LBL-24100 c.2
UC-48

Annual Report
1987

RECEIVED
LAWRENCE
BERKELEY LABORATORY
JUL 26 1988
LIBRARY AND
DOCUMENTS SECTION

TWO-WEEK LOAN COPY
This is a Library Circulating Copy
which may be borrowed for two weeks.

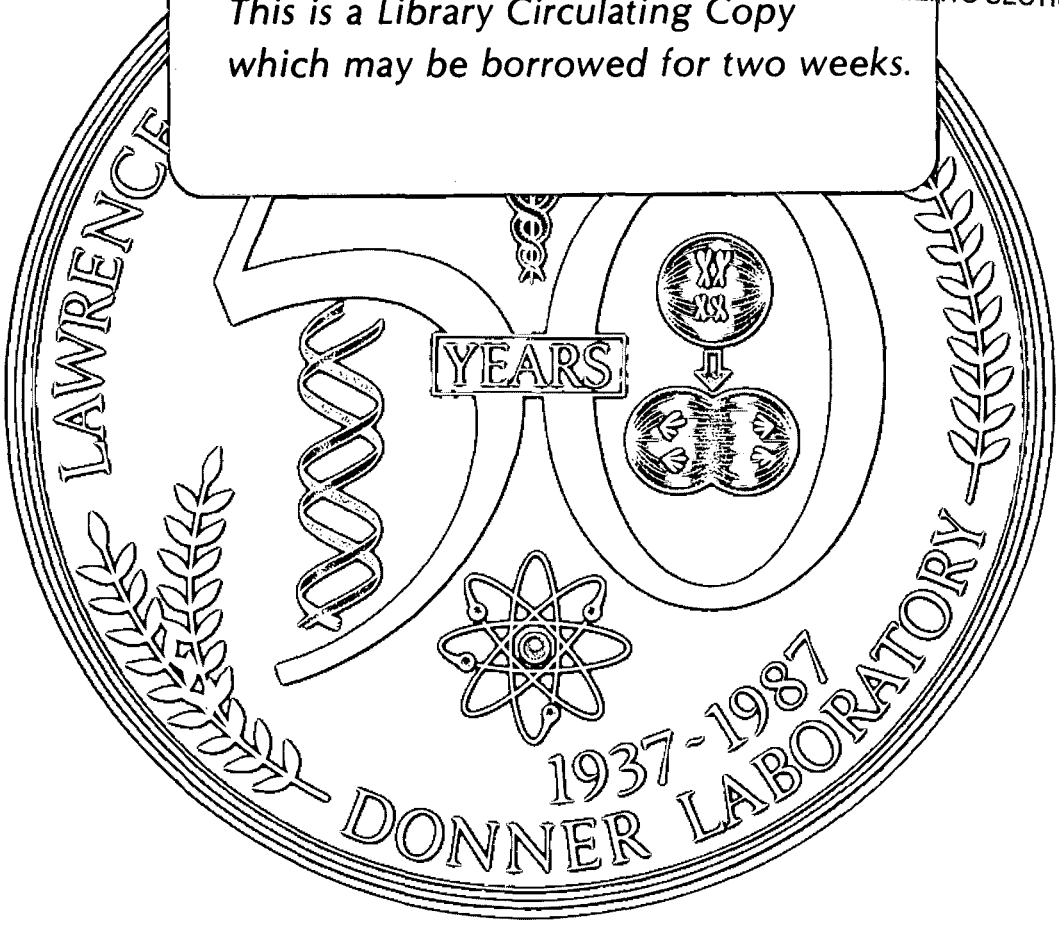

Biology & Medicine Division

Lawrence Berkeley Laboratory
University of California

April 1988

Prepared for the U.S. Department of Energy under Contract DE-AC03-76SF00098

LBL-24100 c.2

DISCLAIMER

This document was prepared as an account of work sponsored by the United States Government. While this document is believed to contain correct information, neither the United States Government nor any agency thereof, nor the Regents of the University of California, nor any of their employees, makes any warranty, express or implied, or assumes any legal responsibility for the accuracy, completeness, or usefulness of any information, apparatus, product, or process disclosed, or represents that its use would not infringe privately owned rights. Reference herein to any specific commercial product, process, or service by its trade name, trademark, manufacturer, or otherwise, does not necessarily constitute or imply its endorsement, recommendation, or favoring by the United States Government or any agency thereof, or the Regents of the University of California. The views and opinions of authors expressed herein do not necessarily state or reflect those of the United States Government or any agency thereof or the Regents of the University of California.

BIOLOGY AND MEDICINE DIVISION ANNUAL REPORT 1987

Lawrence Berkeley Laboratory
University of California
Berkeley, California 94720

April 1988

This work was supported by the Office of Health & Environmental Research of the United States Department of Energy under Contract DE-AC03-76SF00098. Portions of this work were also supported by the National Institutes of Health, Department of Health and Human Services, the Armed Forces Radiobiology Research Institute, the National Aeronautics and Space Administration, the Nuclear Regulatory Commission, the Office of Naval Research, Liposome Technologies Inc., and Monsanto. The DOE projects, the contracts and grants with the above, and the subcontracts with the University of California San Francisco, the University of Southern California Medical Center, the University of Colorado, and Stanford University are listed in Appendix A.

Preface

This year an attempt has been made to develop a Biology and Medicine Division annual report that presents a coherent, integrated, and balanced portrayal of the research activities of the Division.

The decisions on the program emphasis for this new format were made by an editorial committee made up of Group Leaders and Deputy Group Leaders. As a result a much heavier burden fell on them as the contact points between the contributors and the Associate Laboratory Director's Office. In this capacity Eleanor Blakely, Mina Bissell, Thomas Budinger, Aloke Chatterjee, Michael Esposito, Trudy Forte, and Bing Jap deserve special mention.

Credit for the coordination of the overall effort and much of the fine editing goes to Jan DeMoor, as it has in previous years. The efforts and interest of R.G. Barton and the staff of the Technical Information Department contributed in many ways to make this a more readable document than it might otherwise have been.

Jack Bartley

CONTENTS

Introduction 1

Section 1. Structural and Macromolecular Biology 5

Electron Microscopy and Electron Crystallography 6
- Chemical Element Localization in the Microenvironment of Epithelial Cells 6
- Analytic Electron Microscopy 6
- X-Ray Microscopy 6
- Development of Freezing Techniques for Biological Material 8

Electron Crystallography of Membrane Proteins 8

Spectroscopy of Nucleic Acids and Proteins 11
- Fluorescence Detected Circular Dichroism 11
- Differential Polarization Microscopy of Changes in Structure of Spermatocyte Nuclei 11
- The Effect of Speed of Deoxygenation on the Percentage of Aligned Hemoglobin in Sickle Cells: Application of Differential Polarization Microscopy 13

Lipoprotein and Membrane Protein Biochemistry 13
- Lipoprotein Structure and Metabolism 13

Genetics and Gene Expression of Lipoproteins 16
- Genetic Factors that Influence LDL Subclass Patterns 16
- Expression of Lipoprotein Genes by Liver Cells 17
- Atherosclerotic Plaque Proteins 19

Publications 20

Section 2. Cell and Molecular Biology 25

Molecular and Genetic Studies of DNA Damage and Repair 27
- Molecular Mechanisms of DNA Damage by Carcinogens 27
- Processing of Lesions in the Vicinity of Replication Forks 28
- Efficiency of Repair and Transcriptional Activity 28
- Oxidative Damage and Direct Adduct Formation in Carcinogenesis 29

DNA Replication and Recombination 30
- Introduction 30
- Postreplication Recombinational Repair 30
- Mitotic Recombination and DNA Repair 31
- Recombinational Repair Mediated by *RAD* Genes 32

Differentiation 34
- Mammary Cells as a Model for Studies of Gene Expression and Polarized Secretion 34
- Tendon Cells 37
- Hemopoiesis 38

Carcinogenesis 42
- Introduction 42
- Environmental Carcinogens 42
- Human Mammary Cancer 43
- Novel Approaches to Viral Carcinogenesis: Host-Virus Interactions in Differentiation and Malignancy 43

Publications 46

Section 3. Radiation Biophysics 51

Ionizing Radiation 54
Radiological Physics and Radiation Chemistry 54
Molecular and Cellular Studies 59
Theoretical Modeling of Cellular and Molecular Effects 63
Cell Transformation and Somatic Mutation Studies 64
Oxygen-Glucose Deprivation as the Cause of Necrosis in a Tumor Analog 65
In Vivo Biophysics 66

Nonionizing Radiation 70
Field-Induced Changes in Membrane Permeability 70
Structural Changes in Eukaryotic Cell Membranes 70
Cardiovascular Effects 70
Applications of Electromagnetic Fields in Spectroscopy and Chromatography 71

Future Studies 71

Publications 72

Section 4. Research Medicine 75

Introduction 75

Brain Function and Disease Studies 77
Schizophrenia and Affective Disorders 77
Clinical and Metabolic Significance of Cerebral White Matter Lesions Seen on NMR Imaging 78
Quantitative NMR Measurements of Brain Atrophy in Normal Aging and Alzheimer's Disease 78
Investigation of Cerebral Serotonin Receptor Sites with Radiolabeled Amphetamine Analogs 80
Differentiation of Actively Growing Tumor from Inactive Tumor *In Vivo* Using Positron Emission Tomography 82
Quantitation of Hypoxia with Misonidazole Derivatives 82

Heart and Atherosclerosis Studies 84
Imaging Atherosclerosis 84
Heart Studies 86

Therapy with Charged Particle Beams 88
Review of Heavy Charged Particle Research Trial for FY 1987 88
Treatment Planning Developments in Radiotherapy 88
Stereotactic Heavy Charged Particle Radiosurgery 90
Neurobiological Effects of Heavy Particle Irradiation 92

Imaging, Instrumentation, and Methods 93
New Positron Emission Tomograph Instrumentation 93
NMR Methods 95

Publications 98

Appendix A. Project, Contract, and Grant Suppport 103

Appendix B. Biology and Medicine Division Staff 108

Introduction

The continuity and tradition of research in biology and medicine at LBL—devoted to "advancing the application of physics, chemistry, and the natural sciences to biology and medicine" (as inscribed on the 1941 dedication plaque of the Donner Laboratory)—was emphasized this past year by the celebration of our 50th Anniversary. The current research in life sciences at LBL remains compatible with this mission. There is a continuing commitment to basic studies of biological and molecular function, particularly as they relate to carcinogenesis, mutagenesis, and atherogenesis, to the development and application of advanced nuclear medical techniques, and to studies basic to radiation damage and therapy utilizing the unique selection of particle radiations available at LBL. These efforts entail application of state-of-the-art techniques derived from immunology, cell biology, molecular genetics and the traditional disciplines basic to medicine such as biochemistry, biophysics, physiology, and hematology.

Planning

During the past year, two unusual panels dealt with new and ongoing research at LBL. LBL Director Shirley received recommendations on research in life sciences from the Panel to Explore New Directions (PEND) and from the multicampus Life Sciences Task Force. These reports have recognized the potential importance of life sciences in the future of LBL.

The PEND Subcommittee for Life Sciences evaluated several potential new programs in the context of the LBL/DOE mission. Their recommendations designated two initiatives as being appropriate for development at LBL at this time. The first was a biotechnology initiative that would utilize strengths in 1) molecular and cellular biology at LBL/UCB to explore means for optimization of host/vector systems for bioprocessing and 2) instrumentation and bioengineering to develop a pilot plant to facilitate scale-up of the optimized systems and to develop noninvasive means of monitoring cellular activity and productivity. The second initiative was a plan to bring to bear the combined activities of several divisions on the question of the extent and biological significance of free radical generation in the environment during energy conversion. The first of these initiatives has received funding from the Director's Program Fund and the UC Biotechnology Research and Education Program for bioprocess engineering. A pilot program in biotechnology will be initiated in FY 1988 that will include components from the Cell and Molecular Biology, Applied Sciences, and Engineering Divisions.

Reorganization

The Life Sciences Task Force was charged with assessing current strengths and future opportunities for the LBL life sciences program and to recommend an appropriate organizational structure. The recommendations included retaining and nurturing existing strengths in chemical biodynamics and in research medicine and to promote cell and molecular biology. A new organizational structure, implemented at the beginning of 1988, essentially embraces the organizational aspects of the Task Force's recommendations. This new organization brings together, under the leadership of Paul Silverman as Associate Laboratory Director for Life Sciences, those divisions in which the major research effort is in life science. Concurrent with these organizational changes, Life Science was added to Energy Science and General Science in the LBL mission statement to reflect the recognized importance of this research area.

Paul Silverman remained head of the Biology and Medicine Division until January 4, 1988 when it was divided into two major research components: the Research Medicine Division, under the leadership of Thomas Budinger, and the Cell and Molecular Biology Division under the direction of Mina Bissell. This organizational structure meets the recommendation of the Task Force to provide a more prominent role for the research program in cell and molecular biology.

Internal and external reviews have recognized the strengths in the research effort at LBL and affirmed the appropriateness of its emphasis on research medicine, cell and molecular biology, and structural biology. The opportunity to combine these efforts with research in life sciences in other divisions was explored at a retreat late in the fiscal year. The potential of this integration to develop an even stronger program in life sciences is being realized and will be reflected in next year's report.

New Initiatives

Any quality research program requires infusion of new concepts, innovative approaches to ongoing programs, and addition of complementary new initiatives if it is to maintain its scientific stature. In an effort to confront this necessity, several new projects were initiated last year and significant new directions were added to several ongoing programs. The new initiatives include development of a multidisciplinary program to examine the biophysical, cellular, and molecular aspects of radon exposure; the use of molecular epidemiology based on restriction length polymorphism to provide a molecular link to the incidence of familial diseases, particularly atherogenesis and breast cancer, and the addition of the hemopoietic system to the studies of the relationship between perturbations in gene expression and carcinogenesis.

The Human Genome Center became the major new initiative developed in life sciences at LBL during the past year. As a result of this effort, LBL was designated by the Secretary of Energy as one of the two DOE-sponsored centers for the national Human Genome Project. The Center at LBL is designed to focus strengths in cell and molecular biology, instrumentation, data management and analysis, and structural biology on the formidable and challenging task of physically mapping and sequencing large portions of the human genome. This project exemplifies the new emphasis on the importance of research in life sciences to the total research effort at LBL. The Human Genome Center has the potential of becoming one of the largest single biomedical initiatives attempted at LBL.

In addition to the the two major programs initiated during FY 1987–the Human Genome Center and Cell Transformation by Radon Progeny–several ongoing programs are being significantly expanded. The goal is to encourage the research effort in nuclear medicine and in the cellular and molecular aspects of radiobiology, mutagenesis and carcinogenesis, and gene expression.

Specific programs targeted for expansion include advancing our understanding of the mechanisms for repairing damaged DNA, the cellular and molecular consequences of radiation-induced DNA damage, the role in carcinogenesis of perturbations in differentiation, and diagnostic and therapeutic applications of radiation and related instrumentation developed in research medicine.

Accomplishments

The research effort in DNA repair was mounted at LBL several years ago with major emphasis in bacterial and yeast systems. This work has progressed and coalesced to produce four new projects on DNA repair, three of which involve human cells. These projects use concepts and techniques refined in simpler systems to increase our understanding of DNA repair in human cells. This is complemented by the expanding effort of radiobiologists at LBL to characterize chemically the damage induced in DNA by various types of radiation, the biological consequences of this damage, and how this damage is recognized and repaired in the cell. The research effort at LBL in gene expression, particularly in mammary epithelial cells, has achieved international recognition. Continued growth of this program is expected, and the emphasis will remain on modulation of the differentiated state by cytokines, tissue substrata and other cells, and the role of aberrations in these modulations in carcinogenic processes.

Research in nuclear medicine continues to advance investigations of physiology and disease processes, the development of special instruments to aid in these investigations, and the development of treatment regimens using the variety of radiation sources available at LBL. The use of nuclear magnetic resonance (NMR) for imaging tissues and blood flow was pioneered at LBL, and a new positron emission tomograph (The Donner-600) that provides 2.5 times finer spatial resolution than previously possible was designed and developed here. A significant expansion of the medicine program will include the research and development necessary to transfer this instrumentation to the clinic. Construction of a biomedical isotope facility has been proposed in support of the PET-imaging effort. LBL has the staff necessary to develop radiolabeled imaging agents, but productivity is hampered by the lack of facilities for producing short-lived tracers and inadequate facilities for meeting the demand for synthesis of new and improved PET-imaging agents.

The research on biomedical applications of heavy-ions is at the forefront in testing and refining

effectiveness as a treatment modality for certain inoperable tumors and for arteriovenous malformations (AVMs) in the brain. The proposed upgrade of the Bevalac, the source of the unique spectrum of charged-particle beams available at LBL, will facilitate the anticipated expansion of this program. One goal of the recent reorganization is to foster a highly integrated program involving heavy-ion therapy in conjunction with imaging by PET and NMR.

There are two major parts to the research effort in atherogenesis. The first is to understand the metabolism of specific lipoprotein subclasses and subspecies and the role of variations in this metabolism, and the underlying molecular and biological causes of these variations, as factors protecting against or related to the onset of premature atherosclerosis. The second part is related to this goal. Preliminary evidence indicates that a predominance of small dense subclasses of low density lipoproteins (LDL) in the circulating plasma is related to the risk of cardiovasuclar disease. The objective of this research to test the hypothesis that the patterns of subclasses of LDL are in large measure determined genetically. This hypothesis is being tested by screening for the presence of various LDL subclasses in carefully defined families and performing both complex segregation analysis in pedigrees and linkage analysis restriction fragment length polymorphisms (RFLP) in DNA.

Technology Transfer

Another goal of the research effort in life sciences at LBL is to transfer new findings to the medical community and to industry for application in the private sector. Recent examples of this activity in nuclear medicine are the discovery of metabolic aberrations in Alzheimer's disease and the newly defined phenomenon of heart muscle flow rebound in coronary artery disease.

Summary

Modern biology is characterized by rapid change. The development of new tools and the results derived from their application to various biological systems require significant shifts in our concepts and the strategies that are adopted to analyze and elucidate mechanisms. In parallel with exciting new scientific developments our organizational structure and programmatic emphases have altered. These changes and developments have enabled the life sciences at LBL to be better positioned to create and respond to new opportunities. The work summarized in this annual report reflects a vital multifaceted research program that is in the vanguard of the areas represented. We are committed to justifying the confidence expressed by LBL through the new mission statement and reorganizational changes designed to give greater prominence to the life sciences.

Paul H. Silverman

Section 1. Structural and Macromolecular Biology

The Structural and Macromolecular Biology Group comprises multidisciplinary investigators whose major objective is to understand the structural-functional relationships of biologically important molecules. The breadth of the program ranges from protein structure studies at the level of atomic detail using highly sophisticated electron crystallography techniques to optical spectroscopy methods utilized to study the orientation and structure of proteins and nucleic acids in intact cells. And because protein structure and synthesis in biological systems are under the regulation of specific genes, the program examines genetic regulation in the formation and metabolism of specific biological structures.

The different research components of our group and the research affinities of its members are indicated below.

ACTIVITIES OF THE STRUCTURAL AND MACROMOLECULAR BIOLOGY GROUP

	Scientists	*Technical and Staff Graduate Students*
Electron Microscopy and Electron Crystallography	J. Bastacky F. Burkhard K. Downing R. Glaeser T. Hayes B. Jap	J. Barr G. Gutman S-H. Kong C. Lee G. Perkins P. Walian
Spectroscopy of Nucleic Acids and Proteins	S. Bicknese R. Glaeser B. Jap F. Livolant M. Maestre A. Nichols	J. Corbett S.Goolsby
Lipoprotein and Membrane Protein Biochemistry	E. Berry S. Bicknese T. Forte B. Jap R. Krauss M. LaBelle F. Lindgren T. Musliner A. Nichols J. Owicki M. Robinson P. Williams	J. Adamson P. Blanche R. Celli D. Chin G. Giotas L. Glines E. Golder E. Gong R. Harvey-Turner S-H. Kong B. Nordhausen V. Obie J. Orr J. Selmek-Halsey J. Slack
Genetics and Gene Expression of Lipoproteins	M. Austin T. Forte R. Krauss M. Labelle M. McCall	L. Abe A. Cavanaugh L. Glines

Electron Microscopy and Electron Crystallography

CHEMICAL ELEMENT LOCALIZATION IN THE MICROENVIRONMENT OF EPITHELIAL CELLS

The chemical elements of the cell's microenvironment are often found to be localized in small particles or microcompartments surrounding the cell. Such localization and compartmentalization can result in individual cell exposure to concentrations of chemical elements (or molecules containing such elements) that are quite different from the exposure calculated from data obtained by bulk chemical analysis of the extracellular fluids. If certain microcompartments or particles tend to concentrate the element, the individual cell exposure can be strikingly different from that estimated from macroenvironmental measurements.

The analysis of the elemental composition of small volumes (on the order of the size of individual cells) has been carried out during the past year using the analytic electron microscope at the National Center for Electron Microscopy (NCEM) at LBL. Both elemental mapping and estimates of concentrations based on characteristic x-ray analysis by a thin-film program at NCEM were carried out. The elements P and Fe, as distributed in red blood cells and lung type II epithelial cells, were used as test specimens. Elemental concentrations and distribution can also be determined by using synchrotron radiation (x rays) to excite characteristic x-ray fluorescence or by measuring the absorption edge structure in scanning transmission x-ray microscopy. An alternative method of x-ray microscopy imaging uses a contact radiograph (lithograph) to record the information and an electron microscope to read the information from the x-ray lithograph. During the past year, investigators in our group provided biological specimens for synchrotron radiation experiments in collaboration with the LBL Center for X-ray Optics. Progress on both x-ray scanning and x-ray lithography methods during the past year are described below.

ANALYTIC ELECTRON MICROSCOPY

The analytic electron microscope (AEM) is a scanning transmission electron microscope (STEM), JEOL 200CX, fitted with both high-angle and ultrathin window x-ray detectors and a Kevex 8000 series spectrometer. The beam is capable of penetrating whole cells.

Figure 1.1a shows the wall from a single lung alveolus in the STEM. The lung had been inflated and maintained under controlled physiologic conditions, then frozen *in situ*. This sample was frozen relatively slowly by pouring liquid nitrogen over the lung; however, techniques are presently being developed for rapid freezing using a metal probe. Sections of frozen lung tissue were transferred to the specimen chamber of the low-temperature scanning electron microscope (LTSEM) in a special vacuum transfer device currently being designed and developed in conjunction with the AMRay and EMScope corporations. After examination under the electron beam of the LTSEM, final freeze-drying was carried out on the stage of the scanning microscope. A single alveolar wall from the lung (approximately 10 μm thick and 100 μm long) was removed using microdissection techniques and mounted between two beryllium grids. Increased magnification of the image [Fig. 1.1(b)] allows selection of individual cells for analysis by beam spot or raster modes [Fig. 1.1(c)]. Characteristic x-ray peaks were measured to determine the concentration of specific elements in individual cells.

Figure 1.2 shows two superimposed spectra; one spectrum was obtained from the red blood cell marked "RBC" in Fig. 1.1(c) and the other spectrum from the type II epithelial cell marked "T_{II}" in Fig.1.1(c). The iron peak (Fe) is present only in the red blood cell and the phosphorous peak (P) is higher in the epithelial type II cell. The type II cell produces phospholipid surfactant, which is critical in preventing alveolar collapse.

The pattern of P and Fe distribution can be recognized more easily by elemental mapping of the alveolar wall. In Fig. 1.3 the microscope generates a spectrum at each point in a 125 × 64 raster then each pixel is displayed with an intensity of red proportional to the concentration of iron and an intensity of green proportional to the concentration of phosphorus.

X-RAY MICROSCOPY

In the past year pilot studies were conducted to assess specimen preparation and mounting for the first trials of x-ray microscopy on lung tissue. Sequential correlative microscopy before and after x-ray imaging was conducted using the analytic electron microscope and high voltage electron

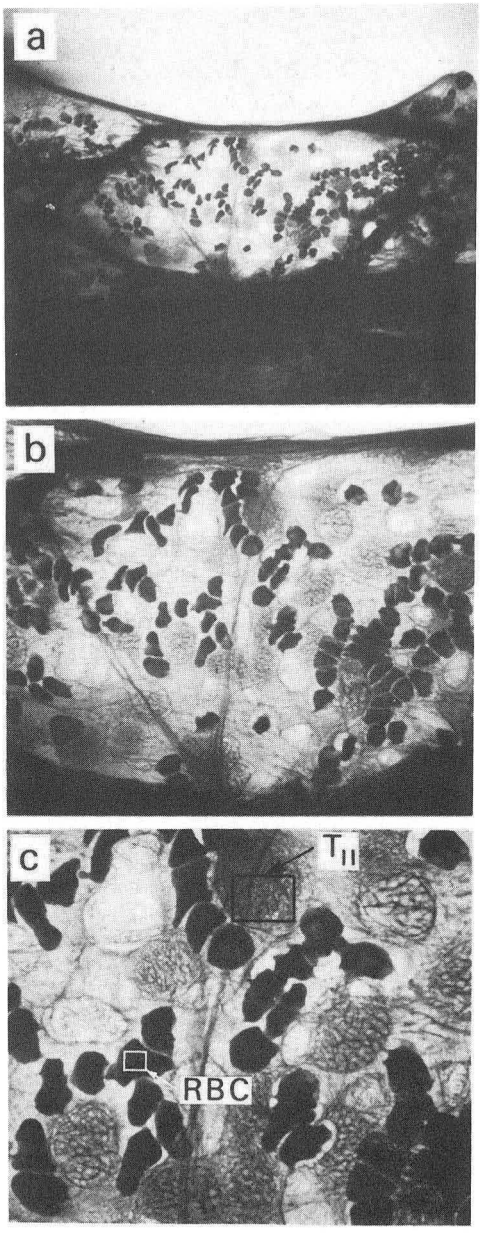

Fig. 1.1 The scanning transmission electron microscope transilluminates the wall of a single air sac or alveolus from the lung. Red blood cells line up within the thin sheet of capillaries that make up this gas exchange membrane. This sample of dog lung was frozen while inflated then freeze-dried. No chemical fixatives, stains nor metal coats were used. Figures 1.1b and 1.1c are increasing magnifications of the center of the field in Fig. 1.1a. Red cells are approximately 5 μm in diameter. The rectangles marked RBC and T_{II} indicate the electron beam raster areas during the collection of the spectra in Fig. 1.2. RBC is the red blood cell, T_{II}, the alveolar epithelial Type II cell. (XBB 882-866)

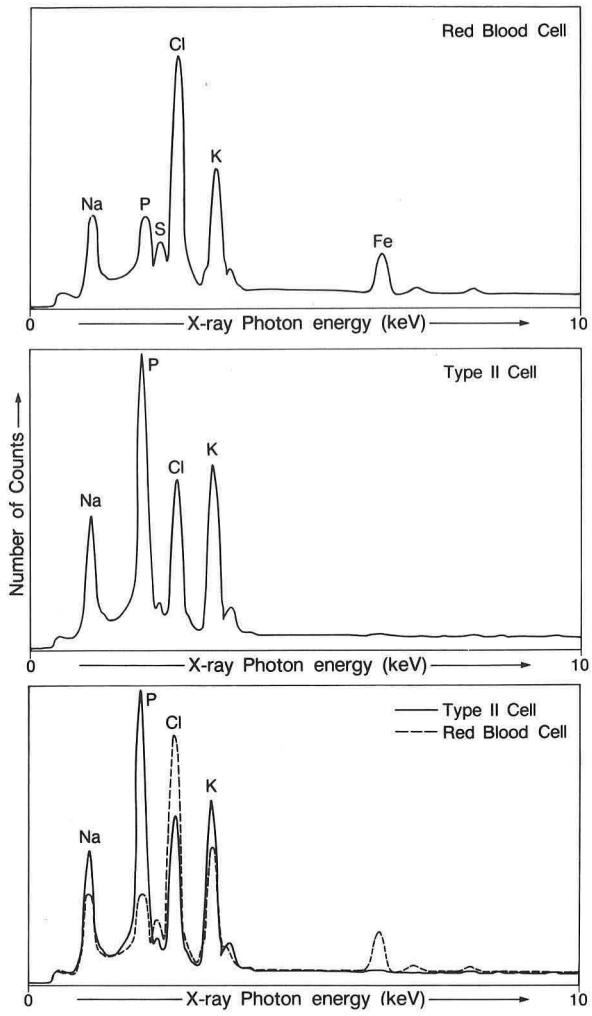

Fig. 1.2. Characteristic x-ray fluorescence spectra from red blood cell and alveolar epithelial type II cell in Fig. 1.1. (XBL 881-7240)

microscope at the National Center for Electron Microscopy. Freeze-dried alveolar wall preparations similar to those described above were photographed in the transmission light microscope and examined with the LBL prototype scanning x-ray microscope system operated by the LBL X-Ray Optics Group at the National Synchrotron Light Source at Brookhaven National Laboratory. This instrument was able to focus monochromatic x rays to an elliptical spot of 10 × 5 μm and to scan this spot in a line across the alveolar wall, taking a characteristic x-ray spectrum at each of 12 to 14 points along the line. The specimens were returned to LBL, the lung was mounted on Be grids, and the same area was analyzed with the AEM. X-ray spectra excited by the AEM electron beam were compared with those excited by the x-ray beam. STEM images were compared with the original transmission light images. The sample was also transilluminated by the 1.5-MeV electron beam of the high voltage electron microscope to obtain fine structural detail as a first step in the evaluation of beam damage with the scanning x-ray microscope.

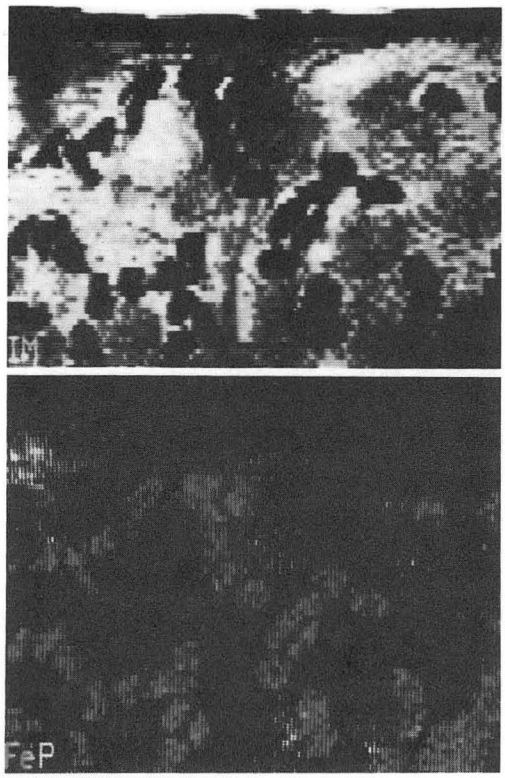

Fig. 1.3. (a) Digitalized image of the same alveolar wall in Fig. 1.1(c). The analytic electron microscope collects a characteristic x-ray spectrum at each point in the 125 × 64 pixel field then in in (b) paints each pixel red if Fe is present and green if P is present. In this x-ray map of the alveolar wall, the intensity of color at each point is proportional to the amount of the element present. In the above black and white print of this map the distribution of the elements is still discernible but the pattern is much less evident than in the orginal. (CBB 882-1346)

DEVELOPMENT OF FREEZING TECHNIQUES FOR BIOLOGICAL MATERIAL

A joint study with Dr. Patrick Echlin at the Botany School, Cambridge University was directed toward a better understanding of the cellular changes that take place in specimens held at subzero temperatures during microscopic examination and analysis. Relatively unaltered biological material can be cryofixed at temperatures from –20 to –2°C, held at the fixation temperature until cellular electrolyte equilibrium is established and then snap-frozen for analysis by SEM-characteristic x-ray techniques. The experiments were carried out using primordial tissue found in the low-temperature-resistant turion or bud of the aquatic plant *Lemna* (Duckweed), which had been the specimen used in previous studies of frozen hydrated material examined at liquid-nitrogen temperatures. Viability studies were carried out in the upper ice-temperature range and the transition from liquid to solid phase was monitored on individual turions by microcalorimetry and thermal analysis of the exotherm that accompanies the freezing of the supercooled tissue. Preliminary results indicate that the turion of *Lemna* is an excellent test specimen for experiments that would develop techniques for the examination of unaltered biological specimens by soft x-ray microscopy.

T. Hayes and J. Bastacky. Affiliate Members: J. Goerke (UCSF) J. Underwood, A. Thompson, R. Giaque, Y. Wu., and M. Howells (Center for X-ray Optics, LBL), C. Echer (NCEM, LBL).

Electron Crystallography of Membrane Proteins

Electron crystallography has been used widely in structural studies of biological molecules at a resolution of 20 Å, and in a few cases to somewhat better than 10 Å. Information obtained at that resolution is useful in identifying major structural domains. However, the full understanding of functional mechanisms of protein molecules requires a knowledge of molecular structure in atomic detail. Electron crystallography has great potential to become a powerful technique for determining the atomic structures of membrane proteins. The best resolution that is currently attainable by the electron crystallography technique is about 6–7 Å, which is somewhat short of that needed to discern the atomic structure of the proteins. Until recently, several problems have limited the attainable resolution.

In the past year, technical breakthroughs have been made in electron crystallography for determination of atomic structures of membrane proteins. The first is a technique that improves the signal-to-noise ratio of the high resolution details in the images of biological samples, thus allowing high resolution images to be routinely obtained; the

other is the crystallization of membrane proteins for molecular structure determination. These breakthroughs have contributed major steps toward making electron crystallography become a routine technique for molecular structure determination of proteins.

Specimen movement that occurs in response to incident electron radiation has been a major problem in obtaining high resolution images of biological samples. It has long been known that radiation damage limits the resolution of images of organic specimens. This damage results in breakage of covalent bonds and puts stress on the specimen. These effects produce movement in the specimen during electron radiation that results in smearing of the image and a resulting loss of contrast of the high resolution details. To overcome this problem, a small-spot illumination technique was developed that produces a dramatic increase in the contrast of high resolution details of images. This is demonstrated by the quality of images of a monolamellar paraffin crystal obtained in this way (Fig. 1.4). The crystalline lattice spacing of 3.7 Å is clearly visible in these images. In contrast, such a lattice spacing is not visible or appears with much lower contrast when images of paraffin crystals are obtained using conventional methods. The small-spot technique has recently been applied to obtain high resolution images of bacteriorhodopsin, a light-driven proton pump, and of outer membrane channels from *E. coli*. The small-spot technique therefore provides a major step in developing electron crystallographic technique for routine three-dimensional structure determination at the atomic level. This technique can be similarly applied to improve the contrast of high resolution details for crystalline fibers, such as actin filaments and microtubules. Images of these samples have been limited in the past to give low resolution details as a result of specimen movement and of radiation damage. The small spot technique opens a new dimension to electron crystallographers for structural determination of biological macromolecules.

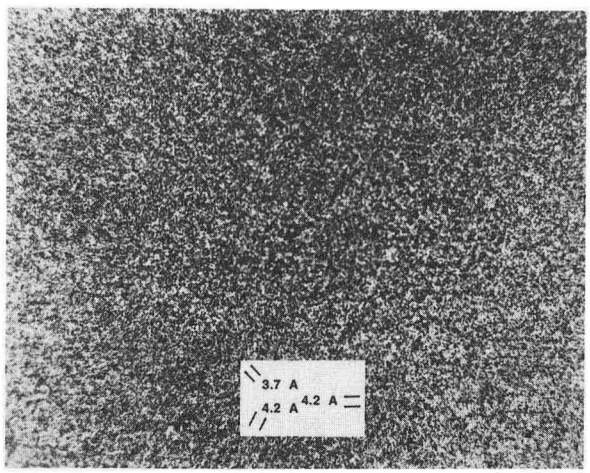

Fig. 1.4. *An image of a monolamellar paraffin crystal obtained directly with the small spot technique. The image is somewhat noisy; lattice lines can be seen more clearly by viewing the figure at an angle along the direction of the lines. Lattice lines with spacings of 3.7 and 4.2 Å as indicated are visible. The dark spots at the intersections of lines correspond to the image of the paraffin chains seen end-on. (XBB 876-5429)*

Specimen flatness and/or the interaction of biological samples with the support film have reduced the success rate of obtaining high resolution images and the diffraction pattern of bacteriorhodpsin in purple membrane at high tilt angles. Images at various tilt angles are needed in order to obtain the three-dimensional molecular structure. The success rate of obtaining high resolution images diminishes at increasingly high tilt angles. This is now the only known limiting factor in obtaining the high resolution structure of bacteriorhodopsin by electron crystallographic methods. A recent study focuses on ways to change the surface properties of the support film to ensure that the sample remains flat. The use of support films with holes and the frozen hydrated specimen technique have provided some encouraging results, but further work is needed.

Crystallization of membrane proteins forming two-dimensional crystals is a necessary step in obtaining the three-dimensional molecular structure of a protein by electron crystallography. Crystallographic averaging provides a way to enhance the signal-to-noise ratio of high resolution details with a minimum dose of electron radiation, damage from which limits the dose allowed to obtain high resolution structural details of biological samples. In the past, purple membrane, which naturally forms highly ordered arrays, was the only specimen from which one could successfully obtain a high resolution structure to 6.5 Å by electron crystallography. There was an urgent need to show that membrane proteins that are not naturally crystalline can be reconstituted to form two-dimensional crystals that diffract to high resolution. Such reconstitution has now been successfully done for a membrane protein, PhoE porin, and the crystals diffract to at least 3.4 Å (Fig 1.5).

The specimen flatness problem, which clearly hindered progress in obtaining high resolution data

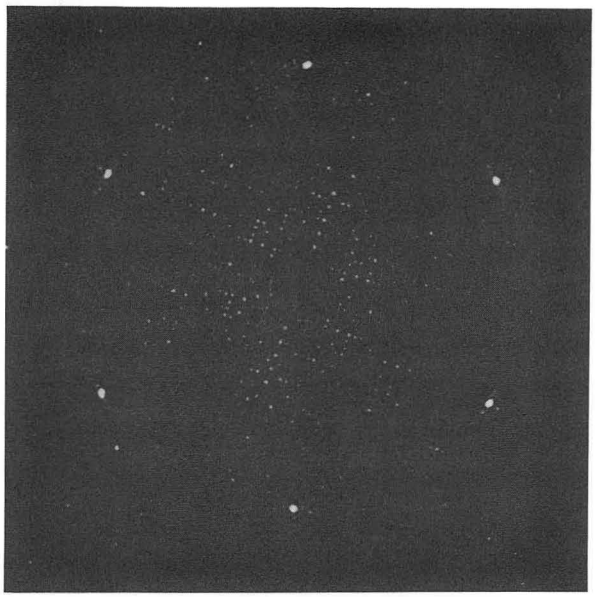

Fig. 1.5. A high resolution electron diffraction pattern of PhoE porin embedded in glucose. The pattern has been procesed by computer to reduce the background intensity. The diffraction pattern was obtained at a temperature of -120 ℃. The pattern shows reflections extending to at least 3.4 Å. (XBB 870–10681)

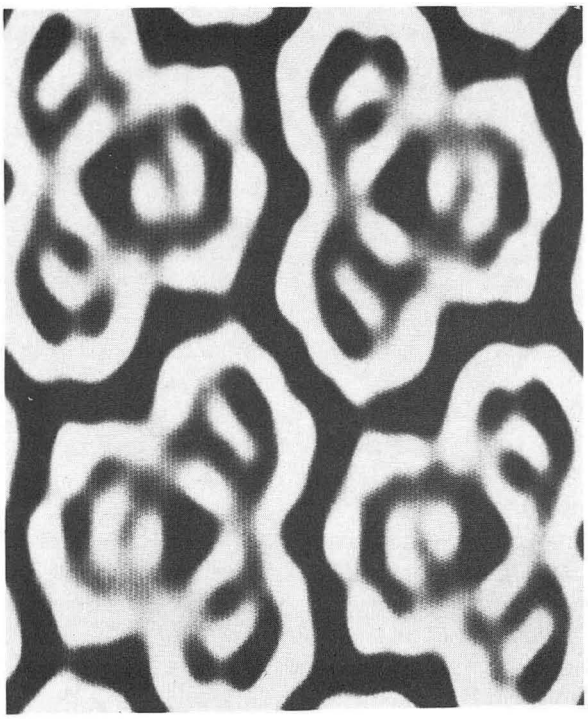

Fig.1.6. A projected map of PhoE porin embedded in glucose. The map is obtained from an image by computer processing that enhances the contrast. The structural information is limited to a resolution of about 10 Å. There are four trimers in a unit cell. Each trimer appears as three cylindrical structures (dark rings) of β sheet, where the central dark region of each cylinder represents a glucose-filled channel. (XBB 881-8)

at high tilt angles for bacteriorhodopsin, appears to be less severe for PhoE porin. It was possible to obtain high resolution diffraction of PhoE porin at 45 degrees tilt without significantly degrading its quality. The interaction of the PhoE membrane with the support film as compared to that of bacteriorhodopsin may be the main difference: bacteriorhodopsin crystals diffract only when the support film is hydrophobic while PhoE porin crystals diffract even when the support film is highly hydrophillic. It is currently believed that the surface properties of the support film and of the sample suspension determine the degree of stress on the support film, resulting in varying degrees of bending of the support film. The bending of the support film, in turn, results in the fading of the diffraction pattern as the sample is tilted.

Significant progress has been made in obtaining a high resolution three-dimensional structure of PhoE porin. A projection map of PhoE porin (Fig. 1.6) with a resolution better than 10 Å has been obtained. The projected map shows that the structure of porin consists of a hollow cylinder with outer diameter of about 40 Å. The diffraction pattern of PhoE porin shows strong reflections at approximately 4 and 10 Å suggesting that the β sheets, which are known to make up its secondary structure, are oriented approximately normal to the membrane plane. Assuming that the cylindrical structure extends across the membrane, about 40 Å thick, the number of β strands needed to form such a hollow cylinder is about 19, each strand being 12 residues long. The total number of residues needed to form such a channel is about 230. Since PhoE porin consists of 330 residues, there are about 100 remaining residues for linker peptides and for forming a possible gating structure. This type of model is consistent with our three-dimensional map of negatively stained PhoE porin at a resolution of better than 20 Å. Our three-dimensional map shows trimeric channels, each of which is about 35 Å long and 20 Å wide. The trimeric channels traverse the membrane, but they do not merge. Each channel probably has an extended narrower segment that may play an important role in both its molecular selectivity and possible gating mechanism. Currently, the three-dimensional structure of PhoE porin at high resolution is being determined in order to provide more detailed information about the molecular design of the channel.

Great effort has been given to crystallize halorhodopsin (hR), a light-driven chloride pump. Reconstituted hR with lipids, extracted from purple

membrane, forms two-dimensional patches, indicating that our crystallization condition is not too far from the ideal one. The reconstituted patches have not yet shown any ordered arrays. Work is currently underway to refine the crystallization protocol in order to obtain well-ordered crystals.

A new project has been initiated to purify mitochondrial transport enzymes, the adenine and phosphate transporters, for subsequent crystallization into two-dimensional crystals suitable for electron crystallographic studies. When these proteins have been purified to homogeneity, attempts will be made to crystallize them following the same technique that has been used successfully in the reconstitution of PhoE porin into crystals. The natural abundance of the two transporters in mitochondria from beef heart and their stability when purified are certainly positive factors for successful two-dimensional crystallization.

Robert M. Glaeser, Bing K. Jap, Kenneth Downing, and Edward Berry. Affiliated Members: Paula Flicker, Peter Walian, and Seok-Hwan Kong.

Spectroscopy of Nucleic Acids and Proteins

FLUORESCENCE DETECTED CIRCULAR DICHROISM

Fluorescence-detected circular dichroism (FDCD) is a powerful tool for studying the structure of proteins that possess fluorophores such as the amino acid tryptophan. In normal FDCD measurements, a large part of the fluorescent signal is lost by the phenomenon of photoselection. This latter spectroscopic artifact arises when fluorophores are excited by linearly polarized light and emit anisotropically due to long rotational times and transition dipoles that are closely aligned with the plane of polarization. Residual linearly polarized light occurs in most FDCD instruments, thus decreasing sensitivity. A technical breakthrough has been made in the past year by members of our spectroscopy group in developing an ellipsoidal mirror system that virtually eliminates the signal from photoselection. The design of the elliptical mirror system that is placed inside the sample chamber of the Jasco spectropolarimeter is schematically shown in Fig. 1.7. Fluorescent emission reaching the photomultiplier tube is increased by a factor of 18. By increasing the signal-to-noise ratio, the mirror assembly will be extremely useful for other forms of spectroscopy, and will be important for resolving the structure of complex biological macromolecules. Experiments are presently underway to study the structure of apolipoproteins and changes induced in the structure of the protein molecule during interaction with specific lipids.

DIFFERENTIAL POLARIZATION MICROSCOPY OF CHANGES IN STRUCTURE OF SPERMATOCYTE NUCLEI

Phase-dependent forms of microscopy (phase contrast, interference, polarization, and so forth) have been used for many years; they use the amount of phase retardation to measure the isotropic or anisotropic index of refraction. Investigators in our group have developed a microscope that forms images dependent on small differences in extinction for different forms of incident polarized light. By modulating the polarization of incident light on the sample and digitally recording the

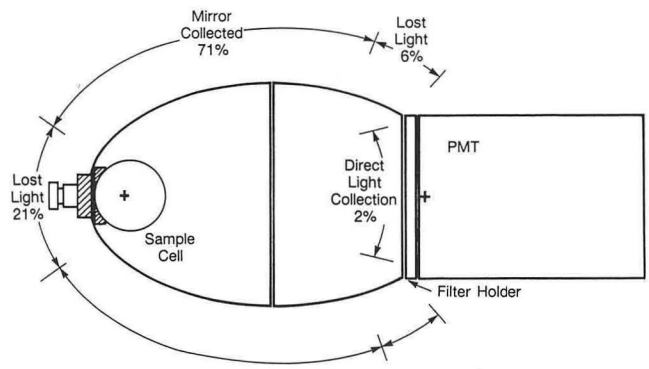

Fig. 1.7. The basic ellipsoidal mirror configuration showing the sample cell with its collar, the modification of one mirror, and the position of the photomultiplier tube (PMT) (+ indicates the ellipsoidal foci). The positions and percentages of light collection and loss are also indicated. (XBL 875-7731)

difference in intensities of transmitted light, images have been obtained that reveal specifically either linear or chirally ordered structures. Linear polarized light, incident alternately with two perpendicular directions of polarization, forms images of structures that have linear order or linear orientation. Right and left circular polarized light incident alternately on a sample forms images of chiral structure. Structures with neither linear order nor chirality are essentially invisible. Thus, linear dichroism, circular dichroism, and linear and circular differential scattering images can be used to detect specific types of structures that may be obscure by conventional methods. The structure of the nucleolus (the site of RNA synthesis) in live primary spermatocytes of *Drosophila* when they are transcriptionally active and inactive has been elucidated by linear and circular differential imaging techniques. The active nucleolus is separated into regions of differing amount of linear and chirally scattering material while the inactive nucleolus and the heterochromatic region of the Y chromosome show the same uniformity of linearly and chirally scattering material (Fig. 1.8). Thus polarization-dependent images reveal structures that correlate with the transcriptional activity of cells.

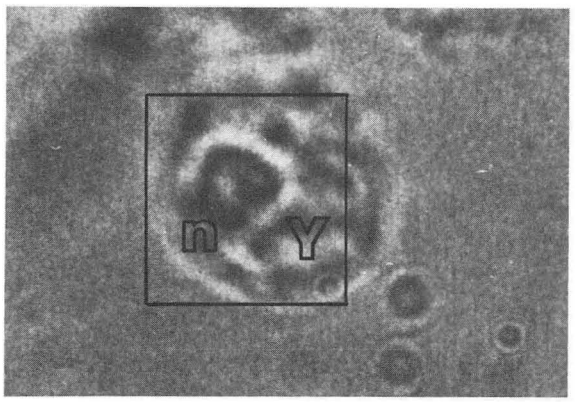

(a)

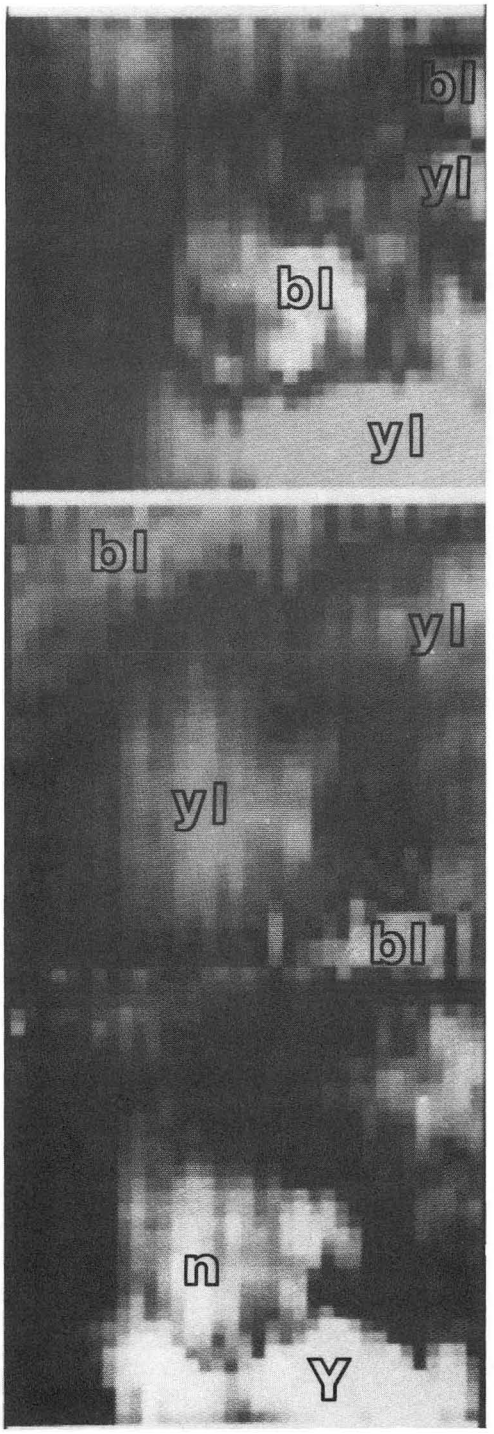

(b)

(c)

(d)

Fig. 1.8. *Four views of the nucleus of an early stage primary spermatocyte: more than ten such cells were imaged. The morphology of this cell is as expected; most of the cytoplasm is contained in a small region still attached to part of the cyst above. The nucleus (with its prominent nucleolus) takes up the remainder of the cell. The nucleolus (n) and the presumed Y chromosome (Y) are labeled. (a) The transmission image of a primary spermatocyte. The field of view in the differential images is 7 μm on each side; the wavelength used to image is 430 nm. The white bar with the differential images is 2 μm long. A square outlines the area of this cell that was imaged in the differential polarization images. Both linear and circular differential extinction are color coded with blue (bl) representing +0.002 to 0.0; yellow (yl) represents 0.0 to -0.002. (b) A circular differential image showing the nucleolus and part of the Y chromosome. (c) A linear differential image of the same area in (b) showing the single domain nucleolus (center, yellow) and part of the lampbrush chromosome (upper right, blue). (d) The image of the amount of linearly aligned material. The image is obtained from two linear dichroism images [one is shown in (c)] with the principal axes of polarization differing by 45 degrees. The norm of these two images gives the amount of oriented material independent of the direction of orientation. The nucleolus and part of the lampbrush chromosome are readily visible in (a) through (d). Note that the circular and linear differential images show different structures at this stage in development. [(a)XBB 860-8866, (b,c,d)XBC-869-7926]*

THE EFFECT OF SPEED OF DEOXYGENATION ON THE PERCENTAGE OF ALIGNED HEMOGLOBIN IN SICKLE CELLS: APPLICATION OF DIFFERENTIAL POLARIZATION MICROSCOPY

Differential polarization microscopy (linear dichroism) has been used to measure the percentage of aligned hemoglobin (Hb) in 1086 deoxygenated red blood cells from subjects with sickle cell anemia. The percentage was found to be only slightly dependent on the speed of deoxygenation, thus showing that the percentage of aligned Hb was thermodynamically controlled (as has been found previously for the percentage of polymerized Hb). The slight decrease in the percentage of aligned Hb due to increasing speed of deoxygenation is primarily due to the increase in number of cells containing no detectable aligned Hb. This class of cells was also the most variable between the different subjects studied. Two other groups of cells were identified that contain different numbers of domains of aligned Hb, and these groups contain statistically different percentages of aligned Hb. The differences between these classes of cells were shown to be primarily due to different numbers of initial nucleation sites within each cell. It appears that the presence of preformed nucleation sites within cells at room oxygen tension results in the thermodynamic control of aligned Hb polymer.

Marcos Maestre, William Mickols, Stephen Bicknese, and Alex Nichols. Affiliated Member: Ignacio Tinoco (Chemical Biodynamics, LBL).

Lipoprotein and Membrane Protein Biochemistry

LIPOPROTEIN STRUCTURE AND METABOLISM

Lipoproteins are macromolecules that transport triglycerides and cholesterol in the plasma. Normally these lipids are important as sources of energy for cells, and they are required for cell growth and repair. However, it is well known that exaggerated levels of plasma lipids, particularly cholesterol, increase risk to atherosclerosis. Lipoproteins do not represent a single population of particles but rather are best described as distinct families or classes that are distinguished by the protein(s) called apolipoproteins (apo), associated with the lipid. The protein associated with the lipoprotein ultimately determines the metabolic fate of the particle.

The metabolism of various lipoproteins and the interactions between classes of lipoproteins are extremely complex. Abnormalities in lipoprotein metabolism or processing can lead to the onset of atherosclerosis. The complexity of lipoproteins and their role in atherogenesis is schematically represented in Fig. 1.9.

The goal of investigations in the lipoprotein subgroup is to understand the origin and fate of specific lipoprotein subclasses and subspecies, and their contribution as possible risk factors in atherosclerosis or their capacity to protect against premature atherosclerosis. To this end, members of our group are carrying out extensive *in vitro* modeling studies in order to delineate how lipoprotein macromolecules are assembled and subsequently modified by specific enzymes.

Plasma HDLs are associated with decreased risk to premature atherosclerosis; this property of HDL has led to studies aimed at understanding the structural-functional aspects of their molecules. Extensive progress has been made in understanding the origin of specific high density lipoprotein subclasses. HDLs are composed of at least five different components and are associated with three major apolipoproteins, apo AI, AII, and E. Specific details on conversion of apo AI (or AII or E) precursors to representative plasma components have been delineated with protein-lipid models interacted with the enzyme lecithin:cholesterol acyltransferase (LCAT). Model complexes formed with three apo AI molecules, phospholipid, and cholesterol are discoidal structures, of 13.5-nm diameter. Following incubation with LCAT, spheres of 9.2-nm diameter that contain three apo AI molecules are generated (Fig. 1.10). Starting with discoidal complexes containing two apo AI

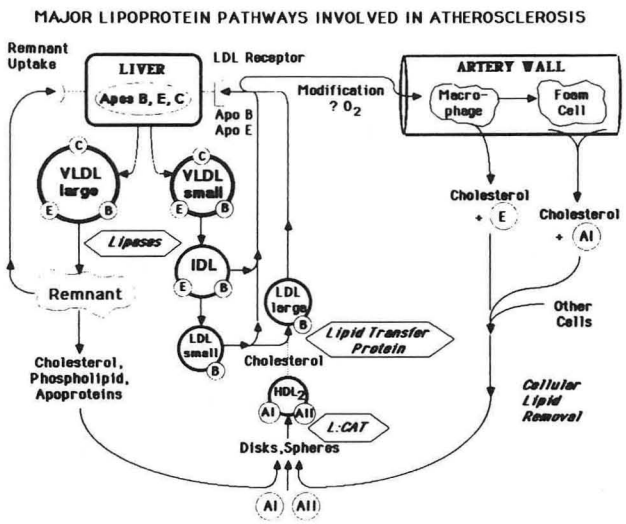

Fig. 1.9. Schematic of major lipoprotein pathways involved in atherosclerosis. The liver is the major source of apolipoproteins (apo)B, E, and C. The major particles secreted by the liver are triglyceride-rich structures, VLDLs. VLDL-triglyceride is hydrolyzed, thus forming smaller particles, including IDL and LDL, that transport most of the blood's cholesterol. LDLs that are abnormally modified in the blood are thought to be taken up by arterial macrophages that then give rise to foam cells that are the beginning of the atherosclerotic lesion. The HDL lipoproteins associated with apoAI and apoAII are believed to remove excess cholesterol from cells with the help of apoE, which is synthesized by many cells and is believed to transport cell cholesterol into the blood. The HDL are often termed "good" lipoproteins because of their ability to reverse cholesterol transport, i.e., remove it from cells. The precursor HDL associated with cholesterol is discoidal in shape but is rapidly converted to the mature spherical HDL by the enzyme lecithin:cholesterol acyltransferase (LCAT). The cholesterol accumulating in large HDL is transferred to LDL and is ultimately degraded in the liver. (BBC 8710-8579)

molecules, LCAT produces a spherical product 8.5 nm in diameter that contains three apo AI molecules per particle. During transformation, fusion occurs with the formation of a particle containing three apo AI molecules and the liberation of one apo AI. The properties of the core-containing particles (spheres) with three apo AI molecules closely resemble those of the major plasma apo AI without apo AII HDL subpopulation, which also contains three apo AIs and is between 8.2–8.8 nm in diameter. This apo AI HDL model strongly suggests that three apo AI proteins are required to stabilize an HDL core containing 13–22 cholesteryl ester molecules. Model complexes employing apo AII were developed to study the molecular dynamics of HDL particles containing this protein. Normally, plasma apo AII is found in association with

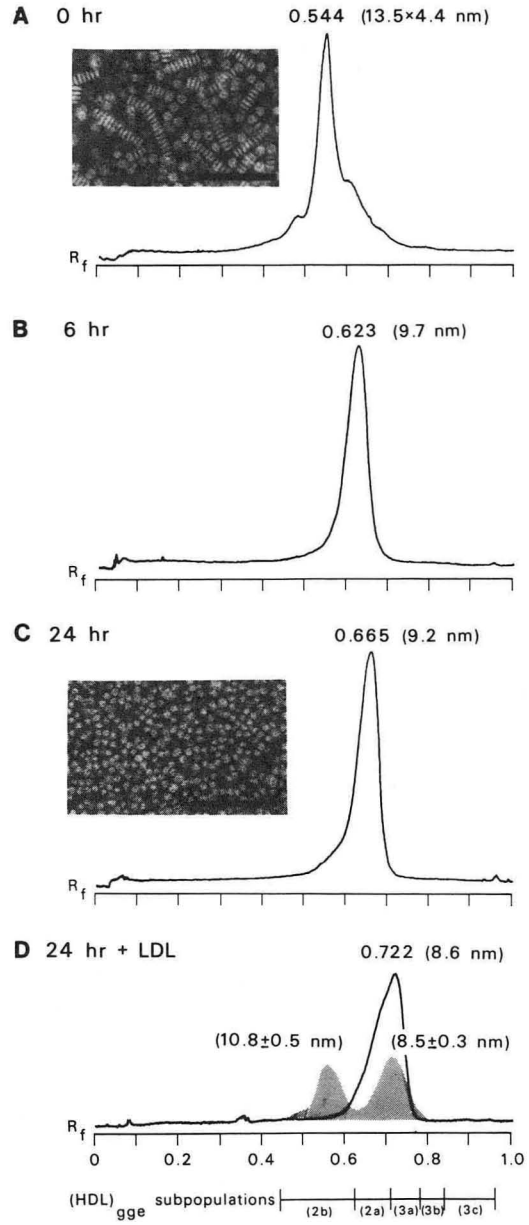

Fig. 1.10. Gradient gel electrophoresis patterns of transformation products from fractions isolated from incubation mixtures comprised of three apoAI-unesterified cholesterol complexes, partially purified LCAT, human serum albumin, and 15-mM b-mercaptoethanol. Patterns correspond to the following incubation (37° C) periods: (A) 0 hr; (B) 6 hr; and (C) 24 hr. Electron micrographs (Formvar grids) of material in fractions from 0-hr and 24-hr mixtures are shown with corresponding electrophoretic patterns. Pattern (D) is of 24-hr transformation product isolated from mixtures with same composition as in (A)–(C) above, but containing LDL as source of additional cholesterol. The shaded pattern in (D) is a schematic representation of the R_f distribution of the two major subpopulations observed in the human plasma HDL population containing apoA-I without apoA-II (Lp(A-I without A-II)). For reference, the particle size intervals of the major subpopulations of total HDL are indicated below pattern (D). (XBL 866-4890)

apo AI, except for the genetic abnormality in which apo AI is not synthesized. Using cholate dialysis for association of apo AII and phospholipid, several discrete complexes are generated. These complexes, which probably mimic nascent apo AII-containing HDL, are separated by gel filtration into subfractions that have specific numbers of apo AII molecules and electron-microscopic size. The minimum number of apo AIIs required to stabilize the discoidal HDL is three; with increasing disc diameter the number of apo AII molecules per particle increases. The well-defined apo AII model complexes are currently being used to understand the role of this protein by itself and in association with apo AI to participate in formation of plasma HDL subpopulations.

Apo E, which is known to play a role in reverse cholesterol transport is also currently under investigation. Model complexes are being generated that promise to be extremely useful in understanding formation and processing of apo E-rich HDL. In addition, collaborative studies on the physical-chemical properties of apo E have been carried out with investigators at the Gladstone Foundation, San Francisco. This 34,000-dalton protein is readily fragmented into two proteolytic fragments of 10 kDa and 22 kDa. The 10-kDa fragment aggregates into tetramers while the 22-kDa portion remains monomeric and has a globular conformation. This important work indicates that the protein has two independently folded domains that may mediate its lipid and receptor-binding functions

Unlike HDL, the lower density lipoprotein classes contain subpopulations that are positive risk factors for coronary artery disease. Important breakthroughs have been made in the past year in understanding the intricate interrelationships between subpopulations of very low density lipoproteins (VLDL), intermediate density lipoproteins (IDL), and low density lipoproteins (LDL). LDLs consist of a spectrum of several subpopulations on nondenaturing gradient gels as outlined in Fig. 1.11, where peaks I and II are large less dense particles and LDL-III and IV are small denser particles. As indicated in Fig. 1.11, IDLs appear in the region before LDLs and are precursors of LDL subspecies. A novel experimental approach was developed in order to determine which VLDL or IDL subclass was the precursor of specific LDL subpopulations. Human plasma lipoproteins of known density (VLDL or IDL) were isolated, isotopically labeled with ^{125}I, and injected into rats, which possess an active lipolytic pathway but no

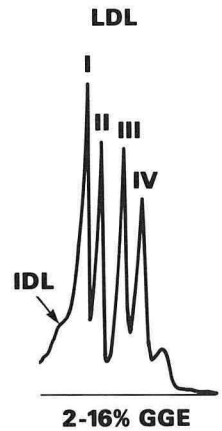

Fig. 1.11. Densitometric scan of IDL and LDL subpopulations separated by electrophoresis 2 to 16% nondenaturing polyacrylamide gels. (XBL 854-8243)

lipid-transfer activity. *In vivo* transformations of VLDL → IDL → LDL were charted by electrophoretic blotting of the radiolabeled products. This unique method of following *in vivo* metabolism of human triglyceride-rich VLDL particles revealed that normal small-sized VLDLs can give rise to IDL-1s and ultimately cholesterol-rich LDL-IIs. Somewhat smaller sized IDL-2s were found to generate larger LDL-I species. VLDLs from patients with familial type 3 hyperlipoproteinemia produce cholesterol-rich particles intermediate in size between IDL-1 and IDL-2. These unusual species are also found in patients with familial hypercholesterolemia and may represent atherogenic particles responsible for increased risk of cardiovascular disease in these disorders.

Recent work with LDL-I enriched *in vitro* with triglyceride indicates that lipolysis of triglyceride in such particles generates the smaller denser LDL-III particle associated with increased atherosclerosis risk. This suggests that LDL-I and LDL-III are metabolically related, which is consistent with previously reported inverse correlations between these two subclasses of LDL.

Lipoprotein lipase is a key remodeler of triglyceride-containing lipoproteins along with lipid transfer proteins. Pursuing this aspect of triglyceride-rich lipoproteins, members of the Lipoprotein Research Group have recently shown that VLDL and LDL form an association complex during lipolysis, which suggests a mechanism whereby lipids can be transferred from one lipoprotein class

to another. Current studies are underway that are specifically addressing the role of HDL during lipolysis. Preliminary studies suggest that HDLs are able to inhibit VLDL-LDL complex formation. Moreover, during lipolysis, lipids can be transferred to HDL apolipoproteins, thus indicating a metabolic interaction between triglyceride-rich particles and anti-atherogenic HDL.

Alex V. Nichols, Trudy M. Forte, Ronald M. Krauss, Frank T. Lindgren, and Thomas A. Musliner. Affiliated Members: Michael La Belle, Miguel Robinson (LBL), Virgie G. Shore, (Lawrence Livermore National Laboratory), and Lon Aggerbeck, Karl Weisgraber, John Wetterau, and David Chappell (all of Gladstone Foundation, San Francisco).

Genetics and Gene Expresion of Lipoproteins

GENETIC FACTORS THAT INFLUENCE LDL SUBCLASS PATTERNS

Based on nondenaturing gradient gel electrophoresis, investigators in this Group have provided data on more than 400 individuals that reveal the existence of two distinct LDL subclass patterns, denoted A and B in Fig. 1.12. In these examples of patterns A and B the three component curves correspond to LDL subclasses I, II, III, and IV. Pattern A is characterized by a major peak of large, buoyant LDL subclasses I and II, and a minor peak representing smaller LDL-III. In contrast, pattern B has a major peak of smaller denser LDL-III or

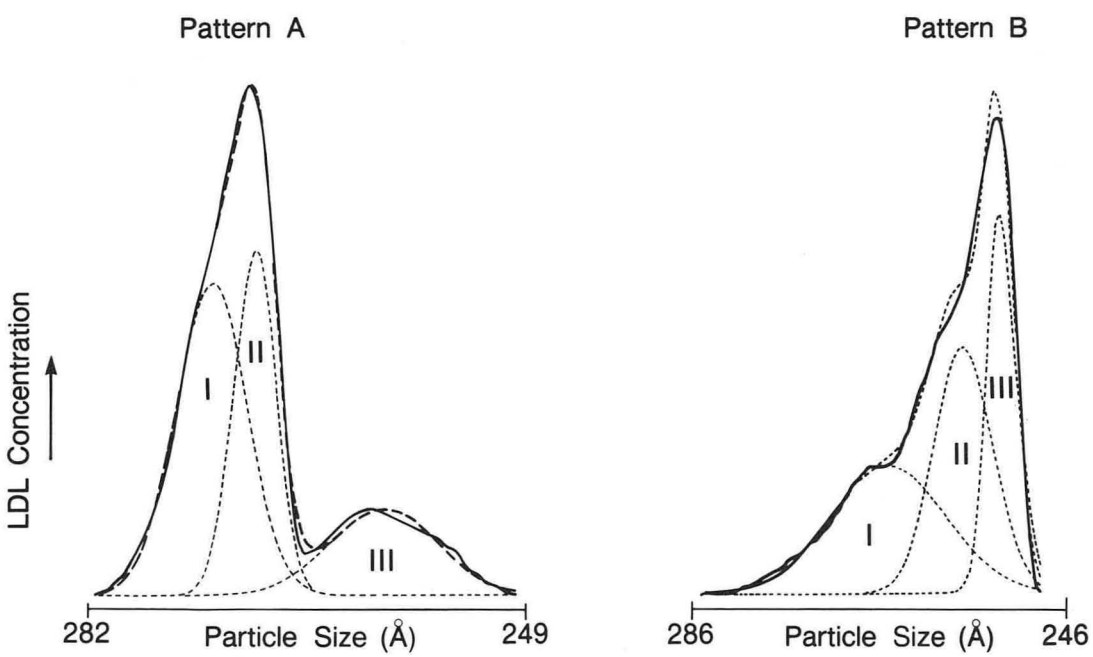

Fig. 1.12. *Low density lipoprotein subclass patterns A and B, as determined by gradient gel electrophoresis. The solid lines represent densitometric tracings of the gradient gel bands. The dotted lines were determined by mathematical modeling to facilitate identification of the LDL subclasses. Pattern A is characterized by a major peak of large LDL subclasses (LDL-I and II) and a minor peak of smaller LDL. In contrast, pattern B is characterized by a major peak of small LDL (LDL-III or IV), often with skewing of the curve to the left. (XBL 853-8233E)*

LDL IV particles, with skewing of the curve toward the larger particle diameters. LDL subclass pattern A is, in general, defined as an LDL subclass pattern with the major gradient gel peak at a particle diameter of 255 Å or greater, and skewing of the minor components of the curve to the right. Pattern B has the major peak at a particle diameter less than 255 Å, with skewing of the minor components of the curve to the left.

To test the hypothesis of genetic control of LDL subclasses in a healthy population, 200 healthy Mormon families are currently being recruited and screened for LDL subclass distribution. To date 29 large kindreds, including 61 nuclear families and 300 members, have been screened among the relatives in these families.

The distribution of pattern A and pattern B shows apparent sex, age, and hormonal effects. That is, only 17% of males under age 40 demonstrate LDL subclass pattern B, while more than 40% of the males over that age have pattern B. Among females, the highest prevalence of pattern B, 50%, was seen among postmenopausal women. Subjects with LDL subclass pattern B have higher mean triglyceride levels, lower HDL cholesterol levels, and higher apo B levels. These trends are seen despite the fact that these families are healthy and lipid values are generally within normal ranges.

Segregation analysis has been performed on these families using a mixed model incorporating both a major gene effect and a polygenic component. The best-fitting model included a major gene effect influencing LDL subclass pattern B with a dominant mode of inheritance, an allele frequency of 0.28 for the allele leading to LDL subclass pattern B, and a small but significant polygenic component. The observed segregation ratios for the 49 families with both parents screened and the expected ratios based on the above model are summarized in Table 1.1. Based on this sample, the allele leading to LDL subclass pattern B is present in a large proportion of the healthy population. If so, this trait may be a marker for genetic predisposition to lipid disorders, and possibly increased coronary heart disease risk.

A collaboration was conducted with the Boston Area Health Study that suggests that there is indeed a correlation between LDL pattern types and cardiovascular disease. In this case-control study, it was found that 54% of male subjects with myocardial infarction had pattern B. Subjects with pattern B also had elevated plasma triglyceride and apo B levels. LDL subclass pattern B is associated with a high-risk lipoprotein profile, i.e., higher triglycerides and apo B levels and lower HDL cholesterol. Future studies will probe the molecular basis for LDL patterns A and B. It is possible that genes coding for apo B structure include DNA polymorphisms that are associated with a given LDL pattern. Specific DNA restriction enzymes will be used to determine whether there are differences in restriction fragment length polymorphisms (RFLP) in DNA coding for apo B, and whether such RFLP's correlate wtih either pattern A or pattern B.

Table 1.1 Segregation ratios by parental mating type and age of offspring.

Parental mating		Number of matings	Number of offspring Age <40 pattern A	B
A×A	Observed	14	41	0
	Expected		41.0	0
A×B	Observed	27	66	28
	Expected		66.1	27.9
B×B	Observed	8	13	7
	Expected		10.9	9.1

Melissa A. Austin and Ronald M. Krauss.
Affiliate Member: Karen Vranizan.

EXPRESSION OF LIPOPROTEIN GENES BY LIVER CELLS

The human hepatoma line Hep G2 has been extensively used to study synthesis of HDL and LDL precursors; a major drawback with this line is its inability to secrete very low density lipoproteins (VLDL) under basal conditions. A major breakthrough in the past year was the identification of two other human hepatoma-derived cell lines that secrete precursor or nascent lipoproteins. One, Hep 3B, is able to produce VLDL in basal medium. The three lines presently under investigation are phenotypically distinct in their expression of apolipoproteins in defined medium as noted in Table 1.2.

Table 1.2 Expression of apolipoprotein in defined medium.

Cell line	Major apolipoprotein
Hep G2	B and AI
Hep 3B	B and AII
NPLC	E

An important observation in the past year is that Hep G2 apo AI is secreted primarily as a lipid-free form. This led to the hypothesis that HDL may be assembled extracellularly. Extracellular assembly was demonstrated by model incubations using Hep G2 lipid-free apo A and phospholipid. Such products were discoidal in shape and represent *in vitro* analogs for nascent HDL harvested from the culture medium. Nondenaturing gradient gel scans and complementary views of the electron microscopic structure of HDL-like complexes formed by incubation of Hep G2 lipid-free protein fraction with the phospholipid, dimyristoylphosphatidylcholine, are shown in Fig. 1.13. At a molar ratio of phospholipid to apo AI of 100:1, a complex 9.7 nm in size is formed that is similar to the intact lipoprotein isolated from the medium. A higher molar ratio, 300:1, results in the formation of even larger-sized complexes. The inference from such studies is that HDL may not necessarily be pre-assembled in the liver; rather some may be assembled extracellularly through interaction of lipid-free apo AI with membranes and/or other lipoproteins. This premise remains to be tested experimentally.

Another important observation made in the past year is that newly synthesized LDLs, i.e., those secreted by Hep G2 and Hep 3B cells, differ electrophoretically from plasma counterparts. Several possible factors contributing to the increased negative charge are that the carbohydrate moiety of the protein is different in newly secreted particles and/or that the apo B protein conformation may be different on nascent LDLs. Altered properties of the LDL surface may guarantee that the newly synthesized particles are not taken up by the cells that secrete them. The liver has numerous receptors that recognize LDLs (the LDL receptor or apo B-E receptor) subsequently leading to the

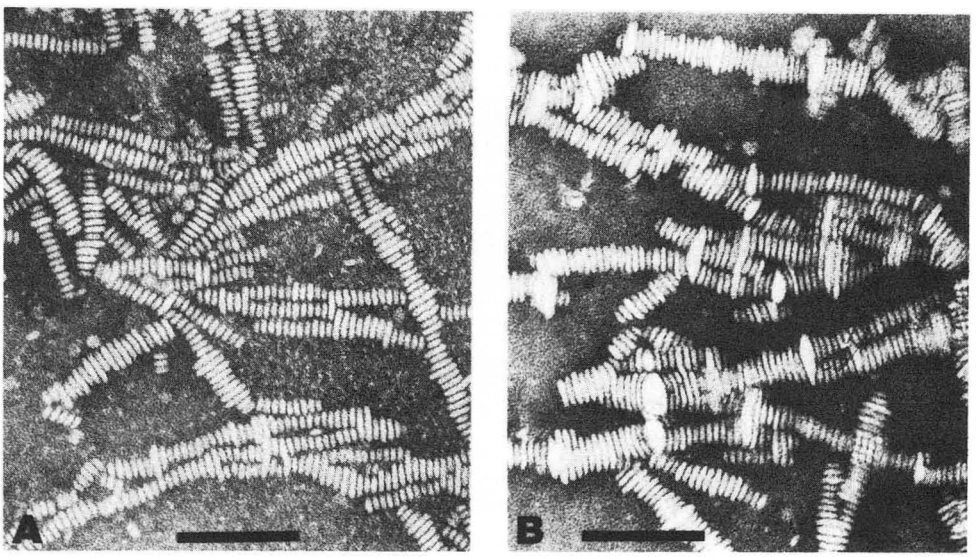

Fig. 1.13. *Electron micrographs of negatively stained complexes formed by incubation of Hep G2 lipid-free apoAI with the phospholized, dimyristoylphosphatidylcholine. (A) Phospholipid: protein molar ratio 100:1; (B) ratio 300:1. Bar represents 100 mm. (XBL 871-438)*

internalization and degradation of LDLs (Fig. 1.14). Newly synthesized LDL may not be recognized by the receptor by reason of altered conformation of the ligand. Clearly, two aspects of nascent LDLs are yet to be explored: 1) that the apo B protein is structurally different from circulating plasma LDLs that have probably undergone modification in the plasma, and 2) that nascent LDLs do not recognize normal LDL receptors. To assess apo B protein structure, future studies will utilize monoclonal antibodies that recognize specific apo B epitopes to determine whether there are differences between nascent and plasma apo B which could account for the observed difference in electrophoretic behavior. Ligand blotting techniques will be used to assess to what extent nascent LDLs bind to normal LDL receptors.

Melissa A. Austin, Ronald M. Krauss, Trudy M. Forte, and Michael La Belle. Affiliated Members: Alex Nichols, Mark R. McCall, Miguel Robinson, Karen Vranizan, and Virgie G. Shore (Lawrence Livermore Laboratory).

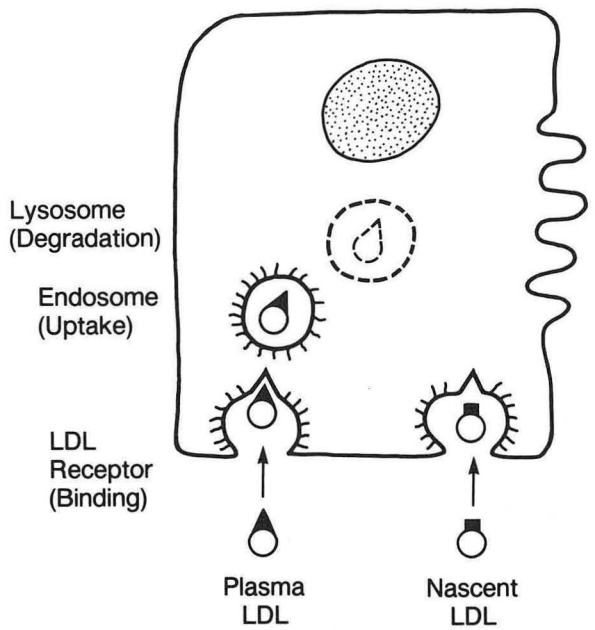

Fig. 1.14. *Schematic showing interaction of normal plasma LDL with the LDL receptor on cell surfaces. A possible scenario for nascent LDL is also shown; subtle changes on the surface of the particle may prevent its recognition of and binding to the LDL receptor. (XBL 8711-8007A)*

ATHEROSCLEROTIC PLAQUE PROTEINS

The objective this study was to use anion exchange and reverse-phase HPLC to provide new knowledge about the properties of plaque proteins and to determine whether different protein species are present in plaque harvested from two anatomical sites: the coronary artery and thoracic aorta. Protein extracts were characterized by anion exchange and reverse-phase HPLC and the integrated chromatographs revealed significant differences in both peak retention times and areas for protein species from coronary artery compared to thoracic aorta artery plaque. Coronary artery plaque proteins possessed a high degree of cationic charge and polarity compared to those present in thoracic aorta plaque and normal mammary artery. This suggests that specific protein makers may be expressed in plaque of different anatomical origin, and that the processing of protein may be distinct to plaque sites. In constrast, characterization of molecular weight by gel electrophoresis resolved no major differences between plaque types. These findings indicate that proteins in human plaque lesions of different anatomical origin can be resolved by HPLC methodology and that they exhibit different charge and polarity. Such an HPLC approach may prove useful in the quantitative identification and ultimate isolation of specific protein markers present in plaque during atherogenesis, and in the study of mechanisms of protein involvement in plaque formation.

Robert Liburdy.

PUBLICATIONS: Lipoprotein and Structural Biology

CONTRIBUTIONS TO JOURNALS

Abney, J.R., Braun, J., and Owicki, J.C. Lateral interactions among membrane proteins: implications for the organization of gap junctions. *Biophys. J. 52,* 441–454 (1987).

Austin, M.A., King, M.C., Bawol, R.D., Hulley, S., Friedman, and G.D. Risk factors for coronary heart disease in adult female twins: genetic heritability and environmental influences. *Amer. J. Epidemiol. 125,* 308–318 (1987).

Bastacky, J., Hook, G.R., Finch, G.L., Goerke, J., and Hayes, T.L. Low-temperature scanning electron microscopy of frozen hydrated mouse lung. *Scanning 9,* 57–70 (1987).

Braun, J., Abney, J.R., and Owicki, J.C. Lateral interactions among membrane proteins: valid estimates based on freeze-fracture electron microscopy. *Biophys. J. 52,* 427–439 (1987).

Bustamante, C., Maestre, M.F., and Wells, K.S. Recent advances in polarization spectroscopy: perspective of the extension to soft x-ray techniques. *Radiation Biophysics 44,* 331–341 (1986).

Carr, K.E., Hayes, T.L., Indran, M., Bastacky, S.J., McAlinden, G., Ellis, S., and Ainsworth, E.J. Morphological criteria for comparing effects of x-rays and neon ions on mouse small intestine. *Scanning Electron Microscopy 1,* 799–809 (1987).

Carr, K.E., Hayes, T.L., Watt, A., Bastacky, S.J., Klein, S., and Fife, M. Specimen handling and data interpretation in x-ray microanalysis of frozen hydrated etched gastrointestinal tract. *J. Electron Microscopy Technique 4,* 371–381 (1986).

Carr, K.E., Hayes, T.L., Watt, A., Klein, S., McKoon, M., Bastacky, S.J., and Ellis, S. Biological variation in cryomicroanalytic data from mouse small intestinal villi. *J. Elect. Microscopy Tech. 5,* 65–69 (1987).

Chiu, W., Downing, K.H., Dubochet, J., Glaeser, R.M., Heide, H.G., Knapek, E., Kopf, D.A., Lamvik, M.K., Lepault, J., Robertson, J.D., Zeitler, E., and Zemlin, F. Cryoprotection in electron microscopy. *J. Microscopy 141,* 385–391 (1986).

Downing, H. and Glaeser, R.M. Improvement in high resolution image quality of radiation-sensitive specimens achieved with reduced spot size of the electron beam. *Ultramicroscopy 20,* 269–278 (1986).

Finch, G.L., Bastacky, S.J., Hayes, T.L., and Fisher, G.L. Low-temperature scanning electron microscopy of particle-exposed mouse lung. *J. Microscopy 147,* 193–203 (1987).

Finch, G.L., Fisher, G.L., and Hayes, T.L. The pulmonary effects and clearance of intratracheally instilled Ni_3S_2 and TiO_2 in mice. *Environmental Research 42,* 83–93 (1987).

Forte, T.M., Nichols, A.V., Selmek-Halsey, J., Caylor, L., and Shore, V.G. Lipid-poor apolipoprotein A-I in Hep G2 cells: formation of lipid-rich particles by incubation with dimyristoylphosphatidylcholine. *Biochimica et Biophysica Acta 920,* 185–194 (1987).

Franceschini, G., Calabresi, L., Tosi, C., Sirtori, C.R., Fragiacomo, C., Noseda, G., Gong, E., Blanche, P., and Nichols, A.V. Apolipoprotein $A\text{-}I_{Milano}$: correlation between high density lipoprotein subclass distribution and triglyceridemia. *Arteriosclerosis 7,* 426–435 (1987).

Goldberg, I.J., Le, N.-A., Leeman, B., Brown, W.V., and Lindgren, F.T. Evidence for heterogeneity of low density lipoprotein metabolism in the cynomolgus monkey. *Biochim. Biophys. Acta 879*, 197–185 (1986).

Henderson, R., Baldwin, J.R., Downing, K.H., Lepault, J., and Zemlin, F. Structure of purple membrane from *Halobacterium halobrium*: Recording, measurement, and evaluation of electron micrographs at 3.5 Å resolution. *Ultramicroscopy 19*, 147–178 (1986).

Hook, G.R., Bastacky, J. Conhaim, R.L., Staub, N.C., and Hayes, T.L. A new method for pulmonary edema research: scanning electron microscopy of frozen-hydrated edematous lung. *Scanning, Vol. 9,* 71–79 (1987).

Hughes, T.E., Sasak, W.V., Ordovas, J.M., Forte, T.M., Lamon-Fava, S., and Schaefer, E.J. A novel cell line (Caco-2) for the study of intestinal lipoprotein synthesis. *J. Biol. Chem. 262*, 3763–3767 (1987).

Jaffe, J.S. and Glaeser, R.M. Difference Fourier analysis of "surface features" of bacteriorhodopsin using glucose embedded and frozen hydrated purple membrane. *Ultramicroscopy 83*, 17–28 (1987).

Krauss, R.M. Relationship of intermediate and low density lipoprotein subspecies to risk of coronary artery disease. *Amer. Heart Journal 113,* (No. 2, Part 2), 578–582 (1987).

Krauss, R.M. Effects of oral contraceptives on lipid metabolism. *J. Reprod. Med. 31 (Suppl. 6)*, 549–550 (1986).

Krauss, R.M., Lindgren, F.T., Williams, P.T., Kelsey, S.F., Brensike, J., Vranizan, K., Detre, K.M., and Levy, R.I. Intermediate density lipoproteins and coronary artery disease progression in hypercholesterolemic men. *Lancet ii (July 11, 1987),* 62–66 (1987).

Kwiterovich, P.O., Jr., White, S., Forte, T., Bachorik, P.S., Smith, H., and Sniderman, A. Hyperapobetalipoproteinemia in a kindred with familial combined hyperlipidemia and familial hypercholesterolemia. *Arteriosclerosis 7*, 211–215 (1987).

LaBelle, M. Computer-assisted collection and analysis of enzyme-linked immunosorbent assay data. *J. Immunol. Methods 102*, 251–258 (1987).

Lamon-Fava, S., Ordovas, J.M., Mandel, G., Forte, T.M., Goodman, R.H., and Schaefer, E.J. Secretion of apolipoprotein AI in lipoprotein particles following transfection of the human apolipoprotein AI gene into 3T3 cells. *J. Biol. Chem. 262*, 8944–8947 (1987).

Maestre, M.F. The effect of anisotropic properties of randomly oriented particles on polarized light: an operational calculus for spatially heterogenous distributions. *Biopolymers 26*, 1357–1379 (1987).

Mickols, W., Maestre, M.F., and Tinoco, I., Jr. Differential polarization microscopy of changes in structure in spermatocyte nuclei. *Nature 328*, 452–454 (1987).

Musliner, T.A., McVicker, K.M., Iosefa, J.F., and Krauss, R.M. Lipolysis products promote the formation of complexes of very low density and low density lipoproteins. *Biochim. Biophys. Acta 919*, 97–110 (1987).

Musliner, T.A., McVicker, K.M., Iosefa, J.F., and Krauss, R.M. Metabolism of intermediate and very low density lipoprotein subfractions from normal and dysbetalipoproteinemic plasma: *in vivo* studies in the rat. *Arteriosclerosis 7,* 408–420 (1987).

Nichols, A.V., Gong, E.L., Blanche, P.J., Forte, T.M., and Shore, V.G. Pathways in the formation of human plasma high density lipoprotein

subpopulations containing apolipoprotein A-1 without apolipoprotein A-11. *J. Lipid Research 28*, 719–732 (1987).

Palmer, R.H., Nichols, A.V., Dell, R.B., Ramakrishnan, R., Lindgren, F.T., Gong, E.L., Blum, C.B., and Goodman, D.S. Lack of relationship in humans of the parameters of body cholesterol metabolism with plasma levels of subfractions of HDL or LDL, or with ApoE isoform phenotype. *J. Lipid Res. 27,* 637–644 (1986).

Shore, V.G., Smith, M.E., Perret, V., and Laskaris, M.A. Alterations in plasma lipoproteins and apolipoproteins in experimental allergic encephalomyelitis. *J. Lipid Res. 28*, 119–129 (1987).

Stefanick, M.L., Williams, P.T., Krauss, R.M., Terry, R.B., Vranizan, K.M., and Wood, P.D. Relationships of plasma estradiol, testosterone and sex hormone-binding globulin with lipoproteins, apolipoproteins, and high density lipoprotein subfractions in men. *J. Clin. Endocrin. Metab. 64*, 723–729 (1987).

Tinoco, I., Jr., Mickols, W., Maestre, M.F., and Bustamante, C. Absorption, scattering, and imaging of biomolecular structures with polarized light. *Ann. Rev. Biophysics and Engineering 16*, 319–349 (1987).

Williams, P.T., Krauss, R.M., Kindel-Joyce, S., Dreon, D.M.,Vranizan, K.M., and Wood, P.D. Relationship of dietary fat, protein, cholesterol, and fiber intake to atherogenic lipoproteins in men. *Am. J. Clin. Nutr. 44*, 788–797 (1986).

CONTRIBUTIONS TO BOOKS AND PROCEEDINGS

Baldwin, J.M., Ceska, T.A., Glaeser, R.M., and Henderson, R. Structure analysis of bacteriorhodopsin by electron crystallography. Pages 101–115 in *Crystallography in Molecular Biology*, D. Monas, J. Drenth, B. Standberg, D. Suck, and K. Wilson, eds. Plenum Publ. Corp., New York (1987).

Bastacky, J. Review of G.F. Marshall, ed., "Laser Beam Scanning", Opto-Mechanical Devices, Systems, and Data Storage Optics. *Scanning 9*, 45 (1987).

Downing, K.H. Overcoming beam-induced specimen motion: a major advance in improving image contrast for organic specimens. Pages 6–9 in *Proceedings of the 45th Annual Meeting of the Electron Microscopy Society of America,* G.W. Bailey, ed. San Francisco Press, Inc., San Francisco, CA (1987).

Downing, K.H. and Glaeser, R.M. Effect of illumination spot size on high-resolution image contrast for radiation-sensitive specimens. Pages 35–36 in *Proceedings XII International EM Congress,* Kyoto, Japan (1986).

Finch, G.L., Hayes, T.L., Mossman, B.T., Chang, M.J.W., and Fisher, G.L. SEM of tracheal respiratory epithelium exposed *in vitro* to Ni_3S_2. Pages 391–393 in *Microbeam Analysis — 1986*, A.D. Romig, Jr. and W.F. Chambers, eds. San Francisco Press, Inc., (1986).

Glaeser, R.M. High resolution electron microscopy of radiation sensitive crystals. Pages 17–18 in *Proceedings XII International EM Congress*, Kyoto, Japan (1986).

Krauss, R.M. Physical heterogeneity of apolipoprotein B-containing lipoproteins. Pages 15–21 in *Proceedings of the Workshop on Lipoprotein Heterogeneity*, K. Lippel, ed. NIH Publication No. 87–2646 (September 1987).

Krauss, R.M. Lipids and lipoproteins in postmenopausal women. Pages 56–60 in *Postgraduate Medicine: A Special Report*, W.A. Peck and R.A. Lobo, eds. Custom Communications, New York, (1987).

Krauss, R.M. and Nichols, A.V. Metabolic interrelationships of HDL subclasses. Pages 17–27 in *Advances in Experimental Medicine and Biology, Volume 201: Lipoprotein Deficiency*

Syndromes, A. Angel and J. Frohlich, eds. Plenum Press, New York (1986).

Nichols, A.V., Gong, E.L., Blanche, P.J., Forte, T.M., and Shore, V.G. Origin and heterogeneity of HDL subspecies. Pages 331–340 in *Proceedings of the Workshop on Lipoprotein Heterogeneity,* K. Lippel, ed. NIH Publication No. 87–2646 (September 1987).

Norum, R.A., Forte, T.M., Alaupovic, P., and Ginsberg, H.N. Clinical syndrome and lipid metabolism in hederitary deficiency of apolipoproteins A-I and C-II, variant 1. Pages 137–149 in *Proceedings of Symposium on Lipoprotein Deficiency Syndromes,* A. Angel, ed., Plenum Press. (1986).

Perlman, J.A., Krauss, R.M., Ray, R., Russell-Briefel, R., Ezzati, T., and Lieberknect, G. Smoking, oral contraceptive use and other risk factors for atherosclerotic heart disease. Pages 27–35 in *Smoking and Reproductive Health,* M.J. Rosenberg, ed., PSG Publishers, Littleton, MA, (1987).

Section 2. Cell and Molecular Biology

These are exciting times for biology in general and for the cell and molecular biology effort at LBL in particular. The Cell and Molecular Biology Group was formed four years ago. Through its own activities and by its representation on the LBL Panel to Explore New Directions (PEND), it succeeded in an effort to foster a coordinated programmatic approach to research in life sciences at LBL. This effort has integrated ongoing research and is one of the driving forces behind attempts to initiate programs in hemopoiesis, in biotechnology and bioprocessing, and with the cooperation of the Chemical Biodynamics Division, in the Human Genome Center. The activity of the Group was part of the impetus for reorganization and formation of the Cell and Molecular Biology Division that took effect in January 1988, implementing a recommendation of the LBL Life Sciences Task Force. During FY 1987, an important consolidation was the integration of hemopoietic research into other efforts in cell and molecular biology and differentiation. Formation of the Cell and Molecular Biology Division consolidates and integrates programs in atherogenesis, macromolecular structure, and radiation biology with the historic four subgroups, DNA repair, DNA replication and recombination, carcinogenesis, and differentiation. These investigators will all continue to interact and produce pioneering research.

The following summary of research activities outlines the major scientific goals and recent achievements of the Group and shows the direction of future studies.

ACTIVITIES OF THE CELL AND MOLECULAR BIOLOGY GROUP

	Scientists	*Technical Staff and Graduate Students*
Carcinogenesis		
Generation of active species	M. Alhadeff	L.G. Hayashi
Mixed function oxidase	J.C. Bartley	C. Hatier
Arachindonate cascade	M.J. Bissell	M.M. Hosobuchi
Characterization of damage to DNA	R. Goth-Goldstein	A.C. Pang
Alkylation products	A.R. Howlett	M. Sieweke
Bulky adducts	S.A. Leadon	
Oxidative damage	B. Singer	
Induction of transformation	S.J. Spengler	
Characterization of stages, target population, cellular substrates	M.R. Stampfer	
Development of selective and quantitative assays for human epithelial cells	A.W. Stoker	
Role of viral and cellular oncogenes	A.N. Tischler	
Factors involved in promotion and progression		
Active oxygen/inflammatory response		
Cell agonists and antagonists		
Cell-cell and cell-stromal interactions		

Continued on following page

	Scientists	*Technical Staff and Graduate Students*
Differentiation		
Regulation of normal differentiation and development cell types	M. H. Barcellos-Hoff	L-H. Chen
Mammary epithelial cells (rodent and human)	J.C. Bartley	B.L. Cullen
Fibroblasts	J.C. Beck	D.J. DeManicor
Hemopoietic cells	M.J. Bissell	U.N. Dinh
Factors	G. Brecher	D.E. Erkenbrack
Hormonal, extracellular matrix	G.K. Clemons	B.R. Kullgren
Relationship between normal gene and expression and carcinogenesis	K.L. Miller	G.A. Levine
	G. Parry	L.Moss
	D.E. Prosen	L.J. Mahlmann
	R.I. Schwarz	S.S. Neben
	P.H. Silverman	T.G. Ram
	M.R. Stampfer	J.S. Scherer
	J.D. Stubbs	K.R. Zettl
DNA Replication and Recombination		
Analysis of molecular mechanisms of recombinational events	J.T. Brown	M.Aker
Coordinate control of DNA replication and recombination	P.K. Cooper	M. Bell
Characterization of multiprotein-DNA replication and Recombination complexes	M.S. Espositio	Q.E. Gipson
Protein-protein and protein-DNA interactions	J.C. Game	J.A. Kans
In vitro and *in vivo* model plasmidic systems	J. Hosoda	T.J. McKey
Physical monitoring of chromosomal recombination	R.K. Mortimer	H.W. Moise
Purification and characterization of proteins involved in recombination	N.L. Rudin	
Maintenance of genomic integrity during recombination	D. Schild	
Effects of DNA damage on replication		
Repair of Induced DNA Damage		
Characterization of inducible networks repairing DNA Damage	P.K. Cooper	F. Chavez
Repair of DNA damage in specific sequences or at specific sites	M.S. Esposito	S.L. Gee
Transcribed and nontranscribed sequences analysis of importance of excision repair at or near growing forks	J.C. Game	M.K. Hughes
Influence of DNA-protein interactions	R. Goth-Goldstein	C.B. Kinglsey
Use of model substrates and purified polymerases to examine coding properties of DNA containing defined lesions	J. Hosoda	D.A. Lawrence
Isolation and molecular characterization of genes involved in cellular responses to DNA damage	S.A. Leadon	
	L.S. Miller	
	R.K. Mortimer	
	D. Schild	
	B. Singer	
	S.J. Spengler	

Molecular and Genetic Studies of DNA Damage and Repair

The DNA of living cells is continuously subject to damage, both from endogenous events within the cell and from a variety of exogenous environmental agents to which humans are routinely exposed, ranging from ordinary sunlight to naturally occurring carcinogens present in foods. Organisms at all levels of complexity have evolved an elaborate array of enzymatic mechanisms to maintain the integrity of their genetic material, and the mutagenic or cytotoxic consequences of any particular lesion in DNA will depend in large part on the nature and timing of the cellular processing of that lesion and on the interaction of repair processes with other aspects of DNA metabolism such as replication, recombination, and transcription. The broad objectives of our DNA repair studies are to understand the biochemical and molecular basis for the processing of damaged DNA and the genetic control of repair processes (also described in the section on DNA Replication and Recombination). Individual research groups approach these questions using a variety of systems ranging from purified enzymes *in vitro* to *in vivo* studies employing phage, bacteria, yeast, rodent and primate cell lines, established human cell lines, and primary cultures of human cells.

MOLECULAR MECHANISMS OF DNA DAMAGE BY CARCINOGENS

Mono- and Bifunctional Aldehydes

The biochemistry of mono- and bifunctional aldehydes is being studied *in vitro* to provide accurate and well defined conditions permitting the isolation and identification of metabolic products. The aldehydes arise both from environmental carcinogens, such as vinyl chloride, as well as metabolic processing of natural substrates. Monofunctional aldehydes are being used to study the initial reaction with nucleosides and the further reaction between these products and other molecules present in the cell. Bifunctional aldehydes can form DNA derivatives that contain an additional ring on the base. This ring destroys at least one base-pairing site in the nucleoside and distorts DNA structure to varying degrees. The mutagenic efficiencies of these etheno derivatives have been determined by measuring the levels of errors introduced following replication *in vitro* with a variety of polymerases. High mutagenic efficiency coupled with small amounts of physical distortion of the DNA helix may be the hallmark of a derivative, such as N^2,3-ethenoguanosine, that is likely to be an initiator of carcinogenesis (Fig. 2.1). Bifunctional aldehydes can also form interstrand crosslinks in DNA. Although the extent of formation of this type of damage may be low, the biological consequences are likely to be severe. Thus, *in vitro* studies are being extended to measuring the extent of crosslinks formed in DNA in animals exposed to vinyl chloride by inhalation, the normal route of human exposure.

Bea Singer and Sylvia Spengler.

N-nitroso Alkylating Agents

The reaction products of another class of ubiquitous carcinogens, N-nitroso alkylating agents, have been well characterized. The biological consequences of this damage involve both mutation and cell killing. Mutagenicity has been associated most frequently with alkylation of exocyclic oxygens of both purines and pyrimidines. Mammalian cells and *E.coli* have similar enzymes to repair alkylation damage. N-alkyl-purines are removed by N-glycosylases while O^6-alkylguanine (the principle lesion responsible for the carcinogenicity and mutagenicity of alkylating agents) is repaired by a rather unique mechanism. A small protein, O^6-alkylguanine alkyltransferase (MT), directly transfers the alkyl group in a stoichiometric manner to a cysteine residue on the protein, resulting in suicide inactivation of the protein. Both the MT and N-glycosylase activities can be measured in crude cell extracts using *in vitro* alkylated DNA as a substrate. There is evidence that the common baker's yeast *Saccharomyces cerevisiae* might differ from *E.coli* and mammalian cells in the repair of alkylation damage. No MT

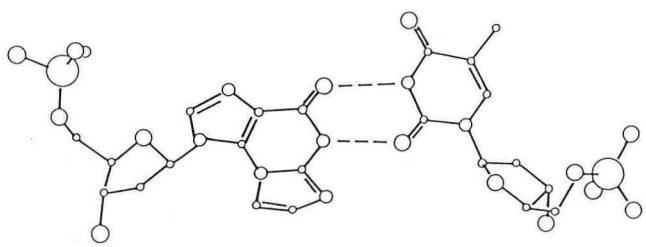

Fig. 2.1. *N^2,3-ethenoguanosine can form two hydrogen bonds with thymidine. The mutgenic base pair does not distort the helix significantly, and the additional etheno ring can be accommodated in the groove. (XBL 881-7237)*

activity or N-glycosylase activity can be detected in extracts from yeast cells. However, using a radioactively labeled alkylating agent, it was found that methylated purines and O^6–methylguanine are lost from the yeast DNA relatively rapidly and therefore, are presumably repaired. DNA repair mutants of yeast, described later in this report, will be used to determine whether alkylated bases are repaired by a different repair system in yeast.

It is less well understood which alkylated DNA bases cause cell death. In *E.coli*, 3-methyl purines could be identified as lethal lesions. However, in mammalian cells no specific lesion has been implicated in alkylating-agent-induced cell death. The identification of such lethal lesions has been attempted by two approaches: 1) comparison of the cytotoxic effects of alkylating agents which form different spectra of alkylated bases, and 2) comparison of DNA repair in alkylating agent sensitive and resistant cell variants. Neither approach was successful in identifying a specific lethal lesion. Rather, there seem to be several alkylated bases that can contribute to cell death and as yet unidentified factors that modify the cytotoxic effect of specific DNA alterations. Since the alkylating agent resistant cells apparently do not differ from sensitive cells in repair of methylated DNA bases, other cellular responses to alkylation damage were investigated. It was found that following treatment with N-methyl-N'-nitro-N-nitroso-guanidine, intracellular levels of diadenosine tetraphosphate (Ap4A) are elevated to a greater extent in resistant than sensitive cells. Since cellular Ap4A levels are increased in response to various environmental stressors, they might trigger a cellular mechanism that increases cellular survival. This mechanism apparently does not function as efficiently in a number of tumor-derived cell strains characterized by hypersensitivity to the cytotoxic effects of alkylating agents and by lack of repair of O^6-methylguanine.

Regine Goth-Goldstein and Mildred Hughes.

PROCESSING OF LESIONS IN THE VICINITY OF REPLICATION FORKS

The mutagenic or lethal consequences of any particular lesion in DNA depend on cellular processing of that lesion, often by responses that are induced by the damage itself. A damage-inducible repair process in *E.coli*, long patch excision repair, has been shown to be of general importance in resistance to lethal and replication-blocking effects of DNA damage. Results from a variety of experiments have suggested that the inducible process is required for repair of lesions near DNA replication forks, where structural constraints might hinder constitutive excision repair. Our recently developed technique for resolving DNA fragments containing replication forks from linear DNA fragments by two-dimensional agarose gel electrophoresis has been used to detect the replication of a specific gene in a synchronously dividing culture. Determinations of the timing of replication of a gene near the origin of replication (*polA*) was made by hybridization of a cloned probe to slot blots of CsCl density gradient fractions of DNA prepared from samples taken at various times after initiation of replication in bromouracil. Parallel samples of purified DNA were digested with a restriction endonuclease, analyzed in the two-dimensional electrophoresis system, blotted to nitrocellulose by capillary transfer under neutral conditions, and hybridized with the probe DNA. Hybridization in the position of replicating DNA (the minor arc) was detected at the time predicted by the CsCl gradient results. The two-dimensional gel electrophoresis system and the ability to detect the replication of specific genes will allow the investigation of human genetic repair deficiency diseases such as the variant form of xeroderma pigmentosum and ataxia telangiectasia, both of which may have a defect in the processing of lesions in the vicinity of replication forks. In addition, this system will be used to determine whether the integration of transfected plasmid DNA into the mammalian genome takes place via replicative intermediates.

Priscilla Cooper and Sherry Gee.

EFFICIENCY OF REPAIR AND TRANSCRIPTIONAL ACTIVITY

The analysis of DNA repair in eukaryotic cells is complicated by the various levels of DNA condensation in chromatin structure and by the complexity of the multiple tandem replication units. An increasingly important aspect of DNA damage and excision repair is whether all sequences in the eukaryotic genome are affected by damage to the same extent. The repair of uv damage in the human metallothionein (MT) gene family is being studied using an immunological method that isolates DNA fragments containing bromouracil in repair patches by means of a monoclonal antibody that recognizes bromouracil. The presence of the MT genes in the repaired and unrepaired DNA

fragments can be detected by using a cDNA probe for the genes. Repair in four members of this gene family was measured: the expressed MT-IA and MT-IIA genes, the MT-IB gene whose expression is tissue specific, and the non-expressed MT-IIB pseudogene. Ultraviolet damage was repaired at least twice as fast in the transcribed MT-IA and MT-IIA genes than in the genome overall. Repair in the MT-IB and MT-IIB genes was about the same as in the rest of the genome. When the expression of the MT-IB and MT-IIB genes is increased 15- to 20-fold by incubation of the cell cultures with cadmium, the rate of repair in these genes was 4- to 5-fold faster than in the genome overall (Fig. 2.2). The rate of repair in the MT-IB and MT-IIB genes, whose expression cannot be induced by cadmium, remained about the same as in the rest of the genome. These results indicate that the efficiency of repair of DNA damage in a particular sequence is influenced by the transcriptional activity of that sequence.

Steven A. Leadon and Margaret M. Snowden.

OXIDATIVE DAMAGE AND DIRECT ADDUCT FORMATION IN CARCINOGENESIS

There is increasing evidence implicating the involvement of free radicals, particularly those derived form molecular oxygen, in many stages of chemical carcinogenesis. The production and repair of two types of DNA damage, direct benzo(a)pyrene adducts and indirect oxidative damage, produced during the metabolic activation of the carcinogen benzo(a)pyrene by human mammary epithelial cells, have been examined. Thymine glycols, one type of oxidative DNA damage, were detected using a monoclonal antibody specific to this base modification (Fig. 2.3). The number of thymine glycols formed in the DNA was similar to that of benzo(a)pyrene-DNA adducts. Since thymine glycols represent only a portion of the oxidative damage possibly produced, these results indicate that the total amount of oxidative damage induced by exposure of human mammary epithelial cells to benzo(a)pyrene greatly exceeds the amount of direct adduct formation and that complete carcinogens such as benzo(a)pyrene may exert their biological effects by both direct DNA binding and the production of indirect damage.

Jack.Bartley, Steven A. Leadon, and Martha Stampfer.

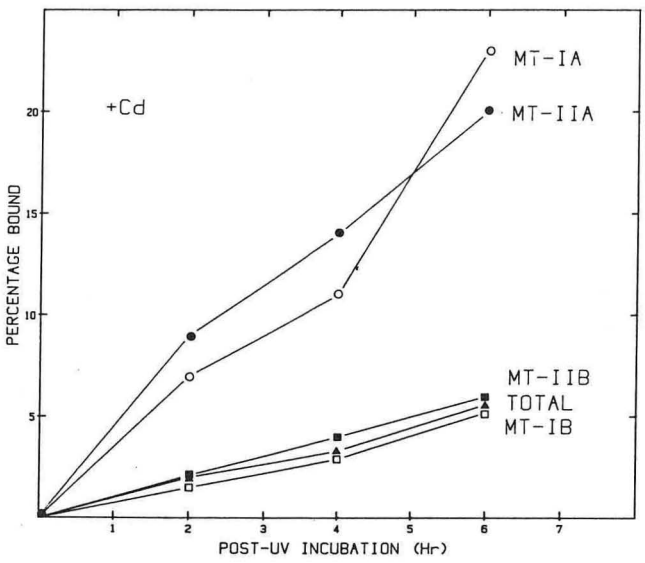

Fig. 2.2. *Repair of uv damage in the metallothionein IA and IIA genes, under conditions where their transcriptional activity is induced, is 4- to 5-fold faster than in the genome overall. The rate of repair in the metallothionein IB and IIB genes, whose expression cannot be induced, is about the same as in the rest of the genome. (XBL 881-7238)*

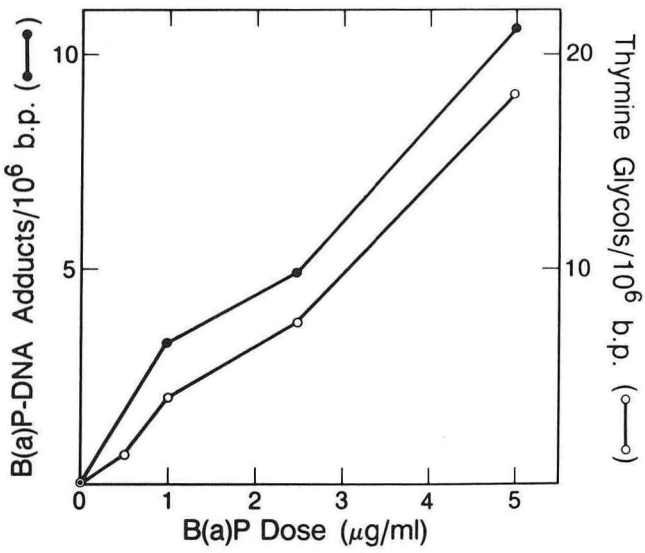

Fig. 2.3. *Benzo(a)pyrene produces both direct DNA adducts and thymine glycol. Human mammary epithelial cells were exposed to [^{3}H]-benzo(a)pyrene and the DNA isolated. Benzo(a)pyrene-DNA adducts (•–•) were determined from the specific activity of the DNA. Thymine glycols (o–o) were determined from competitive immunoassays with a monoclonal antibody to thymine glycol. (XBL 881-7239)*

DNA Replication and Recombination

INTRODUCTION

An understanding of the mechanisms of DNA replication and recombination is a fundamental prerequisite to studies of the role of genomic changes in normal development and disease states. The molecular and biochemical studies of genes and proteins required for DNA replication, repair, and recombination complement the studies of DNA repair and carcinogenesis described above. The focus of one program is to characterize the activities, DNA-protein, and protein-protein interactions of bacteriophage T4 gene products that function as an integrated replication-repair-recombination multiprotein complex during the T4 life cycle. A related research goal is to identify the biological roles of spontaneous mitotic recombination in *Saccharomyces cerevisiae* and to identify and characterize *REC* genes and proteins comprising the partial reactions of mitotic and meiotic recombination. Several investigators are conducting a comprehensive study of *RAD50-57* family of yeast genes involved in repair of double strand breaks, recombination, homothallic mating type switching, chromosome disjunction, and meiosis.

POSTREPLICATION RECOMBINATIONAL REPAIR

The major genes encoding proteins involved in postreplication recombinational repair (PRR) of bacteriophage T4 have been identified in previous studies and provide an opportunity to examine the DNA-protein and protein-protein interactions of gene 32 protein (gp32), a helix destabilizing protein; the uvsX gene product, a RecA-like protein; and the product of genes 46 and 47 (gp46 and gp47), a putative exonuclease.

Functional Domains of gp32

Previous studies employing limited proteolysis products and an *in vitro* DNA replication system provided support for the model that gp32 consists of three functional domains and that the carboxy terminal A-domain not only participates in DNA replication, recombination, and PRR activities, but also controls the the properties of replication-repair-recombination multiprotein complexes through direct protein interactions. Recent studies have been focused on the structural and functional roles of Zn(II) and "Zn-finger" sequence located in the central domain of gp32.

The "zinc-finger" emerged in the last few years as a novel protein motif for nucleic acid recognition and binding. Although it was originally discovered in repeated tandems in the Xenopus transcription factor IIIA(TFIIIA), similar sequences have been found widespread throughout many different organisms–from human cells to bacterial viruses. They are present within the structure of a large number of regulatory proteins and seem to serve as modules for the building up of specific nucleic acid binding domains.

Our preliminary studies indicate that many Zn-suppressible gene 32 mutations induce conformational changes that make the normally protease resistant central domain susceptible to proteases. Such conformational changes have been analyzed by limited proteolysis of crude lysates from mutant infected cells, followed by Western-blot detection of the proteolysis products. These findings demonstrate that Zn(II) is essential for stability of the protein and that mutations within the zinc-finger alter the conformation of that portion of the molecule where the terminal domain A connects to the central core (the hinge of the A domain). The functional significance of relationships between the zinc-finger and the terminal domains is currently being investigated.

Purification of gp46/gp47

Properties of temperature sensitive and amber nonsense mutants of genes 46 and 47 provide evidence that they encode an exonuclease activity that expands single strand nicks into gaps, an activity required for biparental recombination and production of concatenated DNA, a precursor of mature bacteriophage. Purification of gp46/47 to near homogeneity has been achieved, as shown in the SDS-gel picture (Fig. 2.4). The gp46/47 preparation contains a nuclease activity that converts both double-stranded and single-stranded T4 DNA to acid soluble material. Purification of the gp46/47 protein from temperature sensitive mutants is in progress. The purified proteins from the wild-type and mutants will provide direct evidence of the catalytic role of gp46/47, its involvement with other proteins such as gp32 and uvsX, and its role in DNA strand exchange, DNA unwinding, DNA annealing, and branch migration. In collaboration

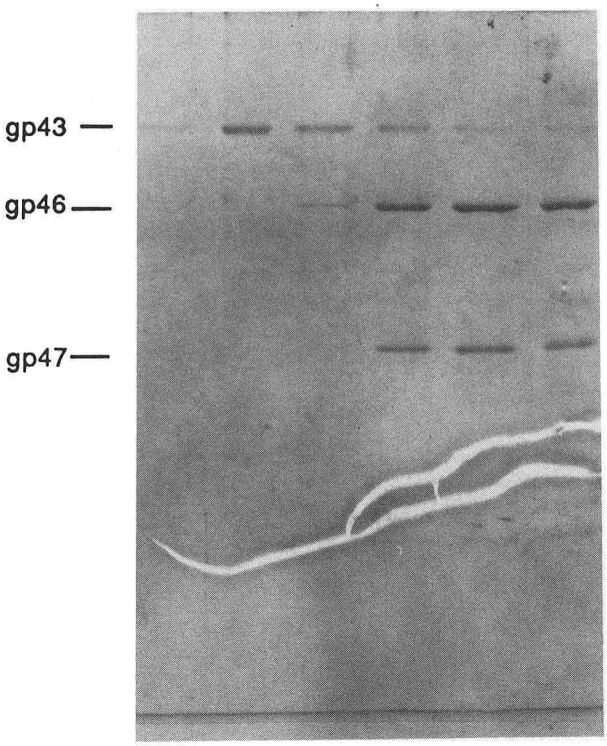

Fig. 2.4. 1D-PAGE of DEAE-cellulose column fractions containing T4, gp46, and gp47. (XBB 882-887)

with Michael S. Esposito, differential DNA affinity chromatograpy and *in vitro* assay methods developed for T4 studies are being adapted to characterize analogous proteins of *Saccharomyces cerevisiae* and *rec* mutants. This approach is particularly appropriate since the yeast *RAD52* gene (also known as *REC2*) complements gp46/47 mutations of bacteriophage T4 *in vivo*.

Junko Hosoda, Herbert Moise, and Ellen Sisk.

MITOTIC RECOMBINATION AND DNA REPAIR

Previous studies demonstrated that interhomolog mitotic recombination of *Saccharomyces cerevisiae* differs from meiotic recombination with respect to the time of initiation of recombination relative to chromosomal replication, the lengths of conversion tracts, mismatch repair modalities, the relative frequencies of Holliday structure intermediates containing asymmetric or symmetric heteroduplex DNA, and reciprocality of intergenic recombination. A broad spectrum of hyporecombination and hyperecombination mutants affecting spontaneous mitotic single site gene conversion, intragenic recombination, intergenic recombination, and genomic stability were isolated to attempt to understand the differences between spontaneous mitotic and meiotic recombination and to test the predictions of current molecular models of chromosomal recombination.

Isolation of REC Gene Mutants

An N+1 hyperhaploid strain disomic for chromosome VII (LBL1) was employed for direct isolation of *rec* mutants affecting spontaneous recombinational events and chromosomal segregation. Heterozygous and heteroallelic markers on chromosome VII permit simultaneous monitoring of recombination in several genetic intervals and detection of dominant and recessive *rec* mutations induced in the remainder of the genome. Spontaneous mitotic recombinational proficiency *per se* was used to identify ultraviolet-light-induced *rec* mutants of novel *REC* loci comprising five phenotypic classes: 1) conversion negative, intergenic recombination negative; 2) conversion positive, intergenic recombination negative; 3) conversion negative, intergenic recombination positive; 4) conversion positive, intergenic recombination elevated; and 5) conversion elevated, intergenic recombination elevated. Several *rec* mutations affect *in vitro* plasmidic recombination and exhibit meiotic defects when *rec/rec* diploids are exposed to meiosis inducing sporulation medium (Table 2.1).

Characterization of the REC1 *Gene and Protein*

Ongoing research focuses upon cloning and sequencing of the *REC1* gene and isolation of the *REC1* gene product since it is required for all modes of mitotic recombination, chromosomal stability and meiosis (Table 2.2). Since the *rec1*-1 mutation is defective for *in vitro* plasmidic recombination the *REC1* protein will be isolated by *in vitro* complementation. The amino acid sequence of the purified protein will be determined and compared to the amino acid sequence inferred from DNA sequencing of the cloned structural gene to provide confirmation that the correct protein has been purified. The purified protein will be tested for strand transfer activity, exo- and endodeoxyribonuclease activities, and ability to cleave Holliday junctions using protocols developed in collaboration with Junko Hosoda.

Michael S. Esposito, John Brown, Norah Rudin, and Greg Delory.

Table 2.1 Mitotic recombination mutants isolated following ultraviolet light mutagenesis of LBL1.

Phenotypic groups	Average spontaneous mitotic recombination frequencies		
	No. mutants obtained	Cyh^r conversions/ 10^6 cells	Cyh^r intergenic recombinations/ 10^6 cells
I. $Conv^-$ Inter. $Exch^-$	13	1.5	0.8
II. $Conv.^+$ Inter. $Exch.^-$	24	22.8	0.8
III. $Conv.^+$ Inter. $Exch.^{+++}$	13	15.3	121.9
IV. $Conv.^-$ Inter. $Exch.^+$	1	0.8	19.7
V. $Conv.^{+++}$ Inter. $Exch.^{+++}$	3	94.7	1006.4
Control LBL1 (25 colonies)		19.4	29.1

Table 2.2 Properties of four REC gene mutants.

Mutants	rec1	rec2 rad52	rec3	rec46
Mitotic gene conversion	–	–	+	+++
Mitotic intergenic recomb.	–	+	–	+++
Mitotic chromosomal stability	–	–	–	–––
Meiosis of rec/rec diploid	–	–	–	–

RECOMBINATIONAL REPAIR MEDIATED BY *RAD* GENES

The radiation sensitive mutants of *Saccharomyces cerevisiae* are a valuable genetic resource for studying repair in a eukaryote. The main focus of research is to understand the roles played by the *RAD50* to *RAD57* genes in recombinational repair and in mitotic and meiotic recombination. Some important genes, such as *RAD50* and *RAD52* have already been extensively studied. Others such as *RAD24, RAD51, RAD54, RAD55,* and *RAD57* remain to be characterized. Several *RAD* genes have been cloned and sequenced (e.g., *RAD 51, RAD52,* and *RAD54*) providing reagents to characterize the transcriptional control of these genes and whether regions 5' to them bind regulatory proteins.

Transcriptional Regulation

Recent studies of *RAD54* demonstrate that this gene is inducible approximately 3- to 5-fold by x rays, ultraviolet light, and methyl-methane sulfonate, but not by heat shock. Regions 5' to the *RAD54* gene are involved in its regulation. Deletion analysis is being employed to identify the exact sequences involved in regulation both in mitotic and meiotic cells and to determine whether this gene is under positive or negative transcriptional control. A similar analysis of the *RAD51* gene will reveal whether this gene is similarly regulated and whether *RAD51* and *RAD54* are coordinately regulated.

Using *lacZ* fusions of both the *RAD52* and *RAD54* genes, evidence has been obtained that these genes are induced in diploids during meiosis during the period of meiotic recombination. No induction was observed when haploid cells, incapable of meiosis, were incubated in sporulation medium. Preliminary studies indicate that induction of RAD52 and RAD54 is blocked in *rad50*-1 mutant diploids, known to arrest after premeiotic DNA synthesis and before the onset of meiotic recombination.

Characterization of Primary Gene Products

RAD51 and *RAD54* have been sequenced and the sequencing of *RAD55* and *RAD57* is in progress. These data are employed to infer the amino acid sequence of the encoded proteins. *RAD51, RAD54* and *RAD55* have been placed under the control of yeast ADH1 and GAL1 promoters and protein gels are being employed to identify the *RAD* proteins. *RAD* genes are also being overexpressed in *E.coli* as fusion proteins, which will be isolated to produce antibodies for further protein purification. Purified *RAD* proteins will be tested for various enzymatic activities such as ATPase, nuclease and DNA binding activities.

Visualization of Recombination and Recombinational Repair by Pulsed Field Gel Electrophoresis

Pulsed field gel electrophoresis allows DNA molecules the size of yeast chromosomes to be resolved on gels. One form of this technique, orthogonal field alternation gel electrophoresis, OFAGE, has been used to study double strand breaks and repair of linear chromosomes. A novel system has also been developed to detect double strand breaks, inter-homolog recombination, and sister chromatid exchange (SCE) on OFAGE gels. The technique employs a circular derivative of chromosome III. Recombination between this circular chromosome and its linear homolog is topologically equivalent to integration of the circle into the linear molecule. Thus, molecules of a new size class are generated that are detected on OFAGE gels by Southern hybridization. Similarly, SCE between two sister circles generates a new type of molecule, a double circle. The double circle does enter gels until it is linearized by introduction of a double strand break by x-ray exposure. These techniques provide methods to examine repair of linear chromosomes, recombination between homologs, recombination between sister chromatids and the effects of *RAD* gene mutations upon repair of DNA damage and the normal progress of meiosis.

The novel technique for detection of SCE exchange represents a significant advance over methods that detect only unequal SCE events. The circle by circle exchanges detect all SCE events and the *rad50*-1 mutant blocks meiotic SCE. The OFAGE technique further demonstrates that there is a low but detectable number of double strand DNA breaks during meiosis and that there is a two-hour delay between commitment to genetic recombination and actual recovery of physically recombined molecules.

Robert K. Mortimer, John Game, David Schild, and Rebecca Contopoulou.

Differentiation

Understanding how cells precisely regulate tissue-specific function in response to signals from their environment is a fundamental problem in modern biology. In the Cell and Molecular Biology Group, an understanding of this complex problem is sought from three distinct but complementary systems. Mammary cells of epithelial origin are studied as a model of cells with polarized secretion, hormonally regulated gene expression, and great sensitivity to external environment. Tendon cells, archetypal fibroblasts producing very high levels of collagen, are an ideal model for determining molecular mechanisms controlling the production of an extracellular matrix protein. Hemopoiesis encompasses a series of distinct cell lineages leading to the various circulating blood cells derived from a common pluripotent stem cell. Hemopoiesis throughout the life of the organism is a model for many of the critical processes that take place during embryogenesis such as determination and maturation.

MAMMARY CELLS AS A MODEL FOR STUDIES OF GENE EXPRESSION AND POLARIZED SECRETION

Cell-ECM Interaction and Gene Expression

Study of the regulation of gene expression in cultured cells, particularly in epithelial cells, has been both hampered and facilitated by the loss of function that accompanies culture on traditional plastic substrata. However, with the recognition that the unit of function in higher organisms is larger than the cell itself and that gene expression is dependent upon cell interactions with hormones, substrata, and other cells, came the understanding that the epithelial cell is stimulated by its extracellular environment to express its phenotype. In the last decade epithelial cell research has centered on studies of functional differentiation with very promising and important results. Using cultured mammary epithelial cells as a primary model of these interactions, a framework has been delineated in which gene expression may be studied based on three premises:

1) That the unit of function in higher organisms includes the cell and its extracellular environment.

2) That the extracellular matrix (ECM) on which the cells sit is an extension of the cells and an active participant in regulation of their function, i.e., that the ECM is an "informational" entity in the sense that it receives, imparts, and integrates structural and functional signals.

3) The ECM-induced functional differentiation in the mammary gland is mediated through changes in cell shape, i.e., that the structure is a large part of the message to maintain differentiated gene expression.

Based on these tenets and the data generated at LBL, several years ago a model of "dynamic reciprocity" was proposed wherein the ECM is postulated to exert an influence on gene expression via transmembrane proteins and cytoskeletal components. The cytoskeleton, in turn, through its association with polyribosomes may affect mRNA stability and rates of protein synthesis, and through its interactions with the nuclear matrix may affect mRNA processing and, possibly, rates of transcription.

The study of mammary gland epithelial cell biology has addressed the role of the ECM in controlling the expression of tissue specific function by measuring the expression of milk proteins, both at the level of mRNA synthesis and protein secretion. Extension of previous studies led to the identification of transferrin (Tf) as a major mouse milk protein for which a cDNA has also been isolated and characterized. *In vivo* mammary Tf protein and mRNA levels are dramatically increased by pregnancy and lactation, during which time they are comparable to those found in liver (Fig. 2.5). In culture, the steady-state Tf mRNA and protein levels are relatively insensitive to lactogenic hormones compared to those of β-casein. However, mRNAs of both milk proteins' expression are markedly increased in cells cultured on basement membrane over those cultured on plastic (Fig. 2.6). It is therefore postulated that changes in the basement membrane composition that occur *in vivo* play a role in regulation of transferrin and possibly other milk proteins.

In the past year, the form and function of mammary epithelial cells cultured on a substratum of reconstituted basement membrane prepared from EHS tumors (Engelbreth-Holm-Swarm) have been characterized. In comparison to cells cultured on plastic, and even to those cultured on floating collagen gels, EHS elicits a dramatic increase in tissue-specific function. β-casein mRNA was shown to increase 70-fold in cells cultured on EHS atop a floating collagen gel. Cells on EHS are characterized by a unique three-dimensional organization into matrix-adherent spheres surrounded by a

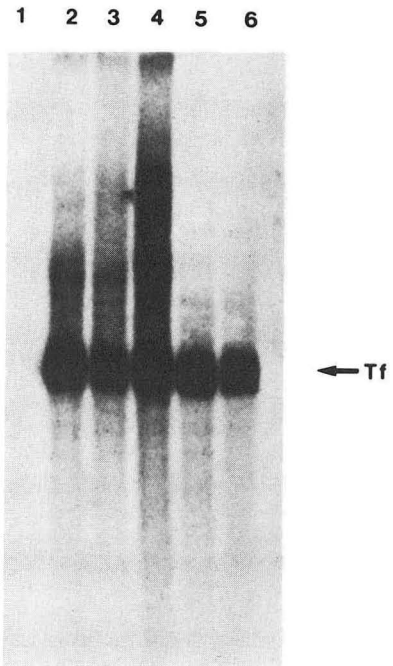

Fig. 2.5. The identification of mammary gland transferrin (Tf) mRNA and its modulation by pregnancy and lactation. Total cellular RNA (10 μg) was extracted from mammary glands of virgin (lanes 1 and 2), pregnant (lanes 3 and 4), and lactating (lanes 5 and 6) mice. The RNAs from mammary glands (lanes 1, 3, and 5) and from liver (lanes 2, 4, and 6) were separated on formaldehyde-agrarose gel, blotted to Gene Screen Plus membrane, and hybridized with nick-translated TF probe by standard procedures. (XBB 882-884)

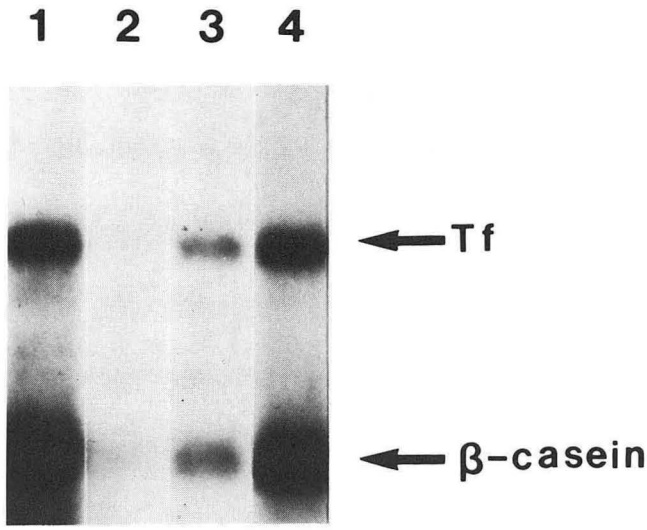

Fig. 2.6. Effect of culture substrata on transferrin (Tf) expression. Cells were isolated from mammary glands of pregnant mice and cultured in the presence of lactogenic hormones on plastic (lane 2), EHS (lane 3), and EHS on floating gel (lane 4). Lane 1 was RNA isolated from lactating mammary gland. Northern blot was probed with nick-translated pMTf-5 and β-casein cDNA simultaneously. Transferrin-specific mRNA was detectable in lane 2 after longer autoradiographic exposure. (XBB 873-2013)

distinct basement membrane, in which the apical surfaces of the polar columnar cells face a central lumen (Fig. 2.7). That this morphology is accompanied by vectorial secretion of milk proteins was determined by comparing the protein composition of the medium exposed to the basal surfaces of the cells to that obtained after opening junctions between cells. This procedure extracts the medium sequestered within the lumina of the spheres. Immune-precipitation using a polyclonal antibody to skim mouse milk proteins of the basal medium versus the luminal medium indicates that a greater proportion of the luminaly secreted proteins are milk proteins (Fig. 2.8). These data indicate that in addition to the dramatic changes in gene expression reported previously, EHS allows formation of functional three-dimensional structures resembling secretory alveoli *in vivo*. Thus basement membrane plays a role in both the structure and the function of the mammary gland and the underlying mechanism of this influence on gene expression is being pursued. Preliminary data have been obtained suggesting that EHS may stimulate the production of basal lamina by mammary epithelial cells in culture. How the production of new basement membrane may affect cellular function and whether a specific disruption in cell-ECM interaction leads to loss of polarity and hence function are under study. The level of regulation of milk protein by substrata (i.e., transcriptional or post-transcriptional) is also being investigated using nuclear run-on and pulse-chase experiments.

Mina Bissell, Mary Helen Barcellos-Hoff, Li-How Chen, Tracy Ram, and Charles Streuli.

Cell Polarity and Secretory Activity

Research in the area of epithelial cell polarity has focused on two areas: 1) the generation and maintenance of plasma membrane polarity; and 2) the significance of cell polarity for expression of differentiation in culture. In studying plasma membrane polarity, monoclonal antibodies have been used that are reactive with a high molecular weight glycoprotein (PAS-0), that is restricted to the apical plasma membrane of differentiated epithelial cells in the lactating mammary gland. PAS-0 is also expressed on the surface of cultured human mammary carcinoma cells (734B), a model system for these studies. PAS-0 is polarized to the

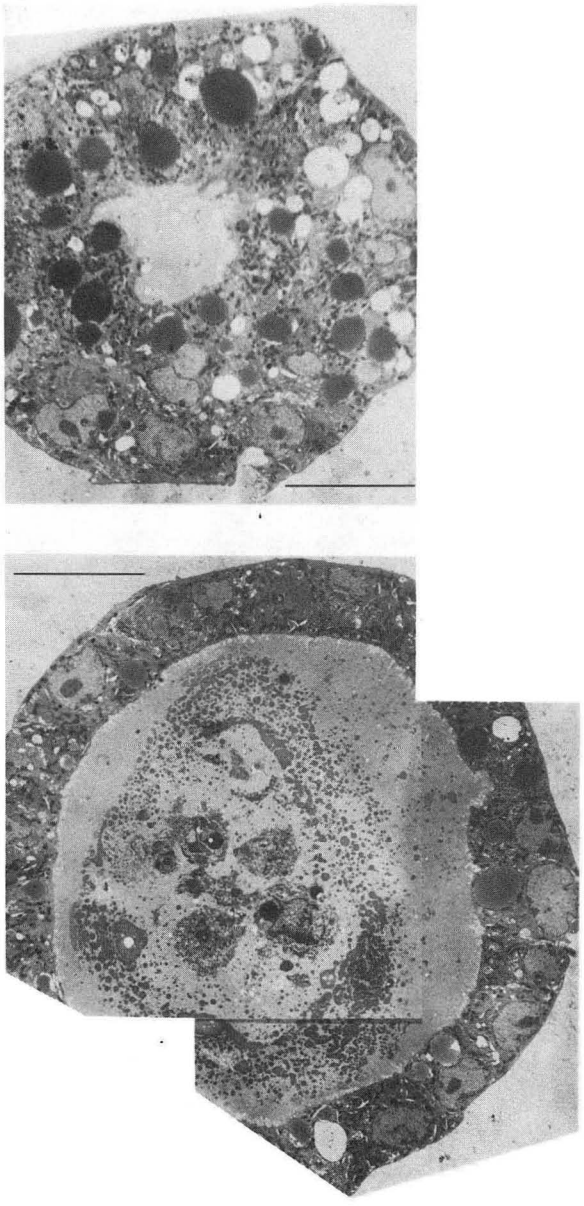

Fig. 2.7. Morphology of primary mammary cells on a reconstituted basement membrane (EHS). These structures resemble functional secretory alveoli in vivo. *(XBB 882-883)*

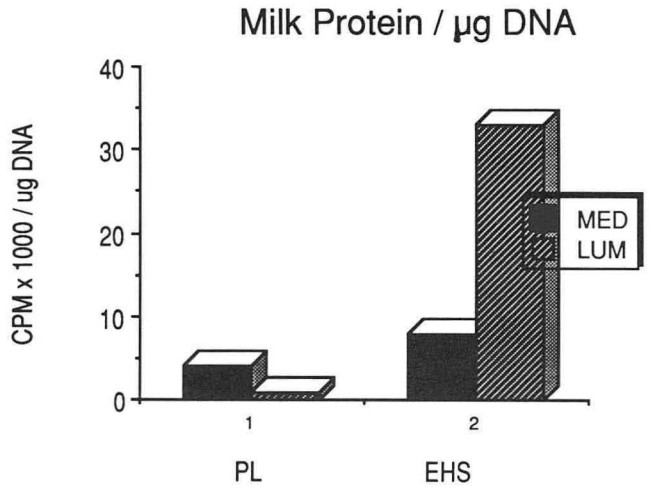

Fig. 2.8. Cells secrete much higher levels of milk proteins on the EHS matrix. In addition, almost all the caseins are secreted vectorially into the lumin. (MED = medium; LUM = lumin). (XBL 881-7273)

apical domain of the plasma membrane in the cultured cells independently of culture density. Experiments were designed to determine the relative significance of cell-cell, cell-substratum, and membrane-cytoskeleton interactions in controlling the domain distribution of PAS-0. Immunofluorescence and immunoelectronmicroscopy experiments (Fig. 2.9) demonstrated that all three interactions were important for maintaining a polarized distribution of PAS-0, and that they were interrelated. Experiments using drugs that disrupt cytoskeletal elements in the cell, and in particular, the actin-containing microfilaments, led to the conclusion that PAS-0 was restricted in its distribution by association (either direct or indirect) with submembranous microfilaments (Fig. 2.10). The stability and organization of this network, however, was dependent upon cell-cell and cell-substratum interactions.

While these results present a novel view of how specialized domains are established in the membrane of epithelial cells, they also provide insight into one of the ways by which cell-cell and cell-substratum interactions can influence structural differentiation in epithelia. Further studies of this simple model system may well contribute significantly to our understanding of cell-cell and cell-substratum effects in more complex epithelial cells.

The fact that epithelial cells are polarized has important implications for the way in which they interact with their environment. In the mammary gland, the basal surface exclusively is involved in uptake of nutrients into the cells and in interacting with hormones and growth factors. The apical surface, in contrast, is active in secretion. The importance of such a polarized interaction with the environment for optimal differentiation was studied in mouse mammary epithelial cell strains (COMMA-1-D) in culture. Experiments utilizing a variety of exogenous extracellular matrices as culture substrata demonstrated that culture conditions that met the polarity constraints of the cell permitted differentiation and secretion. This was shown directly by culturing cells on nitrocellu-

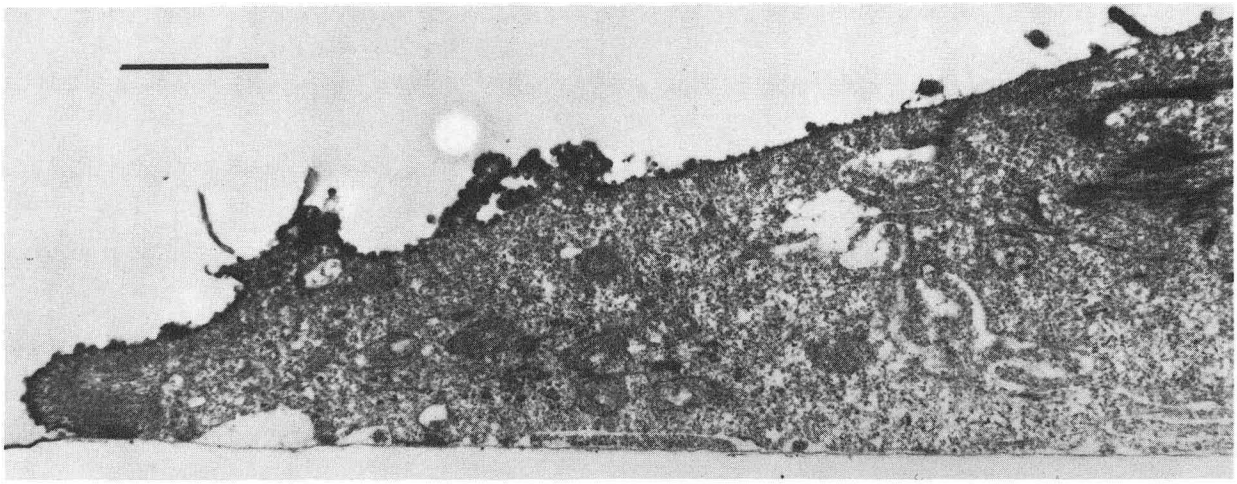

Fig. 2.9. Electronmicrograph of cultured 734B cells stained with monoclonal antibodies to PAS-0 and visualized with peroxidase conjugated second antibody. The antibody decorates the apical surface of the cell up to the point of contact with the substratum. No staining of the basal or lateral membranes is apparent. (XBB 879-7806A)

lose filters in Millicell chambers in which the basolateral surface of the cells was exposed. Under these conditions the cultures differentiated and secreted their differentiated products, namely milk proteins, in a highly polarized fashion (Fig. 2.11).

These studies thus indicate that cell-extracellular matrix and cell-cell interactions influence expression of differentiation in terminally differentiated cells. Whether cell-ECM interactions lead to establishment of polarity which in turn leads to changes in gene expression remains to be determined.

Gordon Parry, Lenny Moss, Betsey Cullen, and James Beck.

TENDON CELLS

In higher organisms, tissues involved in structural organization must synchronize their own growth in relation to that of the whole organism.

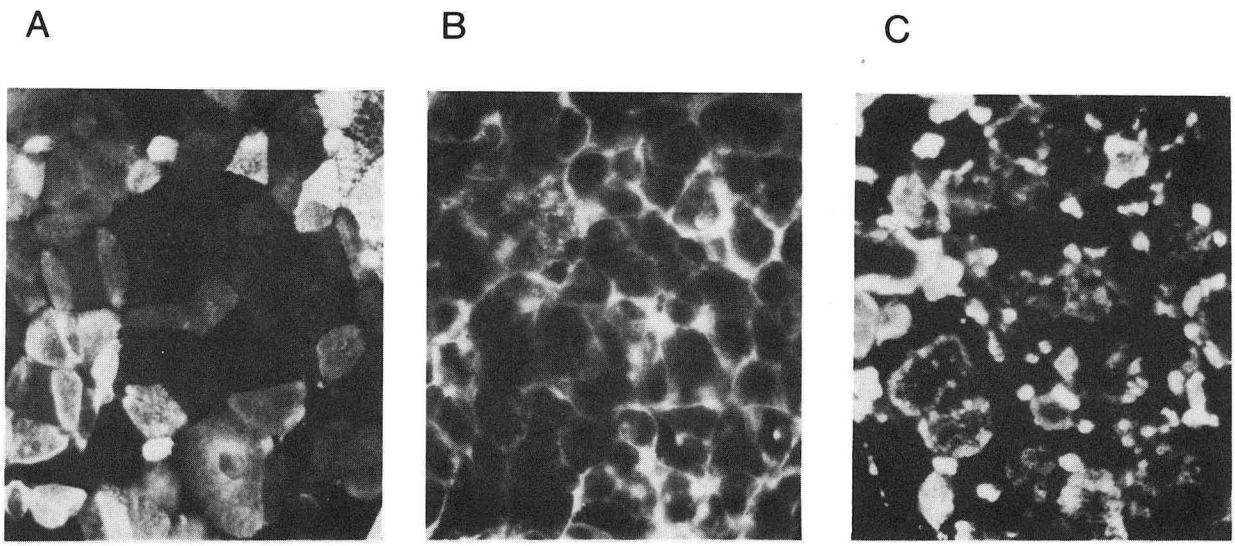

Fig. 2.10. Immunofluorescence analysis of PAS-0 distribution on untreated and cytocholasin-B treated 734B cells. The PAS-0 molecules were visualized using a polyclonal antibody to PAS-0. (A) Untreated cells where the antigen is found exclusively on the apical surface; (B) cytocholasin-B treated cells where the PAS-molecule has redistributed to the basolateral membranes; (C) antibody-induced patching of PAS-0 after cytocholasin treatment. Patching did not occur in the absence of cytocholasin (A). (XBB 870-9177)

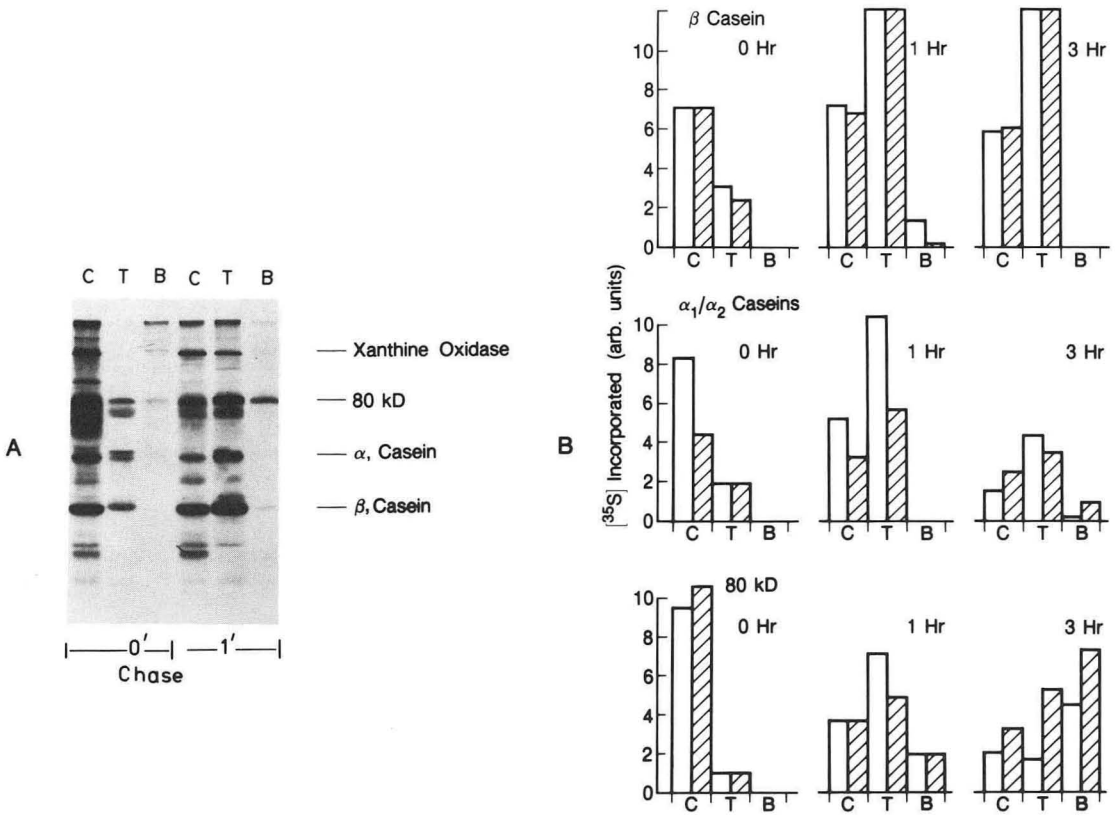

Fig. 2.11. Polarized secretion of mouse milk proteins from COMMA-1-D cells cultured in "Millicell" chambers. (A) An autoradiogram showing immunoprecipitated proteins present in the cell C, top chamber T, and bottom chamber B after 30-minute labeling (O'chase) and a 1-hour chase. (B) Quantitation of data such as that in (A), with additional data for a 3-hour chase. The caseins (α_1, α_2 and β) are secreted in a polarized manner into the top chamber, while transferrin is secreted into both the top and bottom chambers. Coating the "Millicell" chambers with extra-cellular matrix proteins (▨) did not affect the polarized secretion process. (□ =uncoated chambers.) (XBB 873-2117)

Since overall growth rate changes radically over the course of development, this raises important questions as to how tissues regulate their own size. In tendon, the important growth parameter is length, and this is determined to a first approximation by the level of collagen production, since collagen is the major protein component. Deciphering the mechanisms controlling collagen production in tendon cells has importance not only because it is crucial to understanding the regulation of the differentiated state of a tendon cell but also because it sheds light on how tissues coordinate growth regulation.

In this regard two important facts have emerged from studies of tendon cells in culture. First, the steps in the collagen pathway are tightly coupled allowing for feedback control. Second, the cell responds to the density of its neighbors and only produces high levels of collagen at high cell density. In the past it was shown that the level of a collagen modifying enzyme, prolyl hydroxylase, and procollagen mRNA are cell-density dependent. To further pursue how a cell detects its neighbors, the cell density increase in procollagen mRNA was used to develop a quantitative *in situ* hybridization assay (Fig. 2.12) so that the level of procollagen mRNA could be measured in individual cells. Using this assay it can be shown that a tendon cell can detect the presence of other cells over a 1-mm distance. Whether this is due to chemical gradients or physical changes such as expression of extracellular matrix components is under investigation.

Richard I. Schwarz.

HEMOPOIESIS

The basic problems in hemopoiesis are fundamental to many systems in biology. What directs a pluripotent stem cell to a specific lineage? How does this differ from self-replication? What are the factors that cause a committed cell to mature? In addition, there are also unique characteristics of

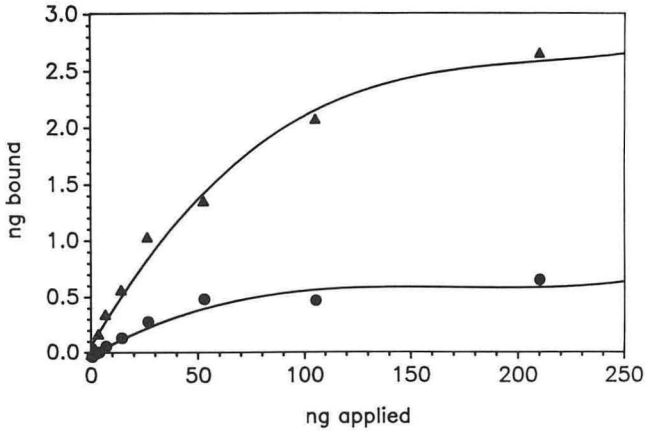

Fig. 2.12. Saturation of hybridizable sites of procollagen mRNA molecules in tendon cells in situ. *Tendon cells were grown with (▲) and without (•) ascorbate. The 6-fold increase in procollagen mRNA induced by ascorbate (as shown previously by dot hybridization using purified total BNA) is quantitatively reproduced by* in situ *hybridization. (XBL 881-7236)*

hemopoiesis that are poorly understood. A hemopoietic stem cell can wander throughout the blood stream but will be functional only in a few sites in the body. The factors that contribute to this "hemopoietic inductive microenvironment" are not well understood, and yet its influence cannot be doubted. A single stem cell injected into the peripheral blood can repopulate the bone marrow and start producing the 3×10^8 red blood cells per day and all the other blood types necessary for the survival of a lethally irradiated mouse. In addition, numerous factors play a role in the induction and proliferation of hemopoietic cells and their mode of action needs to be understood. For example, erythropoietin is one of the first factors shown to stimulate the erythroid lineage, but neither the exact producer cell in the kidney nor the receptor cell in the marrow have been clearly identified. With this lack of understanding of normal control, it is not surprising that the underlying mechanisms that cause this tightly controlled cell system to malfunction (leading to anemias, leukemias, immunodeficiency, etc.) are also poorly understood. Our approach is multidisciplinary, combining classical hemotological techniques with those of modern molecular biology. Each activity below focuses on a specific subset of questions in hemopoiesis but all share overlapping techniques and interest in the process as a whole.

Erythroid Lineage

Identifying Early Committed Stem Cell and the Inductive Microenvironment: The technique of *in situ* hybridization has been adapted for use with bone marrow smears. Using a hemoglobin mRNA probe, one can readily identify the late progenitor cells, normoblasts and reticulocytes, as well as earlier committed stem cells that would be impossible to identify by histological stains (Fig. 2.13).

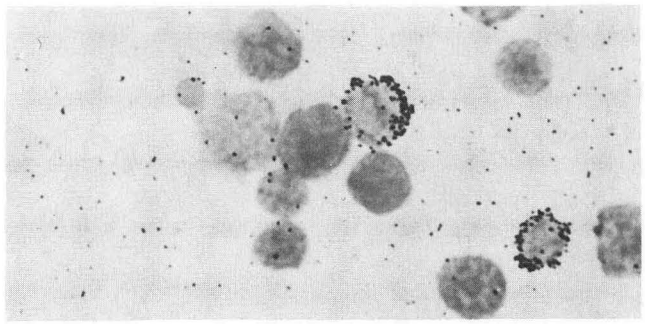

Fig. 2.13. Cytospin of bone marrow cells from mice blocked in erthropoiesis by hypertransfusion. Committed stem cells can still be detected by their ability to hybridize in situ *to a β-hemoglobin probe. The hemoglobin in mRNA content is estimated to be about 10 molecules/cell. (XBB 882-885)*

The ability to stimulate erythropoiesis by injection of erythropoietin or to inhibit erythropoiesis by hypertransfusion allows one to manipulate the flow through this lineage. Currently, *in situ* hybridization is used to follow a synchronous stimulation of the erythroid lineage by first repressing the marrow by hypertransfusion and then stimulating the committed stem cells with erythropoietin. Combining this information with ability of *in situ* hybridization to give spatial information about the organization of the various erythroid precursor cells in frozen sections of bone marrow should aid in our understanding of the hemopoietic inductive environment.

Richard I. Schwarz and Mark Hertle.

Action of Erythropoietin (Ep): The main objectives of this research are to investigate 1) the ontogeny and physiology of erythropoietin producing tissues, 2) the action of Ep at the receptor level in blood forming tissues, and 3) whether the expression of the Ep receptor gene is modulated by other hormones or growth factors during fetal, neonatal, and adult life.

The production of red blood cells in the normal animal is regulated by Ep. However, as in other hormonal systems, the endocrine control of blood forming tissues, while Ep dependent, is also the result of complex interactions with other factors. Conversely, our recent finding of high Ep levels in the fetus and neonate indicate that Ep, besides being responsible for red blood cell production, might also have additional functions. Very high Ep levels were found in salivary glands, and it was shown that these glands are not the source of extrarenal Ep. Rather, they may be the result of accumulation after puberty because no mRNA for Ep can be demonstrated in tissues derived from hypoxic rats. In addition, sexual dimorphism exists in rodents in that more Ep is found in male saliary glands than in females. Whether Ep plays a role in wound healing similar to nerve, epidermal, and transforming growth factors derived from the salivary gland is under investigation. Renal Ep production is also being investigated in the adult animal as a function of insulin-like growth factor 1 (IGF1) and growth hormone.

To further define the action of Ep, a radioreceptor assay for Ep is presently being developed. Our laboratory is the first to show that radiolabeled Ep retains its full biological activity, a fundamental prerequisite for the development of such an assay. The use of a radioreceptor assay is manifold. It will allow the study of the kinetics and affinity of the receptor in membrane preparations, the action of Ep at the receptor level during development and maturation, the modulation of the receptor gene expression as a function of other hormonal interactions, and the ontogeny of Ep receptors in blood forming tissues.

Gisela K. Clemons and Darlene DeManincor.

Megakaryocyte Lineage

The overall goal is to understand the mechanisms that regulate megakaryocytopoiesis leading to the formation of platelets. Several approaches are being used:

A culture system has been developed where megakaryocytes can be stimulated by the plasma from thrombocytopenic rabbits to undergo changes that show many features of platelet formation *in vivo*. Plasma from normal rabbits is inactive. Current models predict that thrombopoietin, an as yet uncharacterized hormone, is elevated during thrombocytopenia and is responsible for the changes we observe in these cultures. Part of the observed changes are dependent on extension of microtubules that provide structural support for long cytoplasmic processes. In addition, microtubule coils that are characteristic of mature blood platelets may also form in the cytoplasmic extensions of the cultured megakaryocytes before intact platelets are released. Small cytoplasmic fragments that are ultrastructurally similar to platelets and respond to platelet activators are found in these cultures. Currently, a detailed analysis of cytoskeletal organization during the process of megakaryocyte fragmentation is being undertaken. This work is primarily by the use of immunocytochemistry and electron-microscopy.

A study is being made of the Wistar Furth rat, a strain that has a genetically controlled abnormality of platelet size and number. Ultrastructural analysis has led to our belief that there may be a biochemical abnormality in the megakaryocyte membranes of these rats that leads to abnormal platelet formation. This work has been done in collaboration with Dr. Fern Davis at the University of California, Davis. In addition, lipid and proteoglycan analyses of the platelets from these animals have been underway to resolve biochemical alterations that may underlie the observed abnormalities in membrane structure.

Studies of the unique characteristics of the gene expression in megakaryocytes are being initiated. Techniques for isolation of megakaryocyte RNA have been developed, and currently the expression of protooncogenes and platelet alpha granule proteins is under investigation. It is thought that protooncogene expression may play a role in the development of polyploidy, an unusual characteristic of megakaryocytes. Several alpha granule proteins appear to be specific for megakaryocytic cells. Therefore detection of the expression of these proteins may be a useful tool to detect otherwise unrecognizable early-committed percursor cells in the bone marrow.

Shirley Ebbe, Robert Leven, Dorothy Carpenter, and Tamlyn Yee-Neben.

Disease Models: Malaria

The cellular mechanisms involved in the anemia and immunosuppression associated with malaria infection are being investigated. Anemia, a major complication of malaria, accounts for the major morbidity and mortality of this disease. Our current focus is on how products of the immune system, such as interleukins and tumor necrosis factor (TNF), may mediate these pathological sequelae via their regulatory effects on stem cell

proliferation and/or differentiation.

It has been shown that infection of mice with three strains of malaria (*Plasmodium vinckei, P. berghei,* and *P. chabaudi adami*) results in the depletion of bone marrow pluripotent stem cells (from which all erythroid and myeloid cells derive) and a concomitant increase in stem cells in the blood and spleen. Apparently, an increase in stem cells in the spleen does not compensate for the loss of erythropoietic activity of the bone marrow. Mice infused with recombinant TNF, a product of activated macrophages, show a similar depletion of bone marrow stem cells and an increase in spleen stem cells. Studies are now under way to determine whether such mobilized stem cells are functionally altered during malaria infection and therefore contribute to the anemia and immunosuppression observed in malaria-infected mice.

Studies using *in vitro* colony assays for erythroid progenitor cells and an *in vitro* assay to measure erythroid precursor cell proliferation in response to erythropoietin (Ep), the hormone required for mature red blood cell development, demonstrated that committed erythroid progenitor cells as well as pluripotent stem cells are altered by malaria infection. Both early erythroid progenitor cells, colony forming unit erythroid (CFU-E), and later erythroid progenitor cells, burst forming unit erythroid (BFU-E), are present in reduced numbers in the bone marrow and spleen over the course of malaria infection (Fig. 2.14). Evidence suggests that a soluble factor may be responsible for the ineffective erythropoiesis observed in infected mice. Conditioned media produced from spleen cells of malaria infected mice, or normal spleen cells incubated with malaria infected red blood cells, are able to inhibit the proliferative response of erythroid precursor cells to erythropoietin. What factor(s) is/are involved is not known. Interleukin-1 (IL-1), a product of macrophages and other cell types, has been shown by J.C. Schooley and colleagues to suppress the proliferative response to Ep in the same assay.

In addition to anemia, malaria infection is also associated with immunosuppression, as shown by the depression of the *in vitro* response of lymphocytes from malaria-infected mice to mitogens and/or antigens. The relationship of the immunosuppression to the inhibition of erythropoiesis and whether similar mechanisms are involved is currently under investigation.

In conclusion, it has been shown that malaria infection leads to alterations in the kinetics of

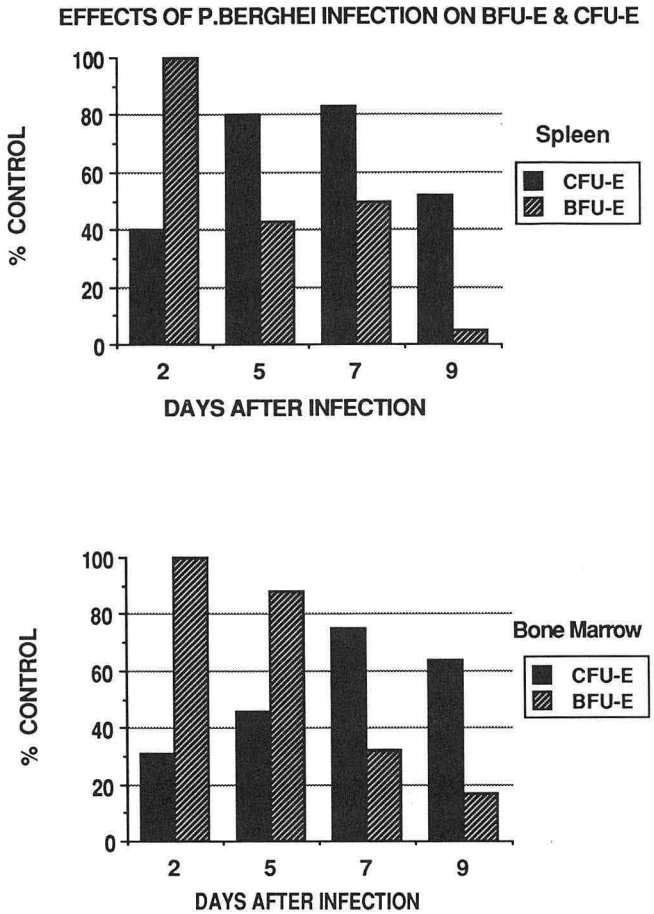

Fig. 2.14. *The number of colony forming units erythroid (CFU-E) and burst forming units erythroid (BFU-E) in the spleen and bone marrow of BALB/c mice at various times after infection with* P. berghei. *CFU-E and BFU-E were determined by* in vitro *colony assays. Results are expressed as the percentage of control values for normal BALB/c mice. (XBL 8711-4911)*

pluripotent stem cells and in the functional capacity of committed erythroid progenitor cells and lymphocytes.

Investigations continue into the nature of the inhibitory factor(s) in conditioned media from malaria infected spleens, whether the target cell is a pluripotent stem cell or a committed erythroid progenitor cell, the molecular basis of the inhibition, and the role played by factors such as IL-1 and TNF. This research will not only increase our understanding of how hemopoiesis is normally regulated but will also aid in the development of therapeutic strategies for the anemia and immunosupression that are associated with a number of infectious diseases such as malaria.

Paul H. Silverman, Kathleen L. Miller, Lynn J. Mahlmann, and Birgitta Kullgren.

Bone Marrow Transplantation and the Pluripotent Stem Cell

Both pluripotential stem cells and precursor cells committed to the different lineages have been cultured and characterized *in vitro*. However, the relationship of pluripotential and precursor cells is poorly understood *in vivo*, because there are no methods to identify the early stem cells. Such methods must be highly sensitive, because the pluripotential stem cells represent a vanishing small number in the bone marrow. At the moment, only the progeny of these cells can be studied, most satisfactorily after transfusion of marrow into a new host in which the pluripotential stem cells seed and proliferate. Present methodology requires samples of at least 15,000 cells for this purpose. The development of a much more sensitive method for the recognition of a few hundred transplanted stem cells is thus badly needed for understanding of the kinetics and physiology of stem cells. A major effort is under way to produce a monoclonal antibody to meet this methodological requirement.

In the meantime, work is in progress on the progeny of donor pluripotential stem cells While a single stem cell can repopulate a lethally irradiated mouse completely and permanently, it has been demonstrated, in collaboration with E.P. Cronkite, that there exist other stem cells that can repopulate the irradiated recipient only partially. The host's own stem cells may then recover and repopulate the entire animal. The ecology of the bone marrow stroma is being investigated to clarify these findings. Marrow transfused into a lethally irradiated mouse was retransfused subsequently into both secondary lethally irradiated hosts and normal-nonirradiated secondary hosts. The marrow exposed to a lethally irradiated environment repopulated the entire marrow of the secondary lethally irradiated host, but failed to grow at all in the normal host. This was the case, even when the number of marrow cells was increased to contain as many CFU-S as sufficed to produce a 30% level of donor cells in a normal, nonirradiated secondary host.

George Brecher, Marilyn Yee, and Steven Neben.

Carcinogenesis

INTRODUCTION

The transformation of normal cells to malignancy is a multi-step process, involving derangements in cellular growth control, differentiation, and senescence. Many factors are known to affect this process as initiators or promoters of carcinogenesis. These include chemical and physical agents (such as chemical carcinogens and radiation), viruses and cellular oncogenes, and dietary components. An individual's genetic makeup can also influence relative susceptibility to development of cancer. Members of the Cell and Molecular Biology Group are examining several different aspects of the carcinogenic process, ranging from assessments of the effect of chemical carcinogens, radiation, and viral infection on cells and animals. These studies should provide an increased understanding of both the causes of, and mechanisms occurring during oncogenic transformation, and should draw upon insights into DNA repair, replication and recombination, and responses to carcinogens described in the preceding sections.

ENVIRONMENTAL CARCINOGENS

In an effort to evaluate the potential hazard to human health of exposure to chemical carcinogens, the Group has developed a Carcinogenic Potency Database (CPDB). This database includes the published results of chronic animal carcinogenesis bioassays from about 4000 experiments involving 1000 different chemicals. Estimates of the TD_{50} values of rodent carcinogens vary more than 10-millionfold. These TD_{50} values have been used to rank possible hazards to humans from exposure to chemicals known to be carcinogenic in rats or mice, in particular, 41 chemicals for which there are also defined OSHA Permissible Exposure Levels (PEL). When the PEL (mg/kg/day) for these chemicals are compared to the rodent TD_{50} the resulting ratios differ by more than 100,000-fold from each other. It therefore seems reasonable to give particular attention to the reduction of allowable worker exposure to those substances that appear to be

hazardous by this index, and that some workers may be exposed to full-time near the PEL, namely ethylene dibromide, ethylene dichloride, 1,3-butadiene, tetrachloroethylene, propylene oxide, chloroform, formaldehyde, methylene chloride, dioxane, and benzene.

Bruce Ames and Lois Gold.

HUMAN MAMMARY CANCER

Interaction of Human Mammary Cells with Growth Factors and Oncogenes

Much of the work in the carcinogenesis group utilizes a human mammary model system developed by Martha Stampfer. This culture system permits long-term active growth of normal human mammary epithelial cells (HMEC) in a serum-free medium. *In vitro* exposure of normal HMEC to the chemical carcinogen benzo(a)pyrene has also led to the development of two immortalized cell lines. Transformation to malignancy can occur when these cell lines are further exposed to tumor virus oncogenes. These unique cell substrates are being used in many laboratories at LBL and around the world to study and compare the properties of normal and transformed human epithelial cells. A major effort in the past year (in collaboration with Marc Lippman and Bob Dickson at NIH) has involved examining these cells' requirements for, responses to, and production of growth factors, hormones, and their receptors. In particular, TGF-β growth inhibition and receptor levels are being assessed as a function of transformation, age in culture, and presence of other growth factors, while TGF-α and EGF receptor mRNA and protein synthesis have been shown to be active in all the HMEC types examined. Subpopulations of the immortalized cell lines that have altered growth requirements or responses have been isolated to aid in the dissection of the mechanisms of cell responses to growth factors. Growth in restrictive media also appears to select for cells altered by further exposure to a chemical carcinogen. It is hoped that this selective growth will assist quantitation of the transformative potential of different carcinogens.

Interaction of Human Mammary Epithelial Cells with Carcinogenic Hydrocarbons

The normal HMEC have been used to study another aspect of chemical carcinogenesis, the metabolism of pro-carcinogens such as benzo(a)pyrene (BaP) to their ultimate carcinogen form, in this case, the benzo(a)pyrene-diolexpoxide (BPDE). Reaction of BPDE with DNA may result in mutation or cellular transformation. The group has previously shown that HMEC readily convert BaP to the active BPDE form, whereas fibroblast cells from the same tissue are much less capable of this reaction. This work is continuing by determining whether arachidonic acid, particularly cyclooxygenase, plays a role in this conversion by the HMEC. Pretreatment of normal HMEC with cold BaP has been found to increase the overall conversion of tritiated BaP to BPDE, as measured by BP-7,8-diol and tetraol hyrolysis products of BPDE identified by reversed-phase HPLC. Methods to quantitate the BPDE-derived tetraols by periodate oxidation and calcium oxide treatment are being developed. Cyclooxygenase inhibitors appear to partially inhibit this tertraol production, while thus far, inhibitors of lipoxygenase have no effect. Hence, of these two pathways the cyclooxygenase appears to be the predominant one in HMEC. Recently, ^{3}H-BaP-7,8-diol was found to be a superior substrate to ^{3}H-BaP in that it produces BPDE-derived tetraols both more readily and cleanly. Use of this substrate should allow a quantitative dissection of the key step, the conversion of BP-7,8-diol to BPDE by evaluating the effect of inhibitors of cytochrome P-450 as well as inhibitors of the arachidonic acid cascade. In a collaborative effort with Mina Bissell and co-workers, the possible role of the arachidonic acid cascade in wound-promoted tumors in Rous sarcoma virus infected chicks is under investigation.

Martha Stampfer, Jack Bartley, Allan Tischler, Myriam Alhadeff, Linda Hayashi, Midori Hosobuchi, Gerri Levine, and Annie Pang.

NOVEL APPROACHES TO VIRAL CARCINOGENESIS: HOST-VIRUS INTERACTIONS IN DIFFERENTIATION AND MALIGNANCY

The recent advent of techniques for the incorporation of foreign genetic information into animal hosts *in vivo* has allowed us to embark on a systematic and ambitious project to apply modern cell and molecular biology to answer basic questions in tumor biology. Since it has been shown that the embryo is capable of regulating the malignant properties of Rous sarcoma virus (RSV), the system affords the exciting opportunity to evaluate some of the key elements in the transformation process. In the past year it has been shown that while the level of pp60src (the product of the transforming gene of

RSV) is not proportional to the expression of other viral structural proteins such as p19 (a compound of group-specfic antigens), nevertheless *src* is expressed in the early embryo and further, it is active because it phosphorylates tyrosine residues of proteins. To trace the lineage of the target cells and to investigate whether the older embryo could become permissive for sarcoma, it was first necessary to prevent viremia and to prolong the life of the embryo. To achieve these goals, we developed a

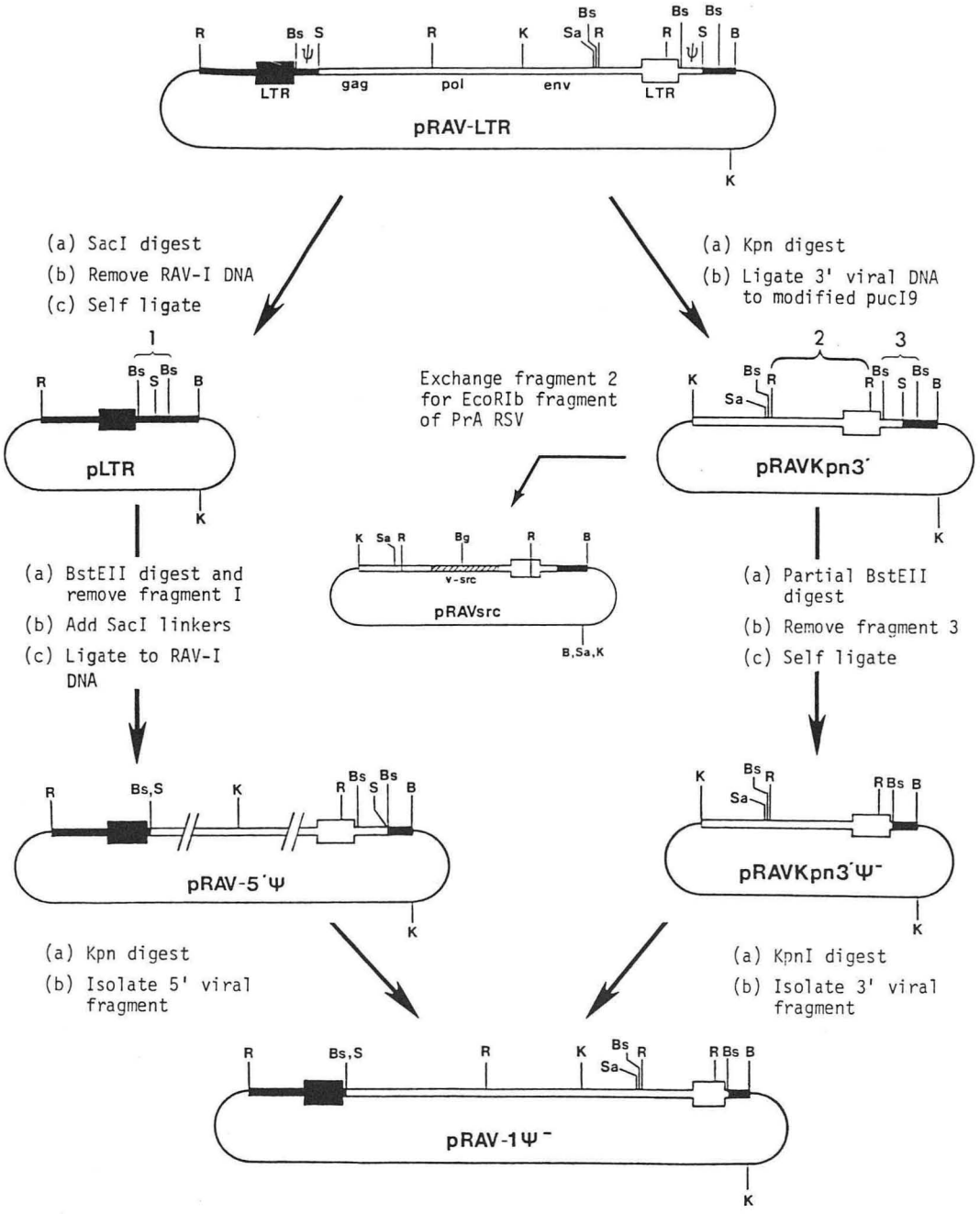

Fig. 2.15. Schematic representation of pRAV-1ψ construction. Boxed regions represent proviral DNA, RAV-1 (open boxes), AEV10 (closed boxes). Single lines represent bacterial plasmid DNA. Duplicated RNA encapsidation sequences, ψ, are indicated in pRAV-LTR. Relevant enzyme cleavage sites are indicated: B, BamHI (sites within RAV-1 DNA are not shown); Bg, Bg1II; Bs, BstEII; K, KpnI; R, EcoRI, S, SacI; Sa, SalI. (XBL 876-2640A)

vector-packaging quail cell line, stably infected with an avian leukosis virus-derivative deficient in packaging sequences ψ. The construction of this derivative (named pRAV-1ψ) is shown in Fig. 2.15. Novel replication-defective v-src constructs containing drug-resistant genes were transfected into pRAV-1ψ, and the resulting colonies were shown to stably produce up to 2×10^5 replication-defective (RD) infectious viral particles. These viruses are currently being injected into the embryo. Preliminary results indicate that unlike the wild type virus that was expressed early in the skeletal muscle only and would not allow viability beyond days 12–14, the RD virus appears to be expressed in the limb connective tissue post-day-12, but allows embryo survival at least to day 18 at which time it appears to form sarcoma. These experiments verify the versatility of the embryo system and should lead to identification of factors that appear (or disappear) between days 12–18 that allow the expression of the malignant phenotype. In another complementary approach, we are exploring the mechanism by which wounding acts as a cocarcinogen in RSV tumorigenicity in hatched chicks. Techniques have been developed for sectioning through the wounded area (Fig. 2.16) to follow the course of activation of silent integrated virus, for subsequent localization of virus and dividing-cells using antibodies, immunohistochemistry, and *in situ* hybridization with riboprobes of viral genes. In collaboration with Michael Sporn of NIH, the pattern of TGF-β expression after wounding and its possible role in RSV-tumorigenicity is also being investigated.

Mina J. Bissell, Anthony Howlett, Andrew Stoker, Michael Sieweke, and Jill Hatier.

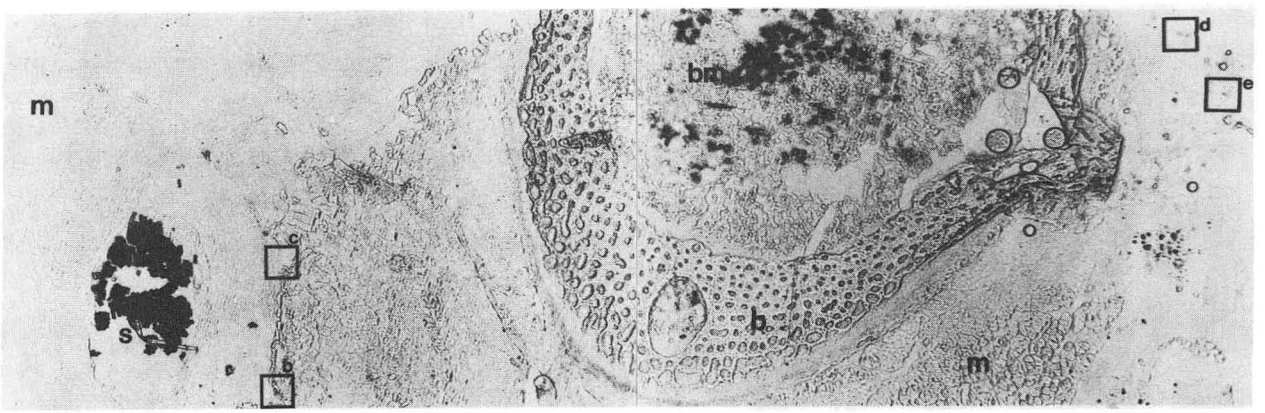

Fig. 2.16. *Phase contrast image of a transverse frozen section (6 μm) of a suture wound at the midpoint of the radius-ulna region 1 of the right wing of a 15-day-old chicken 20 hours after wounding. The suture allows the precise localization of wounded tissue in the section. Boxes indicate areas with high incidence of growing cells. (b = bone, bm = bone marrow, m = muscle, s = suture). (XBB 882-886)*

Publications: Cell and Molecular Biology

CONTRIBUTIONS TO JOURNALS

Ames, B.N., Magaw, R., and Gold, L. S. Ranking possible carcinogenic hazards. *Science 236,* 271–280 (1987).

Bernstein, L., Gold, L.S., Ames, B.N., Pike, M.C., and Hoel, D. Some tautologous aspects of the comparison of carcinogenic potency in rats and mice. *Fundamental and Appl. Toxicol. 5*, 79–86 (1985).

Brecher, G., Beal, S.L., and Schneiderman, M. Renewal and release of hemopoietic stem cells. Does clonal succession exist? *Blood Cells 12*, 103–112 (1986).

Chan, L.-M., Hatier, C., Parry, G., Werb, Z., and Bissell, M.J. Collagen-fibronectin interactions in normal and Rous sarcoma transformed avian tendon cells: Possible mechanism for increased extracellular matrix turnover after transformation. *In Vitro Cell and Molec. Biology 23*, 308–314 (1987).

Chandra, M., McVicar, M., Clemons, G., Mossey, R.T., and Wilkes, B.M. Role of erythropoietin in the reversal of anemia of renal failure with continuous ambulatory peritoneal dialysis. *Nephron 46*, 312–315 (1987).

Clemons, G.K., DeManincor, D., Fitzsimmons, S.L., and Garcia, J.F. Immunoreactive erythropoietin studies in hypoxic rats and the role of the salivary glands. *Exp. Hematology 15*, 18–23 (1987).

Cole, G.M., Schild, D., Lovett, S.T., and Mortimer, R.K. Regulation of *RAD54-* and *RAD52-lacZ* gene fusions in *Saccharomyces cerevisiae* in response to DNA damage. *Molecular and Cellular Biology 7*, 1078–1084 (1987).

Contopolou, C.R., Cook, V.E., and Mortimer, R.K. Analysis of DNA double strand breakage and repair using orthogonal field alternation gel electrophoresis. *Yeast 3*, 71–76 (1987)

Dixon, M.L. and Mortimer, R.K. A yeast screening system for simultaneously monitoring multiple genetic endpoints. *Mutation Research 161*, 49–64 (1986).

Eckhardt-Schupp, R., Siede, W., and Game, J.C. The *RAD24*(=*Rs*) gene product of *Saccharomyces cerevisiae* participates in two different pathways of DNA Repair. *Genetics 115*, 83–90 (1987).

Gold, L.S., Bernstein, L., Kaldor, J., Backman, G., and Hoel, D. An empirical comparison of methods used to estimate carcinogenic potency in long-term animal bioassays: Lifetime vs. summary incidence data. *Fundamental and Appl. Toxicol. 6*, 263–269 (1986).

Gold, L.S., Wright, C., Bernstein, L., and de-Veciana, M. Reproducibility of results in "near-replicate" carcinogenesis bioassays. *J. Natl. Cancer Inst. 78*, 1149–1158 (1987).

Goth-Goldstein, R. MNNG-induced partial phenotypic reversion of the Mer- cells. *Carcinogenesis 8*, 1449–1453 (1987).

Goth-Goldstien, R. and Hughes, M. Cell killing by various monofunctional alkylating agents in Chinese hamster ovary cells. *Mutation Ressearch 177*, 267–276 (1987).

Goth-Goldstein, R. and Hughes, M. Characterization of a CHO variant in respect to aklylating agent-induced biological effects and DNA repair. *Mutation Research 184*, 139-146 (1987).

Guzman, R.C., Osborn, R.C., Bartley, J.C., Imagawa, W., Asch, B., and Nandi, S. *In vitro* transformation of mouse mammary epithelial cells grown serum-free inside collagen gels. *Cancer Research 47*, 275–280 (1987).

Howlett, A.R., Cullen, B., Hertle, M., and Bissell, M.J. Tissue tropism and temporal expression of Rous sarcoma virus in embryonic avian limb *in ovo* and after transfer to cell culture. *Oncogene Res. 1*, 255–263 (1987).

Kusmierek, J.T., Jensen, D.E., Spengler, S.J., Stolarski, R., and Singer, B. Synthesis and properties of N^2,3-ethenoguanosine and N^2,3-ethenoguanosine 5'-diphosphate. *J. Organic Chem. 52*, 2374–2378 (1987).

Leadon, S.A. Production of thymine glycols in DNA by radiation and chemical carcinogens as detected by a monoclonal antibody. *Brit. J. Cancer 55 (Suppl. VIII)*, 113–117 (1987).

Lee, E.Y.-H., Barcellos-Hoff, M.H., Chen, L.H., Parry, G., and Bissell, M.J. Transferrin is a major mouse milk protein and is synthesized by mammary epithelial cells. *In Vitro Cellular and Molecular Biol. 23*, 221-226 (1987)

Li, M.L., Aggeler, J., Farson, D.A., Hatier, C., Hassell, J., and Bissell, M.J. Influence of a reconstituted basement membrane and its components on casein gene expression and secretion in mouse mammary epithelial cells. *Proc. Natl. Acad. Sci. USA 84*, 136–140 (1987).

Lin, J.P., Aker, M., Sitney, K., and Mortimer, R.K. First position wobble in codon-anticodon pairing: amber suppression by yeast glutamine tRNA. *Gene 49*, 383–388 (1986).

Lovett, S.T. and Mortimer, R.K. Characterization of null mutants of the *RAD55* gene of *Saccharomyces cerevisiae*: Effects of temperature, osmotic strength and mating type. *Genetics 116*, 547–553 (1987).

Medina, D., Li, M.L., Oborn, C.J., and Bissell, M.J. Casein gene expression in mouse mammary epithelial cell lines: Dependence upon extracellular matrix and cell type. *Exp. Cell Res. 172*, 192–203 (1987).

Menon, R., Bartley, J.C., Som, S., and Banerjee, M.R. Metabolism of 7,12-dimethylbenz(a)anthracene by mouse mammary cells in serum-free organ culture systems. *European J. Cancer and Clin. Oncology 23*, 395–400 (1987).

Parry, G., Cullen, B., Kaetzel, C.S., Kramer, R., and Moss, L. Regulation of differentiation and polarized secretion in mammary epithelial cells maintained in culture: Extra-cellular matrix and membrane polarity influences. *J. Cell Biol. 105*, 2043–2051 (1987).

Pavlovíc-Kentera, V., Clemons, G.K., Djukanovíc, L., and Biljanovíc, L. Erythropoietin and anemia in chronic renal failure. *Experimental Hematology 15*, 785–789 (1987).

Preston, B.D., Singer, B., and Loeb, L.A. Mutagenic potential of O^4-methylthymine *in vivo* determined by an enzymatic approach to site-specific mutagensis. *Proc. Natl. Acad. Sci. USA 83*, 8501-8505 (1986).

Preston, B.D., Singer, B., and Loeb, L.A. Comparison of the relative mutagenicities of O-alkylthmines site-specifically incorporated into ϕX174 DNA. *J. Biol. Chem. 262*, 13821–13827 (1987).

Roth, R.M., Game, J.C., and Peak, M.J. Sensitivities to monochromatic 254-nm and 365-nm radiation of closely related strains of *Saccharomyces cerevisiae* with differing repair capabilities. *Photochem. Photobiol. 45*, 479–843, (1987).

Schooley, J.C., Kullgren, B., and Allison, A.C. Inhibition by interleukin-1 of the action of erythropoietin on erythroid precursors and its

possible role in the pathogenesis of hypoplastic anemia. *Brit. J. Haematology 67*, 11–17 (1987).

Schwarz, R.I., Kleinman, P., and Owens, N. Ascorbate can act as an inducer of the collagen pathway because most steps are tightly coupled. *N.Y. Acad. Sci. 498*, 172–185 (1987).

Silverman, P.H., Schooley, J.C., and Mahlmann, L.J. Murine malaria decreases hemopoietic stem cells. *Blood 69*, 408–413 (1987).

Singer, B., Spengler, S.J., Chavez, F., and Kusmierek, J.T. The vinyl chloride-derived nucleoside, N^2,3-ethenoguanosine, is a highly efficient mutagen in transcription. *Carcinogenesis 8, 745–747* (1987).

Smith, H.S. and Bissell, M.J. Cancer at the cellular level. *Cancer Res. 47*, 3337–3338 (1987).

Stoker, A.W. and Bissell, M.J. Quantitative immunocytochemcial assay for infections avian retroviruses. *J. Gen. Virology 68*, 2481–2485 (1987).

Teramo, K.A., Widness, J.A., Clemons, G.K., Voutilainen, P., Saarinen, R., McKinlay, S., and Schwartz, R. Amniotic fluid erythropoietin correlates with umbilical plasma erythropoietin in normal and abnormal pregnancy. *Am. J. Obst. Gynecol. 69*, 710–716 (1987).

Tischler, A., Bailey, P., Dallob, A., Witzel, P., Durette, P., Rupprecht, K., Allison, D., Dougherty, H., Humes, J., Ham, E., Bonney, R., Egan, R., Gallagher, T., Miller, D., and Goldenberg, M. L-652,343: A novel dual 5-lipooxygenase/cyclooxygenase inhibitor. *Advances in Prostaglandins, Thromboxanes and Leukotrienes Research 16*, 63 (1986).

Tischler, A.N. and Lanza, T.J. 6-Substituted indoles form o-halonitrobenzenes. *Tetrahedron Letters 27(15)*, 1653 (1986).

Tyndall, M.R., Teitel, D.F., Lutin, W.A., Clemons, G.K., and Dallman, P.R. Serum erythropoietin in patients with congenital heart disease. *J. Pediatrics 110*, 538–544 (1987).

Walle, A.J., Wong, G.Y., Clemons, G.K., and Garcia, J.F. Erythropoietin-hematocrit-feedback circuit in the anemia of endstage renal disease: effects of transfusions, hemorrhage and hemodialysis. *Kidney International 31*, 1205–1209 (1987).

CONTRIBUTIONS TO BOOKS AND PROCEEDINGS

Bissell, M.J. and Aggeler, J. Dynamic reciprocity: How do extracellular matrix and hormones direct gene expression? Pages 251–262 in *Mechanisms of Signal Transduction by Hormones and Growth Factors*, M. Cabot, ed., Alan Liss Inc, New York (1987).

Bissell, M.J. and Hall, H.G. Form and function in the mammary gland: The role of extracellular matrix. Pages 97–146 in *The Mammary Gland*, M.C. Neville and C.W. Daniel, eds., Plenum Publ. Corp., New York (1987).

Bissell, M.J., Li, M.L., Chen, L-H., and Lee, E. Y-H. Regulation of milk proteins in the mouse mammary epithelial cells by extracellular matrix and hormones. Pages 155–186 in *Growth and Differentiation of Mammary Cells in Culture*, J. Enami and R. Ham, eds., Japan Scientific Societies Press, Tokyo, Japan (1987).

Brecher, G. Commentary on M. Rosendaal, S. Villa, and C. Hooper: Correspondence between the development of hemopoietic tissue and the time of colony formation by colony-forming cells. *Blood Cells 12,* 625–626 (1987).

Brecher, G., Commentary on M. Rosendaal and J. J. Adam, Hemopoietic progenitors in different parts of the femur perform different functions during regeneration. *Blood Cells 12*, 641–643 (1987).

Brecher, G., Beal, S.L., and Schneiderman, M. Reply to commentary: Renewal and release of hemopoietic stem cells: does clonal succession exist? *Blood Cells 12*, 127 (1987).

Clemons, G.K. Some endocrine aspects of renal and extrarenal erythropoietin in normoxic and hypoxic rats. Pages 177–186 in *Molecular and Cellular Aspects of Erythropoietin and Erythropoiesis*, I.N. Rich, ed., NATO ASI Series, Volume H8. Springer-Verlag Berlin Heidelberg (1987).

Esposito, M.S. Book Review: "Meiosis." P.M. Moens, ed., Academic Press, Orlando, Florida; 1987. (391 pp) *Cell 50,* 821–822 (1987).

Goth-Goldstein, R. and Hughes, M. Characterization of two CHO variants in respect to MNNG-induced cell killing, mutations, and repair of methylated DNA bases. Pages 447–451 in *Radiation Carcinogenesis and DNA Alterations*, F.J. Burns, A.C. Upton, G. Sillini, eds., Plenum Publ. Corp., New York (1986).

Ham, R.G., Hammond, S.L., Stampfer, M.R., and Bartley, J.C. Normal human mammary epthelial cells in serum-free medium. Pages 59–108 in *Growth and Differentiation of Mammary Cells in Culture*, J. Enami, ed., Japan Scientific Societies Press, Tokyo (1987).

Hanawalt, P.C., Bohr, V.A., Leadon, S.A., Mansbridge, J.N. and Reusch, M.K.H. Comparative analysis of cutaneous DNA repair *in vivo* and *in vitro*.. Pages 217–231 in *Proceedings of 4th U.S.-Japan Conference on the Processes in Epidermal Differentiation*, I. Bernstein and T. Hirone, eds., Praeger, New York (1987).

Hosoda, J., Holbrook, E.L., Moise, H., Bjornstad, K., Maleas, D., and Esposito, M.S. Fractionation of DNA metabolic proteins of *Saccharomyces cerevisiae* by DNA cellulose chromatography: SSB-1, ssDNA-dependent ATPase, DNA polymerase, DNA primase, topoisomerase I, and resolvase. Pages 171–192 in *Biological Research on Industrial Yeasts*, Volume II; G.G. Stewart, I. Russell, R.D. Klein, and R.R. Hiebsch, eds., CRC Press, Inc., Boca Raton, Florida (1987).

Klitz, W., Kuhner, M.K., Robinson, W.P., and Esposito, M.S. Analysis of genetic and serological traits typed in multiply affected IDDM families. Presented at NIH-NATO-INSERM Advanced Research Workshop, September 1987. *Genetic Analysis Workshop 5,* 1–5 (1987).

Leadon, S.A. Immunological probes for lesions and repair patches in DNA. Pages 331–336 in DNA Repair: *A Laboratory Manual of Research Procedures*, Volume III, E.C. Friedberg and P.C. Hanawalt, eds., Marcel Dekker, New York (1987).

Singer, B., Spengler, S.J., Chavez, F., Sagi, J., Kusmierek, J.G., Preston, B.D., and Loeb, L.A. O-alkyldeoxythymidines are recognized by DNA polymerase I as deoxythymidine or deoxycytidine. Pages 37–40 in *N-Nitroso Compounds: Occurrence, Biological Effects and Relevance to Human Cancer*, J.K. O'Neill, et al., eds., IARC, Volume 84, Lyon (1987).

Stampfer, M.R. and Bartley, J.C. Growth and transformation of human mammary epithelial cells in culture. Chapter 20 in *Cellular and Molecular Biology of Experimental Mammary Cancer*, D. Medina, W. Kidwell, G. Heppner, and E. Anderson, eds., Plenum Publishing Corp., New York (1987).

LBL REPORTS ISSUED

Hosoda, J., Bell, M., Bjornstad, K., Hosobuchi, M., Moise, H., and Esposito, M.S. Single-strand specific DNA binding proteins of *Saccharomyces cerevisiae*. Lawrence Berkeley Laboratory report LBL-22091 (1986).

Section 3. Radiation Biophysics

The Radiation Biophysics Group brings an interdisciplinary approach to understanding both the harmful and beneficial effects of a large variety of ionizing and nonionizing radiations. This understanding is being developed through fundamental studies at all levels of biological organization — the physical, chemical, molecular, cellular, tissue, and organ levels. The ultimate goals are 1) to determine the health risk from very low levels of radiation such as those found in space, or the natural and occupational environments; 2) to develop procedures to mitigate the risks due to long term radiation exposures; and 3) to optimize the utilization of different qualities of radiation for the treatment of cancer and certain non-neoplastic brain disorders.

The research activities related to these goals are quite broad in scope. The formal training or background of each member of the group is in either physics, chemistry, or biology. However, over the years, several have crossed their boundaries and extended themselves into other areas. The members and their affiliated activities are shown below.

Our main interest in nonionizing radiations concerns the biological effects of static magnetic fields and radio-frequency (rf) radiation. A new 9.0-tesla (90,000 gauss) superconducting magnet facility has recently been installed to study the responses of cellular, tissue, and animal systems when exposed to such ultrahigh magnetic fields.

Ionizing radiation studies center around the Bevalac, a unique source of energetic heavy particles that is capable of accelerating ions of masses ranging from hydrogen to uranium. These accelerated ions are extremely valuable for probing various cellular properties. In addition, some of these ions are currently used in cancer therapy and in treatment of certain brain disorders. Many basic radiobiological studies are being extended to understand the health effects of alpha particles (energetic helium ions) emitted from the decay products of radon gas. Radon, a natural pollutant, is of national concern because of its effect in inducing lung cancer. The central focus of research activities in ionizing radiations will continue to be the elucidation of the effects of heavy charged particles in biological materials at various levels of organization. It is becoming increasingly clear that the knowledge gained from particle studies can improve the understanding of the effects of x rays and gamma rays in biological materials.

Physicists are engaged in research related to 1) the qualitative and quantitative aspects of the physical nature (charge, mass, energy loss, etc.) of radiation fields associated with heavy charged particles, and 2) the energy deposition patterns within regions equivalent in size to cellular dimensions. This information is essential for basic studies as well as for planning radiation exposure in clinical applications, and for ensuring the radiologic safety of personnel in space.

The information obtained from physical studies then becomes the basis for evaluating chemical changes in a biological target. The end result is establishing a better quantitative relationship between the radiation quality and the initial cellular damage.

The DNA inside the cellular nucleus is considered to be the most critical radiological target because it contains all the genetic information. Any chemical change in this important molecule has far reaching biological consequences. Chemical changes associated with a given site (sugar or base) on a DNA molecule caused by ionizing radiation have been considered through two mechanisms: 1) by hydroxyl radicals produced from water in the cell, and 2) by direct deposition of energy on the DNA itself. These two mechanisms then define the molecular nature of the damage and become the starting point for our studies in molecular radiobiology.

Research in molecular radiobiology is concerned with investigation of the repair, misrepair, and unrepair of the various types of damage to mammalian DNA caused by ionizing radiation. Chromatin and chromosome breaks are also included in these studies. The central problem is the identification of those initial chemical changes that lead to either mutation or transformation if not repaired adequately. The chemists and molecular biologists work together to understand the correlation between chemical changes and their possible biological consequences. They exploit high-LET radiations to better understand the processes leading to repair or misrepair of radiation-induced lesions. Preliminary studies indicate that high-LET radiation causes a larger number of unrepaired (or possibly misrepaired) lesions per unit dose than do x rays or toxic chemicals. While most basic studies

in molecular radiobiology are done *in vitro*, the fundamental knowledge acquired is subsequently further studied in cellular environments.

One focal point in the overall research efforts by physicists, chemists, and molecular radiobiologists is understanding the responses of mammalian cells when insulted by ionizing radiation. They interact with the cellular biologists to analyze cellular data in terms of the fundamental physical, chemical, and molecular processes involved. Cellular radiobiologists are trying to understand the correlation between damage and repair processes in the cellular environment to characterize cell-cycle-dependent changes. They also try to understand the correlation between molecular changes in DNA and chromosomal changes. The overall research efforts of cellular radiobiologists pursue understanding of the relationship between formation of DNA adduct and cell transformation. Several current studies concern various biological end points, including acute dose-survival effects, cell progression delays, cellular repair, and transformation as a function of radiation quality (including nuclear fragmentation processes). A major emphasis is given to work with synchronized human cells. In addition to basic research, cellular radiobiologists are also providing important data for applications in clinical therapy. Cancer patients are being treated with heavy ions from the Bevalac (see Section 4, Research Medicine) and, before treatment planning can be done, it is essential that radiobiological data concerning cell killing, oxygen effect, and the efficiency of cell killing by the heavy charged particles in comparison to x rays or gamma rays are available. All this information is provided by the cellular radiobiologists in collaboration with radiation therapists.

Theoretical models are being developed and, as we learn more and more about the basic physical, chemical, and biological processes involving ionizing radiation, the time-evolution and the mechanistic aspects of radiation damage are becoming more apparent.

The section on *in vivo* biophysics describes research radiation effects at the tissue and organ levels. The objective is to obtain data to develop models for the assessment of health-risk and to elucidate mechanisms that relate lethal and nonlethal damage in *in vivo* systems to different qualities of radiation (natural and man-made). The focus is principally on carcinogenesis, *in vivo* cellular radiobiology, and early and late damage to tissues and organs where cell loss, altered function including metabolism, and regulation of cell proliferation are important. The *in vivo* biophysics program complements and extends the molecular and cellular studies conducted with pro- or eukaryotic systems *in vitro*: it uses organized tissues or intact rodents to address questions that cannot be studied productively *in vitro* where cell, tissue, and organ system interactions and homeostatic regulatory mechanisms are absent. However, much attention is being given to determination of the molecular and cellular basis for these tissue effects.

A strong component of this program is the application of accelerated charged particles in the treatment of cancer and for radiosurgery. It is important to assess possible damage to normal and healthy cells during this radiation therapy, and the evaluation of such damage to critical organs adjacent to a tumor volume to be treated by radiation is one of the special concerns in the *in vivo* biophysical studies.

ACTIVITIES OF THE RADIATION BIOPHYSICS GROUP

	Scientists	*Technical Staff and Graduate Students*
Physics		
Physical nature of high-LET radiation field (nuclear interactions), dosimetry associated with high-LET charged particles and magnetic fields	A. Chatterjee S. Curtis W. Holley W. Schimmerling T. Tenforde	
Transport of heavy ion beams	M.Wong	
Mechanism of energy deposition and track structure in water, DNA, and cells.		
Statistical fluctuation in energy loss for low dose studies.		
Chemistry		
Energy deposition and the initial yield of chemical species (•OH •H, etc.).	J. Afzal A. Chatterjee W. Holley	J. Scherer
Radical attack (•OH) on DNA, Chemical nature of DNA damage	R. Roots	
Excitation and ionization of DNA, chemical nature of DNA damage		
Molecular Biology		
Chemical nature of DNA damage and repair and misrepair, chromatin and chromosome breaks	E. Blakely M. Dixon R. Liburdy	K. Bjornstad P. Chang K. Goncz
Molecular characterization of mutation	R. Roots C. Tobias	E. Goodwin G. Ivery
Protooncogene activation and neoplastic transformation.	T. Yang	
Cellular Biology		
Damage and repair processes in a cellular environment; cell cycle effects	E. Blakely M. Decker M. Dixon	K. Bjornstad P. Chang K. Goncz
Human chromosome in a hybrid cell line	L. Hlatky A. Rodriguez	E. Goodwin G. Ivery
Role of protein synthesis	R. Roots T. Tenforde	
Role of intra- and extra-cellular matrix	C. Tobias T. Yang	

Continued on following page

	Scientists	*Technical Staff and Graduate Students*
***In Vivo* Biophysics**		
Molecular and cellular basis for tissue effects	J. Afzal J. Ainsworth	R. DeGuzman K. Kavanau
Tumor radiobiology and cell kinetics	E. Alpen S. Curtis	P. Powers-Risius
Cellular mechanism of early and late effects in critical organs	P. Durbin C. Gaffey R. Liburdy	
Carcinogenesis at low dose and low dose rates	A. Rodriguez T. Tenforde	
Effects of magnetic and electromagnetic fields		
Actinide element biokinetics		
Modeling		
Initial damage	A. Chatterjee S. Curtis	
Repair-misrepair model	C. Tobias	
Lethal and potentially lethal model		
Carcinogenesis		

Ionizing Radiation

RADIOLOGICAL PHYSICS AND RADIATION CHEMISTRY

Over the years, from experience in doing research with ionizing radiations, it has become very clear that studies with energetic charged particles (also called high-LET radiations) are extremely important for an overall understanding of biological effects. There are many intrinsic properties of cells that cannot be explored by using only x rays or gamma rays (also called low-LET radiations). Hence, a strong component of this program has been the utilization of accelerated charged particles from the Bevalac, a Lawrence Berkeley Laboratory national resource accelerator complex.

The Bevalac can produce energetic particles across the periodic table from helium to uranium. These particles can penetrate to depths of 30 cm or more in human tissue or in a tissue-like medium. For a given energy, each particle has a precise depth of penetration with little scattering as compared to x rays, and about 90% of the radiation dose is deposited near this stopping point. These features make such particles especially useful (as compared to x rays) for the treatment of localized tumor volumes. However, physical processes associated with these particles, such as their microscopic energy deposition patterns or the occasional break-down of their heavy nuclei during propagation, introduce complexities that must be understood for optimal utilization.

In FY 1987, these physical processes were investigated through experimental and theoretical studies. Specifically, results were obtained on the break-down, or nuclear fragmentation, of 670-MeV/u neon ions. At this energy these ions penetrate a depth of about 32 cm in water (a tissue-like me-

dium). Along their flight-path, some of the neon nuclei break down into protons, carbon, oxygen, etc., with the resulting nuclei having mass numbers lower than neon. The extent of fragmentation depends upon the parent nucleus and the depth of the medium traversed. This research involves identification of each of the fragments at a given depth, and thereby provides information on the spectral nature of the radiation field.

Analysis of fragmentation data for 670-MeV/u neon nuclei in a water absorber at the Bevalac Biomedical Facility has continued. An identification algorithm for particle charge was developed based on the relationship between average energy loss in a thick detector and the stopping power calculated for a proton using the measured time of flight (TOF). With this algorithm, fluence spectra (i.e., number of particles per unit area) were obtained for particles with charges between Z = 4 (Be) and Z = 10 (the primary neon and its isotopes) as a function of water-absorber thickness. At each depth the number of particles per square centimeter emitted with a given value of linear energy transfer (LET) was obtained. Typical LET spectra at the entrance and at the Bragg peak of neon, are shown in Figs. 3.1 and 3.2. At the entrance to the Bragg curve the LET spectra are narrow, even for the fragments accompanying the beam. These fragments are due to residual material in the beam line such as vacuum windows, beam flattening lead foils, etc.

The measurement of radial distribution of energy around a charged particle trajectory is of

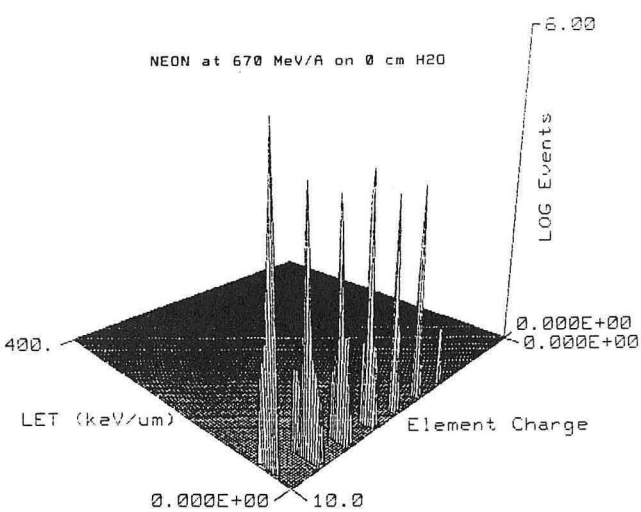

Fig. 3.1. LET spectra of neon at 670 MeV/A incident on a water column; beam contaminants,also shown, are present at the 1% level. (XBL 811-111)

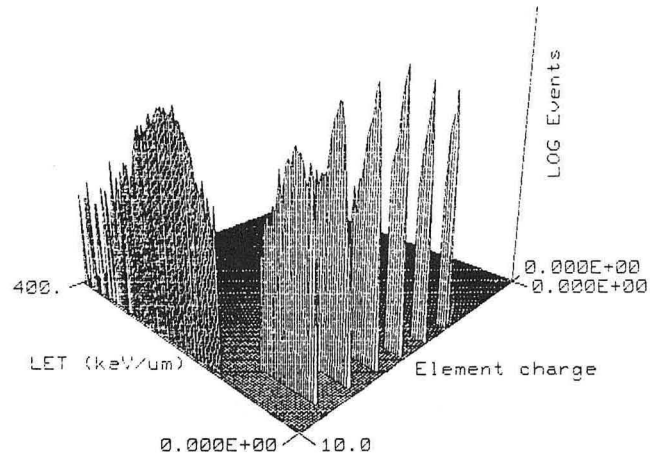

Fig. 3.2. LET spectra of neon and fragments produced after 32 cm of water on which neon was incident at 670 MeV/A. (XBL 881-110)

primary importance to the overall research effort. Recently Metting and co-workers from Battelle Pacific Northwest Laboratory completed an analysis of single-event energy deposition distributions measured in a 1.3-μm diameter site, using iron beams extracted into the Bevalac Biomedical Facility. These had been measured as a function of radial distance *b* from the trajectory of 600-MeV/u iron ions. Specific energy $(\bar{z}_b)_F$ spectra of single energy deposition events, and the frequency mean $(\bar{z}_b)_F$ were obtained as function of *b*. Figure 3.3 shows the experimentally determined values of $(\bar{z}_b)_F$, where the width of each rectangle indicates the range of *b* over which each $(\bar{z}_b)_F$ was averaged to obtain adequate statistics, and where the height of each rectangle is based on the number of events detected. Beyond 5 μm, $(\bar{z}_b)_F$ is determined mainly by single electrons, whose energy spectrum no longer changes appreciably as a function of *b*. These single-electron events occur more rarely, but when they do, the energy they impart in a microscopic volume can be significantly greater than the average absorbed dose, calculated as $D(b) = R_b(\bar{z}_b)_F$ (where R_b is the number of events at the same distance *b*) and also is shown in Fig. 3.3 to be in substantial agreement with homogeneous track models.

Heavy nuclei undergo multiple scattering during their passage through matter. A quantitative understanding of this physical process is needed, primarily for purposes of dosimetry. The physicists are involved in measuring these scattering phenomena in order to make comparisons with

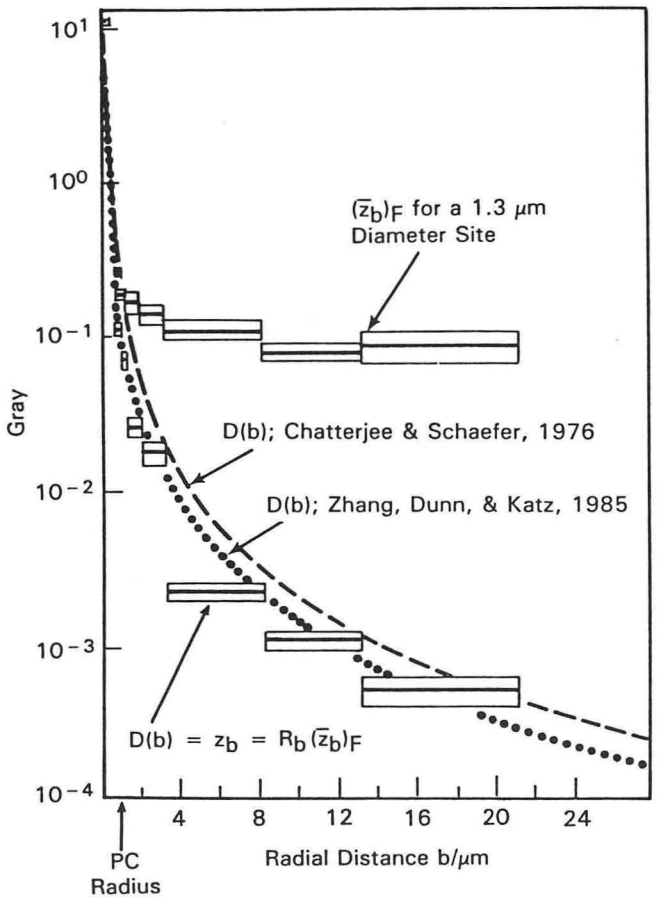

Fig. 3.3. Single-event mean specific energy $(\bar{z})_F$ and radial absorbed dose (rectangles) and homogeneous track structure predictions (curves). (XBL 881-113)

the existing theoretical formulae. The multiple scattering studies are categorized as 1) measurement of heavy charged particle multiple scattering angular distributions, 2) development of calculational methods to compare the results of experiment with multiple scattering theory, and 3) calculation of the loss of particles to multiple scattering in nuclear fragmentation experiments.

Measurements of the multiple scattering of ~600-MeV/u beams of neon, iron, and uranium ions in targets of water, aluminum, copper, and lead have been made. Position-sensitive detectors (psd's) are used to determine the spatial trajectories of individual particles before and after target scattering. The angle through which an incident trajectory is deflected is then a measure of the multiple Coulomb scattering of the beam particle by the target nuclei. In this method there is no physical collimation of the beam, so that possible effects of collimator edge scattering or particle fragmentation are eliminated. The method is also independent of beam divergence.

The focus is an analysis of data obtained for the most massive particle accelerated at the Bevalac, uranium, to provide a stringent test of the theoretical descriptions of the multiple scattering of very heavy charged particles relative to those for protons.

The psd's make possible differential measurement of the multiple scattering deflection angle. A computer simulation of the experiment using Monte Carlo techniques has been made to allow detailed studies. In this simulation, individual particles are tracked through the system, with the effects of particle energy loss, multiple scattering, and detector resolution all taken into account. The overall angular resolution of the system is measured with the "target-out data." The conclusion from this analysis of uranium data is that the standard theory of multiple Coulomb scattering for elementary charged particles appears to describe adequately the scattering of very heavy charged particles from target nuclei.

To understand the chemical stage in the evolution of radiation-induced damage, an attempt has been made to understand the effects on biological material at the molecular level by studying the physical phenomena of the energy deposition process and the subsequent physico-chemical and chemical processes leading to DNA strand breaks. Both the indirect and direct mechanisms of damage have been studied theoretically. Initial studies were confined to a linear form of DNA, but during the past year a systematic study of the effects of higher order structures in the formation of damage has been started.

In conjunction with the theoretical studies above, the experimental program aimed at testing and verifying the theoretical models and, in particular, attempting to understand the detailed mechanism involved in radiation-induced DNA strand breaks have been continued.

Theoretical Studies

The earlier work—studying the indirect effects of radiation on isolated DNA using SV40 viral DNA in dilute aqueous solution as a model system—has continued. These calculations involve the following main features: 1) computer simulation of the SV40 DNA molecule using standard geometric stereochemical parameters (obtained from x-ray diffraction studies); 2) simulation of the production of OH

radicals and other water radiolysis products around the DNA by the track of an ionizing particle; and 3) simulation of the diffusion of the radicals and their reactions with each other, with other scavenging agents in the solution (Tris buffer), and ultimately with the DNA molecule. Reactions with the deoxyribose ring lead to strand breaks while reactions with the bases lead to other forms of damage.

These studies have been carried out using a series of Monte Carlo computer codes to simulate the actual process. The probabilities of single strand break (SSB) formation for a variety of incident radiation qualities and scavenger concentrations (to mimic the cellular environment) have been calculated.

During the past year, these calculations have been extended to include the effects of the presence of associated proteins by studying the effects of nucleosomes (see Fig. 3.4) on the probability of strand break formation. The results are given in Table 3.1. The presence of the histones reduces the probability of single strand break formation by approximately a factor of two for the DNA that is in contact with the proteins. When moving away from the histones onto the linker DNA the probability of strand breaks gradually increases until it reaches approximately the uncomplexed DNA value after about 170 base pairs. Future studies will investigate the effects of organized groups of nearby nucleosomes to more closely simulate the complex structure of chromatin.

The development of computer codes to model the direct action of radiation on DNA has also continued. This model is based on concepts of track

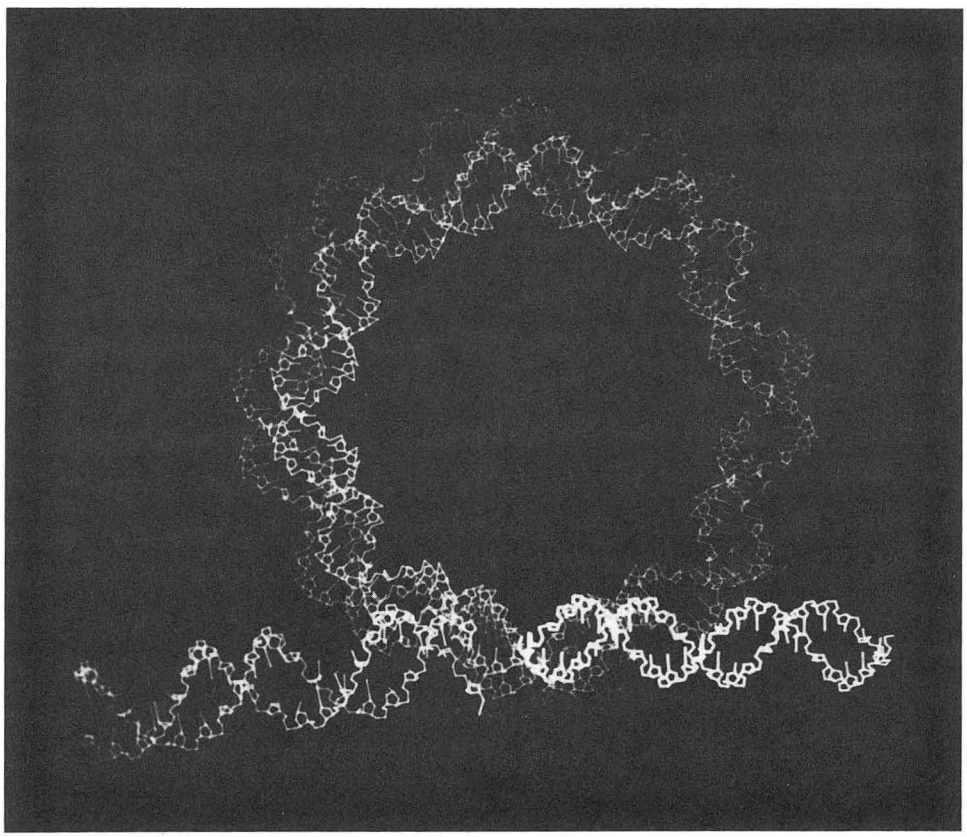

Fig. 3.4. A computer graphic representation of a DNA molecule wrapped around a central histone core, which is not visible in this figure. Such a representation has provided us with a three-dimensional consideration of damage caused by the diffusive motion and subsequent attack by water radicals. Based on theoretical calculations, it appears that the histone protects the DNA from damage by a factor of two when compared to similar damage to DNA without histone. However, the linker part of the DNA is not protected to any significant extent by the presence of histone. (CBB 869-7725)

Table 3.1. Comparison between B-DNA with and without histones.

DNA structure	$\langle P \rangle_{sugar}$	$\langle P \rangle_{base}$	% sugar attack	% base attack
Linear (No Histones)	4.70×10^{-3}	1.83×10^{-2}	20.0	80.0
Linker 1 (171 Base Pairs)	4.59×10^{-3}	1.90×10^{-2}	19.5	80.5
Nucleosome (210 Base Pairs)	2.04×10^{-3}	7.18×10^{-3}	22.1	77.9
Linker 2 (171 Base Pairs)	4.10×10^{-3}	1.87×10^{-2}	18.0	82.0

structure, stopping-power theory, and the Bragg rule. Monte Carlo computational techniques are used to treat both glancing and knock-on collisions.

Previous studies made use of a simple smooth radial energy distribution to calculate the direct effects of the penumbra (knock-on electrons). During the last year, these calculations have been incorporated into a more detailed model for electron interactions.

Furthermore, these electron results have been combined with the results for the core of heavy-ion tracks to calculate the single- (SSB) and double-strand break (DSB) yields as functions of LET for a series of particles.

Strand-break production in oxygenated cells is generally considered to be due mainly to indirect effects at low LET and to direct effects at high LET. The calculated yields (normalized to breaks rad^{-1} $dalton^{-1}$) in Fig. 3.5 shown as solid lines (direct) and dotted lines (indirect) are compared in the adjacent plot with a selection of experimental measurements of radiation-induced primary single- (SSB) and double- (DSB) strand-break yields as functions of LET. In addition, recent results for the yields of chromatin breaks are also shown. The satisfactory agreement of the theoretical results with experimental data suggests that most of the important effects are at least approximately accounted for in these calculations.

In addition to the indirect effect studies, there is also an interest in looking at the influence of the higher order organization (nucleosome, chromatin, and eventually chromosome) of DNA in cellular nuclei on directly induced strand-break yields and on the spatial distribution and correlations of the damage along the DNA chain.

Experimental Studies

Through collaboration with Dr. G. Kraft (GSI, Germany), data have been accumulated on the formation of strand breaks in viral DNA irradiated in dilute aqueous solution (pH 7.6) with a large

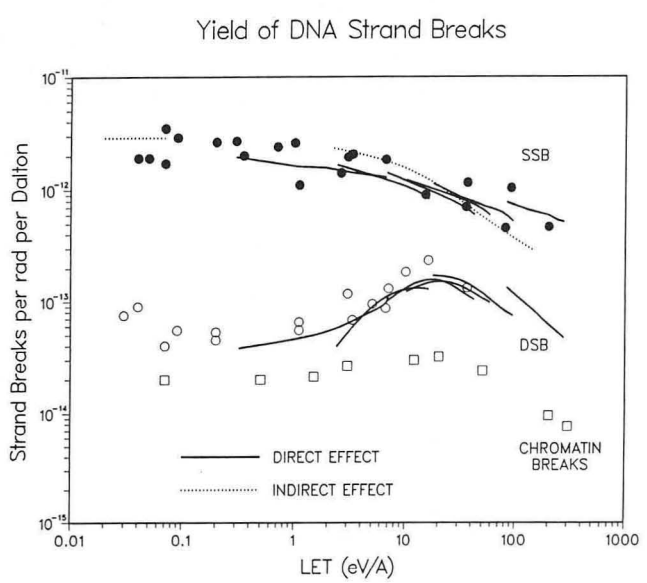

Fig. 3.5. *Theoretical yields of DNA strand-breaks in cells for direct effects (solid curves) and indirect effects (dotted curves). For comparison selected experimental measurements are shown for yields of single-strand (•), double-strand (o), and chromatin (□) breaks. (XBL 881-112)*

number of charged particles, ranging from helium to uranium. A plot of the DSB/SSB ratios plotted against LET for several ion species is shown in Fig. 3.6. It becomes evident that a biological effect that varies because of radiation quality must be studied separately for each particle species. Data collected should cover a range in velocities for each particular ion species, with a series of curves thereby obtained. The number of DSBs relative to the number of all breaks (or SSBs) increases as the LET of the specific ion species increases, as shown with SV40 DNA irradiated in a buffered solution. However, this same relationship also holds true for irradiation of mammalian cellular DNA with alpha particles, shown by the dashed line in Fig. 3.6.

Aloke Chatterjee, William Holley, and Ruth Roots.

MOLECULAR AND CELLULAR STUDIES

In the field of molecular radiobiology, the efforts are focused in three areas: 1) detection of radiation-induced DNA damage and repair; 2) LET dependence of chromatin breaks and rejoining; and 3) evaluation of neon-ion-induced rearrangements in the single human chromosome using a dual species-specific fluorescence hybridization method.

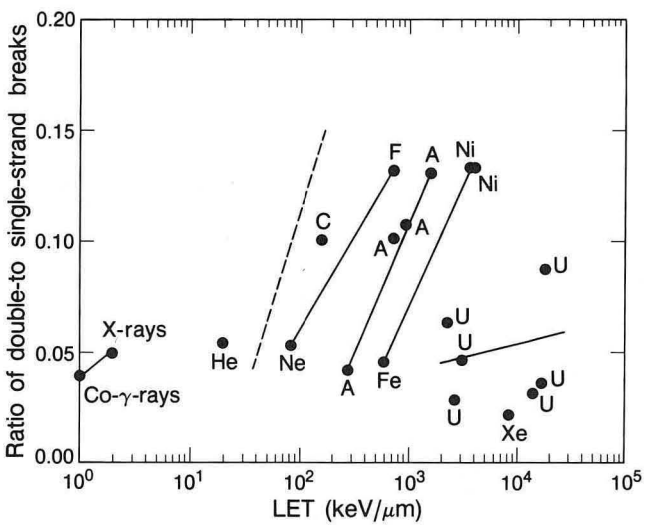

Fig. 3.6. Measurements of the yields of DNA, DSB, and SSB as a function of ionization density (keV/μm). A variety of ion species were used, ranging from alpha particles to uranium. Particle energies at the DNA target ranged from 5 to 900 MeV/u, approximately. Data obtained for DNA irradiated in solution are represented by solid lines. The dashed line represents data obtained for mammalian cellular DNA irradiated with alpha particles. These data were calculated from a publication by Kampf and Eichhorn, 1983. (XBL 881-7219)

In each of these studies, heavy charged particles have been used and the comparison of the data with measurements from x rays are in progress. A brief summary of each of the studies is reported here.

Detection of Radiation-Induced DNA Damage

In these experiments intact cells were irradiated and assays of the damage and repair processes were done by pulsed-field-gradient electrophoresis techniques that have been successfully employed to separate restriction fragments ranging from 50 kb to 3000 kb. The objective is to study the effect of radiation-induced DNA strand breakage and rejoining in normal and repair-deficient synchronous and asynchronous human and Chinese hamster (CHO) cells. The restriction enzymes used include the eight-base cutters NotI, SfiI and six-base cutters MluI and EagI. Preliminary results using LKB Pulsaphor electrophoresis equipment in conjunction with a unique Pulsewave switcher from BioRad indicate that DNA preparation is a critical step in obtaining consistent repeatable results. Factors include age of cells, control of trypsinization, grade of agarose employed, temperature used in each procedure, and the use of sterile quality-grade solutions to avoid shearing the DNA samples. The human lymphoblastoid cell line TK6, irradiated with 320-MeV/u silicon ions has yielded results that show a dose-dependent banding and show repeatedly that with or without irradiation there is a different restriction pattern with NotI, SfiI, and EagI than with hamster or other human-cell lines. Work is in progress to determine if these different restriction patterns are due to differences in radiosensitivity, or are an artifact of cell preparation, methylation, or incomplete digestion with enzyme. Breakage and repair of specific TK6 fragments are being studied by probing with a thymidine kinase gene using Southern procedures to identify molecular alterations due to radiation exposure and to determine if repair incubation periods will allow restitution of the radiation-induced changes. In addition to these studies, results from irradiated wild-type and temperature-sensitive CHO cells are being analyzed and show a disappearance of a band with heat following irradiation. Synchronous G_1 cells with and without irradiation run more completely out of the well and down the gel than do the asynchronous cell populations. Therefore, future research will involve synchronous cell populations in G_1 phase to evaluate dose-dependent DNA damage and repair.

LET-Dependence of Chromatin Breakage and Rejoining

The RBE for cell survival is well known to be LET-dependent, first rising with increasing LET to a broad peak in the 100–200 keV/μm range and then steadily decreasing. If the postulate that chromatin breaks are the only lesions that influence cell survival is accepted, then the premature chromosome condensation (PCC) technique can be used. This allows one to fuse an irradiated cell with a mitotic inducer cell, prematurely condense the chromatin of the test cell, and examine chromatin breaks in individual interphase cells within 30 minutes after irradiation, permitting evaluation of the chromatin damage before it is altered by the processes of repair and cell cycle progression. Three hypotheses to explain why the RBE for survival is a function of LET can then be examined. These hypotheses, which are not mutually exclusive, are that 1) the initial number of chromatin breaks produced per cell per cGy is LET-dependent, that 2) high-LET lesions are less repairable than low-LET lesions either because there is an LET-dependent fraction of the initial chromatin breaks that cannot be rejoined by cellular repair mechanisms, or because high-LET-induced lesions are more likely to be misrepaired, and that 3) clustering of lesions (the production of multiple chromatin breaks per cell by single high-LET particle traversals) may affect the efficiency of cell killing. Results from the ongoing study with the PCC system indicate that the RBE for survival vs. LET curve reflects an LET dependence on the initial number of lesions per cGy, but this alone may not fully account for the magnitude of the RBE at 10% survival in radioresistant cell lines. A comparison between survival and chromatin breakage RBE values is shown in Fig. 3.7 for radioresistant T-1 cells, hamster cells of intermediate sensitivity, and radiosensitive A-T cells. Beyond ~100 keV/μm, the survival RBE consistently exceeds the chromatin breakage RBE in the radioresistant T-1 and hamster cell lines, but not in the radiosensitive A-T cell line. There appears to be a slow or nonrejoining fraction of chromatin breaks that increases with increasing LET, and clustering of chromatin breaks at high LETs resulting in non-Poisson distributions of initial lesions has been demonstrated. The average number of chromatin breaks produced by a single particle passing through a cell nucleus was found to be a sigmoidal function of LET. At ~65 keV/μm, each particle yields an average of one chromatin break per cell in the hamster cell system. In the high-LET region above 65 keV/μm, single particles produce multiple chromatin breaks—a process known as clustering of radiolesions. These investigations should provide a more quantitative explanation of the LET dependence of the survival in both radioresistant and radiosensitive cell lines.

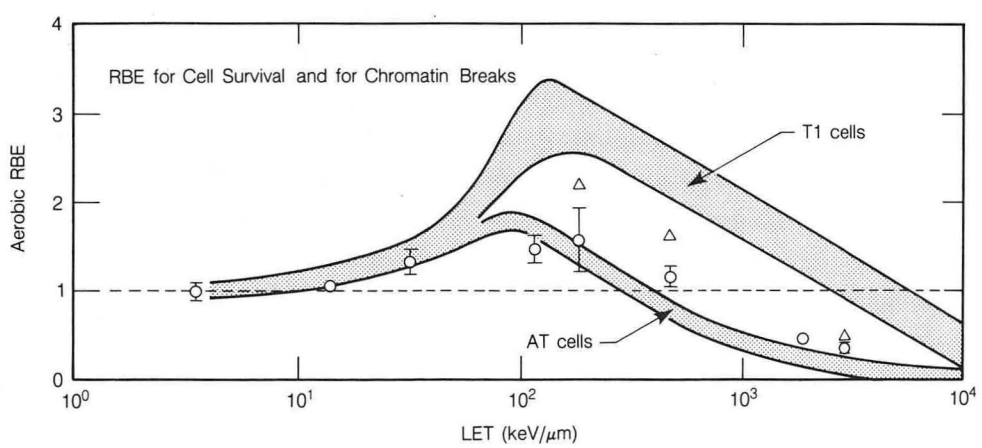

Fig. 3.7. *Comparison between survival and chromatin breakage RBEs. For CHO cells, circles (o) and triangles (Δ) indicate RBEs for chromatin breakage and survival, respectively. Only the envelopes for the previously reported T1 and AT cell survival RBEs are shown (no PCC data are available for T1 and AT cells). Beyond ~100 keV/μm the survival RBE consistently exceeds the chromatin breakage RBE in the radioresistant T1 anc CHO cell lines, but not in the radiosensitive AT cell line. (XBL 877-10828)*

Evaluation of Neon-Ion Induced Rearrangements in a Single Human Chromosome Using a Dual Species-Specific Fluorescence Hybridization Method

Experiments using a human-hamster cell line that has a karyotypically stable hamster genome containing a single copy of human chromosome number 2 have been initiated in which plateau phase cultures have been irradiated with single doses of Bragg-peak neon ions at an LET of 183 keV/μm and are processed with the premature chromosome condensation technique either immediately or after a 37°C incubation period of up to 8 hours. Fixation and dual-fluorescence staining then permitted a scoring of the immediate number of human chromosome fragments produced and an evaluation of rejoining events during the post-irradiation repair period. Preliminary results indicate a dose-dependent increase in production of neon-ion-induced fragments and a time-dependent decrease in the total number of fragments. There is also evidence for a time-dependent increase in illegitimate fusions between human and hamster chromatin. Results of these experiments are to be compared to x-ray studies that are in progress.

In cellular radiobiology, fundamental research as well as research applicable to radiation therapy continue to be carried out, using high-LET and low-LET radiation qualities. The various studies initiated were 1) the effects of clastogenic factor on normal cells irradiated with x rays, 2) the role of protein synthesis in repair of lesions, 3) the effects of cell cycle and survival of synchronized human cells when irradiated with split doses of heavy ions, and 4) clinical radiobiology. A brief summary of each follows.

Effects of a Clastogenic Factor

A diffusible clastogenic factor in the culture medium of ataxia telangiectasia (A-T) cells that increases the incidence of chromosome aberrations of normal cells cultivated with this medium has been reported. This clastogenic factor is a peptide with a molecular weight of 500 to 1000 daltons. Conditioned media from both A-T and normal fibroblasts were collected after 8 days of growth when the clastogenic factor was reported to be maximum. These media were used to cultivate normal fibroblasts transferred to the conditioned media either 3 days before or just before irradiation. In both cases, the irradiated cells were trypsinized and plated into the conditioned media, which were then removed after 3 days and replaced with fresh media. Preliminary studies indicate there is an increased x-ray sensitivity of 20–30% (at 1% survival) for normal cells grown in A-T conditioned medium presumably containing this clastogenic factor compared to the controls cultivated with either normal conditioned or fresh unconditioned media. This effect was most pronounced when the cells were grown in the conditioned media prior to irradiation. This clastogenic factor is being isolated from the conditioned medium by a series of filtration steps to be used for further studies.

Role of Protein Synthesis

CHO wild-type cells (SCI) and temperature-sensitive mutants (TSHI) have been subjected to 42°C continuous heat treatment and assayed for heat shock proteins (hsps) using one-dimensional polyacrylamide gel electrophoresis. Autoradiograms indicate that constitutive levels of proteins in the two cell lines are identical, but upon heat shock, SCI have elevated levels of heat shock proteins and TSHI do not. If the cells were subjected to a trigger dose of 5 minutes at 45°C, then incubated at the permissive temperature of 35°C for up to 5 hours, both cell lines showed hsps. A parallel experiment with a trigger dose of 5 minutes at 45°C, followed by incubation at the nonpermissive temperature of 40°C for up to 5 hours, showed that SCI cells have hsps but the TSHI cells do not. In another experiment the temperature-sensitive mutant and wild-type cells were each exposed to a priming dose of radiation to kill down to 10% survival (4.5 gray of 150-kVp x rays or 2.0 gray of neon) and heated to 41.5°C for up to 6 hours. The temperature-sensitive mutant cells heated to inhibit their protein synthesis indicated an additive response with the radiation killing but with no synergism, whereas the same experiment with wild-type cells showed the expected enhanced cell killing reported in the literature for both radiation qualities. This suggested that protein synthesis plays an important role in the repair of lesions produced by high- and low-LET radiations. Lack of protein synthesis protects the mutant cells from the combined effects of the two deleterious treatments. Hyperthermia following radiation is more effective when the radiation is low-LET than when it is high-LET; this points to differences in the types or quantity of lesions produced or in the mechanisms of repair. Preliminary survival results also indicate that thermotolerance is still expressed in the wild-type cells and is absent in the mutant cells after chronic exposure to heat post-irradiation,

but confirmatory studies still have to be carried out using polyacrylamide gel electrophoresis.

Effects of Cell Progression Kinetics and Survival of Synchronized Human Cells Irradiated with Split Doses of Heavy Ions

The rationale for this work is to extend early hamster cell work that indicated 1) a lack of split-dose recovery and perhaps even a potentiation of cell killing with dose fractionation of neon Bragg-peak ions and 2) a lack of independent action of sequential doses of high and low-LET radiations. There is particular interest in the cell-cycle-dependent kinetics of these dose fractionation effects in a human cell with longer cell-cycle times. Figures 3.8 and 3.9 summarize the results. Figure 3.8 (A) illustrates split-dose survival kinetics of asynchronous cell populations irradiated with two low-LET or two high-LET doses. Figure 3.8 (B) illustrates similar data obtained with cell populations synchronized either in the middle of G_1 phase or S phase. Recovery occurs in the exponentially growing cells irradiated in the plateau, but not in the Bragg peak, resulting in an enhanced peak-to-plateau differential effectiveness with dose fractionation. Figure 3.9 summarizes data obtained from synchronized cell populations irradiated with a sequence of high-LET radiation followed by low-LET radiation. The sequential doses of neon Bragg-peak and plateau ions administered within several hours can result in human cell killing that is greater than expected from the independent action of each radiation. The cell-cycle-dependent sensitivity to sequential doses of high-LET and low-LET radiations can be further modified by cell progression to more radiosensitive or radioresistant cell cycle phases occurring with elapsed time between the two doses. Future extensions of these experiments are planned that will be of value to improved clinical dose fractionation schemes.

Clinical Radiobiology

Several cellular experiments have been completed by members of the Radiobiology Group to directly support clinical radiotherapy with heavy-ion beams. These included studies of enhanced biological effectiveness of particle radiotherapy beams controlled by magnetic wobbling and an evaluation of the potential of combined chemotherapy with cisplatinum and particle treatment. The latter investigation has been completed by Mary Decker, a UCSF Radiation Oncology Resident, who is working 50% time in the heavy-ion radiobiology experimental program.

Eleanor Blakely, Cornelius Tobias, Tracy Yang, Martha Dixon, Edwin Goodwin, Polly Chang, Kathy Bjornstad, Gayla Ivery, and Kaarin Goncz.

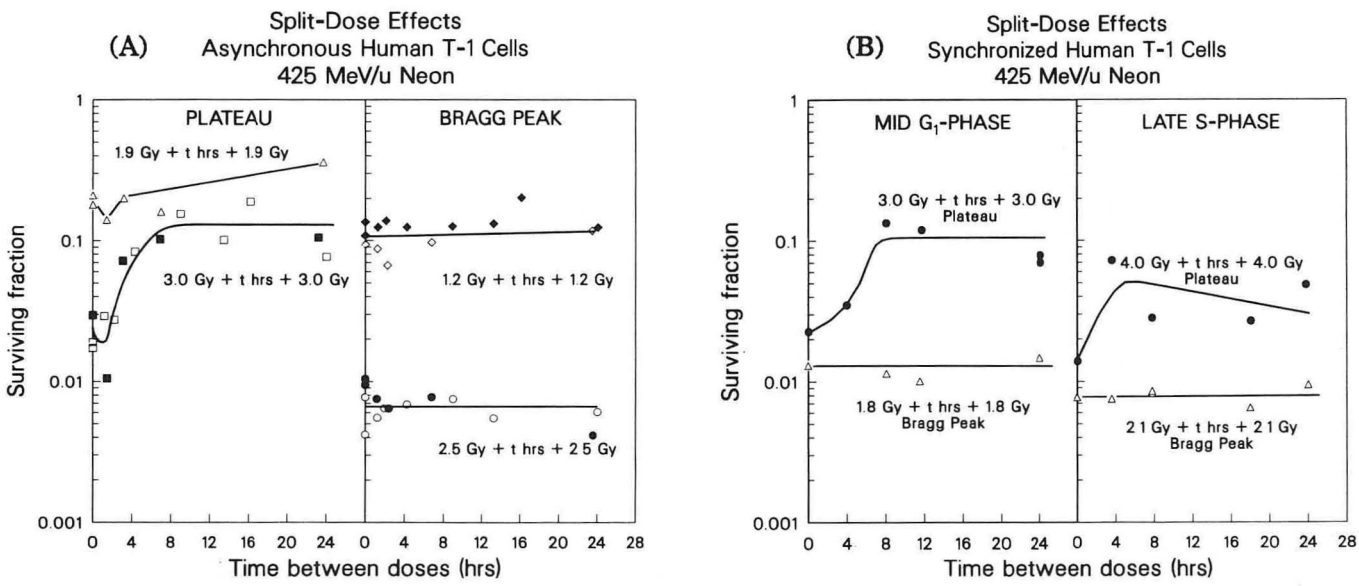

Fig. 3.8. *Split-dose effects of asynchronous and synchronized human T-1 cells. (A) Complilation of data from replicate experiments to investigate split dose effects of 425-MeV/u neon plateau or Bragg-peak ions on asynchronous human T-1 cells. The data show dose-dependent recovery in the plateau, but relatively negligible recovery in the Bragg peak. (B) Effects of 425 MeV/u neon-plateau (•) or Bragg-peak (Δ) ions on synchronized cell populations in mid G_1 phase or late S phase at the time of the first dose. The data show split-dose recovery with plateau and a lack of recovery with Bragg-peak ions. [(a) XCG 872-6773, (b) XCG 872-6778]*

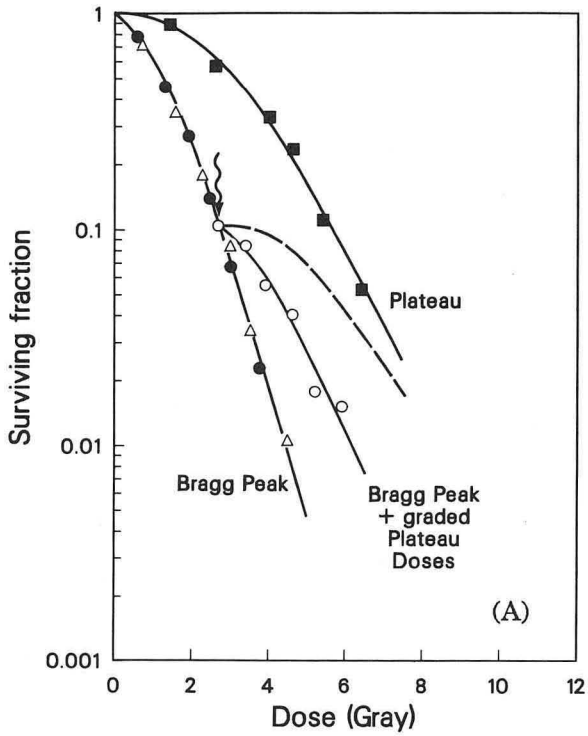

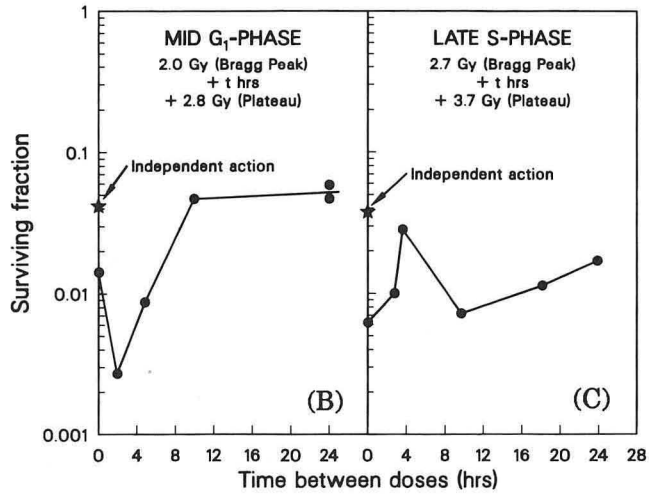

Fig. 3.9. *Comparisons of high-LET and low-LET radiations. (A) Late S-phase human T-1 cells (425-MeV/u neon). Complete dose-response curves for late S-phase cells cooled to ice temperature and irradiated with single doses of plateau ions alone (■) or single doses of Bragg-peak ions alone (•). Some cells were also irradiated with Bragg-peak ions at room temperature (Δ). Also shown are the survival data for cooled cells irradiated sequentially with 2.7-Gy Bragg-peak ions followed within 2 minutes by graded doses of plateau ions (o). The survival of this last group was significantly less than that expected from the independent action of the two radiations (---). (B) Mid G_1-phase and (C) late S-phase or late S phase at the time of a first dose of Bragg-peak ions followed at various times by a dose of plateau ions. The stars represent the survival level expected from the independent action of each radiation. The data show that G_1-phase cells are more sensitive than expected and become even more radiosensitive with a 2-hr interval between the two doses as the cells move to the G_1/S border. The cells then show increasing radioresistance that levels off with an 8-hr fractionation interval. The late S-phase cells are also much more sensitive than expected with the combined radiation treatment, but become more resistant with split-times up to 4 hr and then more radiosensitive when the cells divide and enter G_1 phase (confirmed by flow cytometry). [(a) XCG 872-6774, (b) XCG 872-6776]*

THEORETICAL MODELING OF CELLULAR AND MOLECULAR EFFECTS

The experimental program has been accompanied by the development of mathematical models. A goal is to describe the essential nature of processes that take place when ionizing radiation or other environmental variables perturb the mechanisms that control cell progression and proliferation. One such model is the "repair misrepair (RMR) model," which has been under development for several years. Its central theme is that cells attempt to repair injuries in their own genome using enzymatic processes: macroscopic expressions of observable effects are the consequences of misrepair, defined as the inability to finish the repair process, or the occurrence of molecular mistakes as this process occurs.

Another model that has been developed is the "lethal-potentially lethal (LPL) model." The difference between it and the RMR model is that the former assumes two distinct classes of lesions, irreparable (lethal) and repairable (potentially lethal), while the RMR model assumes one type of lesion that is initially "uncommitted" and whose fate is determined by lesion interaction and the fidelity of the repair process. One consequence of the LPL model is that sublethal and potentially lethal damage repair are manifestations of the same repair process.

The intent is to examine various mechanisms that may occur in interactions between the progeny of transformed cells and the tissues of the living organism. It must be kept in mind that, while developing quantitative approaches for modeling transformation processes, the events leading to cell division and proliferation are statistical processes.

Aloke Chatterjee, Cornelius Tobias, and Stanley Curtis.

CELL TRANSFORMATION AND SOMATIC MUTATION STUDIES

The induction of neoplasms and of somatic mutations are two of the major damaging effects of ionizing radiation. Our focus is to determine how effective energetic heavy charged particles (primary cosmic rays) are in producing these effects. Using the results from these studies, it may be possible to assess potential risk for space workers on a long-term space mission.

Low Dose Rate Effects

The oncogenic effects of high-LET radiation, using accelerator-produced heavy-particle radiation and mouse embryo cells (C3H10T1/2), have been studied for many years. The exposure dose rate of space travelers is very low, less than 1 cGy/min, and thus it is important to have data on this low dose rate of heavy ions for risk assessment. The earlier dose-rate studies with energetic iron particles (600 MeV/u, 200 keV/μm) indicated an enhancement effect of low dose rate (2 cGy/min) for cell transformation, as shown in last year's Annual Report. In FY 1987 the dose-rate studies have been extended to other ions, and LETs and dose response curves for 425-MeV/u neon and 400-MeV/u argon ions have been obtained. A similar enhancement effect for cell transformation was observed for argon ions, but not for neon particles. These results clearly suggest that the low-dose-rate effect for cell transformation is LET-dependent, enhanced at about 140–200 keV/μm and reduced at about 32 keV/μm. Whether there is an enhancement effect of low dose rate for LETs greater than 200 keV/μm is uncertain at present, because some recent data have indicated that 300-MeV/u iron particles (430 keV/μm) were equally effective at 47 and 2.7 cGy/min in inducing neoplastic cell transformation.

RBE Repair and LET

Human skin fibroblasts and rat embryonic cells (Rat-2) at a confluent state have been used as model systems in continuing studies to determine the mutagenic effect of heavy ions, and investigations on the repair of potential mutation lesions have been initiated. An analysis of dose-response curves for various heavy ions, including uranium particles, showed that the RBE and LET relationship for the 6–thioguanine resistant mutation is very similar to that for cell transformation. This good correlation suggests that the mutation lesion, possibly deletion, may be important for cell transformation by ionizing radiation. Studies on the repair of potential mutation damage indicated that heavy ions produce fewer repairable lesions than photons and that no repair of potential lesions could be detected in cells irradiated by 320-MeV/u silicon ions (85 keV/μm). The molecular nature of repairable and irreparable mutation lesions has not been carefully investigated and is totally unknown.

Systematic studies with heavy ions, which are effective in producing irreparable mutation lesions, may provide insights on the initial lesions for mutation.

Initial Primary Lesions

Neoplastic cell transformation is a multi-step process, including initiation, fixation, promotion, and progression to the malignant state. Various experimental findings suggest that nuclear DNA is the primary target for radiogenic cell transformation. The nature of the primary DNA lesion(s) responsible for initiation of cell transformation is unclear, although double-strand breaks have been suggested as possibly important ones. In the past several years, considerable dose-response data with carbon, neon, silicon, argon, iron, and uranium particles have been collected, and information on the repair of potential transformation damage as a function of LET has been obtained. A simple analysis of these data indicates that two specific primary ionizations within 80 Å in DNA may form transformation damage. Further studies with restriction endonucleases are being undertaken to verify this interesting finding.

Genetic Changes in Transformants

Numerous instances have now been provided on the links between protooncogene alterations in some form or another and the presence of various forms of neoplasms. To understand the genetic basis for radiation-induced cell transformation, some investigations on the radiation-mediated genetic changes in specific genes have been initiated. At present, this research concentrates on the molecular changes of the c-myc protooncogene in transformed cells.

Normal diploid Syrian hamster embryo cells at secondary or tertiary passages were transformed by x rays. The transformed foci were then isolated and tested for anchorage-independent growth in

soft agar medium. Large colonies formed in soft agar medium were cloned again, grown into large cell populations in culture, and tested for alterations in gene expressions of specific genes at various times after cloning. To date, the changes in the c-myc protooncogene of one transformed clone have been analyzed. By using Southern and Northern analyses, it was found that restriction-fragment-length polymorphism (RFLP) occurred in the c-myc locus during the progression of cell transformation and that the c-myc gene expression (the c-myc mRNA level) also changed.

It appears that some changes developed at a Pst-1 site in c-myc gene during the progression and that certain changes of c-myc mRNA species also occurred at the same time. Figure 3.10 shows the mRNA changes of the c-myc gene.

Current studies are attempting to find out if specific chromosomal alterations have occurred in the c-myc locus by applying the *in situ* hybridization technique to metaphase chromosome spreads. In the near future these studies will be extended to include other protooncogenes (e.g., the ras family), and to determine whether these observed changes are general phenomena in radiation-induced cell transformation.

Tracy Yang and Ruth Roots.

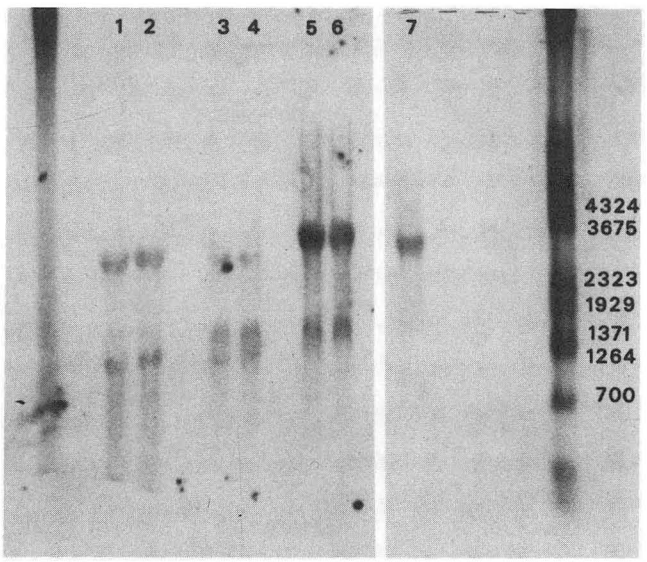

Fig. 3.10. *Northern plot of cytoplasmic C-MYC mRNAs. (Left panel) C-MYC mRNA is shown for normal (lanes 1,2) vs. transformed (lanes 3,4) hamster cells. The (2.7-kb) C-MYC mRNA from normal human cells (IMR-90) is shown in lanes 5,6. (Right panel) The characteristic 2.7-kb mRNA of C-MYC in human cells (IMR-90) is shown in lane 7 together with lambda molecular weight markers at the right. (XBB 877-5732A)*

OXYGEN-GLUCOSE DEPRIVATION AS THE CAUSE OF NECROSIS IN A TUMOR ANALOG

A sandwich system was recently developed as an *in vitro* tumor analog. Like spheroids, sandwiches are organized, multicellular systems in which the interplay between diffusion and consumption leads to the formation of spatial gradients; a necrotic center and a viable cell border subsequently develop. Adjacent to the necrotic center is a region of hypoxic cells. Within the viable border, there are gradients of oxygen, nutrients, cell-cycle state, morphology, and ultrastructure. These gradients of biological state result in gradients of radiation response and response to chemical perturbations or labeled substances. All cells are viewable during the time the sandwich matures. The gradients can be avoided by removing the top slide; this reoxygenates the cells and restores them to favorable growth conditions. Sandwiches of the 9L, V79, and EMT6 cell lines have been used to investigate questions relevant to formation of necrosis in solid tumors, the presence and behavior of hypoxic cells, the radiation response of the tumors, and the results of reoxygenation.

The effects of oxygen and glucose deprivation on the onset and formation of necrosis were investigated. The data indicate that in sandwiches necrosis is a result of a joint shortage of both substances. Complementary cell monolayer experiments to determine a number of consumption parameters were performed. On the basis of the data, a joint oxygen-glucose deprivation model for V79 cell necrosis was proposed. It is assumed a cell dies when oxygen deprivation in conjunction with glucose deprivation lowers the cell's ATP production rate below a critical value. Interactions of the concentrations and consumptions of oxygen and glucose were analyzed theoretically; concentration profiles are obtained by numerically solving coupled nonlinear integral equations arising from the diffusion equation. The predicted viable border widths are in good agreement with the observed values.

Sandwiches were labeled with ^{3}H-misonidazole. Location of cells within a sandwich was preserved by fixation and misonidazole binding was assessed by autoradiography. Heavy binding was seen in all cells bordering the necrotic center, with a greater than 50-fold difference between cells in the innermost hypoxic region vs. the outer oxygenated region. Misonidazole binding profiles were, at least approximately, consistent with oxygen profiles

computed previously for V79 sandwiches from the model described above. It was possible to count grains per cell rather than grains per unit area. No preferred binding in the nucleus, other organelles, or cytoplasm was noted. Detailed statistics on per-cell binding are consistent with a two-fold intrinsic variation of misonidazole binding per cell in the outer region of the viable border, where most cells are normally cycling, with a smaller intrinsic variation in the hypoxic region near the necrotic center. The results suggest misonidazole binding is proportional to cell size. The cell kinetics and response to other labels of those sandwich cells that bind misonidazole heavily were investigated both before and after reoxygenation.

There was a gradient of ^{3}H-thymidine labeling index for the sandwich cells, with the index dropping to less than 10% for the cells adjacent to the necrotic center. When these cells were reoxygenated and restored to favorable nutrient conditions by removal of the top slide, the ^{3}H-thymidine labeling index rose considerably within 24 hours; the minimum value after removal of the top slide occurred for the cells adjacent to the necrotic center and was 60%. Using the DMIPS, viability was assessed using formation of mini-colonies as a criterion after removal of the top slide. It was found that 80% of the cells in the hypoxic region were viable. Thus such hypoxic cells could contribute to repopulation. The biology of the hypoxic cells after reoxygenation was analyzed using a number of additional labels, including fluorescent labels; the results were compared to labeled R1 tumors from rats shortly after the removal and sectioning of the tumors.

The conclusion was that sandwich hypoxic cells are viable and resume cycling after restoration of favorable growth conditions, a property relevant to tumor repopulation after radiation therapy. It was also concluded that the cell state continues to reflect their former hypoxia for at least 24 hours, a property relevant to diagnosis using tumor sections.

Because of the presence of self-induced or imposed gradients, the potential usefulness of sandwiches is not confined to their role as tumor analogues. They can be used to study situations where diffusion gradients are relevant, cells in a continuum of local environments, cells subjected to a continuum of toxin or drug concentrations, and cell populations heterogeneous with respect to kinetic states.

Lynn Hlatky.

IN VIVO BIOPHYSICS

Normal Tissue Studies

There are two main objectives of studies on radiation effects in normal tissues. The first is to determine the relationship between the relative biological effectiveness (RBE) in normal tissues and the linear energy transfer (LET) of heavy charged particles. It has been shown that the highest RBE for acute effects after single doses of radiation occurs at about 90 keV/μm (Fig. 3.11). Fractionated doses are being used at present to determine the RBE and the repair capacity of mouse kidney and rat spinal cord, which are late responding tissues. The purpose is to test the hypothesis that the RBE for late effects after heavy ion irradiation is higher than for early responding tissues.

The second is to study the effects of radiation on differentiated normal tissue cell function and the regulation of function. These studies are being performed with cultured pig kidney cells (LLC-PK1) and rat proximal tubule kidney cells. Implications of these studies are fundamental as well as applied.

Mouse kidney functions are measured to determine the target cell type responsible for the kidney late radiation syndrome. Urinary frequency (tubular damage) changes are found to occur early (4 days) after neon irradiation, with an RBE of 1.9. This effect is clearly separate from hemodynamic effects (glomerular filtration, plasma flow) that do not occur before 10 to 12 weeks postirradiation. By 20 weeks all the functions have similar dose-response relationships (RBE of 1.45). Data analysis indicates that there is less repair after neon radiation.

Rat spinal cord paralysis studies with neon indicate a large sparing effect with fractionated helium plateau and neon plateau (α:β of 1.51 and 2.23 respectively). There is much less sparing for fractionated doses of distal Bragg peak neon (α:β of 12.85). The RBE is 2.0 for neon plateau and 5.2 for the distal Bragg peak. It appears that the RBE for late effects after fractionation is higher than for early-responding tissues.

Studies on the regulation of sodium-activated glucose transport in pig kidney cells indicate that this process can be impaired in a dose-dependent manner and there is no sparing effect on glucose transport regulation with fractionated doses. However cell killing is spared. These studies implicate a target or targets other than DNA that are inactivated for functional impairment.

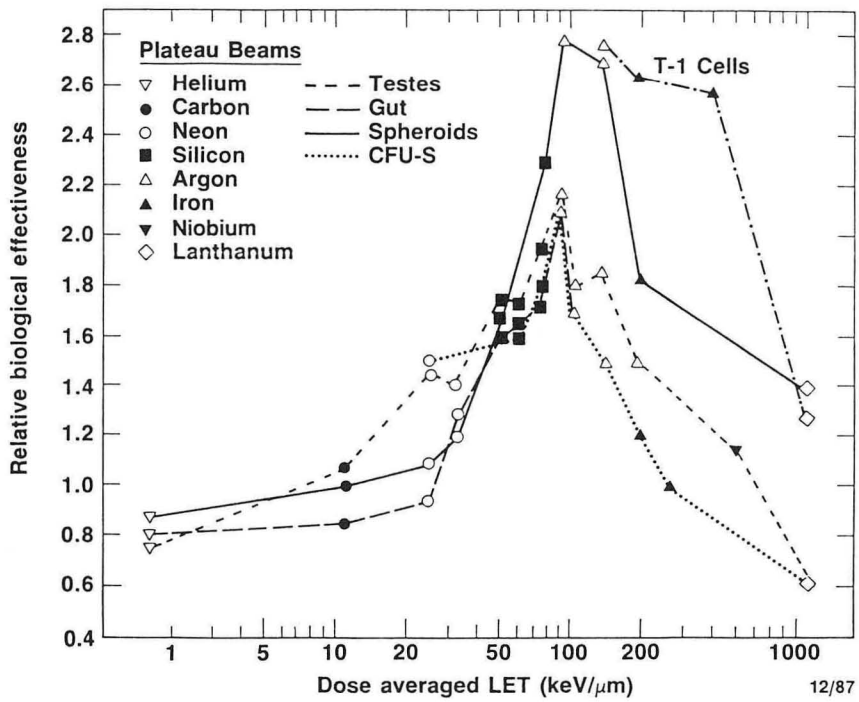

Fig. 3.11. *RBE for acute effects in normal tissues. Relative biological effectiveness (RBE) as a function of linear energy transfer (LET) for T1 (kidney) cells and multicellular spheroids, and the following murine normal tissue systems: testes weight loss, intestinal crypt cell survival, and colony-forming units: spleen. (XBL 8611-6485B)*

Future studies include 1) irradiation of normal tissues with 1-2 Gy per fraction of low- and high-LET radiation, and 2) determination of the radiation-sensitive target of functional impairment in pig kidney cells.

Radiation Carcinogenesis in Mouse Harderian Gland

The pituitary-promoted mouse Harderian gland tumorigenesis model was used to examine carcinogenic effects of heavy ions representing LET values from 1.6 to 650 keV/μm. High LET radiation carcinogenesis for doses in the range of 5 cGy to 40 cGy in the mouse Harderian gland has an RBE range of 2 for plateau helium ions at 1.6 keV/μm to values in excess of 25 for the highest LET of 650 keV/μm (argon distal peak) as shown in Fig. 3.12. The important generalization from these data is that there is no evidence for a peak in the RBE-LET relationship as is found for cell killing and other tissue late effects. Future studies will include induction of Harderian gland tumors with low doses (0.02–0.4 Gy) of plateau heavy ions.

Life Shortening Effects in Mice

The goal of this project is to relate carcinogenic effects *in vivo* to particle LET, track structure, or other physical parameters so that cancer risk models may be formulated. Life-span shortening in irradiated mice reflects the total radiation-induced tumor burden in terms of increased tumor incidence and/or shortened tumor latency. From the results of pilot studies on life shortening in CB_6F_1 male mice irradiated (total body) with particles ranging in LET from 30–200 keV/μm, several important conclusions were drawn. The hypothesis that LET has predictive value was rejected because stopping carbon particles are far less effective than fission neutrons for life shortening after either a single dose or 24 weekly fractions. Surprisingly, iron particles produced no detectable life shortening at doses of 40, 80, or 160 cGy. Cataract evaluations indicated that weekly fractionation with carbon particles significantly enhanced cataract severity.

Results from these pilot studies are an essential prerequisite for the design of future tumori-

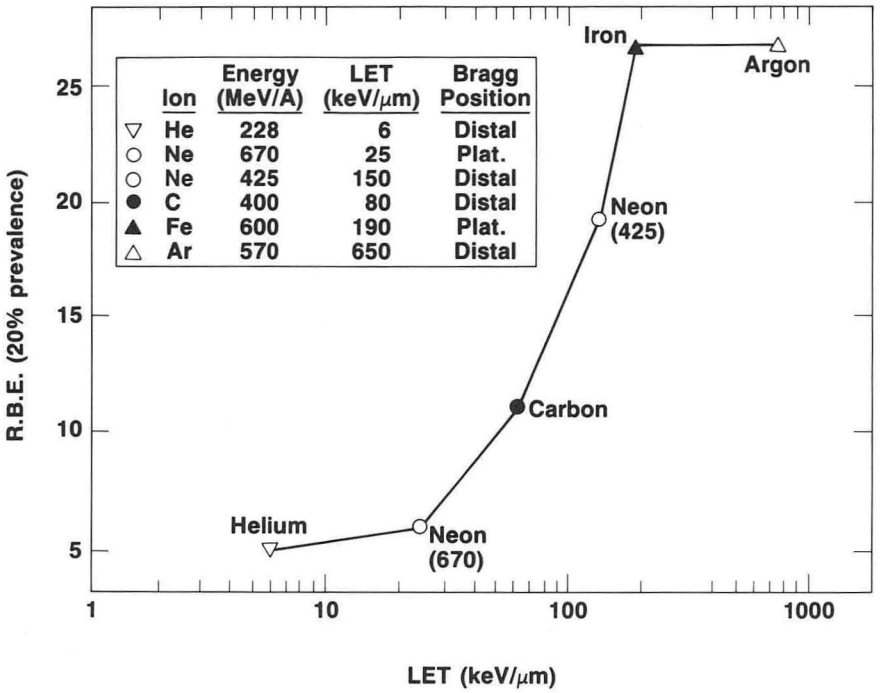

Fig. 3.12. RBE for murine Harderian gland tumors as a function of LET. At the 20% prevalence level the RBEs are about 10 times higher than for normal tissue RBEs and the RBE remains elevated at a high LET. (XBL 8611-6484)

genesis studies, probably with high-energy silicon particles. The objective will be to define the initial slopes of dose-response curves for various radiation-induced/promoted tumors over a range of low single or fractionated doses.

Marrow Stem Cell Inactivation

The RBE-LET relationship for CFU-S inactivation *in vivo* has been defined for both high energy and stopping particles. Results indicate a maximum RBE or cross section, at about 80 keV/μm, and no detectable differences between high energy or stopping particles where LET estimates are the same. New data collected for high energy protons (150 MeV/u) and stopping argon particles (330 MeV/u) indicate RBEs of 1.0 and 0.8 respectively compared with gamma photons. Future inactivation studies will focus on fragmentation of iron particles to determine how RBE increases as the ratio of primary particles to fragments decreases.

Studies continue on the mechanisms of charged particle damage to CFU-S using the radioprotectors WR 2721 and prostaglandins. Results indicate independent action, if not synergism, when Misoprostol is given at 2 hours and WR 2721 at 0.5 hours before exposure to gamma radiation. Future studies will focus on metabolic and membrane alterations produced by Misoprostol.

Tumor Radiobiology

The response of a rat rhabdomyosarcoma tumor system to irradiation with heavy charged particles is being evaluated from experiments conducted both *in vivo* and *in vitro*. The radiobiological endpoints studied include tumor volume response, cellular survival after *in situ* tumor irradiation, and cell kinetic parameters measured by flow cytometry. The primary emphasis of research during the past year has been in the following areas: 1) tumor repopulation kinetics following fractionated doses of low- and high-LET radiations; 2) phase-specific cell survival and cell kinetics following low- and high-LET radiations, and 3) studies on the immune system response to irradiated tumors.

Measurements were made of the time course of clonogenic cell survival in rat tumors after fractionated doses of either 225-kVp x rays or 557-MeV/u neon ions in the distal position of a 4-cm extended peak. Rhabdomyosarcoma R-1 tumors (the R2C5

subline) were irradiated *in situ* with daily fractionated doses (4 fractions in 3 days) of either peak neon ions (1.75 Gy per fraction) or x rays (6 Gy per fraction). These doses were administered to achieve a cell survival of approximately 2–3% by the end of the four-fraction schedule. The most significant new finding of these experiments was that with both radiation modalities a large delayed decrease in cell survival was observed at 1 to 3 days after completion of the fractionated dose schedule as shown in Fig. 3.13. The rate of cellular repopulation was consistent with the postirradiation tumor volume regression and regrowth pattern for both radiation modalities.

Several factors related to tumor-host interactions and to tumor cell environment following irradiation are being considered in an attempt to explain the delayed decrease in clonogenic cell survival. These studies have clearly implicated a specific host immune response against x-ray-irradiated R2C5 tumors as a factor that influences post-irradiation tumor cell survival properties. Future studies will focus on determining the relative role of this factor in producing the post-irradiation dip in cell survival.

The results of experiments reported here suggest several new treatment regimens that may prove to be highly efficient in achieving tumor cure. Because the clonogenic cell survival is dramatically decreased following fractionated doses of either x rays or peak neon ions, a top-off dose of radiation administered at that time may be highly efficient in sterilizing the small residual fraction of clonogenic cells. In addition, the results suggest the possible advantages of using monoclonal or polyclonal antibodies directed against tumor antigens that are expressed following irradiation. By combining immunotherapy and radiotherapy, it may be possible to achieve tumor sterilization with radiation doses that are substantially less than the tolerance limit of normal tissue structures within the radiation field.

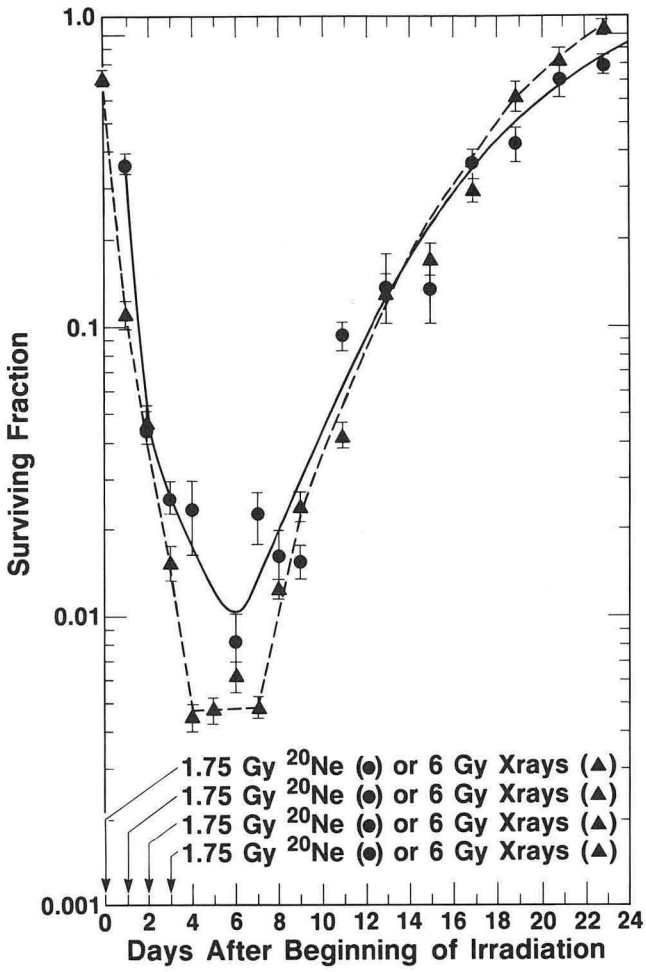

Fig. 3.13. *Surviving fraction of rat rhabdomyosarcoma tumor cells as a function of time during and after* in situ *exposure to daily fractionated doses (4 fractions in 3 days) of either 557-MeV peak neon ions in the distal position of 4-cm extended peak (•, 1.75 Gy per fraction) or 225-kVp x rays (▲, 6.0 Gy per fraction). Groups of 3 to 4 tumors were assayed at each time point. (Error bars represent ± 1 SEM.) (XBL 881-7211)*

Edward Alpen, Adrian Rodriguez, John Ainsworth, Stanley Curtis, and Javed Afzal.

Nonionizing Radiation

The primary objectives of the nonionizing radiation program are 1) the development of a detailed experimental and theoretical understanding of the mechanisms through which static magnetic fields, extremely-low-frequency (elf) electromagnetic fields, and radiofrequency (rf) fields interact with biological systems; 2) the use of static magnetic fields and rf fields to facilitate the release of encapsulated chemotherapeutic drugs from liposomes into target cells; 3) the application of static magnetic fields with intensities up to 9.0 tesla (90,000 gauss) for magnetic circular dichroism analysis of DNA structure; and 4) the development of novel chromatographic procedures in which rf fields and pulsed electric fields are used to enhance the separation of chemical species such as DNA fragments and arterial plaque proteins. Progress in selected areas of the nonionizing radiation program are described here.

FIELD-INDUCED CHANGES IN MEMBRANE PERMEABILITY

The interactions of static magnetic fields and rf radiation with the phospholipid bilayer membranes of liposomes and various eukaryotic cell membranes were analyzed using several structural and functional end points. The liposome vesicle membrane is normally not permeable to solutes at temperatures below the thermal phase transition. However, when exposed to static magnetic fields at prephase transition temperatures, liposomes were observed to release an encapsulated chemotherapeutic drug, cytosine arabinofuranoside. This observation indicates that it may be possible to medically control drug release in a given target tissue by manipulating membrane permeability with a focused magnetic field. A detailed theoretical model of liposome membrane interactions with magnetic fields at prephase transition temperatures has provided a structural explanation for these findings. These investigations will be extended to eukaryotic cell membranes in future research.

In related experiments, the ability of rf fields to facilitate solute transfer from liposomes into various target cells was investigated using a fluorescent dye marker: 6-carboxyfluoroscein (6-CF) was self-quenched inside liposome bilayer membranes comprised of lecithin or other phospholipids with 14- and 16-carbon chain lengths. Human erythrocytes and lymphocytes, rodent lymphocytes, rodent tumor cells, and rodent macrophages were treated with 6-CF-liposomes to promote cell-surface binding. Washed liposome-cell complexes were subsequently exposed to 2.45-GHz microwaves or sham-treated at identical temperatures below the phase transition for the liposome system, and fluorescent dye transfer between the bound liposomes and the target cells was assessed by fluorescence microscopy and by a spectrofluorometric assay. The microwave exposure was found to significantly facilitate dye transfer from the liposomes as compared to the sham-treated control samples maintained at the same temperature. This finding indicates that the membrane permeability changes leading to dye transfer are not attributable to thermal interactions with the microwave field. Future studies will explore the feasibility of using microwaves to facilitate drug delivery from liposomes into various target tissues *in vivo.*

STRUCTURAL CHANGES IN EUKARYOTIC CELL MEMBRANES

Studies have demonstrated that microwaves physically alter the structure of eukaryotic cell membranes. It is known that erythrocytes shed proteins from the membrane surface at the thermal phase transition. When human erythrocytes were placed in a 2.45-GHz microwave field, it was observed that the total protein released in the phase transition temperature range was doubled. Further, the type of proteins shed as a consequence of microwave exposure were relatively nonpolar and possessed a positive electrostatic charge, which distinguished these proteins from those released as a result of conventional heat treatments.

CARDIOVASCULAR EFFECTS

The magnetohydrodynamic interaction of high-intensity static magnetic fields with blood flow have been studied in monkeys, dogs, and rodents at field levels up to 1.5 tesla. Circulating blood in an applied magnetic field generates electric currents, and a volume force on the fluid is produced from the interaction of these induced electric currents with the magnetic field. Theoretically, this volume force can cause a retardation of axial blood flow velocity. Mathematical models of this magnetohy-

drodynamic phenomenon have predicted the slowing of blood flow in intense magnetic fields. However, studies on carotid artery blood flow rates in rats have shown no effects from a 1.5-tesla uniform field. Further studies are planned using magnetic field intensities up to 9.0 tesla in order to determine the threshold field level for producing a measurable magnetohydrodynamic effect on blood flow dynamics. Cardiovascular effects of prolonged exposure to high-intensity magnetic fields are also being studied by continuous radiotelemetry monitoring of the electrocardiogram (ECG) in rodents subjected to a 1.5-tesla static magnetic field. At this field level, the magnetically-induced currents within the central circulatory system are 2–3 times as large as the endogenous currents normally present in the region of the sinoatrial node that controls cardiac pacing. Data obtained from implanted ECG radiotelemeters in 12 adult rats have demonstrated that a 3–4% decrease in heart rate occurs during a continuous 10-day exposure to a 1.5-tesla field relative to the heart rate measured during the 10-day pre-exposure interval. However, this change in heart rate is completely reversible upon termination of the magnetic field exposure. The results of these experiments indicate that the induced electrical potentials and currents present in the central circulatory system during prolonged magnetic field exposure have only a small, and probably insignificant effect on cardiac pacing.

APPLICATIONS OF ELECTROMAGNETIC FIELDS IN SPECTROSCOPY AND CHROMATOGRAPHY

Progress in this research area includes 1) the completion of instrumentation for magnetic circular dichroism analysis of DNA structure using a 9.0-tesla uniform magnetic field produced by a superconducting magnet; 2) the demonstration that the separation of arterial plaque protein species using reverse-phase HPLC can be enhanced by the application of an rf field at nonthermal intensities; and 3) a pulsed-electric-field chromatography system designed for use in the separation of large DNA fragments. These applications of nonionizing radiation in spectroscopy and chemical separation procedures will be an integral component of the future research program.

Thomas Tenforde, Cornelius Gaffey, and Robert Liburdy.

Future Studies

Most of the research efforts described above will continue in order to achieve the defined goals. Within the scope of these studies, efforts in the area of molecular radiobiology will be expanded. The key questions to be addressed are related to mechanisms underlying radiation effects, such as damage mechanisms, protective mechanisms, response mechanisms leading to irreversible changes, etc. Emphasis will be given to the late somatic and genetic effects of external radiation (low- and high-LET). The problem of low-level radiation effects on human health will be specifically addressed in the coming years. It is hoped that the knowledge gained from present ongoing studies of basic processes involved in radiation damage and repair (including misrepair) will be sufficient so that many of the low-level effects can be understood from simple statistical considerations.

A recent new initiative deals with the problem of cell transformation by radon progeny. The goal of this study is to provide experimental evidence at the physical, chemical,and molecular levels for a causal link between the incidence of lung cancer and the presence of radioactive nuclides deposited in the air passageways of the lung by the progeny of the decay of radon gas. The primary interest is in the sector of the DNA damage that eventually results in a malignant transformation and the induction of a tumor.

The Radiation Biophysics Group is also going to be involved in technology transfer with respect to the recent interest in the medical community regarding heavy-particle accelerators. The Merritt Peralta Medical Center (MPMC) in Oakland, California, is planning to build a light ion biomedical research accelerator and supporting laboratories for expanded medical research and cancer therapy with high-LET particles. The MPMC has asked the Group to provide input for the determination of the beam characteristics for this accelerator. In addition, the Group will provide assistance in dosimetry and beam development for a variety of clinical applications.

Publications: Radiation Biophysics

CONTRIBUTIONS TO JOURNALS

Afzal, S.M.J. and Ainsworth, E.J. Radioprotection of mouse colony forming units—spleen (CFU-S) against heavy charged particle damage by WR 2721. *Radiat. Res. 109,* 118–126 (1987).

Ainsworth, E.J. Early and late mammalian responses to heavy charged particles. *Adv. Space Res. 6,* 153–165 (1986).

Chatterjee, A., Koehl, P., and Magee, J.L. Theoretical consideration of the chemical pathways for radiation-induced strand breaks. *Advances in Space Research 6 (11),* 97–105 (1986).

Curtis, S.B. Track structure in biological models. *Adv. Space Res. 6,* 179–185 (1986).

Curtis, S.B., Atwell, W., Beever, R., and Hardy, A. Radiation environments and absorbed dose estimations on manned space missions. *Adv. Space Res. 6,* 269–274 (1986).

Doss, K.G., Gustafsson, H.A., Gutbrod, H.H., Kampert, K.H. Kolb, B., Lohner, H., Ludewigt, B., Poskanzer, A.M., Ritter, H.G., Schmidt, H.R., and Wieman, H.H. Nuclear collective flow as a function of projectile energy and mass. *Phys. Rev. Lett. 57,* 302 (1986).

Gauger, G.E., Tobias, C.A., Yang, T.C., and Whitney, M. The effect of space radiation on the nervous system. *Adv. Space Research 6(11),* 243–249 (1986).

Hagen, M.P., Holahan, E.V., and Ainsworth, E.J. Effect of heavy ions on cycling stem cells. *Adv. Space Res. 6,* 201–211 (1986).

Hanson, W.R., Fry, R.J.M., Sallese, A.R., Frischer, H., Ahmad, T., and Ainsworth, E.J. Comparison of intestine and bone marrow radiosensitivity of Balb/c and the C57BL/6 mouse strains and their B6CF1 offspring. *Radiat. Res. 110,* 340–352 (1987).

Kraft, G., Kraft-Weyrather, W., Blakely, E.A., and Roots, R. Heavy-ion effects on cellular and subcellular systems: inactivation, chromosome aberrations and strand breaks induced by iron and nickel ions. *Adv. in Space Research 6(11),* 127–136 (1986).

Liburdy, R.P. Neuroimmunomodulation and cancer. *The Cancer Journal 1,* 198 (1987).

Liburdy, R.P. and Tenforde, T.S. Magnetic-field induced drug permeability in liposome vesicles. *Radiation Research 108,* 102–111 (1987).

Liburdy, R.P. and Vanek, P.F., Jr. Microwaves and the cell membrane: III. Protein shedding is oxygen dependent and temperature dependent: evidence for cation bridge involvement. *Radiation Research 109,* 382–395 (1987).

Renner, T. and Chu, W.T. Wobbler facility for biomedical experiments. *Med. Phys. 14,* 825–834 (1987).

Schimmerling, W., Rapkin, M., Wong, M., and Howard, J. The propagation of relativistic heavy ions in multielement beam lines. *Med. Phys. 13,* 217–228 (1986).

Swiegert, S.E. and Alpen, E.L. Dynamics of cell kinetic parameters during 9L spheroid growth. *Cell Tissue Kinetics 19,* 567–576 (1986).

Swiegert, S.E. and Alpen, E.L. Radiation-induced division delay in 9L spheroid versus monolayer cells. *Radiation Research 110,* 473–478 (1987).

Tenforde, T.S. and Kaune, W.T. Interaction of extremely low frequency electric and magnetic fields with humans. *Health Phys. 53*, 585–606 (1987).

Urie, M., Goitein, M., Holley, W.R., and Chen, G.T.Y. Degradation of the Bragg peak due to inhomogenieties. *Phys. Med. Biol. 31*, 1–15 (1986).

Wren, M.W., Durbin, P.W., Willis, D.L., and Singh, N.P. The potential toxicity of uranium in water. *J. Amer. Waterworks Assn.*, 177–184 (April 1987).

Yang, T.C., Craise, L.M., Mei, M., Tobias, C.A. Dose protraction studies with low- and high-LET radiations on neoplastic cell transformation *in vitro*. *Adv. Space Research 6(11)*, 137–147 (1986).

CONTRIBUTIONS TO BOOKS AND PROCEEDINGS

Blakely, E.A., Tobias, C.A., Ludewigt, B.A., and Chu, W.T. Some physical and biological properties of light ions. Pages 19–41 in *Proceedings of the Fifth PTCOG Meeting and International Workshop on Biomedical Accelerators* , (Lawrence Berkeley Laboratory, Dec. 1–2, 1986), LBL-22962 (1987).

Chatterjee, A., Llacer, J., Collier, M., Renner, T., Henderson, S., and Chu, W. Diagnostic applications of radioactive beams. Pages 213-230 in *Proceedings of the Fifth PTCOG Meeting and International Workshop on Biomedical Accelerators* , (Lawrence Berkeley Laboratory, Dec. 1–2, 1986), LBL-22962 (1987).

Chatterjee, A. and Magee, J.L. Track models and radiation chemical yields. In *A Textbook of Modern Radiation Chemistry* , M.A.J. Rodgers, ed., Verlag Chimie International (1986).

Chu, W.T. and Kuenning, R.W. Limitations of dynamic beam delivery systems. Pages 185–196 in *Proceedings of the Fifth PTCOG Meeting and International Workshop on Biomedical Accelerators* , (Lawrence Berkeley Laboratory, Dec. 1–2, 1986), LBL-22962 (1987).

Durbin, P.W. Metabolic models for uranium. Pages F–1 to F–65 in *Biokinetics and Analysis of Uranium in Man*, R.H. Moore, ed., United States Uranium Registry, Hanford Environmental Health Foundation Report USUR-05-HEHF-47 (1986).

Goodman, E.M., Greenebaum, B., Marron, M.T., and Tenforde, T.S. *Effects of Electropollution: Brain Tumors and Experimental Models*, S.K. Dutta, R.M. Millis, eds., Information Ventures, Inc., Philadelphia, PA (1986).

Liburdy, R.P. Immunological effects of electromagnetic effects. Section 6, Chapter 9, in *Review of Radio Science 1984–1986*, G. Hyde, ed., International Union of Radio Science, Brussels, Belgium (1987).

Magee, J.L. and Chatterjee, A. Theoretical aspects of radiation chemistry. In *A Textbook of Modern Radiation Chemistry*, M.A.J. Rodgers, ed., Verlag Chemie International (1986).

Metting, N.F., Howard, J., Braby, L.A., Schimmerling, W., Rossi, H.H., Wong, M., Kliauga, P.J., and Rapkin, M. Measurement of energy deposit near high energy, heavy ion tracks. *Pacific Northwest Laboratory Report No. 5950* (1986).

Stannard, N.J., Auxier, J.A., Bair, W.J., Durbin, P.W. Eckerman, K.J., McClellan, R.O., Morrow, P.E., Schlenker, R.A., and Thompson, R.D. *General Concepts for the Dosimetry of Internally Deposited Radionuclides*. Report No. 84, National Council on Radiation Protection and Measurements (1985).

Tenforde, T.S. Static magnetic fields. Pages K-10 to K-11 in *Review of Radio Science 1984–1986*, G. Hyde, ed., International Union of Radio Science, Brussels, Belgium (1987).

Tenforde, T.S., Levy, L., and Veklerov, E. Monitoring of circadian waveforms in rodents exposed to high-intensity static magnetic fields. Pages 307–326 in *Interaction of Biological Systems with Static and ELF Electric Magnetic Fields*, L.E. Anderson, B.J. Kelman, and R.J. Weigel, eds., Proceedings of 23rd Hanford Life Sciences Symposium (Report No. CONF-84), Pacific Northwest Laboratory, Richland, WA (1987).

Yang, V.V. and Ainsworth, E.J. A histological study on the cataractogenic effects on heavy charged particles. *Proc. Nat. Sci. Counc. B.ROC.* (Taipei, Taiwan) *11*, 18–28 (1987).

LBL REPORTS ISSUED

Berger, S.E. The radiation response of murine erythroid-colony-forming units (CFUe). Ph.D. Thesis. Lawrence Berkeley Laboratory report LBL-23843 (July 1987). 129 p.

Tenforde, T.S. Interaction mechanisms, biological effects and biomedical applications of static and extremely-low-frequency magnetic fields. Lawrence Berkeley Laboratory report LBL-22321 (1986) 57 p.

Tobias, C.A. Dynamic models in radiobiology. Presented at the workshop on mechanisms of radiation interaction with DNA "Potential Implications for Radiation Protection" (San Diego, Calif., January 21–22, 1987). Lawrence Berkeley Laboratory report LBL-23334 (1987) 21 p.

White, D.L., Durbin, P.W., Jeung, N., and Raymond, K.N. Specific sequestering agents for the actinides. 16. Synthesis and initial biological testing of polydentate hydroxypyridinonate ligands. Lawrence Berkeley Laboratory report LBL-21714 (1987).

Section 4. Research Medicine

Introduction

The Research Medicine Group has as its principal focus the investigation of physiology and disease processes using nuclear chemistry and nuclear physics methods and instruments. This program of research evolved over the past fifty years with its beginnings in 1937, when Dr. John Lawrence joined a small group at the Radiation Laboratory on the University of California Berkeley campus. Now, in its fiftieth year of progress, the Donner Laboratory and the Biology and Medicine Division have participated in the exploration of various disease diagnoses and therapies using radiotracers and accelerated particles. Though the general characteristics of the research approach have not changed, current topics of focus emphasize the study of mental disorders, including schizophrenia and Alzheimer's disease, the evaluation of metabolism in tumors, and the investigation of atherosclerosis by noninvasive imaging methods and tracer methods that detect abnormal metabolism.

Along with physiologic and disease oriented studies in human subjects, there is a continuing thrust on the development of specialized instruments for understanding human disease. Among these instruments is the high resolution positron emission tomograph, which this year achieved a resolution of 2.3 mm, far beyond the available resolution of instruments elsewhere. Recent instrumentation development includes the establishment of NMR spectroscopy and whole-body imaging instruments at Lawrence Berkeley Laboratory close to the existing positron emission tomographic instruments.

Therapy with charged-particle beams has been successful in clinical trials involving tumor sites of the head, neck, spinal cord, and prostate gland. The program of heavy-ion radiosurgery for the ablation of arteriovenous malformations in the human central nervous system continues to have excellent results in disease situations that are not approachable by neurosurgical methods.

Collaborative programs between researchers creating new instrumentation and radionuclides for the study of disease and those interested in their applications in the clinical environment have increased over the past few years to include investigators from the University of California, Berkeley College of Engineering, and Departments of Physical Education and Nuclear Engineering; the University of California, San Francisco Departments of Neurosurgery, Radiology, and Neuropsychiatry; the University of California, Davis Department of Neurology; the University of Illinois, and Harvard Medical School.

As modern biology has emphasized more fundamental investigations of the molecular biology associated with life and disease processes, the Research Medicine Group has emphasized the basic *in vivo* chemical techniques of tracking metabolism while investigating the time rate of change of metabolic products that can be measured by the integration of HPLC techniques with radiotracer methodology.

The Research Medicine Group has also made major contributions to studies of environmental radiation, radiation used in diagnosis and therapy, and the health effects of oscillating and static magnetic fields.

ACTIVITIES OF THE RESEARCH MEDICINE GROUP

	Scientists	*Technical Staff and Graduate Students*
Physics and Mathematics		
Detector instrumentation	S.E. Derenzo	J. Baker
Positron emission tomography	R.H. Huesman	J. Cahoon
Single photon tomograph	W. Moses	M. Colina
	E. Salmeron	A. Geyer
Computer based algorithms	D. Uber	T. Vuletich
Reconstruction methods		
Statistical analysis		
Kinetics modeling		
Chemistry		
Radiopharmaceutical tracers	J. Gerdes	S. M. Hanrahan
Brain and heart blood flow; metabolism	C. Mathis	
Neuroreceptors	Y. Yano	
New isotope generators		
Medicine and Physiology		
Blood clotting	K.M. Brennan	K. Bristol
Platelets	T.F. Budinger	D. Carpenter
Megakaryocytes	K. Dalal	N. Kusubov
	S.N. Ebbe	M. Morimoto
Atherosclerosis	S. Gregg	J. Twitchell
Coronary artery disease	R. Himelman	
Platelets	S. Knezevic	
Metabolic patterns	W.J. Jagust	
	R. Leven	
Alzheimer's disease	B. Periera	
Diagnosis	D. Prozen	
Cause(s)	T. Sargent III	
	J.P. Seab	
Schizophrenia	P.E. Valk	
Tumor metabolism		
Nuclear Magnetic Resonance		
NMR probes	H. Ikehira	N. Bolo
	R. Newmark	B. Knittel
NMR imaging systems	M. Roos	M. Kessler
		S. Wong

	Scientists	*Technical Staff and Graduate Students*
Heavy Ion Therapy		
Intercranial AVMs	J.R. Castro	K. Baken-Brown
	F. Chuang	N. Dodson
Heavy ion radiotherapy physics	J.M. Collier	M. Foster
	J.I. Fabrikant	E. Holloway
	K.A. Frankel	J. Judnick
Heavy ion radiobiology	S. Henderson	C. Rathbun
	M. Kessler	
Treatment planning and dose localization	R.P. Levy	
	E.H. Lo	
	J.T. Lyman	
Radiotherapy physics	N. Manley	
	P. Petti	
Tumor radiosensitivity predictive assays	M.H. Phillips	
	S. Pitluck	
PEBA		

Brain Function and Disease Studies

Neurological and psychiatric diseases are being studied by using positron emission tomography (PET), nuclear magnetic resonance (NMR), single photon emission computed tomography (SPECT), and metabolic tracers. The research activities with these advanced techniques encompass creation of new instrumentation and new tracers, and physiological investigations with animals and patients. The diseases of interest are Alzheimer's dementia, white matter lesions, stroke, brain tumors, radiation necrosis, schizophrenia, and depression. Each is being studied by two or more of the above techniques.

PET is used to obtain images of the localization of any biochemical that can be labeled with a positron-emitting isotope. From these images accurate data can be obtained to give the amount of activity in any selected region, and these data can be determined over short time intervals after injection to derive kinetics for the time course of the label in the brain. Critical to the usefulness of these kinds of data are the choice of the labeled compound and the knowledge of how it is metabolized. For example, glucose metabolism is measured by fluorodeoxyglucose, labeled with 110–min fluorine–18. This is used to measure regional cerebral metabolic rate (rCMR), which is reduced in specific areas in Alzheimer's dementia, stroke, and brain tumors. An important additional measure is the regional cerebral blood flow (rCBF), which is altered by the brain in accord with metabolic demand. A new radiopharmaceutical, ^{122}I-HIPDM [N,N,N'-trimethyl-N'(2-hydroxyl-3-methyl-5-iodobenzyl)-1,3-propanediamine], has been developed by our group for measuring rCBF.

SCHIZOPHRENIA AND AFFECTIVE DISORDERS

These psychotic diseases are being investigated to find the biochemical abnormality that is believed to underlie their clinical manifestations. For schizophrenia there is evidence that the abnormality is in methyl metabolism, and an abnormal oxidation of the methyl carbon of methionine has been demonstrated by our group in these patients. This is studied by administering methionine labeled in the methyl group with carbon-14 and measuring the expired $^{14}CO_2$. The abnormality found in schizophrenia is a reduced rate of oxida-

tion of the methyl carbon, with the total quantity oxidized being reduced to about one-half of normal at 2 hours. Chromatographic methods have been developed to separate the metabolic products that have become labeled with the carbon-14. To detect and measure these metabolites use of the new Cyclotrino developed by the Nuclear Science Division is being investigated, which is expected to increase the sensitivity for detection of the ^{14}C-labeled metabolites by a factor of 1000. With such sensitive methods, it is hoped that the abnormal biochemical step in metabolism that is associated with schizophrenia will be identified. Early preliminary data suggest that the methyl carbon is also oxidized abnormally in depression; studies with such patients have been started to confirm these findings.

Investigations at other laboratories have reported abnormalities in glucose metabolism and blood flow in specific brain areas in schizophrenia and depression. Our investigators have measured glucose metabolism in a carefully controlled group of schizophrenics and did not find the abnormality reported by others, but did find differences in the rate, rather than the total amount of glucose metabolized. With the new radiopharmaceutical (^{122}I-HIPDM) for measuring brain blood flow developed here, our investigators have the capability for this measurement, and studies may be undertaken to confirm the findings reported by other laboratories. However, it is felt that these measurements are not as contributory to understanding the basic cause of schizophrenia as the methionine work, where our effort is concentrated.

Thornton Sargent III and Natalia Kusubov.

CLINICAL AND METABOLIC SIGNIFICANCE OF CEREBRAL WHITE MATTER LESIONS SEEN ON NMR IMAGING

Introduction of nuclear magnetic resonance imaging has revealed the presence of deep white-matter lesions (WMLs) in 30% of elderly subjects. It has been suggested that these lesions represent diffuse cerebral vascular disease of the type that leads to dementia, and that patients with deep WMLs have a higher probability of developing dementia than age-matched controls. The purpose of this study is to test these hypotheses.

A five-year study of 120 patients is underway. Half (60) of the patients will be intellectually normal on entering the study and 60 will show mild dementia. Half of each group will have cerebrovascular-disease risk factors, such as hypertension or ischemic heart disease, and the other half will not. All patients are being studied by NMR imaging, to look for WMLs, and by PET with ^{18}F-2-fluoro-2-deoxyglucose (^{18}F-FDG) to look for cortical areas of reduced glucose metabolism. Cognitive testing, NMR imaging, and PET studies will be repeated three years later.

So far, 38 patients have been studied for the first time: 37 were intellectually normal subjects and 1 had mild dementia. Half the patients had CV risk factors. WMLs have been graded 1 to 4 in severity. Eleven of the nondemented patients had grade 1 or 2 lesions and the remainder were normal. The demented patient had grade 3 lesions. None of the subjects has so far shown abnormalities of FDG uptake. NMR images from a demented patient and a control patient are shown in Fig. 4.1.

This study is expected to elucidate the pathophysiological significance of deep WMLs and to determine the relationship of these lesions to cerebrovascular disease, dementia, and gray-matter glucose metabolism, as demonstrated by PET.

Peter E. Valk and Thomas F. Budinger (LBL); Craig Van Dyke and George Fein (VA Medical Center, San Francisco).

QUANTITATIVE NMR MEASUREMENTS OF BRAIN ATROPHY IN NORMAL AGING AND ALZHEIMER'S DISEASE

Alzheimer's disease (AD) is a progressive degenerative dementia of unknown cause with pathological changes occurring first and most severely in the grey matter of the temporal and parietal lobes of the brain, including the hippocampus, as shown by autopsy studies. Positron emission tomography (PET) and single photon emission computed tomography (SPECT) studies of glucose metabolism and blood flow have shown functional correlates of this regional pattern of involvement in AD with the greatest deficits occurring in the same regions as one finds the pathological abnormalities. Anatomic imaging performed to date has shown general differences between AD patients and normal controls; however, these procedures do not specifically evaluate the grey matter regions of the brain that are most prominently involved in AD and that can be clearly visualized with NMR imaging. The purpose of this study was to image and quantify changes in the temporobasal grey-matter regions of the brain in AD patients and in normal aged controls in order to better understand changes in these brain structures and their relation to clinical symptoms and pathophysiology.

BRAIN WHITE MATTER DISEASE

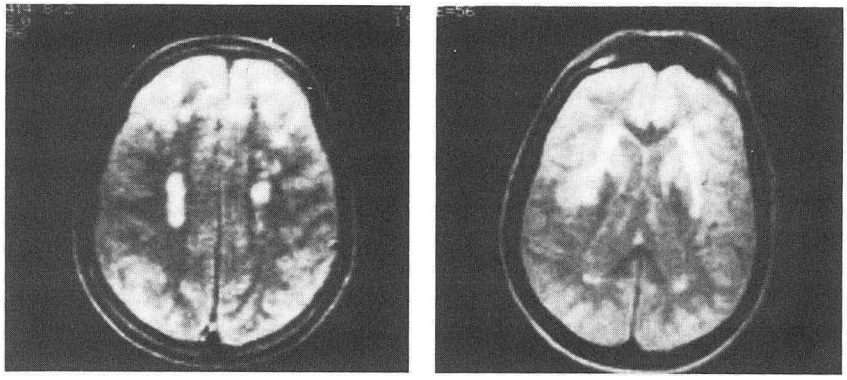

Dementia No Dementia

Fig. 4.1. *White-matter lesions appear as abnormal regions of high signal, deeply located in each hemisphere. They are located in the cerebral white matter, around the lateral ventricles, where only low signal is normally seen. The WMLs are not necessarily accompanied by dementia and the patient with the more severe lesions was cognitively normal in this case. (BBC 870-8736)*

Representative images are shown in Fig. 4.2. There was more than a 40% reduction in mean normalized hippocampal area of the AD patients (0.194 ± 0.025) compared to controls (0.341 ± 0.034, $p < 0.0001$, see Fig. 4.3). Severity of hippocampal atrophy did not correlate with severity of overall dementia as measured by the mini-mental status examination (MMSE) in the AD patients (see Fig. 4.4). It also did not correlate with severity of overall atrophy as measured by percent brain volume, age of onset, or duration of AD.

The percent ventricular size and percent sulcal size were significantly greater in the AD group compared to elderly controls ($p < 0.02$ and $p < 0.01$, respectively). The mean values for overall atrophy also differed significantly ($p < 0.01$), with the AD patients showing a smaller relative brain size (75.1% ± 6.5%) than elderly controls (81.7% ± 2.7%, see Fig. 4.5). The individual values for the two groups overlapped considerably for these three measures of atrophy. There was a correlation between overall atrophy and overall dementia

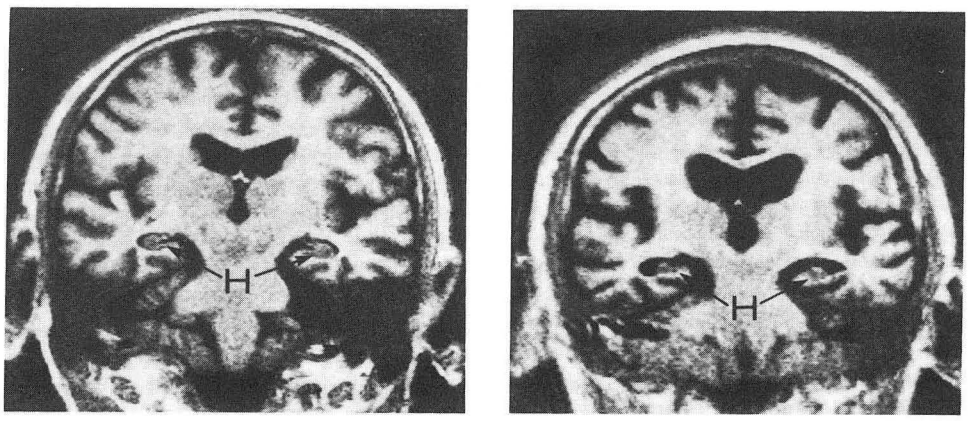

Fig. 4.2. *Representative coronal inversion recovery images showing the hippocampus of a normal aged control (left) and an Alzheimer's disease patient (right). H = hippocampus. (XBB 878-6624A)*

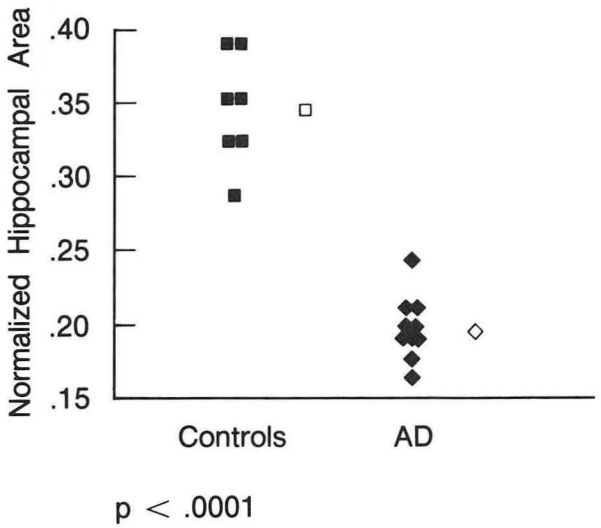

Fig. 4.3. Normalized hippocampal area for the control group and the Alzheimer's disease group (AD). Solid symbols indicate individual subject values; open symbols indicate group means. P < 0.0001 (Student's t-test). (XBL 877-7822)

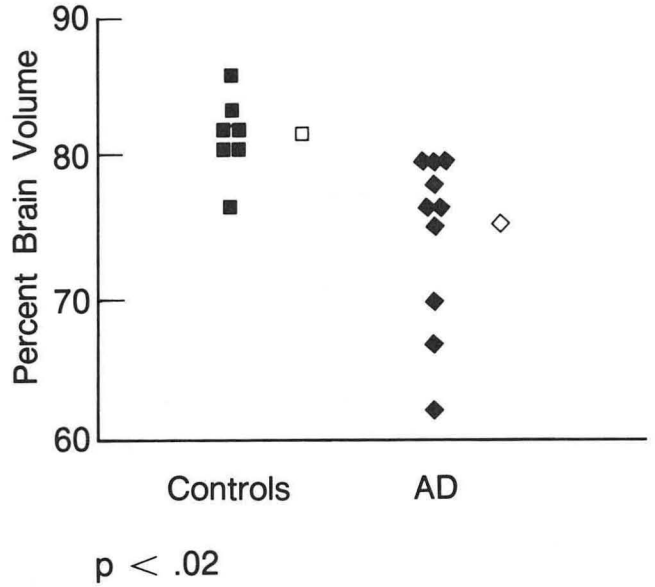

Fig. 4.5. Percent brain volume, a measure of overall atrophy, for the control group and the Alzheimer's disease group (AD). Solid symbols indicate individual subject values; open symbols indicate group means. P < 0.02 (Student's t-test). (XBL 877-7825)

severity as measured by the MMSE (r = 0.89, p < 0.001).

A major finding of this NMR study is that there is atrophy of the hippocampus that can be measured *in vivo*, and which is greater in AD patients then in normal aged controls. Hippocamal atrophy does not correlate with overall brain atrophy, implying that it reflects an aspect of AD pathology that differs from that seen in overall atrophy. While hippocampal size, percent ventricular size, percent sulcal size, and percent brain size were all different between control and AD subjects, only the hippocampal measurements separated the two groups in this study without overlap of individual values. A conclusion from these findings is that hippocampal atrophy occurs early in AD, and may be more sensitive to the presence of the disease than measurements of ventricular size, sulcal enlargement, or overall brain atrophy.

J.P. Seab, W.J. Jagust, S.T.S. Wong, M.S. Roos, B.R. Reed, T.F. Budinger

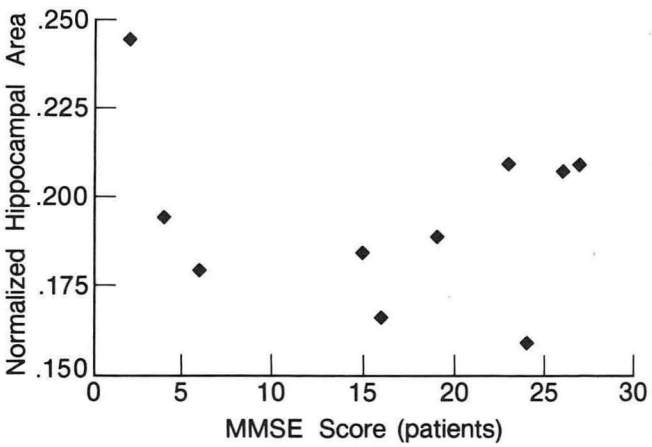

Fig. 4.4. Graph of normalized hippocampal area versus mini-mental status examination score as a measure of dementia severity, illustrating the lack of correlation between these two measures in the Alzheimer's disease group. (XBL 8711-8006)

INVESTIGATION OF CEREBRAL SEROTONIN RECEPTOR-SITES WITH RADIOLABELED AMPHETAMINE ANALOGS

The study of cerebral receptor systems *in vitro* and *in vivo* is an area of active research for many reasons. Receptor systems have been shown to play an important role in normal and abnormal cerebral function. Serotonin receptors have been identified as mediating a number of behavorial and physiological actions, and the 5-HT_2 serotonin receptor subtype has been implicated as playing a role in depression and psychosis. In addition, severe reductions in the density of 5-HT_2 receptors have been noted in Alzheimer's disease. Quantitation of 5-HT_2 receptor densities could yield informa-

tion on normal receptor densities and abnormal densities associated with disease states.

Substituted amphetamine analogs have been studied by this group for many years as potential brain blood-flow agents. Two of these, the 2,5-dimethoxyamphetamines substituted in the 4-position with either iodine (called DOI) or bromine (called DOB), have recently been identified as 5-HT_2 ligands. The compounds were labeled with radioiodine and radiobromine so that they could be utilized to identify 5-HT_2 receptors *in vitro* and *in vivo*. The *in vitro* work to identify the equilibrium receptor binding constants in rat brain was conducted in collaboration with Dr. David Nichols at Purdue University (DOI) and Dr. Steven Peroutka at Stanford (DOB); Dr. Dennis McKenna at the National Institute of Mental Health conducted *in vitro* autoradiographic studies to identify the specific sites of receptor localization in rat brain slices. The results of these studies are shown in Table 4.1 and Figure 4.6.

The values in Table 4.1 indicate that DOI and DOB are strongly bound to a receptor system in the rat brain (low dissociation constant, K_d), and that DOI labels a greater number of sites than DOB (higher B_{max}). Other data (not shown) indicate that these two agents specifically label the 5-HT_2 serotonin receptors. The reason for the higher B_{max} values for DOI is currently under study.

DOI and DOB are known to be potent psychoactive agents that cause hallucinations in man. The cerebral site of action of hallucinogens has not been determined, but the 5-HT_2 receptor system has been implicated as playing a role in the action of these agents. Figure 4.6 is an autoradiograph of rat brain slices incubated with ^{125}I-labeled DOI and ^{125}I-LSD. One of the areas that shows high receptor density with DOI and iodo-LSD is the claustrum; it is known to have extensive afferent and efferent connections to sensory brain regions and is involved in the processing of visual and auditory information. The high density of DOI and iodo-LSD binding in the claustrum suggests that the actions of hallucinogens may involve common receptors in the claustrum.

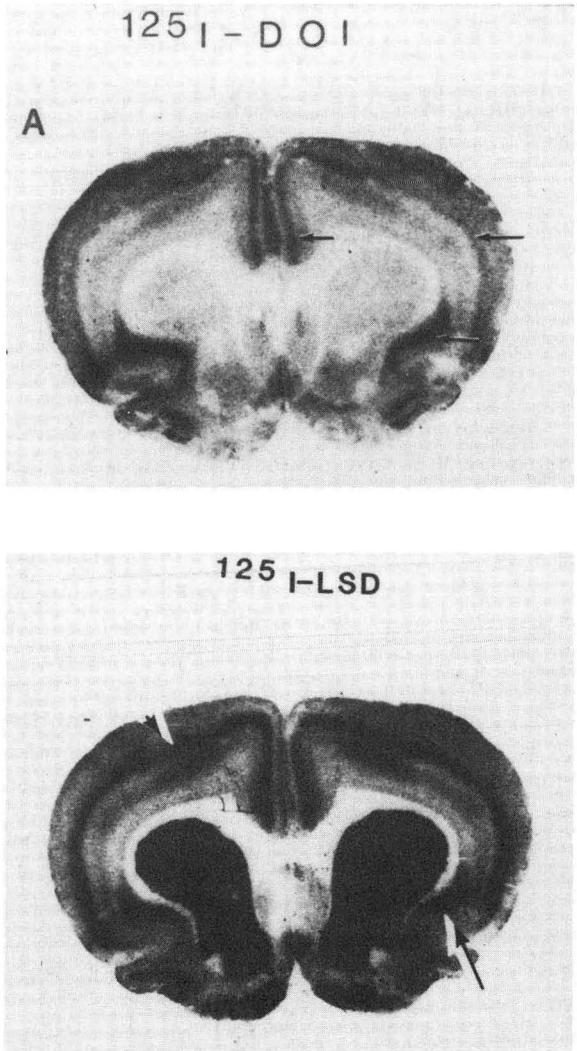

Fig. 4.6 *Autoradiographs of the binding of R-^{125}I-DOI and ^{125}I-LSD in rat forebrain sections. Arrows indicate the claustrum, parietal cortex, and cingulate cortex. The striatum (central grey matter region), which is rich in dopamine receptors, shows significant binding with iodo-LSD, but not with DOI. This indicates that DOI is more a specific ligand for serotonin receptors than iodo-LSD. (XBB 8710-9242)*

Table 4.1. Binding characteristics of DOI and DOB in rat brain homogenates.

	K_D (nM)	B_{max} (nM/g protein)
R-[^{125}I]-DOI	1.3	99
S-[^{125}I]-DOI	2.3	63
R-[^{77}Br]-DOB	0.19	10

The ultimate goal of this research is to quantify serotonin 5-HT_2 receptors *in vivo* in normal and abnormal human subjects utilizing noninvasive imaging techniques such as positron emission tomography (PET) and single photon emission computed tomography (SPECT). Studies such as those described above are necessary to identify and quantitate the binding characteristics of agents

that someday may be useful as radiopharmaceuticals. Future studies will include mapping of the distribution of these agents by autoradiography and evaluation of compounds for use with PET and SPECT studies *in vivo.*

C.A. Mathis, A.T. Shulgin, and T.W. Sargent, III. Collaborators: D. Nichols, S. Peroutka, and D. McKenna.

DIFFERENTIATION OF ACTIVELY GROWING TUMOR FROM INACTIVE TUMOR *IN VIVO,* USING POSITRON EMISSION TOMOGRAPHY

The purpose of this study is the diagnosis of tumor activity in brain tumor patients with histologic evidence of viable tumor.

PET studies using rubidium-82 (^{82}Rb) and ^{18}F-fluoro-2-deoxyglucose (^{18}F-FDG) were done in 18 patients with malignant brain tumors. All patients had presented with deterioration, following initial stabilization, 4 months to 2 years after treatment by interstitial irradiation. Surgery was performed to relieve intracranial pressure and to obtain tissue for a histological diagnosis in order to differentiate tumor regrowth from radiation necrosis. Viable tumor cells were seen in all patients, but clinical follow-up clearly separated the patients into two groups: 9 who deteriorated without anti-tumor therapy and 9 who did not. It was apparent that the tumor tissue was inactive and nonproliferating in half of the patients, despite histologic appearances that were identical to the other group. Assessment by PET with FDG showed a relatively high level of glucose metabolism in 8 of the 9 who had clinically active tumor and relatively depressed metabolism in 7 of the 9 who did not.

This study was originally undertaken with the intention of comparing PET results to histologic diagnosis of tumor recurrence. Initial results, reported in 1986, showed apparently good correlation between the two. However, subsequent clinical follow-up has shown that the histologic diagnosis is unrelated to clinical tumor progression and is of no value for patient management. On the other hand, the results of PET with ^{82}Rb and ^{18}F-FDG do correlate with clinical tumor progression and can be used to determine the need for anti-tumor therapy. This is the first time that *in vivo* PET studies have successfully demonstrated clinical activity or inactivity of tumors that appear histologically identical.

Peter E. Valk and Thomas F. Budinger (LBL); Philip Gutin, Victor A.Levin, and Pamela Silver (UCSF Medical School).

QUANTITATION OF HYPOXIA WITH MISONIDAZOLE DERIVATIVES

Radiolabeled compounds that could be utilized to determine the hypoxic content of tissues *in vivo* would be of considerable benefit. There are a number of potential uses of these agents in conjunction with noninvasive imaging modalities such as positron emission tomograpy (PET); these applications include quantitation of hypoxic cells in solid tumors, stroke, and ischemic heart disease. The ability to quantitate and temporally follow the extent of hypoxia in diseased tissues before and after various therapeutic regimes could be of great clinical value.

Solid tumors in animals and man are known to consist of cells that are heterogeneous in proliferation and oxygenation status. Numerous studies have provided evidence that oxygen concentration is an important factor in tumor growth kinetics and the presence of viable hypoxic cells in tumors has been inferred histologically or by their radiobiological responses since no direct assay or marker for these cells has been available. Hypoxic cells in solid tumors can control radiocurability because they are known to be about 3 times more resistant to ionizing radiation than are oxygenated cells. Radiation therapy is directed at the treatment resistance of hypoxic cells, and their role in tumor responsiveness has clinical relevance. The identification of viable hypoxic cells in stroke and ischemic myocardium to assess potentially recoverable tissue may also be of great benefit in helping to evaluate various therapeutic problems such as selecting patients for cerebral artery and cardiac bypass operations or determining the efficacy of drug, enzyme, and hyperbaric oxygen treatments.

A number of compounds, including quinones, anthracyclines, paraquat, and heterocyclic nitro compounds such as nitrofurans and nitroimidazoles, have been shown to undergo enzyme-catalyzed redox cycles in biological systems. The 2-nitroimidazoles (2-NI), originally developed as antiprotozoal agents, were shown to be effective as radiosensitizers of hypoxic cells in the early 1970s. The 2-NIs enter cells and the nitro group is reduced to the nitro anion free-radical due to the high electron affinity of the compounds. Formation of the nitro anion free-radical can occur either metabolically by enzyme catalyzed redox cycling in the absence of ionizing radiation, or by the transfer of an electron from a transient species formed by ionizing radiation. The nitro radical anion reacts with dioxygen to form the original nitro compound

and accounts for the selective action of these agents upon anaerobic or hypoxic cells. The details of the mechanism of action of these compounds have not been fully elucidated, but it is believed that the nitro anion radical is not the primary alkylating species formed by nitro reduction, but rather that it is an intermediate in the formation of these species. Of concern to the development of hypoxic tissue imaging agents are the observations that 2-nitroimidazoles covalently bind selectively to hypoxic mammalian cells both *in vitro* and *in vivo*. The details of this binding process are not clear, but it is evident that binding rates to intracellular biomolecules (including DNA and macroproteins) occur in inverse proportion to oxygen concentration within the cells; rate differences of 50-fold have been reported for binding of 2-NIs to cells under hypoxic conditions compared to aerobic conditions.

A collaborative research effort was begun with J. Rasey, K. Krohn, and J. Grierson (University of Washington School of Medicine) to label a 2-nitroimidazole derivative with a positron emitter (^{18}F) and conduct organ distribution and imaging studies in normal and tumor-implanted rats. Tumor-implanted rats were provided by S. Curtis and T. Tenforde of the Radiation Biophysics Group (myosarcomas) and by J. Rasey's colleagues at the University of Washington (gliomas).

Labeling experiments were conducted at the 88-Inch Cyclotron at LBL to synthesize ^{18}F-labeled fluoromisonidazole (Fig. 4.7). Labeling yields of 1–10% were achieved, which were sufficient for preliminary studies in small rodents, and animal studies utilizing normal rats and rats in which glioma and myosarcoma tumors were implanted were begun. It was found that the ^{18}F-fluoromisonidazole distributed rapidly to all organs in the rat and cleared from all tissue except bladder, large intestine, and tumor. An Anger positron camera photograph of a rat with implanted myosarcomas is shown in Fig. 4.8. The activity in the two tumors on the animal's shoulders is evident; activity in the caecum was found to be contained in its contents, consistent with the binding of the 2-nitroimidazole by anaerobic bacteria. A PET image taken with the Donner 280-Crystal Tomograph through a longitudinal section of a rat with an implanted glioma is shown in Fig. 4.9; high levels of activity are evident in the tumor and bladder. Bladder activity is consistent with clearance of the compound from the blood via the kidneys.

These preliminary results demonstrate the feasibility of imaging hypoxic tissue *in vivo*. The synthesis and preliminary evaluation of several

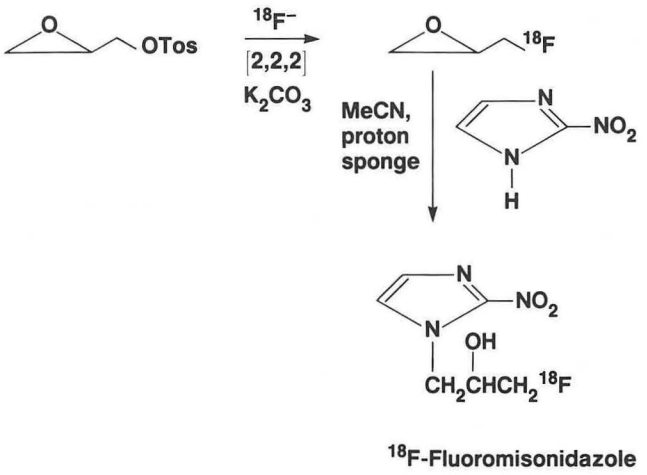

Fig. 4.7. Radiosynthesis of the hypoxic cell marker ^{18}F-labeled misonidazole. The synthesis involves the formation of ^{18}F-epifluorohydrin, its coupling with 2-nitroimidazole to produce ^{18}F-labeled fluoromisonidazole, and was performed in collaboration with John Grierson. (XBL 875-9039)

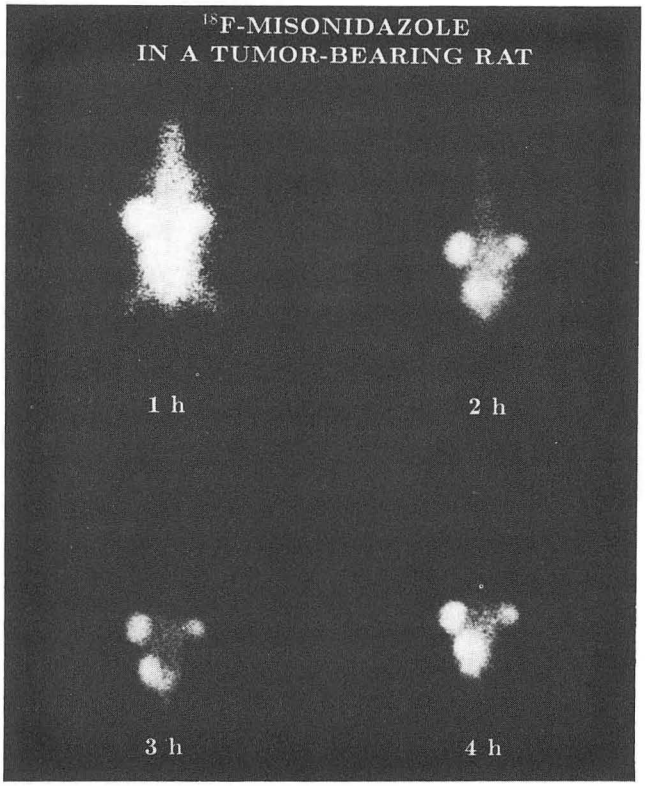

Fig. 4.8. Anger positron camera images of a tumor-bearing rat at various times after the injection of ^{18}F-fluoromisonidazole. At 1 hour the activity is distributed throughout the rat and the tumors on the shoulders contain the highest concentration of activity; at 3 hours and 4 hours only the two tumors on the rat's shoulders are visible along with the contents of its large intestine. (XBL 8710-9082A)

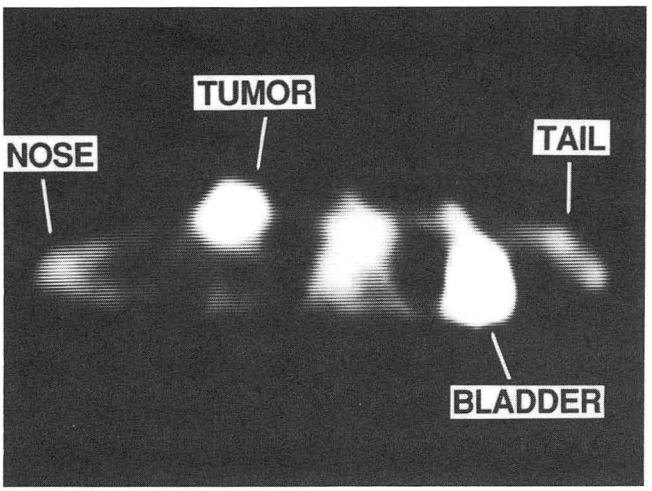

Fig. 4.9. PET image of a tumor-bearing rat 1 hour after injection of ^{18}F-fluoromisonidazole. This longitudinal view was taken on the Donner 280-crystal tomograph. (XBB 874-2970A)

other 2-nitroimidazole derivatives that may be more useful in higher animal species including man are also under investigation. While the rodent is a convenient experimental choice, many metabolic processes are 2–6 times more rapid in the rodent than in dogs and primates. Misonidazole and fluoromisonidazole have been shown to clear slowly from dog blood with a plasma clearance half-time of 9 hours. The eventual application of the 2-nitroimidiazoles to quantitating hypoxia in man will require a plasma clearance time considerably less than the half-life of ^{18}F (110 min). While other longer-lived positron emitting radio nuclides exist, considerations regarding patient dosimetry, ease of radionuclide production, and convenience to eventual clinical application make their use in this application less desirable; fluorine-18 has a relatively low-energy positron and a convenient half-life for radiochemistry and imaging. We plan to evaluate fluoromisonidazole as well as other 2-NI analogs as potential quantitative hypoxic cell markers.

C.A. Mathis, T.F. Budinger, Y. Yano, J. Gerdes, and S. Hanrahan. Collaborators: S. Curtis, T. Tenforde (Radiation Biophysics Group), J. Rasey, K. Krohn, and J. Grierson (University of Washington).

Heart and Atherosclerosis Studies

The studies of cardiovascular diseases encompass investigations of the genetic relations to lipoprotein patterns in patients, the biochemistry of normal and abnormal lipoproteins, the development of methods to measure the lipoprotein receptor activity in the human using tracers, development of methods for detecting arterial lesions, and studies of heart muscle blood flow.

IMAGING ATHEROSCLEROSIS

Arteriosclerosis studies using methods of imaging vessel pathology have focused on human platelet imaging, affinity of atherosclerosis for hematoporphyrins, and use of labeled low density lipoproteins. New findings on porphyrin and LDL distribution that show promise in the development of a method for studying the natural history of the atheromata that block human arteries are presented below.

Evaluation of Radioporphyrins for Uptake in Vascular Lesions

Investigations were continued on the uptake of radioporphyrins in balloon-catheter deendothelialized rabbit aorta relative to normal aorta for the detection of vascular lesions. Whole-body positron emission tomography (WB-PET) and tissue-counting experiments were done to determine the time-course distribution of $^{68/67}$Ga-porphyrins in normal and hypercholesterolemic-diet rabbits.

The uptake of $^{68/67}$Ga-tetra(4-sulfonatophenyl)porphyrin ($^{68/67}$Ga-TPPS4) in various tissues, including normal and damaged aorta was determined from 30–300 minutes postintravenous injection. The ratios of uptake in damaged to normal aorta were calculated and plotted (Fig. 4.10) to show an increase from 2.3 at 30 minutes to a maximum of about 4.7 at 180 minutes and then a decline to 2.8 at 300 minutes.

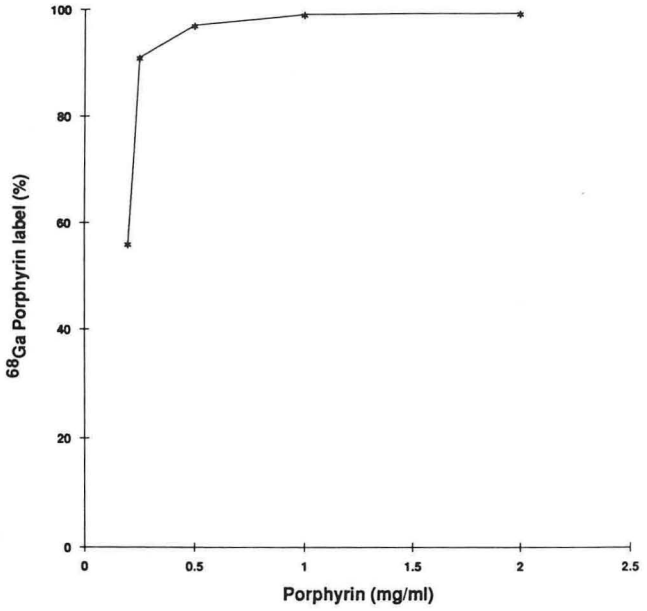

Fig. 4.10. *^{68}Ga-labeling efficiency versus porphyrin concentration (mg/ml). * = ^{68}Ga-TPPS4 (XBL 8710-4373)*

Table 4.2. ^{68}Ga-TPPS$_4$ distribution in rabbits (% injected dose/gram tissue 120 minutes post intravenous injection).

Tissue	Normal diet (n = 3)	Hypercholesterol diet (n = 1)
Blood	0.278	—
Kidneys	0.109	0.103
Lungs	0.122	0.150
Liver	0.123	0.071
Spleen	0.113	0.118
Normal–proximal aorta	0.064	0.062
Scraped–distal aorta	0.258	0.163

Average uptake ratio of scrapped-aorta to normal aorta:

Normal-diet rabbit	4.03
Hypercholesterol-diet rabbit	2.63

WB-PET scans with the 280 BGO detector PET system (7–8 mm resolution) were obtained from 0–30, 30–60, and 60–90 minutes post-intravenous-injection of balloon-catheter deendothelialized-aorta rabbits on normal and hypercholesterolemic diets. Figure 4.11 demonstrates scans done at 0.5 and 1.5 hours showing anteroposterior and lateral views.

Table 4.2 shows the uptake in various tissues of normal and hypercholesterolemic-diet rabbits at 120 minutes postintravenous injection.

The damaged to normal aorta uptake ratio (4.7) at 150–180 minutes is greater than maximum ratios with ^{68}Ga-labeled platelets (3.5) at 30–60 minutes. Furthermore, the radiolabeled porphryins are preferable to platelets, which require separation from plasma.

Tissue distribution results in normal as compared to hypercholesterolemic-diet rabbits showed similar uptake at 120 minutes postintravenous injection, except for the liver and scraped/deendothelialized aorta, which had about 40% less uptake in the hypercholesterolemic-diet rabbits.

Yukio Yano, Kathleen M. Brennan, Shirley N. Ebbe, and Thomas F. Budinger.

Autoradiographic Studies with a Radiolabeled Analog of Low Density Lipoproteins

Preliminary studies on the development of a radiolabeled analog of low density lipoprotein (LDL) for human diagnosis resulted in the successful radioiodination of a tyramine-cellobiose (TC) adduct of LDL. The work reported here extends those studies to autoradiographic imaging of the localization of TC-LDL in the rabbit aorta and gives promise to the possible imaging of the progression and regression of atherosclerosis in humans.

[^{123}I]TC-LDL was injected into male New Zealand white rabbits with control or hypercholesterolemic diets (1.0% cholesterol + 4% peanut oil for 8–15 weeks, or 0.5% cholesterol + 2% peanut oil for 14–21 weeks). The rabbits were sacrificed 4 hours postinjection and the aortas removed, opened longitudinally, and washed several times with saline. The clean aortas were wrapped in plastic-wrap and sandwiched between Kodak diagnostic film, then stored at -70°C for 3.5 days. The exposed film was developed with standard Kodak solutions.

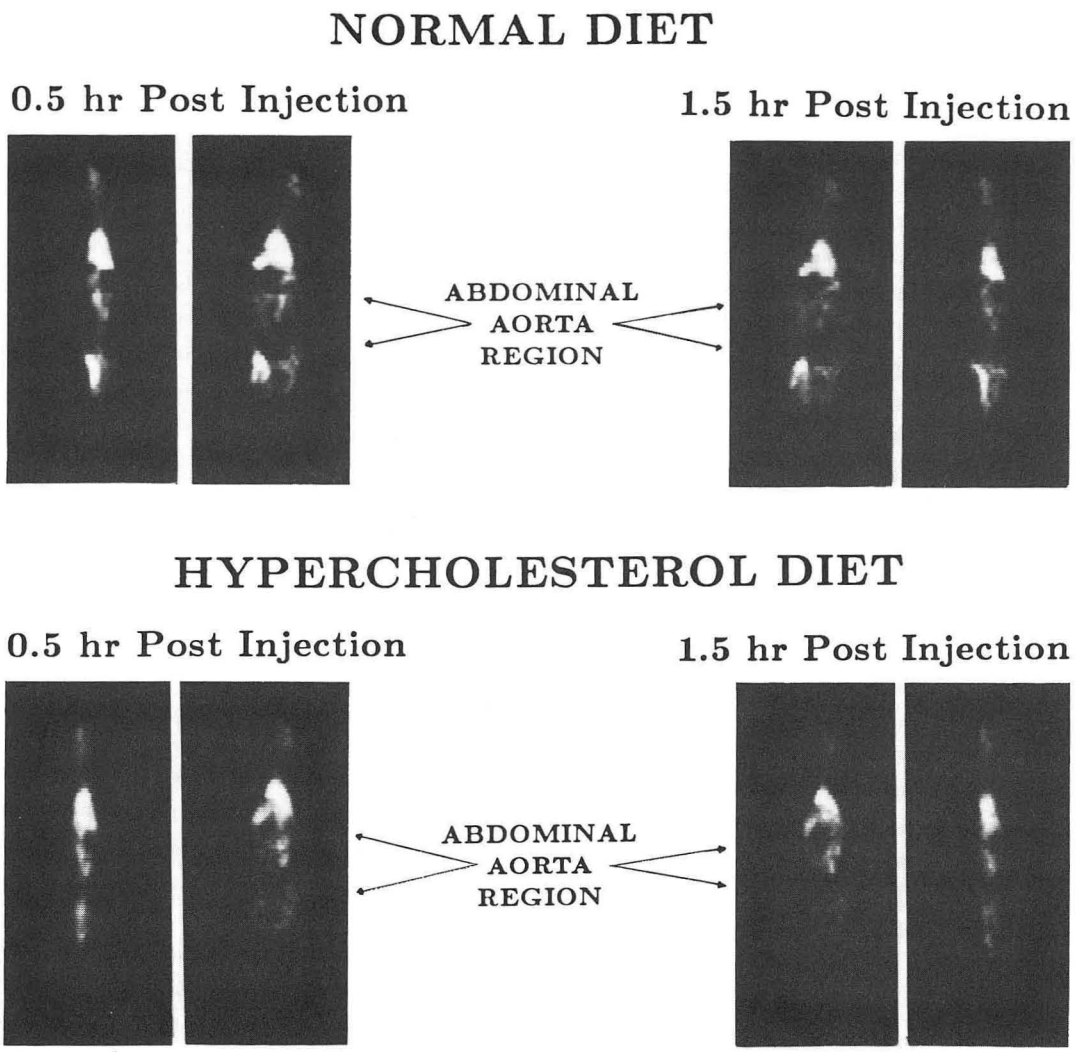

Fig. 4.11. *^{68}Ga-porphyrin activity on the scraped aorta: Normal versus hypercholesterolemic rabbits. (BBC 875-4195)*

The opened aortas are shown in the left half of Fig. 4.12, which shows a marked accumulation of foam cells in an advanced aortic lesion. Autoradiographic images are shown in the right half of the figure, demonstrating the localization of the [^{123}I]TC-LDL in the atherosclerotic areas of the hypercholesterolemic aorta, while the control aorta is virtually free of radiolabeled TC-LDL.

Future work will include imaging with radiolabeled TC-LDL in studies of LDL metabolism in various patient populations and in studies using the rabbit model to evaluate the efficacy of pharmacological intervention in LDL metabolism.

K. Dalal, S. Ebbe, D. Carpenter, T. Yee, Y. Yano, K. Brennan, and T. Budinger.

HEART STUDIES

The efforts to perfect a method of evaluating heart muscle blood flow using radionuclide tracers are motivated by the need for an alternative to coronary catheterization. In the past this need was based on the desire to have a noninvasive diagnostic method. More recently, there has developed a vital need for performing repeated studies to monitor the effects of chemical therapy for lysing clots in coronary arteries and to evaluate the efficacy of intracoronary artery atheromata removal techniques such as laser ablation.

Our radionuclide-tracer method continues to be validated as a good measure of myocardial perfusion. A typical patient study is shown in Fig. 4.13.

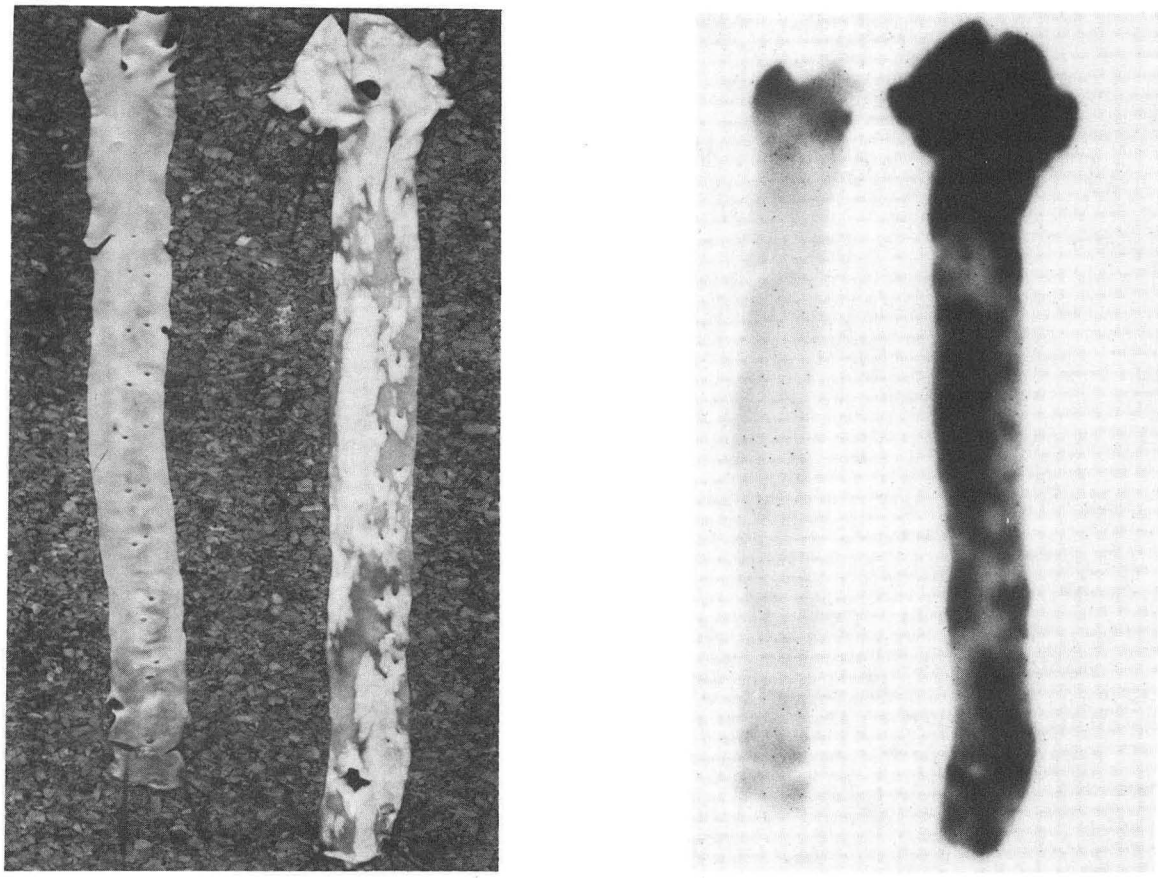

Fig. 4.12. At left is a photograph of aortas removed from a control-diet rabbit (left) and a hypercholesterolemic diet rabbit (right). The hypercholesterolemic aorta shows a great accumulation of foam cells, while the control aorta is relatively free of lesions. At right are the autoradiographic images, demonstrating the accumulation of [^{123}I]TC-LDL in the hypercholesterolemic aorta (right) and the lack of accumulation of the radiolabeled TC-LDL in the control aorta (left). (BBC 876-5413A)

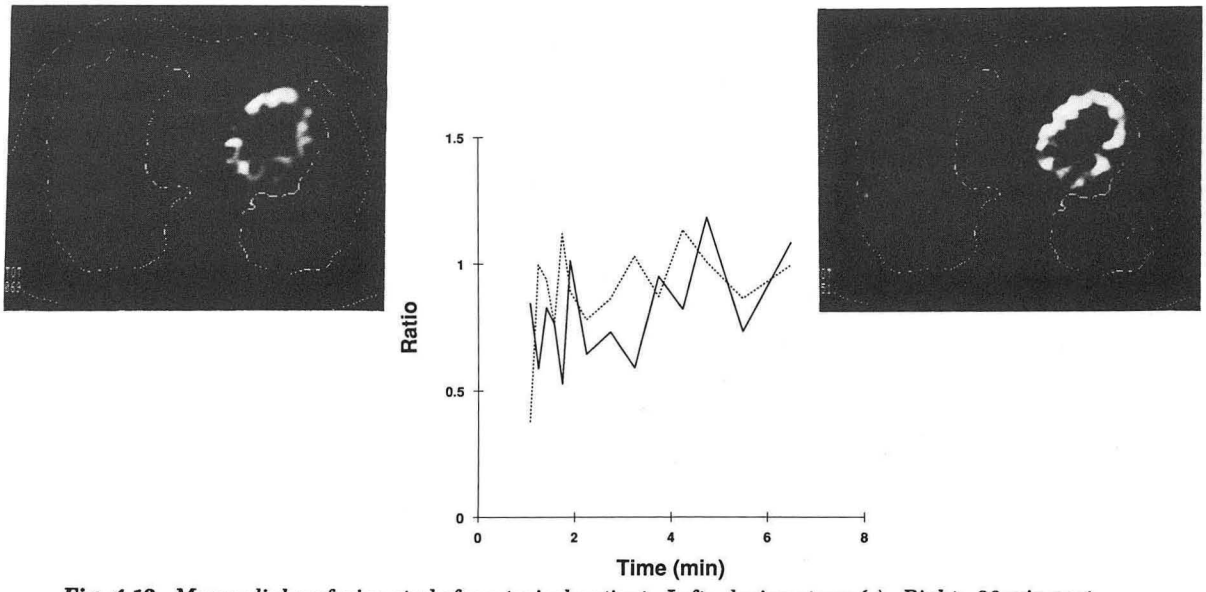

Fig. 4.13. Myocardial perfusion study for a typical patient. Left: during stress (–). Right: 30 min post-stress (.....). Curves show ratio of ^{82}Rb accumulation in defect area to that in the anterior septum. (BBC 875-4047)

Therapy with Charged Particle Beams

REVIEW OF HEAVY CHARGED PARTICLE RESEARCH TRIAL FOR FY 1987

The Heavy Charged Particle Clinical Research Trial continued to accrue patients in studies of dose-localization radiotherapy for uveal melanoma, base-of-skull and para-CNS chondrosarcoma/chordomas, and other histologies.

A randomized Phase II study in conjunction with the Department of Radiation Medicine of Massachusetts General Hospital and the Harvard Cyclotron was opened through the Radiation Therapy Oncology Group to study patients with chordoma/chondrosarcoma in the head and neck. It has accrued 20 patients.

A phase III randomized trial in uveal melanoma has also continued to accrue patients (100 patients to date) in comparing helium-ion therapy against iodine-125 plaque therapy. This is the only randomized study in the world contrasting these two forms of alternative therapy for uveal melanoma.

Other Phase III randomized trials for locally advanced carcinoma of the prostate (12 patients) and unresectable carcinoma of the lung (25 patients) are continuing.

The National Cancer Institute has recently renewed the Program Project Grant supporting the treatment of human cancers with heavy charged particles from October 1, 1987 through February 28, 1992. With the closure of the 184-Inch Cyclotron, the entire charged particle therapy program will be moved to the Bevatron. It is anticipated that it will be possible to carry out the proposed studies at the Bevatron with an accrual rate of about 150 patients per year.

Since local control rates in over 400 patients treated with helium-ion dose-localization therapy range from 50% (residual soft tissue sarcoma) to 70% and 90% (chordoma-chondrosarcoma and uveal melanoma, respectively), this has been highly successful treatment. However it is important that both biological and technological studies of optimization techniques for this therapy continue, as well as the randomized studies in uveal melanoma and head/neck chordoma-chondrosarcoma.

Our major emphasis in 1988 will be on comparing high-LET charged particles (neon) directly against low-LET photon irradiation and helium ion therapy, using randomized protocols in locally advanced tumors of the lung, prostate, brain, nasopharynx, paranasal sinuses, and sarcomas of bone and soft tissue. The key aim will be to establish the role of the high-LET charged particles in the clinical therapy of human cancers.

TREATMENT PLANNING DEVELOPMENTS IN RADIOTHERAPY

Developments in three major areas occurred in treatment planning using charged particles at LBL during the past year. The first was the implementation of PLAN3, a three-dimensional treatment planning system developed at Massachusetts General Hospital by Michael Goitein. With this system it is possible to plan composite treatments with photons and charged particles. It is also possible to plan noncoplanar beams. The program calculates not only nominal dose distributions but also the maximum and minimum distributions that could occur given uncertainties in patient position, CT number, and calibration. This information is extremely useful since it allows one to quantify the maximum possible dose received by a critical structure and the minimum dose to the target volume.

The second major development in treatment planning at LBL was the clinical implementation of image correlation. The ability to transfer volumes of interest from one imaging study to another has become an increasingly valuable treatment-planning tool in defining both tumor volumes and critical structures for brain lesions, in particular chordoma and chondrosarcoma. This technique, developed at LBL over the past few years by Kessler, Chen, Petti and Pitluck, has thus far been used for 11 patients. In all of these cases, target volumes and/or brainstem or spinal-cord contours were transferred from MRI to CT scans (see Fig. 4.14). Two techniques exist for calculating the transformation between two different studies, the point-to-point method, which relies on either external or internal landmarks, and surface-fitting algorithms, which minimize the difference between surfaces (e.g., those defined by the skull) in each study. In general, surface fitting or internal landmarks were used when the MRI scan came from an outside institution. Surface fitting was

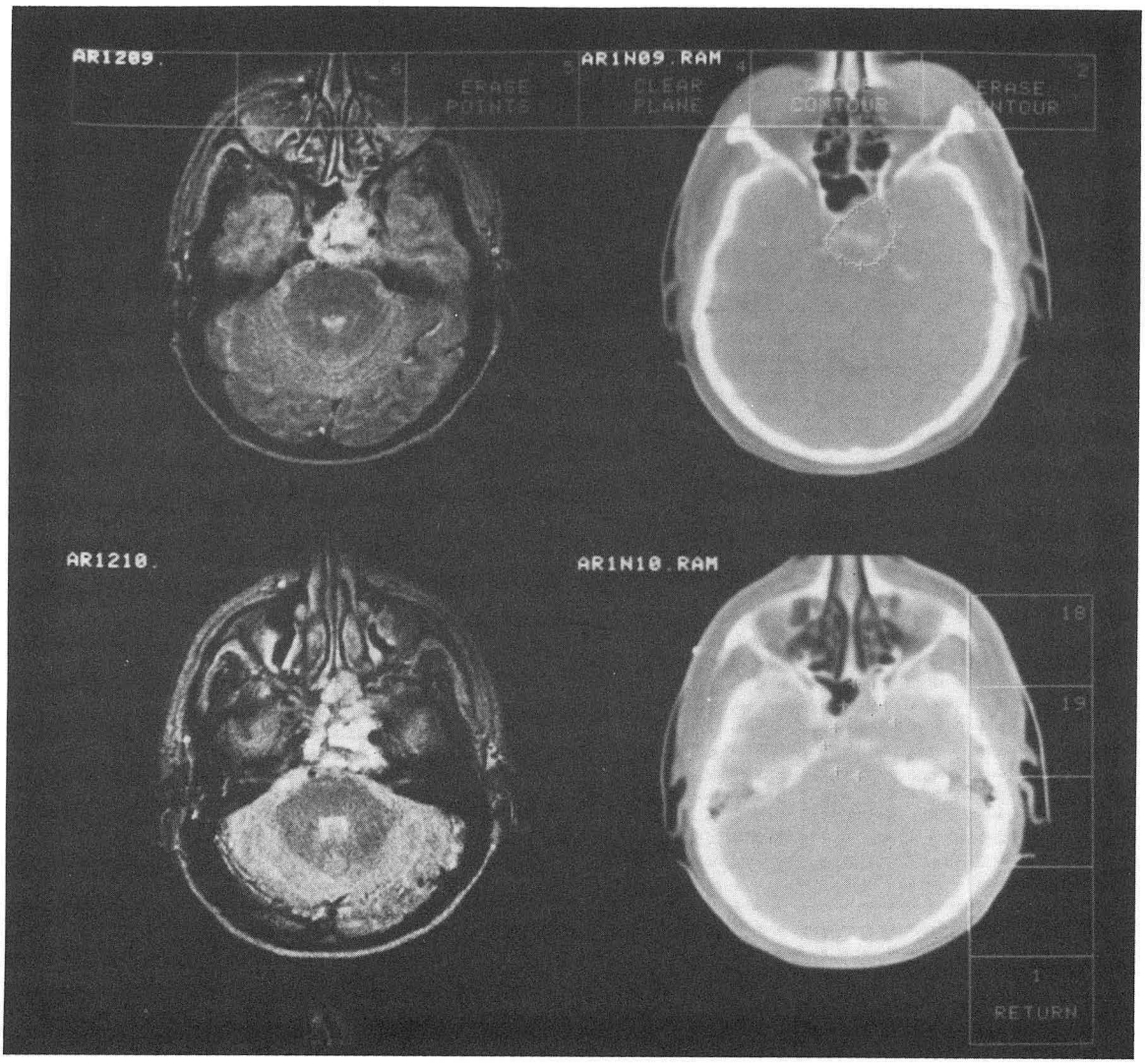

Fig. 4.14 . Contours drawn on MRI are transformed to the reformatted CT scan. (XBC 874-3427)

used in only one of the 11 patients. Of the remaining ten, in three the point-to-point method was used with external landmarks only, in another three only internal landmarks were used, and in the remaining four, a combination of both internal and external landmarks was employed. These techniques have been an important advance in planning treatments for patients when the lesion lies in close proximity to the spinal cord or brainstem, and image correlation will continue to be used on a regular basis for such patients.

The third area is the treatment plan optimization for charged-particle-beam therapy. This optimization is based on the evaluation of a treatment plan by a probabilistic model that was developed with the support of a National Cancer Institute contract for Particle Beam Treatment Planning Intercomparison. This model estimates the probability of an uncomplicated local control of a tumor based on dose-volume histograms of the three-dimensional dose distribution of the target and the critical normal-tissue volumes.

A program has been initiated for the validation of this model based on both retrospective and prospective studies of the expected and observed normal-tissue complication following charged-particle therapy. The validation will be based on dose distributions calculated by the Massachusetts General Hospital treatment-planning program. This is believed to be the most accurate program currently available for calculation of both charged-particle and photon beams; many of the patients in the retrospective study received a significant portion of their therapy with photon irradiation.

The recent developments in treatment plan optimization have been directed to the determination of optimal weighting of the selected beams that will be used for irradiation of the tumor volume. These optimal weightings are determined by a constrained minimization subroutine and the calculated probability of an uncomplicated local control.

A new development in the treatment planning program has been investigation of the improvements that can be expected by development of a variable beam-modulation delivery system with a raster scanner and variable-beam collimator. These improvements in beam delivery will lead to improved dose localization with charged-particle beams.

J.M. Collier, S.D. Henderson, P.L. Petti, M. Kessler, S. Pitluck, J.T. Lyman, K. Baken, J.R. Castro, T. Phillips, and J. Mefferd.

STEREOTACTIC HEAVY CHARGED PARTICLE RADIOSURGERY

Research in the stereotactic radiosurgical treatment of intracranial arteriovenous malformations (AVMs) has continued using the Bragg peak of accelerated charged-particle beams. Intracranial AVMs can be debilitating and life-threatening; they produce hemorrhage, seizures, recurrent headaches, and neurological deficits. These lesions are developmental abnormalities of the newborn, and patients often present with symptoms in youth or middle-age. Once hemorrhage has occurred, the risk of further hemorrhaging is greater. These factors make it desirable that the AVM be treated promptly so that the patient may enjoy a long and productive life.

Neurosurgical removal of the AVM, occasionally combined with flow-directed or intraoperated embolization of the AVM, is the treatment of choice. However, these techniques are not always possible, or if possible, not always completely successful, owing to the position of the AVM in a deep or critical region of the brain, or due to the complex network of feeding arteries and draining veins. These surgically-inaccessible intracranial AVMs have been treated at the LBL 184-Inch Synchrocyclotron using stereotactically-directed heavy charged-particle beams.

Building on the experience and techniques developed at LBL since the use of charged-particle beams for the treatment of pituitary tumors, stereotactic imaging techniques are used to direct the Bragg peak of heavy-charged-particle beams into the lesion while sparing adjacent brain tissue. Properties characteristic of fast charged particle beams that make them very useful in such an application are the fixed range of the beam with rapid fall-off of dose beyond the end of the range, the increased energy loss at the end of the range compared with the plateau region of the beam (Bragg peak), and the small amount of lateral beam scattering.

This clinically applied research focuses on improving treatment planning techniques and following the response of patients clinically and neuroradiologically in order to assess the effects of the radiosurgical treatment. In the past year, 75 patients have been treated, bringing the total since 1981 to 276 patients. These patients are evaluated in collaboration with neurosurgical and neuroradiological colleagues at Stanford University Medical Center and University of California Medical Center, San Francisco. A series of stereotactic imaging procedures (cerebral angiography, computed tomography, and magnetic resonance imaging) is performed in the specially-designed patient immobilization mask and stereotactic frame in order to localize the lesion accurately within the brain. Treatment plans are calculated on a VAX 11-780 computer, using three to five beams, shaped and positioned in order to maximize the dose to the AVM volume and minimize the dose to surrounding normal brain tissue. Treatment occurs over one or two days, depending on the size and location of the intracranial AVM.

This year the use of image correlation techniques with the stereotactic frame and mask have been extended to include nuclear magnetic resonance (NMR) imaging. NMR imaging is extremely useful in that it images the anatomical characteristics of the AVM, the large draining veins, and critical structures in the surrounding brain. It has proven particularly useful in the treatment of cryptic, or occult, AVMs. These are AVMs that cannot be imaged with cerebral angiography but are seen to some extent on contrast CT images and very clearly on NMR scanning. Computer techniques allow the accurate transfer of information between CT and NMR images. Figure 4.15 shows the charged-particle radiation isodose contours overlaid on an NMR image of a patient with an AVM in the brain stem. These contours were calculated using the AVM target imaged by NMR and transferred to the CT scan that contains energy-loss information for the charged-particle beam. The isodose contours were then transferred

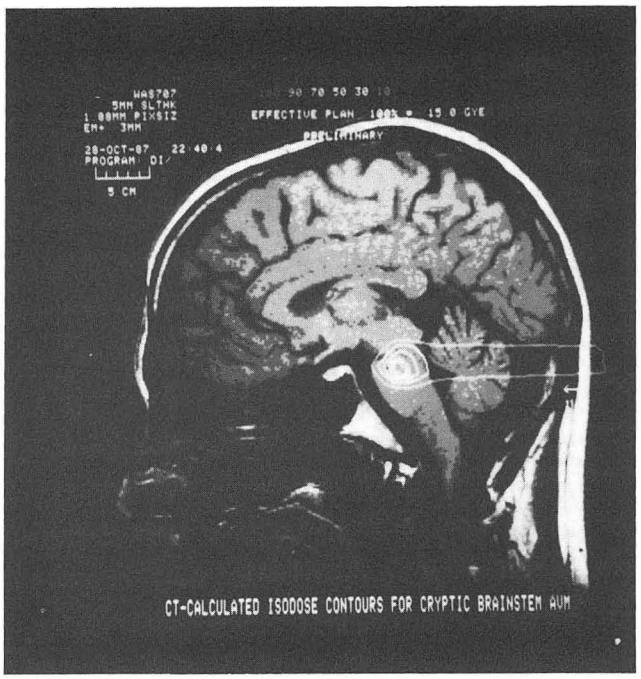

Fig. 4.15. A sagittal NMR image of a patient with a cryptic arteriovenous malformation in the pons: the isodose contours for helium charged-particle treatment are overlaid. The AVM was defined and contoured on the NMR (axial projections) and the target contours were transferred to CT images. A treatment plan was calculated using the CT data. The resulting isodose contours were then transferred to the NMR sagittal images in order to define the radiation dose to adjacent critical brain structures. The treatment plan is for three beams of helium ions; one port is in the sagittal plane shown; the other two ports are in parasagittal planes at ± 30 degrees. (BBC 8712-10668)

back to the NMR image in order to define the dose delivered and the dose distribution to critical structures such as the surrounding brainstem.

Follow-up of patients after radiosurgical treatment consists of clinical examinations either here at Donner Pavilion or by the patients' own neurosurgeons when they do not live in the area. To date, the clinical results show that 67% of the patients have remained normal or improved neurologically, 25% have shown no change neurologically and have remained stable, and the remainder have worsened neurologically. So far, there have been 7 cases of hemorrhage from the AVM prior to 15 months following therapy, well below the expected rate of occurrence in a similar population of untreated patients that follow the natural course of the disease associated with a high spontaneous rate of hemorrhage. Three other types of complications can occur. The first is vasogenic edema in the cerebral white matter extending outside the radiation field; this appears to occur in about 10% of patients, with about 5% experiencing clinical symptoms. The second is a 2–4% incidence of stroke (including arterial occlusion, venous thrombosis, or embolism), frequently occurring during the final phase of obliteration of the AVM. The third is delayed brain injury leading to radiation necrosis; this may have occurred in two patients (unconfirmed without tissue diagnosis). Taken together, the complication rate appears to be low, and less than the surgical risk or the risk of death or neurological damage from the natural course of the disease.

Neuroradiological followup examinations, performed at the Stanford University Medical Center, The University of California, San Francisco, or the patient's local hospital, consist of cerebral angiography, CT, and NMR scanning. For patients followed at least one year post-treatment, 50% of the patients achieve complete obliteration of the AVM in 1 to 2 years. Partial or complete obliteration occurred in 70% of patients by 2 years, and no change (less than 50% obliteration) was apparent in 15% of the patients. The data indicate that protection against hemorrhaging is achieved in most patients even if complete obliteration does not occur.

Current research with other investigators in the Research Medicine Group and colleagues in collaborating university hospitals is exploring the uses of NMR imaging and positron emission tomography (PET) in evaluating radiation-induced changes in the AVM and the surrounding brain tissues. NMR is proving to be useful as a noninvasive procedure for evaluating morphological changes in the AVM, and thereby indicating the optimum time for a more complete and detailed evaluation using cerebral angiography. Vasogenic edema, visible in its early stages only by NMR imaging, can now be recognized and followed before clinical symptoms become apparent. A prospective study using PET and NMR , and correlating these with morphological alterations in brain tissue, is in progress to examine physiological changes following radiosurgery.

Through the end of 1987, all radiosurgical treatments have been performed using the 230-MeV/u helium-ion beam at the 184-Inch Synchrocyclotron at LBL. Beginning in January 1988, the program will move to the Bevalac accelerator. Work in in progress, in collaboration with the Accelerator Division and the radiotherapy physicists to produce and characterize the 165-MeV/u helium beam at the Bevalac, with plans to eventually use carbon-ion beams for stereostactic radiosurgery. Comparative studies are being carried out

to determine the differences between various species of charged-particle beams and photons in the treatment of intracranial AVMs.

J.I. Fabrikant, K.A. Frankel, M.H. Phillips, R.P. Levy, J.T. Lyman, N. Manley, E.H. Lo, M.L. Foster, F. Chuang, and P. Valk.

NEUROBIOLOGICAL EFFECTS OF HEAVY PARTICLE IRRADIATION

In parallel with the heavy-ion radiosurgery research program, fundamental investigations are being carried out to understand the basic physical and biological mechanisms underlying the neurobiological responses to irradiation with focal beams of heavy charged particles (e.g., helium, carbon, neon). The objectives of this research program are to examine cellular and metabolic effects in mammalian (including human) brain in relation to alterations in regulatory control mechanisms, the sites of DNA damage and repair, cellular proliferation and differentiation, the process of myelination and myelin maintenance, and regional cerebral blood flow dynamics; and to develop and apply nuclear medicine procedures for investigating cellular and metabolic events in brain irradiated with heavy charged particles.

Studies of the physical properties of the heavy charged-particle beams have been focused on multiple Coulomb scattering and particle production in heavy-ion collisions. Multiple scattering of the charged particles is a limiting factor in delivering a uniform dose to a target volume, and is one of the criteria in evaluating the dose-localization properties of beams of different ion species. Parallel efforts in computer calculations of the effect of multiple scattering and experimental measurements have proceeded in collaboration with other physicists of the Biology and Medicine Division. Agreement has been found between theory and experiment for clinically important beams, such as protons and carbon ions as well as more exotic ions such as uranium.

Calculation of neutron production in heavy-ion collisions provides further information on the characterization of heavy-ion beams and the distribution of dose. Excellent agreement has been achieved between calculations performed using a cascade code and experimental work by Schimmerling and his colleagues in the Radiation Biophysics Group.

Biological research on the effects of heavy charged particles has proceeded along several directions. In collaboration with Dr. K. Rosander of Sweden, we are studying the induction and repair kinetics of DNA damage in single cerebral and cerebellar oligodendroglial and capillary endothelial cells from rat and mouse brain following selected dose increments of heavy-ion beams, in order to characterize dose-response and time-dependent relationships. The technique involves measuring fluorescent dye intensity as an index of DNA single- and double-stranded breaks using a microscope photometer following DNA unwinding. The data thus far indicate a general increase in DNA damage with neon ions relative to helium ions, and the dose-dependent effect is much greater for oligodendroglial cells than for cerebral endothelial cells. DNA damage *in vivo* is repaired rapidly in both glial and endothelial cells, and the greatest amount of repair occurs within 30 minutes following irradiation with a linear dose-effect relationship for both low-LET and high-LET radiation (Fig. 4.16). The results suggest different post-repair behaviors for the two types of cells; the endothelial cells may be less radiosensitive.

In order to overcome the difficulties in defining changes in cells in the highly integrated brain tissue, techniques have been developed to isolate and maintain defined mammalian brain cell populations in short-term culture, and to identify potential cell-specific properties for use as indicators of cell damage and altered cell metabolism. Of

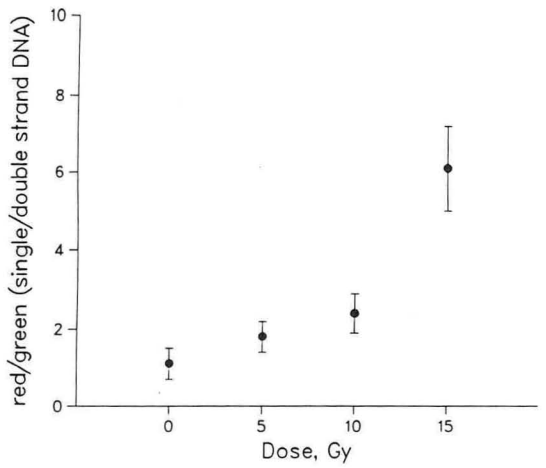

Fig. 4.16. *The dose-response for cerebral endothelial cells 6 minutes after helium-ion irradiation. (Six minutes is the minimum time available after irradiation.) The ratio of red/green fluorescence (single/double stranded DNA) is plotted as a function of dose for mouse brain endothelial cells irradiated* in vivo. *(XBL 8712-8029)*

particular interest is purifying and maintaining glial cell populations in order to examine the effects of heavy-ion irradiation on myelin renewal and the maintenance of myelin.

Pulse-labeled mitosis is one of the techniques being used to study the brain cell population kinetics of the subependymal layer of the mouse brain. Cell-cycle parameters have been measured for these cells in unirradiated mice and in mice irradiated with either helium or neon ions. The responses of different cell population in the subependymal layer to different types of radiation (x rays, helium ions, neon ions) and a range of doses have been measured. Figure. 4.17 illustrates the population doubling times of the subependymal cells following exposure to 230-MeV/u helium ions. The doubling time is markedly reduced after irradiation with 45 Gy, from a normal value of about 140 hours to about 45 hours in the irradiated cortex, and to about 55 hours in the unirradiated cortex of irradiated mice. The glial cell kinetic data in normal and irradiated mouse brain are consistent with the conclusions that in the subependymal plate the light cells remaining after radiation represent a resistant stem cell population with a relatively slow rate of renewal. The dark cells comprise a rapidly proliferating stem cell population, which is relatively radiosensitive, and it is this stem-cell pool that is responsible for recovery following heavy-charged-particle irradiation.

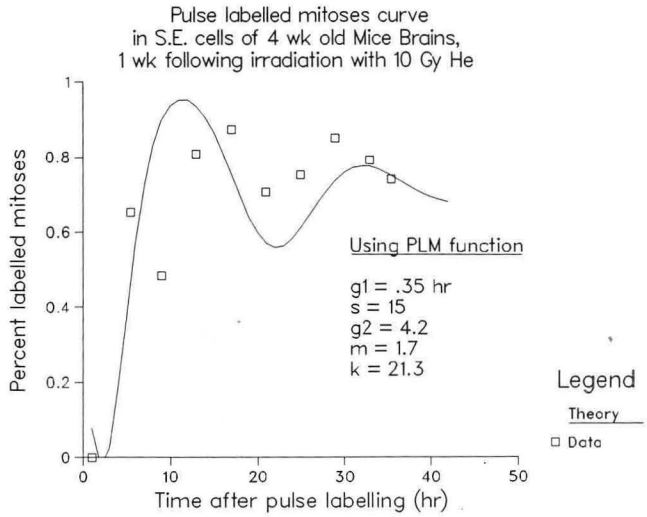

Fig. 4.17. *Percent of labeled mitoses following pulse labeling with tritiated thymidine in the subependymal cells of 4-week-old mouse brain, 1 week following irradiation with 10 Gy He (150 MeV/u). The open squares are the measured points, the smooth curve is a fit to the data using the theory of Takahashi. The durations for the cell cycle parameters derived from the fit are listed. Work is currently in progress to extend the curve fitting to include variations in the cell cycles by means of a Monte Carlo approach. (XBL 8712-8030)*

J.I. Fabrikant, K.A. Frankel, M.H. Phillips, R.P. Levy, J.T. Lyman, N. Manley, E.H. Lo, M.L. Foster, and F. Chuang.

Imaging, Instrumentation, and Methods

NEW POSITRON EMISSION TOMOGRAPH INSTRUMENTATION

Imaging studies using a new very high resolution medical imaging system, the Donner 600-Crystal Positron Tomograph, have recently begun. This system was designed and built at LBL to image positron-emitting tracer isotopes in the human brain and neck with a spatial resolution a factor of two finer than any other tomograph. The instrument consists of a ring of 600 bismuth germanate (BGO) crystals 3-mm wide coupled individually to 14-mm phototubes. When the tracer isotope decays, it emits a positron (the anti-electron) that comes to rest in the tissue nearby and annihilates with an electron. In this process, the positron and electron disappear, and their energy is immediately converted into two photons that fly off in opposite directions. Whenever two BGO crystals detect two photons within 10 billionths of a second, the event is recorded in high speed memory. The image of the tracer distribution is reconstructed from these data using an array processor.

As a test of image sharpness, a very small source of positron emitter was positioned at the center of the instrument. The resulting image was a circle with a diameter (full-width at half-maximum) of 2.6 mm. Another test of image sharpness was performed using the object shown in Fig. 4.18, which consists of a pattern of hollow channels drilled into a solid plastic cylinder. The channels

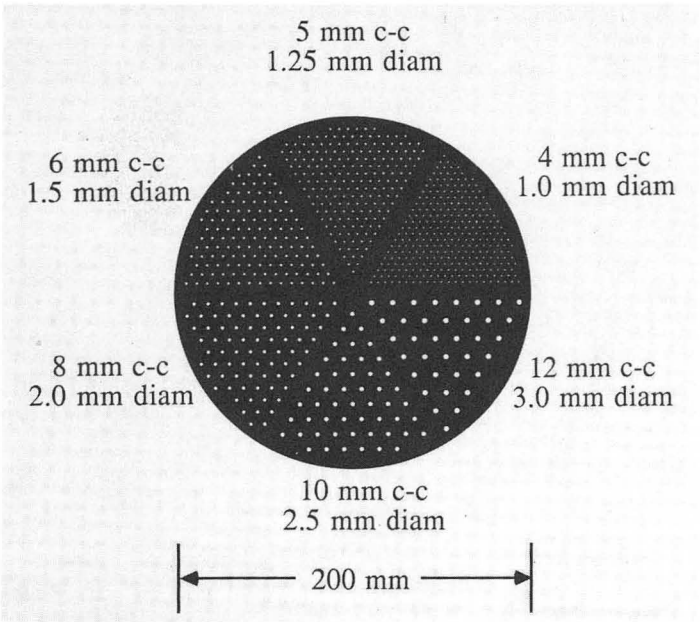

Fig. 4.18 *Sketch of a plastic cylinder containing isotope-filled channels. The finest channels are 1-mm diameter on 4-mm centers. (XBL 8610-4032)*

were filled with a solution of the positron emitting isotope ^{18}F and imaged (Fig. 4.19). Near the center of the tomograph, individual channels with 4-mm center-to-center spacing can be individually resolved. Channels with 5-mm center-to-center spacing can be individually resolved throughout the field of the tomograph.

The detector configuration and electronic circuits were designed for high speed, as well as high spatial resolution. To correct the emission data for absorption of photons in the tissue, a positron source of 20 mCi of ^{68}Ge runs around the outside of the patient, and events are collected at a rate of 800,000 per second. This represents a factor of 8 speed improvement over previous designs and reduces the time to acquire the attenuation correction data from 15 minutes to 2 minutes. These data can be reconstructed to produce an image of the absorption of annihilation photons in the human head [see Fig. 4.20(a)]. This source is withdrawn into the lead shielding for collecting emission data.

The positron-emitting tracer compound ^{18}F-fluoro-deoxyglucose is used to image metabolic

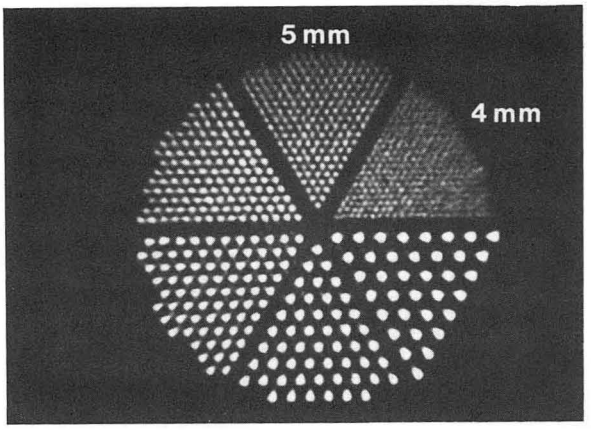

Fig. 4.19 *Image of the isotope ^{18}F in the plastic cylinder taken by the Donner 600-crystal positron tomograph. (XBB 878-7172)*

activity in the brain because its accumulation closely mimics the absorption of glucose, the primary fuel of the brain. This compound is administered with a simple intravenous injection, and data from the ^{18}F are acquired to produce an image of the uptake of glucose in the human brain [Fig. 4.20(b)].

Stephen E. Derenzo, William W. Moses, Ronald H. Huesman, and Thomas F. Budinger.

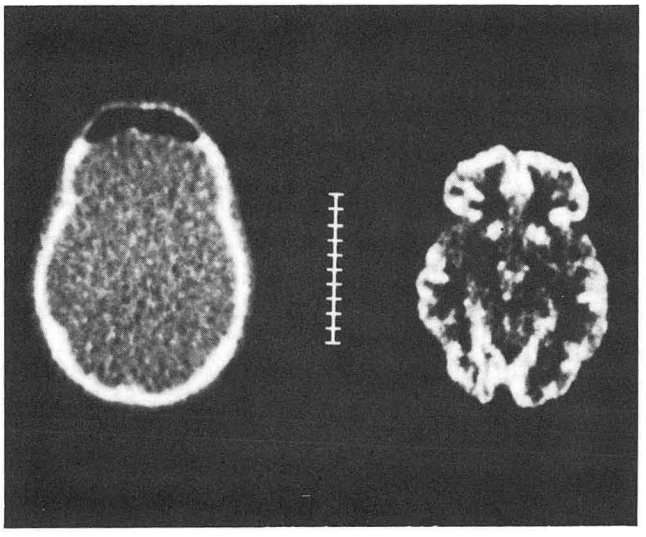

Fig. 4.20 *(Left) Image of a slice through the human head taken by the new tomograph using an external positron source, showing the bones, soft tissues, and nasal passages. (Right) Image of the tracer ^{18}F-fluoro-deoxyglucose in the same slice of the human brain, showing the uptake of sugar. (XBB 875-4261)*

NMR METHODS

Slow Flow Imaging with Steady State Free Precession

Nuclear magnetic resonance studies of moving spins began with diffusion experiments and have evolved to include measurements of bulk flow, including *in vivo* angiography. This study concerns *in vivo* imaging of tissue perfusion without tracers, that is, detection of flow in the capillary bed. Each imaged unit-volume or *voxel* is assumed to contain capillaries with many different orientations, so the flow model shares some properties of both random (diffusive) flow and laminar flow. Typical flow velocities are on the order of 1 mm/sec. Conventional flow imaging experiments require very large magnetic field gradients to detect such small velocities, with accompanying instrumentation problems. Steady-state free-precession (SSFP) imaging is used for improved sensitivity and shorter acquisition time.

The SSFP experiment consists of a sequence of identical rf pulses separated by an interpulse interval τ. For static spins, a steady state is established that is a function of the relaxation times T_1 and T_2, the rf tip angle, and the angle through which the spin precesses during τ. In the presence of an applied gradient $G(t)$, the magnetization is a periodic function of r and has a spatial wavelength λ: $\lambda = 1 / (\gamma G_{eff} \tau)$. G_{eff} is the effective gradient strength, which is the time average of $G(t)$ over the interval t. γ is the gyromagnetic ratio of the proton.

Since the magnetization is a periodic function of position, a moving spin will continually try to approach the local steady state. However, because a finite time is required for the steady state magnetization to be established, moving spins do not attain the maximum response. The response of flowing spins is expressed in terms of the dimensionless parameter ϕ defined as $\phi = v \tau / \lambda = \gamma G_{eff} v\tau^2$ where v is the speed in the spin in the direction of the effective gradient.

The response of moving spins was determined experimentally with a phantom consisting of a tube packed with 3-mm diameter polystyrene spheres. Doped water is introduced at one end and removed at the other, establishing a net flow in the axial direction. The gradient was oriented perpendicular to the tube's axis in order to measure the transverse velocity component. Data were collected while varying the net flow and gradient strength. The response, normalized by the response of static spins, is plotted versus the dimensionless parameter ϕ in Fig. 4.21.

The velocity distribution in the phantom was measured using a spin echo sequence with velocity encoding gradients. The SSFP response was calculated by numerical solution of Bloch's equations using the measured velocity distribution and a simple model in which each spin is assumed to have a constant velocity. This model, shown as a line in Fig. 4.21, predicts a larger response than observed. This is probably due to the constant velocity assumption and magnetic field inhomogeneity near surfaces in the phantom. Work is underway to refine both the model and the experiment.

For imaging slow flow two experiments conducted at different G_{eff} are subtracted (Fig. 4.22). The response from static spins cancels, and G_{eff} can be chosen to yield maximum sensitivity in a desired velocity range. Subtraction experiments have been demonstrated on phantoms, and will be tested in human subjects in early 1988.

S. Wong, M.S. Roos, and S. Patz (Harvard Medical School).

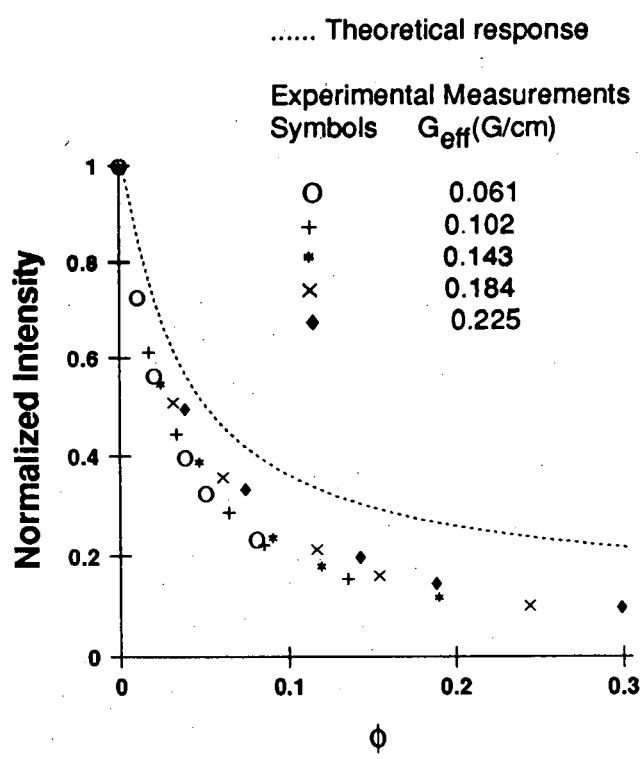

Fig. 4.21. SSFP response is plotted vs dimensionless parameter ϕ. Flow rate is varied at each of five values of G_{eff}. The dotted curve is a prediction based on the simple flow model. (XBL 8712-8032)

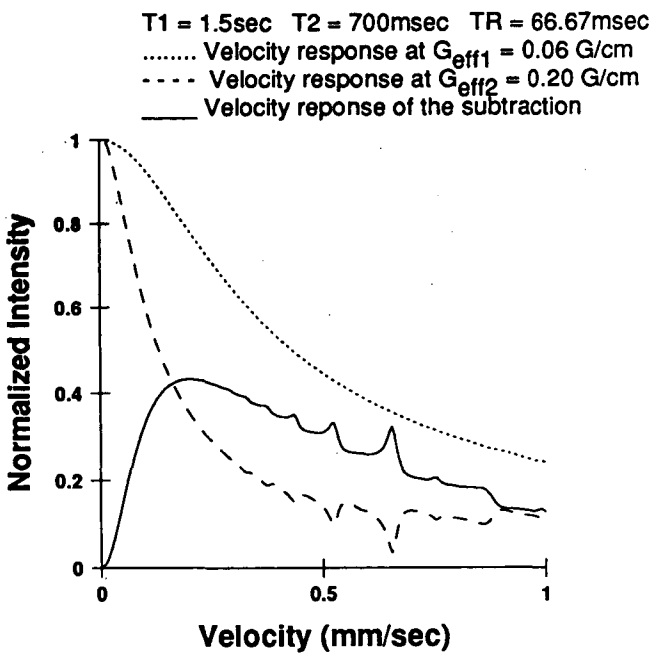

Fig. 4.22. Simulations of SSFP response to uniform velocities illustrate how data acquired at two values of G_{eff} can be subtracted to yield a response that suppresses static spins. (XBL 8712-8033)

Potentials of High Field NMR In Vivo with the Quadrupolar Nuclei Deuterium, Oxygen-17, Sodium-23, Chlorine-35, and Rubidium-87.

In addition to the dipolar spin one-half nuclei, ^{1}H,^{13}C, ^{19}F, ^{31}P, quadrupolar nuclei have been shown to have potential for imaging and spectroscopic studies *in vivo*. For example ^{2}H administered intravenously may be used for the evaluation of blood flow and body-water distribution, and determination of rubidium tissue concentrations is of particular interest in treatment evaluation studies for manic-depressive patients treated with rubidium. These and other biologically important nuclei such as oxygen-17 and lithium-7 have line broadening associated with the interactions of the quadrupole moment with biological media. The feasibility of high magnetic field studies *in vivo* (e.g., at 5 tesla and greater) using either endogenous signals or exogenously administered compounds depends on visibility, which is related to line broadening. The purpose of this study is to determine the visibility of these quadrupolar nuclei in aqueous solution and in biological tissues.

Studies of line shape and broadening in tissues (blood, heart, liver, and kidney) relative to nonorganic media were made at 4.3 tesla in a Nicolet vertical bore spectrometer (^{2}H, ^{17}O, ^{23}Na, ^{35}Cl) and at 2.3 tesla in a Bruker 40-cm horizontal-bore imaging spectrometer (^{87}Rb). The transverse relaxation of quadrupolar nuclei can be characterized by a bi-exponential decay with a fast and slow component. Line broadening associated with tissue interactions was measured as the width at half height that approximates the slow-relaxation component of the broadening. Transverse relaxation times of sodium were measured using the CPMG pulse sequence. The data fit a mono-exponential decay in the case of salt solutions and a bi-exponential decay in the case of tissues. ^{2}H, ^{23}Na, ^{35}Cl, and ^{17}O measurements were obtained from endogenous signals from excised tissue. Recycle delays were between 50 and 100 ms for ^{23}Na, ^{35}Cl, and ^{17}O, and between 400 and 1000 ms for ^{2}H. ^{87}Rb measurements were performed on a White New Zealand Rabbit with a surface coil *in vivo* after intravenous injection of 150 mg/kg of a sterile Rb solution. Signal was acquired at the level of the kidneys for 45 minutes to obtain sufficient signal to noise ratio. Signal was then acquired at the level of the heart for 5 minutes.

Figure 4.23 compares spectra obtained from aqueous solutions and tissues for some of the nuclei studied. Non-Lorentzian line shapes due to the two relaxation components are observed in the spectra from tissue whereas a single Lorentzian line shape is observed in the salt solutions where the nuclei are in the extreme narrowing regime. Figure 4.24 compares the measured line widths and the ratios of line widths from different media. In the case of rubidium, the tissue spectrum and line-width data are for heart tissue *in vivo*. The overall broader line width of rubidium, which has the same quadrupole moment as sodium, is due to the larger inhomogeneity of the B_0 field in the *in vivo* study.

The ratio of the salt solution line width to blood line width or blood to tissue line widths are similar for all nuclei observed except for the chlorine nucleus where broadening due to quadrupolar interactions with tissue is stronger. This is most likely due to the particular outer shell electron

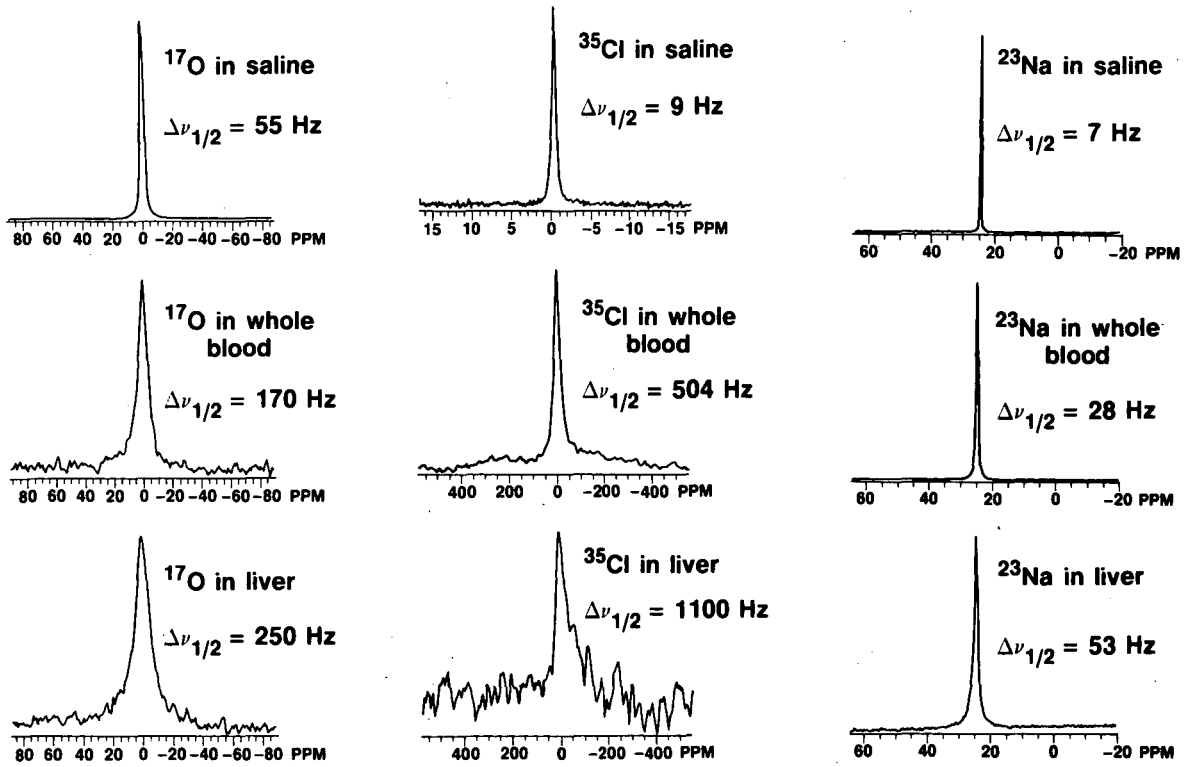

Fig. 4.23. Spectra of some quadrupolar nuclei obtained at 4.3 tesla. (XBL 871-7554A)

configuration of the chlorine atom, which creates stronger electrical field gradients at the nucleus during interaction with tissue components.

The amount of broadening of nuclei with quadrupole moments due to tissue interactions is not so great as to prevent studies of tissue concentrations *in vivo*, and possibly chemical shift, with the exception of intracellular chlorine. Previous studies of chlorine line broadening are summarized elsewhere. We expect chlorine signals to be proportional to the the extracellular fluid space because broadening due to covalent binding and quadrupolar interactions within the cell make it silent to NMR. Interest in evaluation of ^{7}Li and ^{87}Rb tissue concentrations is related to measurements *in vivo* on patients treated for manic-depression and depression.

Nicolas R. Bolo and Thomas F. Budinger.

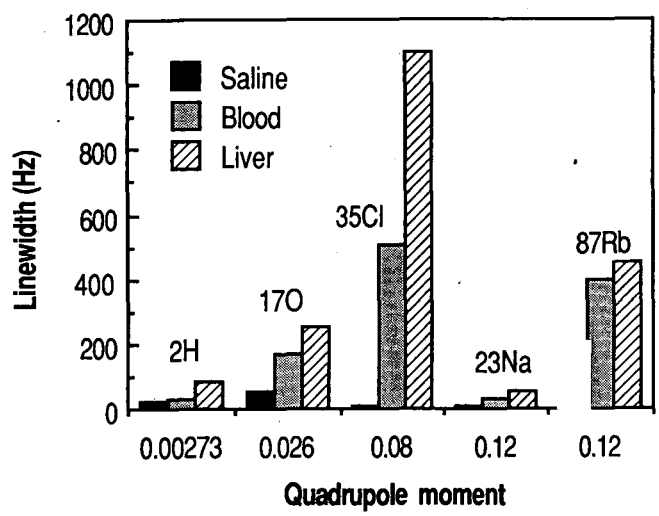

Fig. 4.24. Chart of line widths in hertz of the quadrupolar nuclei studied. The quadrupole moment is given in units of 10^{-28} m². (XBL 8712-8031)

PUBLICATIONS: Research Medicine

CONTRIBUTIONS TO JOURNALS

Castro, J.R., Gademann, G., Collier, J.M., Linstadt, D., Pitluck, S., Woodruff, K.H., Gauger, G.E., Char, D.H., Gutin, P., Phillips, T.L., Chu, W., and Henderson, S.D. Strahlentherapie mit schweren teilchen am Lawrence Berkeley Laboratory der Universität von Kalifornien: Klinische untersuchungen der Northern California Oncolog. Group. *Strahlentherapy und Onkologie 163*, 9–16 (1987).

Doyle, W.K., Budinger, T.F., Valk, P.E., Levin, W.A., and Gutin, P.H. Differentiation of cerebral radiation necrosis form tumor recurrence by ^{18}F-FDG and ^{82}Rb positron emission tomography. *J. Comput. Assist. Tomogr. 11*, 563–750 (1987).

Ebbe, S., Bentfeld-Barker, M., Adrados, C., Carpenter, D., Mortensen, C., Yee, T., and Phalen, E. Functionally abnormal stromal cells and megakaryocyte size, ploidy, and ultrastructure in Sl/Sl^d mice: Normal stromal cells may control megakaryocytopoiesis. *Blood Cells 12*, 217–232 (1986).

Ebbe, S., Leven, J., Miller, K., Yee, T., Levin, F., and Phalen, E. Thrombocytopoietic response to immunothrombocytopenis in nude mice. *Blood 69*, 192–198 (1987).

Fabrikant, J.I. Adaption of cell renewal systems under continuous irradiation. *Health Physics* 52, 561–570 (1987).

Friedland, R.P., Jagust, W.J., Ober, B.A., Dronkers, N.F., Koss, E., Simpson, G.V., Ellis, W.G., and Budinger, T.F. The pathophysiology of Pick's disease: a comprehensive case study. *Neurology 36 (Suppl. 1)*, 268 (1986).

Goodman, D.F., Char, D.H., Crawford, J.B., Stone, R.D., and Castro, J.R. Uveal melanoma necrosis after helium ion therapy. *Amer. J. Ophthalmology 101*, 189–193 (1986).

Jagust, W.J., Budinger, T.F., Huesman, R.H., Friedland, R.P. Mazoyer, B.M., and Knittel, B.L. Methodologic factors affecting PET measurements of cerebral glucose metabolism. *J. Nucl. Med. 27*, 1358–1361 (1986).

Jagust, W.J., Budinger, T.D., and Reed, B.R. The diagnosis of dementia with single photon emission computed tomography. *Arch. Neurology 44*, 258–262 (1987).

Kim, M.K.., Char, D.H., Castro, J.R., Saunders, W.M., Chen, G.T.Y., and Stone, R.D. Neovascular glaucoma after helium ion irradiation for uveal melanoma. *Ophthalmology 93*, 189–193 (1986).

Lagunas-Solar, M.C., Carvacho, O.F., Harris, L.J., and Mathis, C.A. Cyclotron production of ^{122}Xe/^{122}I for positron emission tomography. Current methods and potential developments. *Int. J. Radiat. Appl. Instrum., Part A, Appl. Radiat. Isot. 37*, 835–842 (1986).

Leven, R.M. Megakaryocyte motility and platelet formation. *Scanning Microsc. 1*, 1701–1709 (1987).

Leven, R.M. and Yee, M.K. Megakaryocyte morphogenesis stimulated *in vitro* by whole and partially fractionated thrombocytopenic plasma: a model system for the study of platelet formation. *Blood 69*, 1046–1052 (1987).

Lyman, J.T. and Wolbarst, A.B. Optimization of radiation therapy, III: A method of assessing complication probabilities from dose-volume histograms. *Int. J. Radiation Oncology Biol. Phys. 13*, 103–109 (1987).

McKenna, D.J., Mathis, C.A., Shulgin, A.T., Sargent, T.W., III, and Saavedra, J.M. Autoradiographic localization of binding sites for ^{125}I-DOI, a new psychotomimetic radioligand, in the rat brain. *Eur. J. Pharmacol. 137*, 289–290 (1987).

Mathis, C.A., Moerlein, S.M., Yano, Y., Shulgin, A.T., Hanson, R.N., and Kung, H.F. Rapid labeling of radiopharmaceuticals with iodine-122. *J. Label. Cmpd. Radiopharm.* 23, 1259–1261 (1986).

Moerlein, S.M. Use of aryltrimethylgermanium substrates for facile aromatic chlorination, bromination, and iodination. *J. Organic Chem. 52*, 664–667 (1987).

Moerlein, S.M., and Laufer, P., Stoecklin, G., Pawlik, G., Wienhard, K., and Heiss,W-D. Evaluation of ^{75}Br-labeled butyrophenone neuroleptics for imaging cerebral dopaminergic receptor area using positron emission tomography. *Eur. J. Nucl. Med. 12,* 211–216 (1986).

Moerlein, S.M., Mathis, C.A., Brennan, K.M., and Budinger, T.F. Synthesis and *in vivo* evaluation of ^{122}I- and ^{131}I-labeled iodoperidol, a potential agent for the tomographic assessment of cerebral perfusion. *Int. J. Radiat. Appl. Instrum. Part B., Nucl. Med. Biol. 14,* 91–98 (1987).

Moerlein, S.M., Mathis, C.A., and Yano, Y. Comparative evaluation of electrophilic aromatic iododemetallation techniques for labeling radiopharmaceuticals with iodine-122. *Int. J. Radiat. Appl. Instrum. Part A, Appl. Radiat. Isot. 38*, 85–90 (1987).

Moerlein, S.M., Stoecklin, G., Pawlik, G., Wienhard, K., and Heiss, W-D. Regional cerebral pharmacokinetics of the dopaminergic neurotoxin MPTP as examined by positron emission tomography in the living baboon brain is altered by tranylcypromine. *Neurosci. Lett. 15;66(2)*, 205–209 (1986).

Reimers, M., Castro, J.R., Linstadt, D., Collier, J.M., Henderson, S., Hannigan, J., and Phillips, T.L. Heavy charged particle radiotherapy of bone and soft tissue sarcoma: A phase I-II trial of the University of California Lawrence Berkeley Laboratory and the Northern California Oncology Group. *Amer. J. Clin. Oncol. (CCT) 9,* 488–493 (1986).

Urie, M., Goitein, M., Holley, W.R., and Chen, G.T.Y. Degradation of the Bragg peak due to inhomogenieties. *Phys. Med. Biol. 31*, 1–17 (1986).

Yano, Y. Essentials of a rubidium-82 generator for nuclear medicine. *Int. J. Radiat. Appl. Instrum. Part A, Appl. Radiat. Isot. 38*, 205–211 (1987).

CONTRIBUTIONS TO BOOKS AND PROCEEDINGS

Budinger, T.F. Single-photon emission computed tomography: physics, potentials and limitations. Pages 223–247 in *Technetium in Chemistry and Nuclear Medicine 2*, M. Nicolini, G. Bandoli, U. Mazzi, eds., Raven Press, New York(1986).

Budinger, T.F. Safety of NMR *in vivo* imaging and spectroscopy. Pages 215–231 in *Medical Magnetic Resonance Imaging and Spectroscopy*, T.F. Budinger and A.R. Margulis, eds., Soc. Magnetic Resonance in Medicine, Berkeley, CA (1986).

Budinger, T.F. New technologies for noninvasive imaging in aging and dementia. Pages 175–199 in *Advancing Frontiers in Alzheimer's Disease Research*, Glenner, G.G., Wurtman, R.J., eds., University of Texas Press, Austin, Texas (1987).

Budinger, T.F., Derenzo, S.E., Huesman, R.H., Cahoon, J.L. Vuletich, T. Dynamic positron emission tomography with 2.5 mm resolution. Pages 17–33 in *Biomedical Imaging*, O.

Hayaishi and K. Torizuki, eds., Academic Press, Tokyo (1986).

Castro, J.R. Californium-252. Pages 317–323 (Chapter 33) in *Modern Brachytherapy.*, Pierquin, B., Wilson, J.F., Chassagne, D., eds., Masson Publ. USA Inc. (1987).

Castro, J.R. An update of results of radiotherapy with heavy ions. Pages 148–154 in *Progress in Radio-Oncology III.* (Proceedings of the Third Meeting on Progress in Radio-Oncology, Vienna, Austria, March 27–31, 1985). K.H. Harcher, ed., International Club for Radio-Oncology, Vienna (1987).

Chen, G.T.Y. and Castro, J.R. Charged particle treatment planning. Pages 101–110 in *A Categorical Course in Radiation Therapy: Treatment Planning*, B.R. Paliwal and M.L. Griem, eds., Radiological Society of North American Division of Editorial and Publishing Services, Oak Brook, IL (1986).

Derenzo, S.E. Recent developments in positron emission tomography (PET) instrumentation. *In Physics and Engineering of Computerized Multidimensional Imaging and Processing*, O. Nalcioglu, Z.H. Cho, and T.F. Budinger, eds. *SPIE Vol. 671*, 232–243 (1986).

Derenzo, S.E. Potential improvements in instrumentation for PET. *Physics and Engineering of Medical Imaging, NATO Advanced Studies Institute Series E: Applied Sciences 119*, 913–925 (1985).

Derenzo, S.E. and Budinger, T.F. Advanced instrumentation for positron emission tomography. *Physics and Engineering of Medical Imaging, NATO Advanced Studies Institute Series E: Applied Sciences 119*, 855–873 (1985).

Derenzo, S.E., Huesman, R.H., Cahoon, J.L., Geyer, A., Uber, D., Vuletich, T., and Budinger, T.F. Initial results from the Donner 600 crystal positron tomography. *IEEE Trans. Nucl. Sci. NS-34*, 321–325 (1987).

Draves, D.J., Timiras, P.S., and Manley, N.B. Glial hormone receptors: Thyroid hormones and neurotubules in gliomas and neuroblastomas. Pages 183–201 in *Astrocytes, Volume 3, Cellular Neurobiology*, S. Federoff, A. Vernadakis, eds., Academic Press, New York (1986).

Fabrikant, J.I. Radiation hormesis. *Report to Committee 1 of the International Commission on Radiological Protection*, (4 pages) Jerusalem, Israel (November 1986).

Fabrikant, J.I., Bond, V.P., Modan, B., and Upton, A.C. Probability of causation. Report to Committee 1 of the International *Commission on Radiological Protection*, (33 pages) Jerusalem, Israel (November 1986).

Fabrikant, J.I., Frankel, K.A., Phillips, M.H., and Levy, R.P. Stereotactic heavy charged-particle Bragg peak radiosurgery for intracranial arteriovenous malformations. Pages 23.1–23.34 in *Cerebral Vascular Diseases of Childhood and Adolescence*, M.S.B. Edwards and H.J. Hoffman, eds., Williams and Wilkins, Baltimore, MD (1987).

Fabrikant, J.I., Land, C.E., and Schull, W.J. Risk coefficient for radiation-induced bladder cancer. *Report to Committee 1 of the International Commission on Radiological Protection*, (8 pages) Jerusalem, Israel (November 1986).

Friedland, R.P., Budinger, T.F., Jagust, W.J., Yano, Y., Huesman, R.H., and Knittel, B. Positron emission tomography and the blood brain barrier in Alzheimer's disease. Pages 85–93 in *Acute Cerebrovascular Diseases Pathopharmacology: New Brain Imaging in Cerebrovascular Disease*, N.A. Lassen and J. Cahn, eds., J. Libbey and Co., Ltd. Montrouge, France (1986).

Friedland, R.P., Budinger, T.F., Jagust, W.J., Yano, Y., Huesman, R.H., and Knittel, B. Blood brain

barrier integrity in Alzheimer's disease; Dynamic positron emission tomographic studies using ^{68}Ga-EDTA. In *Proceedings of the Brain 85: XII International Symposium on Cerebral Blood Flow and Metabolism*, Lund, Sweden, June 16–20, 1985 (1986).

Glicksman, A.S. and Fabrikant, J.I. Analysis of post-irradiation sarcomas: correlation of clinical data with experimental results. Pages 4–22 in *International Symposium on Biological Effects of Low Level Radiation*, L. Wei, D.C. Wu, and X.H. Wang, eds., Society of Radiological Medicine and Protection, Chinese Medical Association, Nanjing, China (1986).

Goldman, M., Anspaugh, L., Catlin, R.J., Fabrikant, J.I., and Gudiksen, P. The nuclear reactor accident at Chernobyl. *Interim Report of the Committee on Assessment of Radiological Effects and Consequences (CAREC)*. Prepared for The Office of Health and Environmental Research, U.S. Department of Energy, Washington, D.C. (July 1986).

Goldman, M., Anspaugh, L., Catlin, R.J., Fabrikant, J.I., and Gudiksen, P. Assessment of the Dosimetric and Health Implications of the Chernobyl Reactor Accident. *Interim Report of the Committee on Assessment of Radiological Effects and Consequences (CAREC)*. Prepared for The Office of Health and Environmental Research, U.S. Department of Energy, Washington, D.C. (August 1986).

Goldman, M., Anspaugh, L., Catlin, R.J., Fabrikant, J.I., and Gudiksen, P. Health and Environmental Consequences of the Chernobyl Nuclear Power Plant Accident. *Report to the U.S. Department of Energy, Office of Health and Environmental Research from the Interlaboratory Task Group on Health and Environmental Aspects of the Soviet Nuclear Accident.* Prepared by the Committee on the Assessment of Health Consequences in Exposed Population, U.S. Department of Energy, Washington, D.C. (January 1987).

Jagust, W.J., Budinger, T.F., Reed, B.R., and Colina, M. Single photon emission computed tomography in the clinical evaluation of dementia. Pages 217–233 in *Advancing Frontiers in Alzheimer's Disease Research*, G.G. Glenner and R.J. Wurtman, eds., University of Texas Press, Austin (1987).

Lyman, J.T. Treatment plan optimization. Pages 51–58 in *Proceedings of the Fifth PTCOG Meeting and International Workshop on Biomedical Accelerators*, Lawrence Berkeley Laboratory, December 1–2, 1986, LBL-22962 (1987).

Mazoyer, B.M. and Huesman, R.H. Tomographie d'emission dynamique: analyse des donnees loresque la fonction d'entree est. Pages 183 in Actes du XXVI Colloque de Medecine Nucleaire de Langue Francaise (Deauville-Caen, 18–20 September 1986), *J. Biophysique et de Biomecanique 10*, 183 (1986).

Moerlein, S.M., Laufer, P., Stocklin, G., Wienhard, K., Pawlik, G., and Heiss, W.D. Comparative evaluation of ^{76}br-labelled butyrophenone neuroleptics for PET studies of cerebral dopaminergic receptor area. In *Proceedings of the European Nuclear Medicine Congress*, London, September 3–6, 1985 (1986).

Turko, B.T., Zizka, G., Lo, C.C., Leskovar, B., Cahoon, J.L., Huesman, R.H., Derenzo, S.E., Geyer, A.B., and Budinger, T.F. Scintillation photon detection and event selection in high-resolution positron emission tomography. *IEEE Trans. Nucl. Sci., NS-34*, 326–331 (1987).

Valk, P.E. NMR and PET imaging in beam localization. Pages 199–206 in *Proceedings of the Fifth PTCOG Meeting and International Workshop on Biomedical Accelerators*, Lawrence Berkeley Laboratory, December 1–2, 1986, LBL-22962 (1987).

LBL REPORTS ISSUED

Cullander, C. Local Human Skin Potential—Spatial Distribution, Magnitude, and Origin. (Ph.D. Thesis) LBL-23450 (173 pages) April 1987.

Fabrikant, J.I. BEIR IV. The Effects on Populations of Exposure to Internally Deposited Alpha-Emitting Radionuclides: Health Risks of Radon and other Internally Deposited Alpha-Emitters. LBL-24173 (16 pages) September 1987.

PATENTS ISSUED

Derenzo, S.E. Improved readout for multi-crystal gamma cameras. D.O.E. patent file RL 9482. U.S. Patent 4,672,207, issued to the U.S. Department of Energy, June 9, 1987.

Sargent III, T., Shulgin, A.T., and Mathis, C.A. Rapid Brain Scanning Radiopharmaceutical. U.S. Patent 4,647,446, March 3, 1987.

APPENDIX A

I. Projects supported by the Office of Health and Environmental Research of the United States Department of Energy under Contract DE-AC03-76SF00098

INVESTIGATOR	PROJECT
E.L. Alpen	Long Term Biological Effects
J.C. Bartley	Effect of BaP on Humans
J.C. Bartley	Center for Cellular and Molecular Cancer Biology
A.J. Bearden	Resonance Studies in Photosynthesis
M.J. Bissell	Mechanism of Tumor Promotion
M.J. Bissell	Molecular Carcinogenesis
T.F. Budinger	Experimental Medicine Clinical
A. Chatterjee	Radiological Physics and Chemistry
G.K. Clemons	Endocrine Receptor Studies
A. Chatterjee	Tracer Studies with Radioactive Beams
P.K. Cooper	Carcinogenic DNA Damage
S.E. Derenzo	Positron 3-D Imaging Instrument
S.N. Ebbe	Vascular and Blood Diseases
S.N. Ebbe	Molecular Biology of Hemopoiesis
M.S. Esposito	Mitotic Recombination and DNA Repair
J.I. Fabrikant	Effects of Heavy Particle Radiation
J.I. Fabrikant	Heavy-Ion Radiosurgery
T.L. Hayes	Microdosimetry of Particulates
J. Hosoda	DNA Repair Mechanisms
R.M. Krauss	Human DNA Polymorphisms
R.P. Liburdy	Electromagnetic Field Effects
R.K. Mortimer	Genetic Study on Yeast
R.K. Mortimer	Human Genome Center
G. Parry	Studies of Cell Surface Organization using Monoclonal Antibodies
T.W. Sargent III	Metabolism in Brain Disorders
P.H. Silverman	Hematozoa and Erythropoiesis
J.C. Schooley	Hematopoietic Cell Proliferation
M.R. Stampfer	Rapid Transformation Assay
T.S. Tenforde	Biological Effects of Magnetic Fields
C.A. Tobias	Molecular Mechanisms of Cell Effects
Y. Yano	Experimental Medicine Development

II. Non-DOE Contracts and Grants Supporting Portions of Work Presented in this Annual Report

INVESTIGATOR	CONTRACT OR GRANT
E.J. Ainsworth	NASA P.O. T3516-G Life-Shortening Effects of HzE Particles on Mice/Heavy Ion Cell Transformation
E.J. Ainsworth	AFFRI P.O. N86I014 Murine Bone-Marrow Damage Produced by Charged Particles
E.L. Alpen	PHS Grant CA 30236 Advanced Design Research: Heavy Ion Medical Accelerator
E.L. Alpen	PHS Grant RR 05918 Growth & Radiation Response in an *In Vitro* Tumor Model
E.L. Alpen	PHS Grant CA 44669 Growth & Radiation Response of an *In Vitro* Tumor Model
M.A. Austin	PHS Grant HL 38760 Genetics of LDL Subclasses in Hypercholesterolemia
J.C. Bartley	PHS Grant CA 38889 Human Mammary Cells: Modulation of Differentiated States
M.J. Bissell	Monsanto 1856-29 Mechanisms of Extracellular Matrix Influences on Gene Expression
E.A. Blakely	PHS Grant RR 05918 Repair and Misrepair of Irradiated Single Human Chromosomes
G. Brecher	PHS Grant AM 27454 Kinetics of Transfused Stem Cells in Normal Mice
T.F. Budinger	PHS Grant HL 25840 Cardiovascular Flow and Metabolism
T.F. Budinger	PHS Grant AG 05890 Cerebral Blood Flow Patterns in Alzheimer's Disease
T.F. Budinger	PHS Grant HL 07367 Quantitative Cardiovascular Research, Training Grant
T.F. Budinger	UCSF Subcontract 8378-01 PET Studies
J.R. Castro	PHS Grant CA 19138 Treatment of Cancer with Heavy Charged Particles
A. Chatterjee	PHS Grant CA 27024 Bragg Peak Localization by Radioactive Beams
G.K. Clemons	PHS Grant HL 22469 Radioassay of Erythropoietin
P.K. Cooper	PHS Grant CA 32986 Inducible Responses to Carcinogenic DNA Damage
S.B. Curtis	PHS Grant CA 17411 Response of Rat Tumor Cells to Heavy Ions
K.H. Downing	PHS Grant RR 03637 Macromolecular Surfaces by Scanning Tunneling Microscopy

P.W. Durbin	NRC IAG 60-85-012 Development of Metabolic Models for Alkaline Earth and Actinide Radionuclides
P.W. Durbin	PHS Grant ES 02698 Biological Testing of New Actinide-Chelating Agents
S.N. Ebbe	PHS Grant AM 21355 Kinetics of Megakaryocyte and Platelet Turnover
S.N. Ebbe	PHS Grant RR 05918 Regulation of Megakaryocytes by Bone Marrow Stromal Cells
M.S. Esposito	PHS Grant GM 29002 Comparative Analysis of Mitotic and Meiotic Recombination
T.M. Forte	PHS Grant HL 07279 Lipoprotein Methodology, Structure and Function Training Grant
T.M. Forte	PHS Grant HL 38686 Nonhuman Primate: Development of Lipoprotein Subclasses
C.T. Gaffey	PHS Grant NS 24997 Nerve Bioelectric Activity in Ultrahigh Magnetic Fields
R.M. Glaeser	PHS Grant GM 36884 Membrane Proteins: High Resolution Electron Microscopy
L.S. Gold	PHS IAG 222-Y01-ES-10066 Quantitative Species Extrapolation in Carcinogenesis
R. Goth-Goldstein	PHS Grant ES 03603 Inducible Resistance to Alkylating Carcinogens
R. Goth-Goldstein	PHS Grant RR 05918 Repair of Alkylation Damage in Yeast
T.L. Hayes	PHS Grant TW 01234 Electron Microscopy of Frozen-Hydrated Biospecimens
J. Hosoda	PHS Grant GM 16841 Structure and Function of Helix Stabilizing Protein
J. Hosoda	PHS Grant RR 05918 Purification and Characterization of Yeast Recombination/Repair Enzymes
J. Hosoda	PHS Grant RR 05918 Mapping of Protein Conformational Changes by Limited Proteolysis
L. Hlatky	PHS Grant RR 05918 Chemical Studies Using the Sandwich System
R.H. Huesman	PHS Grant CA 38086 Scatter Compensation in Emission Tomography
B.K. Jap	PHS Grant RR 05918 3-D Crystallization of Bacteriorhodopsin for Molecular Structure Determination
R.M. Krauss	PHS Grant HL 33577 Plasma Lipoproteins in Coronary Artery Disease

R.M. Krauss	USC Medical Center 8072-22 Lipid and Protein Analysis
R.M. Krauss	Stanford University Contract P.O. #PR 4699-3 D & G Analyses
S.A. Leadon	PHS Grant CA 40453 DNA Repair in Specific Sequences of Mammalian Cells
H. Lecar	PHS Grant RR 05918 Distribution of Ion Channels in Stretch-Receptor Neurons
R.P. Liburdy	ONR Contract N00014-84-F-0186 Mechanisms of Microwave Interactions with LiposomeMembranes
R.P. Liburdy	Liposome Technologies Incorporated 1856-31 Electromagnetic-Field Triggered Drug Delivery via Liposome Vesicles into Target Cells
R.P. Liburdy	PHS Grant RR 05918 Electromagnetic Field-Triggered Liposome Drug Delivery
F.T. Lindgren	PHS Grant RR 05918 US-USSR Discrepancies Relating HDL Concentrations and Coronary Heart Disease
J. Llacer	PHS Grant CA-39501 Algorithms and Processing Architectures for Tomography
J.T. Lyman	PHS IAG Y01-CM-20110 Evaluation of Treatment Planning for Particle Beam Radiotherapy
J.T. Lyman	PHS CA 42940 Treatment Planning Optimization
J.T. Lyman	PHS Grant CA 22286 AAPM B682-19 Charged Particle Beam Dosimetry Task Group: Dosimetry Protocol
M.F. Maestre	PHS Grant AI 08427 Physical Structure of Viruses, Chromosomes & Cell Nuclei
M.F. Maestre	PHS Grant RR 02757 Jasco 500C Circular Dichrograph with FDCD and MCD
M.F. Maestre	PHS Grant RR 05918 Duysens Flattening Corrections Technique for Optical Spectra
C.A. Mathis	PHS Grant NS 22899 ^{122}I Blood Flow and Blood Volume Agents for PET Studies
C.A. Mathis	PHS Grant RR 05918 Development of Radiopharmaceuticals for the Quantitation of Hypoxia
M. McCall	PHS Grant RR 05918 Multiuser Inverted Microscope with Phase Optics
R.K. Mortimer	PHS Grant GM 30990 Yeast RAD Genes in Repair, Recombination and Meiosis
T.A. Musliner	PHS Grant RR 05918 Radioisotopic Tracking of Apolipoprotein Associations with Lipoprotein Subspecies

A.V. Nichols	PHS Grant HL 18574 Lipoprotein Methodology and Biomedical Applications
A.V. Nichols S.E. Bicknese	PHS Grant RR 05918 FDCD Spectral Analysis of Synthetic Peptide Models of Apolipoprotein A1
J.C. Owicki	PHS Grant AI 19605 Immunological Recognition of Model Membranes
G. Parry	PHS Grant CA 44398 Proteoglycan Influence on Mammary Cell Differentiation
A. Rodriguez	PHS Grant RR 05918 Radiation Effects on Gene Expression in Differentiated Cells: An *In Vitro* Model
T. Sargent, III	PHS Grant MH 36801 PET Brain Blood Flow & Metabolism in Alzheimer's Disease
D. Schild	PHS Grant RR 05918 Cloning of Human Genes Using Complementation of Yeast Mutations
W. Schimmerling	PHS Grant CA 23247 Physical Characteristics of Heavy Ion Beams
W. Schimmerling	NASA P.O. L22395A To Measure the Production of Neutrons by High Energy Heavy Ions
W. Schimmerling	NASA P.O. L9550C Iron and Oxygen Fragmentation Experiments
R.I. Schwarz	PHS Grant CA 37958 Manipulation of the Differentiated State by Oncogenesis
R.I. Schwarz	PHS Grant RR 05918 Understanding Cellular Control of Oncogene Expression
P.H. Silverman	PHS Grant GM 39143 Pulse Programmer, Automated Measurement System, NMR Probe
B.A. Singer	PHS Grant CA 42736 Alkylation of Polynucleotides *in vitro* and *in vivo*
M.R. Stampfer	PHS Grant CA 24844 Characterization of Human Mammary Cells
M.R. Stampfer	PHS Grant CA 30028 (R.Ham, Univ. Colorado) P.O. 426881 Defined Medium for Human Mammary Epithelial Cells
C.A. Tobias	PHS Grant CA 15184 Heavy Ion Radiobiology Related to Oncology

APPENDIX B: Biology and Medicine Division Staff September 30, 1987

The accomplishments of the Biology and Medicine Division are due in large measure to the capability and dedication of its staff. Listed below are those who have participated in the Division's programs during fiscal year 1987 as full or part-time employees, consultants, and participating guests. The guest staff includes visiting scientists, postdoctoral trainees, resident physicians, graduate and undergraduate students, and summer research participants.

DIVISION HEAD

Paul H. Silverman
John C. Bartley, Deputy

ADMINISTRATION STAFF

Igor R. Blake
Mary P. Curtis
Janice C. DeMoor
Diane E. Duhnke
Wendell Hom
Allan W. Long
Vera Martin
Lucy A. Nixon
Georgia A. Peterson*
Louise Ray
Karen S. Ross
Dolores Ruff
Lori E. Ryan
Robert W. Springsteen
Katherine A. Swenson
Frank T. Upham
Christine P. Villaluz
Mary L. Worth

DIVISION SCIENTIFIC STAFF

James R. Abney
S. Javed Afzal
Judith Aggeler
Lawrence P. Aggerbeck
E. John Ainsworth
Myriam Alhadeff
Julius J. Almasi*
Edward L. Alpen[1]
Bruce N. Ames[1]
Lynn Anderson*
Melissa A. Austin
Mary H. Barcellos-Hoff
S. Jacob Bastacky
Alan J. Bearden[1]
James C. Beck
Andrew S. Belmont*
Eugene V. Benton
Leslie Bernstein
Edward A. Berry
Anthony M. Berson*
Guy M. Besson
Stephen E. Bicknese
Mina J. Bissell
Eleanor A. Blakely
William F. Blakely*
Alan R. Brautigan
George Brecher[2]
Kathleen M. Brennan
Thomas F. Budinger[1,2]
Frederick T. Burkhard
Vincent P. Carabillo*
Joseph R. Castro[2]
Lorraine A. Champion*
David Chappell
Aloke Chatterjee
William T. Chu
Gisela K. Clemons
J. Michael Collier
Priscilla K. Cooper
Christopher Cullander
Stanley B. Curtis
Kanu B. Dalal
Maya M. Das*
Mary M. Decker
Richard L. Deming*
Stephen E. Derenzo
Danielle Dhouailly*

*Left Biology and Medicine Division prior to September 30, 1987.
†Retired during Fiscal Year 1987
[1]Faculty UC Berkeley
[2]Faculty UC San Francisco
[3]Faculty UC Davis

Martha L. Dixon
Odilon M. DoCanto*
David S. Dolberg*
Kenneth H. Downing
Patricia W. Durbin
Shirley N. Ebbe[2]
Barry L. Engelstad
David E. Erkenbrack*
Michael S. Esposito
Jacob I. Fabrikant[2]
James A. Fisher*
Wendy L. Fitch*
Paula F. Flicker
James Fontanesi*
Trudy M. Forte
Heinz Fraenkel-Conrat[1]
Kenneth A. Frankel
Michael Freeling[1]
Cornelius T. Gaffey
John C. Game
Edwin G. Garcia
Grant E. Gauger
Peter S. Geissler*
John M. Gerdes
Sandra H. Gianturco*
Robert M. Glaeser[1]
Michael Goitein
Lois S. Gold
Regine Goth-Goldstein
Martin H. Graham[1]
Stephen G. Gregg
Thomas L. Hayes
Sheri D. Henderson
Ronald L. Himelman
Lynn R. Hlatky
Libby L. Holbrook*
William R. Holley
Yoshio Hosobuchi[2]
Junko Hosoda
Jerry Howard
Anthony R. Howlett
Mirko I. Hrovat*
Li-Shar Huang
John P. Huberty
Ronald H. Huesman
William J. Jagust[3]
Bing K. Jap
John R. Johnston*
Talwinder S. Kahlon
Jonathan A. Kans
Leon N. Kapp*
Parris M. Kidd*
Stevo Knezevic
Ronald M. Krauss[2]
Michael La Belle
John H. Lawrence[1]
Steven A. Leadon
Harold Lecar[1]
Robert M. Leven
Larissa V. Levin*
Richard P. Levy
Ming-Liang Li*
Robert P. Liburdy
Frank T. Lindgren
Jan E. Litton*
Francoise Livolant*
Bernhard A. Ludewigt*
John T. Lyman
Marcos F. Maestre
Andrew C. Magyarosy
Neela B. Manley
Su-Yao Mao
Paul K. Marsden
Manuela Martins-Green
Chester A. Mathis
Mark R. Mc Call
Joyce C. McCann*
Jean M. Mefferd
Howard C. Mel[1]
Kathleen L. Miller
Stephen M. Moerlein*
Robert K. Mortimer[1]
William W. Moses
Brian R. Moyer
Thomas A. Musliner
Nicola T. Neff
Richard Newmark
Alex V. Nichols[1]
Masataka Onizuka*
William G. Owen[1]
John C. Owicki[1]
Charles S. Parkins*
Gordon Parry
Richard Payne*
Ashot Petrossian*
Paula L. Petti
Mark H. Phillips
Theodore L. Phillips[2]
Dennis E. Prosen
Gian M. Ratto*
Miguel T. Robinson
Adrian Rodriguez
Mark S. Roos
Ruth J. Roots
Thornton Sargent, III
David Schild
Walter Schimmerling
John C. Schooley*

Richard I. Schwarz
J. Philip Seab
Alexander T. Shulgin
Bea Singer
Jerome R. Singer[1]
Thomas H. Slone
Sylvia J. Spengler
Martha R. Stampfer
Henry H. Stauffer
Claudio D. Stern*
Andrew W. Stoker
Thomas Swain
Joseph R. Taylor*
Thomas S. Tenforde
Allan Tischler
Cornelius A. Tobias[1]
Peter E. Valk
Karen M. Vranizan
John R. Wetterau*
Paul T. Williams
Mervyn Wong
Tracy C. Yang
Yukio Yano
Michael J. Yezzi*

DIVISION SUPPORT STAFF

Paul Abdul-Malak
Linda D. Abe
Frederick E. Abrams*
Gerald L. Adamson
Mari Aker
David C. Albarian
Nicholas Alexander*
Charles M. Allison
Sharon L. Amacher*
Georganne M. Backman*
Kari P. Baken
John R. Baker
Ashley J. Barboza*
Josephine L. Barr
Elizabeth D. Beattie*
Maren Bell
Sindy E. Berger
Kathleen A. Bjornstad
Judith M. Blair
Patricia J. Blanche
Nicolas R. Bolo
S. Kay Bristol
Gerald L. Brooks
Mark A. Brown*
Mary L. Cabbage
Veronica G. Cabras
John L. Cahoon
Mardel M. Carnahan
Dorothy A. Carpenter
Adelle H. Cavanaugh
Rosemarie L. Celli
Polly Y. Chang
Te Ning Chang*
Frank Chavez
Li-How Chen
Marica Chen*
Steve Chi-Long Chen
Chao-Hstung Cheng
Dennis Chin
Amy L. Choi
Frank Chuang*
Ling-Fong Chung*
Gary M. Cole*
Miguel M. Colina
C. Rebecca Contopoulou
Vincent E. Cook
Douglas Corley*
Benedict J. Costello*
Laurie M. Craise
Freddie L. Crenshaw, Jr.
Betsey L. Cullen
Anne M. Cummings
Maria N. Da Costa*
Massood Darvishzaden
Randy J. De Guzman
Darlene J. De Manincor
Kim Des Rochers*
Andrew M. Dienstfrey*
Uyen Nina Dinh*
Luisa I. Disini
Niedra A. Dodson
Neils M. Dua
Michael L. Dunker
Sujay Dutta
Maria K. Dybbro
Susan L. Eisenberg
Dennis M. Fantin
Deborah A. Farson
Myrtle L. Foster
Rochelle I. Frank*
Roscoe Frazier
Samuel W. French
John Frey
Denis L. Fung*
Jennifer C. Fung
Assefa Gebremichael
Sherry L. Gee
Kalle B. Gehring
Christine Giotas
Queen E. Gipson
Brian J. Glassner

Laura A. Glines
Michael A. Glotzer*
Tennessee W.-Y Gock
Elina Golder
Kaarin Keer Goncz
Elaine L. Gong
Edwin H. Goodwin
Sara P. Goolsby
Anders Greenwood
Robert W. Gribben*
Helena B. Hansen*
Steven M. Hanrahan
William A. Hare
Rita Harvey-Turner
Linda J. Harrison*
Anna R. Hashima
Chris A. Haskell*
Carroll Hatier
Virginia C. Havens†
Lilian E. Hawkins
Linda G. Hayashi
Marjaneh Hedavet*
Mark D. Hertle
Christene S. Ho
Lori L. Hollander*
Elizabeth C. Holloway
Christine S. Hong
Sok C. Hong*
Laura J. Horn
Midori M. Hosobuchi
Mildred K. Hughes
Jacquelyn J. Iler
Gayla P. Ivery
Heather M. Jackson*
Nylan M. Jeung
Jay A. Johnson*
Reese M. Jones*
Mary Jordan
Jay S. Joseph*
Julian S. Joseph*
James W. Judnick*
Norbert V. Kang*
Peter M. Kang*
Aaron B. Kantor
Kristina S. Kavanau
Leah A. Kenaga*
Marc L. Kessler
John Kim
Jeffrey S. King
Chris B. Kingsley
Leslie A. Klein*
Brian L. Knittel
Kenneth J. Knudsen*
Seok-Hwan Kong
Vida W. Kong*
Brian S. Korotzer*
Kari L. Koszdin*
Birgetta R. Kullgren
Mary Lou Kurtz
Natalia Kusubov
Mark T. Lasartemay*
Ann Lee*
Charles Y. Lee*
Joong W. Lee
Kyung-Dall Lee
Peter P. Lee
Gerri A. Levine
Lynette L. Levy
Rebecca H. Lichtenberg*
Eng H. Lo
Leora Lommel*
Janet S. Lowe*
Ryan P. McCormack
Tommy J. McKey
Renae I. Magaw*
Eva J. Mah*
Lynn J. Mahlmann
Dimitrios T. Maleas*
Marc S. Mendonca*
Peter L. Miller
Roger L. Miller
Barbara Modlinski
Herbert W. Moise, III
Charles W. Moniak
Alyssa M. Morimoto*
Marshall L. Morningstar
Lenny Moss*
Steve S. Neben
Tamlyn K. Neben
Robert W. Nordhausen
Virginia I. Obie
Christene Y. Oh*
Lucinda S. Olney
Joseph R. Orr
Lars G. Osterberg*
Laura M. Palanck
Annie C. Pang
Srisawai Pattamakom
Eva A. Penzes
Guy A. Perkins
Denise M. Peterson
Patrick G. Pieper*
Huan N. Phan*
Patricia P. Powers-Risius
John C. Prioleau
Tracy G. Ram
Jose A. Ramirez
Ross A. Ramos

Monica H. Reimers
David Reisman
Gerardo C. Rios*
Ellen Saegerbarth
Laureen Sasaki
Karen R. Schenk
Janis S. Scherer
James B. Schmidt
Annelie D. Schumann
Janet F. Selmek-Halsey
Mark Shavers
Michael Sieweke
Mohindar Singh
Karen C. Sitney*
Jonathan Slack
Karen L. Smith*
Margaret M. Snowden*
Michael T. Solis*
Marcia E. Somers
Dorothy S. Sprague
Karen A. Springsteen
Uhsa Srinivasan
Audrey D. Stapleton
Daniel Straus
John D. Stubbs
Shirley C. Sutton
Herbert C. Szeto*
Annie Tang
Pat Tittiranonda
Jo Ann Trejo*
Sally P. Tubach
Julia A. Twitchell
Greg Y. Uramoto
Vladimir Vacata
Janice Valmassoi*
Dresden D. Van Dusen
Paul F. Vanek*
Peter J. Walian
Alex K-Y Wang
Karly S. Wang*
David K. Warland
Chiahon Wei*
David C. West
Nancy C. White
Monroe Whitney
Eric D. Wieder*
Scot W. Wigert
Jennifer A. Wong*
Sam T.S. Wong
Marilyn Yee
Alice Yeh*
Karen L. Zettl

Committees

DIVISION ADVISORY COMMITTEE

Paul H. Silverman, Chair
John C. Bartley/Priscilla K. Cooper
Mina J. Bissell
Eleanor A. Blakely
Thomas F. Budinger/Thornton Sargent III
Trudy M. Forte/Bing Jap
Robert K. Mortimer
Cornelius A. Tobias/Aloke Chatterjee
Igor R. Blake‡
Lori E. Ryan‡

DIVISION STAFF COMMITTEE

Tony W. Sargent, Chair
Mina J. Bissell
Aloke Chatterjee
Trudy M. Forte
John T. Lyman
Walter Schimmerling

EQUIPMENT COMMITTEE

Shirley N. Ebbe, Chair
Stephen E. Derenzo
William R. Holley
Steven A. Leadon
Marcos F. Maestre
Richard I. Schwarz
Allan W. Long‡

SPACE COMMITTEE

Thomas S. Tenforde, Chair
Priscilla K. Cooper
Kenneth H. Downing
Chester A. Mathis
Richard I. Schwarz
Allan W. Long‡

SALARY COMMITTEE

Paul H. Silverman, Chair
John C. Bartley
Thomas F. Budinger
Trudy Forte
Cornelius A. Tobias
Igor R. Blake‡

DONNER SEMINAR COMMITTEE

Priscilla K. Cooper, Chair
Sheri D. Henderson
Bing Jap
Gordon Parry

HUMAN USE COMMITTEE

Henry H. Stauffer, Chair
J. Michael Collier
Shirley N. Ebbe
Kathleen E. Handron
Mark H. Phillips
Peter E. Valk
Janice C. DeMoor‡

RADIOACTIVE DRUG RESEARCH COMMITTEE

Henry H. Stauffer, Chair
Aloke Chatterjee
Patricia W. Durbin
Jacob I. Fabrikant
Paola S. Timiras
Peter E. Valk
Janice C. DeMoor‡

ANIMAL WELFARE AND RESEARCH COMMITTEE

John C. Bartley, Chair
Hermann Bonasch
Kathleen M. Brennan
Gisela K. Clemons
Janice C. DeMoor
Steve F. Sapontzis
Kent A. Zimmerman
Robert W. Springsteen‡

DONNER LIBRARY COMMITTEE

Stanley B. Curtis, Chair
James C. Bartholomew (LCB)
Jacob Bastacky
J. Michael Collier
Junko Hosoda
John C. Owicki
Adrian Rodriguez
Dorothy F. Denney‡
Hillis L. Griffin‡

SAFETY COMMITTEE

John T. Lyman, Chair
Eleanor A. Blakely
Kathleen M. Brennan
Deborah A. Farson
Regine Goth-Goldstein
Jacqueline Iler
Herbert W. Moise
Robert W. Nordhausen
Patricia Powers-Risius
Robert W. Springsteen
Allan W. Long[‡]

[‡]Ex officio, nonvoting member
[§]Executive Officer

Lawrence Berkeley Laboratory
Technical Information Department
University of California
Berkeley, California 94720